

NORTHWESTERN UNIVERSITY

Nitrogen and Phosphorus Removal and Energy Production via Microbial Nitrous Oxide
Generation from Wastewater

A DISSERTATION

SUBMITTED TO THE GRADUATE SCHOOL IN PARTIAL FULFILLMENT OF THE
REQUIREMENTS

For the degree

DOCTOR OF PHILOSOPHY

Field of Civil and Environmental Engineering

By

Han Gao

EVANSTON, ILLINOIS

September 2018

© Copyright by Han Gao 2018

All Rights Reserved

ABSTRACT

Nitrogen and Phosphorus Removal and Energy Production via Microbial Nitrous Oxide Generation from Wastewater

Han Gao

Reactive Nitrogen (N) and phosphorus (P) pollution is responsible for a vast array of environmental problems, including eutrophication of nutrient limited water bodies, vast dead zones in the ocean margins, and ammonia toxicity to aquatic life. N pollution is also linked to the emission of the potent greenhouse gas nitrous oxide (N_2O), which has a global warming potential 310 times that of CO_2 . In addition, P in fertilizers critical for global food production is derived primarily from phosphate rock, a geographically concentrated nonrenewable resource. P scarcity is an emerging global challenge in its own right, and there is increasing interest in reuse of P from wastewater.

Microbial bioprocesses at Water Resource Recovery Facilities (WRRFs) play a key role in preventing nutrient pollution. Unfortunately, current processes are energy intensive, costly, and characterized by emissions of N_2O . Paradoxically, N_2O is also a powerful potential energy source, as evidenced by its use in propulsion and automotive applications. Recently, a novel nutrient removal process, Coupled Aerobic-anoxic Nitrous Decomposition Operation (CANDO) was introduced to remove N from wastewater and generate N_2O as a biofuel. Here, we developed a second generation of CANDO, termed CANDO+P, that combines N removal and energy recovery via microbial N_2O generation with biological P removal and recovery. Simultaneous N and P removal by CANDO+P will have the chance to make this process more promising and fit a new

vision of wastewater treatment targeting resource recovery in addition to environmental and public health protection.

A proof-of-concept of CANDO+P was provided via long-term operation of a lab-scale bioreactor treating synthetic wastewater with biomass enriched in denitrifying polyphosphate accumulating organisms (DPAOs) for almost 1000 days. Over this period, stable denitrification performance with complete N and partial P removal coupled to high-rate and high-yield N_2O production (>70% influent N) was achieved. Biomass aggregate structure shifted during operation from predominantly flocs to a hybrid mixture of flocs and dense microbial granules. A comprehensive study of both reactor kinetics and the underlying microbial community was conducted to understand the structure and function of the microbiome within CANDO+P, and to shed light on mechanisms of N_2O production in this system. Based on high-throughput 16S rRNA gene amplicon sequencing, the reactor community rapidly shifted away from the inoculum under the selective pressures imposed mainly by high nitrite (NO_2^- , 40-50 mg-N/L) and phosphate (PO_4^{3-} , 5-15 mg-P/L) in the synthetic wastewater feed. A denitrifying Enhanced Biological Phosphorus Removal (EBPR) enrichment dominated by DPAOs, denitrifying glycogen accumulating organisms (DGAOs) and other flanking organisms was selected. 41 near-complete draft genomes including two *Candidatus* Accumulibacter genomes (associated with clade IA and the first published genome associated with clade IC) were extracted through genome-resolved metagenomic sequencing to characterize genomic denitrification potential. To investigate kinetics of the selected microbial consortium, *ex situ* batch assays were performed to evaluate denitrification capabilities and denitrifying phosphate uptake with different nitrogen oxides (nitrate [NO_3^-], NO_2^- and N_2O). Compared with aerobic EBPR reactors and other heterotrophic

denitrifiers enrichments, the selected microbial consortium exhibited a strong preference for NO_2^- utilization, and the propensity to accumulate N_2O in the presence of NO_2^- .

To explain the mechanisms of N_2O formation, three hypotheses were tested: (1) electron competition among denitrification enzymes, (2) the enrichment of *Candidatus Accumulibacter* (PAO) with truncated denitrification pathways, and (3) the selection of flanking organisms (non-PAOs) lacking nitrous oxide reductase (NOS), the terminal enzyme in the complete denitrification pathway. An observed imbalance of denitrification capabilities using different nitrogen oxides as electron acceptors suggested that electron competition was likely not the main driver of N_2O formation in this microbial consortium. By screening denitrification genes within the 41 near-completed genomes, nitrous oxide reductase gene was discovered in the *Accumulibacter* genomes, but not in several flanking bacterial genomes. Taken together, our results suggest that the unusually high levels of N_2O accumulation observed in this microbial consortium may be caused by a combination of different mechanisms, including the selection of flanking microorganisms with truncated denitrification pathways. These findings provide proof the feasibility of the CANDO+P bioprocess, and shed light on biological formation of N_2O and P uptake by providing detailed information on the associated microbial community structure and function.

Thesis Advisor

Dr. George F. Wells

Department of Civil and Environmental Engineering

Final Examination Committee

Dr. George F. Wells, Chair

Dr. Aaron I. Packman

Dr. Erica M. Hartmann

Dr. Keith E. J. Tyo

Thesis Organization

Chapter 1. Introduction

This chapter is an overview of the technical background and research objectives. The discussion of low-energy nitrogen removal processes is adapted from a publication in *Environmental Science Process & Impacts*: Gao, H., Scherson, Y.D. and Wells, G.F. (2014) Towards energy neutral wastewater treatment: methodology and state of the art. *Environmental Science Process & Impacts* 16(6), 1223-1246.

Chapter 2. Complete Nutrient Removal Coupled to Nitrous Oxide Production as a Bioenergy Source by Denitrifying Polyphosphate-accumulating Organisms

The design and implement of lab-scale sequencing batch reactor for CANDO+P proof-of-concept is presented in this chapter. The performance of CANDO+P as well as the comparison of kinetics with other CANDO studies are described in this chapter as well. The overall microbial community structure was also investigated via 16S rRNA gene amplicon sequencing. This chapter has been published in *Environmental Science and Technology*: Gao, H., Liu, M., Griffin, J.S., Xu, L., Xiang, D., Scherson, Y.D., Liu, W.T. and Wells, G.F. (2017) Complete Nutrient Removal Coupled to Nitrous Oxide Production as a Bioenergy Source by Denitrifying Polyphosphate-Accumulating Organisms. *Environmental Science & Technology* 51(8), 4531-4540.

Chapter 3. Differential Kinetics of Nitrogen Oxides Reduction Leads to Elevated N₂O Production by a Nitrite Fed Denitrifying EBPR Bioreactor

This chapter focus on quantification of kinetics of nitrogen oxides reduction and denitrifying phosphorus uptake with different electron acceptors (NO_3^- , NO_2^- and N_2O) by a DPAO enrichment culture via two sets of batch tests with external and internal carbon sources (electron donors). Experimental design and implementation for all the batch tests are described in detail. Electron competition among different nitrogen oxide reductases, our first hypothesis for N_2O generation in CANDO+P, was tested here based on kinetics calculated from the batch studies. The content of this chapter is based on a submitted manuscript: Gao, H., Zhao, X., Zhou, L., Sabba, F., and Wells, G.F. Differential Kinetics of Nitrogen Oxides Reduction Leads to Elevated N_2O Production by a Nitrite Fed Granular Denitrifying EBPR Reactor (*In review*).

Chapter 4. Metagenomic Analysis Reveals Potential N_2O Producers in a Nitrite-fed Denitrifying Biological Phosphorus Removal Process Enriched in *Candidatus Accumulibacter*

In chapter 4, CANDO+P microbial community structure and function were investigated by genome resolved metagenomic analysis. Methods for resolving *Accumulibacter* subpopulation structure and dynamics are described. Two draft genomes of *Accumulibacter* (PAOs) and 39 flanking organisms (non-PAOs) were extracted from five metagenomic sequencing datasets. The other two hypotheses related to N_2O formation were tested in this chapter by extracting and comparing denitrification genes from the recovered PAO and non-PAO draft genomes. The content of this chapter is based on a submitted manuscript: Gao, H., Mao, Y., Zhao, X., Liu, W., Zhang T. and Wells, G.F. Metagenomic Analysis Reveals Potential N_2O Producers in a Nitrite-fed

Denitrifying Biological Phosphorus Removal Process Enriched in *Candidatus Accumulibacter* (*In review*).

Chapter 5. Segregation of Microbial Composition and Function in Granular Denitrifying EBPR Process

Without intentional selection for granules, granulation was observed in the CANDO+P SBR reactor. The spatial segregation of both microbial composition and genetic potential for denitrification are of great interest. After separation of biomass into different size fractions, 16S amplicon sequencing and qPCR were conducted to understand the segregation of microbial community structure and function. The content of this chapter is based on a submitted manuscript: Gao, H., Zhao, X., Zhou, L., Sabba, F., and Wells, G.F. Differential Kinetics of Nitrogen Oxides Reduction Leads to Elevated N₂O Production by a Nitrite Fed Granular Denitrifying EBPR Reactor (*In review*).

Chapter 6. Conclusions

Chapter 6 describes the overall conclusions of the dissertation and suggestions for future work.

ACKNOWLEDGMENTS

I would like to acknowledge my colleagues at Northwestern University as well as my other collaborators outside the University. The work presented here could not be possible without their help and great support.

First and foremost, I would like to thank my advisor, Dr. George Wells, for his great mentoring and tremendous guidance on my research. It has been an amazing experience working with him. I am greatly indebted to him for his endless support, instruction and mentorship on this project.

I would also like to thank all my collaborators. Many thanks to Dr. Wen-tso Liu from University of Illinois Urbana-Champaign (UIUC) for offering valuable suggestions on experimental design and data analysis on my project and publications, and Miaomiao Liu also from UIUC who assists me with some of the molecular biology work. I am particularly grateful to Dr. Yangpin Mao from Shenzhen University and Dr. Tong Zhang from Hong Kong University for their advice and support with the bioinformatics analysis.

I am also very grateful to my colleagues at Northwestern University. Longcheng Xu, Da Xiang, Xiaotian Zhao and Lei Zhou offered me great help on some of the experimental work. I also enjoy working with colleagues in Wells Research Group, Dr. Alex F. Rosenthal, Dr. Yubo Wang, Dr. Fabrizio Sabba, James Griffin, Morgan Petrovich, Paul Roots, Qiteng Feng, and Jeanne LaVerge. Besides, colleagues from other labs in the department, Dr. Nanxi Lv, Dr. Tiezheng Tong, Dr. Xiaobao Li also provided me help on setting up my experiment. I also want to thank the laboratory coordinator Richard Warta for his incredible support for my experiments.

I also owe my greatest gratitude and appreciation to my family and friends. Supports and care from them helped me overcome the obstacles of my research work. With their company, my life becomes more fun and exciting.

TABLE OF CONTENTS

CHAPTER 1

Introduction	25
1.1 Problem Statement	26
1.2 Technical Background	29
1.2.1 Nutrient Pollution in the Environment.....	29
1.2.2 Low Energy or Energy Positive Approaches for NOD Removal.....	32
1.2.3 Enhanced Biological Phosphorus Removal (EBPR) and Polyphosphate Accumulating Organisms (PAOs).....	41
1.2.4 Microbial N ₂ O production.....	47
1.3 Research Objectives	54

CHAPTER 2

Complete Nutrient Removal Coupled to Nitrous Oxide Production as a Bioenergy Source by Denitrifying Polyphosphate-accumulating Organisms	56
2.2 Materials and Methods	60
2.2.1 CANDOP Bioreactor Operation and Strategies for N ₂ O Production.....	60
2.2.2 Bioreactor Performance Monitoring.....	61
2.2.3 DNA Extraction and 16S rRNA Amplicon Sequencing.....	63
2.2.4 Statistical Analyses.....	65
2.3 Results and Discussion	66
2.3.1 Bioreactor Performance and N ₂ O Production.....	66
2.3.2 Overall Microbial Diversity and Population Dynamics.....	69
2.4 Conclusions	74

	13
2.5 Supporting Information	77
2.5.1 Supporting Information - Tables.....	77
2.5.2 Supporting Information - Figures.....	78

CHAPTER 3

Differential Kinetics of Nitrogen Oxides Reduction Leads to Elevated N₂O Production by a Nitrite

Fed Denitrifying EBPR Bioreactor	80
3.1 Introduction	82
3.2 Materials and Methods	84
3.2.1 Bioreactor Setup and Operation	84
3.2.2 Batch Experiments Design.....	85
3.2.3 Chemical Analysis.....	87
3.2.4 Calculation of Electron Consumption and Electron Distribution Among Different Steps of Denitrification	87
3.3 Results and Discussion	89
3.3.1 <i>Ex situ</i> Batch Assays Reveal Distinctive Kinetics with Different Nitrogen Oxides as Electron Acceptors.....	89
3.3.2 Electron Competition and Distribution under Coupled and Decoupled Feeding Strategies.....	99
3.4 Conclusions	103
3.5 Supporting Information	104
3.5.1 Supporting Information - Methods.....	104
3.5.2 Supporting Information - Figures.....	105

CHAPTER 4

Metagenomics Analysis Reveals Potential N₂O Producers in a Nitrite-fed Denitrifying Biological

Phosphorus Removal Process Enriched in <i>Candidatus Accumulibacter</i>	108
--	------------

	14
4.1 Introduction	110
4.2 Materials and Methods	113
4.2.1 DNA Extraction and Metagenome Sequencing, Assembly and Gene Annotation	113
4.2.2 Accumulibacter Genome Binning, Annotation and Comparative Genome Analysis	114
4.2.3 Orthologous Gene Family Detection and Gene Flux Analysis	115
4.2.4 <i>ppk1</i> Clone Library Construction and Sequencing	115
4.2.5 <i>ppk1</i> Gene Screening and Phylogenetic Analysis	116
4.2.6 Flanking Bacterial Genome Binning and Metabolic Potential Analysis.....	116
4.3 Results and Discussion	117
4.3.1 Reactor Characterization and Metagenomic Sequence Data Collection.....	117
4.3.2 Accumulibacter Genome Assembly, Population Characterization, and Assessment of Microdiversity	119
4.3.3 Comparative Genomics of Denitrification Machinery in Type I Accumulibacter Genomes. .	125
4.3.4 Diversity of Denitrification Pathways among Flanking Genomes.....	128
4.4 Conclusions	133
4.5 Supporting Information	136
4.5.1 Supporting Information - Methods.....	136
4.5.2 Supporting Information - Tables	142
4.5.3 Supporting Information - Figures.....	153
 CHAPTER 5	
 Segregation of Microbial Community Composition and Function in Granular Denitrifying EBPR	
Process.....	162
5.1 Introduction	164
5.2 Materials and Methods	166

	15
5.2.1 Biomass Separation by Particle Size	166
5.2.2 DNA Extraction and 16S rRNA Gene Amplicon Sequencing	166
5.2.3 Quantifying Denitrification Genes via Quantitive PCR (qPCR)	166
5.2.4 Statistical Analysis	167
5.3 Results and Discussion	167
5.3.1 Microbial Community Analyses Reveal Predominant PAOs and GAOs and Segregation of Key Functional Guilds in EBPR Biomass Aggregates	167
5.3.2 Genetic Denitrification Potential in Biomass	171
5.3.3 Potential N ₂ O Producers and Consumers in Granular Sludge	175
5.4 Conclusions	177
5.5 Supporting Information	178
5.5.1 Supporting Information - Methods	178
5.5.2 Supporting Information - Tables	180
5.5.3 Supporting Information - Figures	185
 CHAPTER 6	
Conclusions and Future Work	188
6.1 Summary	189
6.2 Future study	191
6.2.1 Potential implications of CANDO+P for mainstream treatment	191
6.2.2 Mechanisms of N ₂ O formation at multiple scales	193
6.2.3 Linking microbial community dynamics to system performance	194
REFERENCES	196

LIST OF FIGURES

Figure 1.1 Schematic of a potential configuration employing the proposed CANDO+P process coupled to upstream anaerobic digestion for sustainable wastewater treatment targeting resource recovery.....	28
Figure 1.2 Global distribution of the size and number of marine dead zones in 2008. Figure from NASA Earth Observatory, by Robert Simmon and Jesse Allen.....	30
Figure 1.3 Biogeochemical N transformation processes and the annual nitrogen fluxes for these processes, modified from Kuypers et al.	31
Figure 1.4 Nitrogen flow for nitrification-denitrification, nitritation-denitritation, and nitritation-anammox. Different colors represent different BNR processes. Numbers on the left denote the oxidation state of the chemical N-species. Figure modified based on Gao et al. (2014) ²⁵ and Schreiber et al. (2012).	33
Figure 1.5 Comparison of four processes for nitrogen removal in terms of oxygen and reducing equivalents from organics consumed, biosolids produced, and energy recovered.	39
Figure 1.6 Net energy consumed or produced (blue) and associated GHG emissions as CO ₂ equivalents (red) for removal of bCOD, nitrogen and salt from 1m ³ of domestic wastewater and seawater.....	40
Figure 1.7 Schematic representation of the configuration a traditional anaerobic-aerobic EBPR process (A), and the profiling of key intracellular and extracellular chemicals (B). Figure from Shaomei He and Katherine D. McMahon 2011.....	42
Figure 1.8 The bacterial tree of life based on 16S rRNA gene maximum likelihood phylogenetic inference in the phylum level. The major putative PAOs and GAOs are classified in phylum	

	17
<i>Proteobacteria</i> and <i>Actinobacteria</i> . Figure modified from Roger S. Laskin and Jeffery S. McLean 2014 ⁸⁸	45
Figure 1.9 Figure at left: Phylogenetic tree for 749 available <i>Accumulibacter ppk1</i> sequences built in MEGA 7.0.18 using the maximum likelihood method with Tamura-Nei model. A total of 1007bp <i>Accumulibacter</i> -specific <i>ppk1</i> gene fragment was included for analysis. Figure at right: Five-way venn diagram depicting shared and unique genes for five <i>Accumulibacter</i> clades (IA, IC, IIA, IIC and IID) from Oyserman et al. 2016.	47
Figure 1.10 Changes in N ₂ O, CO ₂ and CH ₄ concentrations in the atmosphere over the past two centuries ¹⁰⁰ . Numbers in the figure denote the baseline pre-industrial atmospheric N ₂ O concentration and the increased N ₂ O concentration in 2011.	48
Figure 1.11 N transformation and N ₂ O formation pathways in nitrification (blue) and denitrification (red). Figure from Sabba et al. 2018.	50
Figure 2.1 Schematic of the CANDO+P Sequencing Batch Reactor (SBR).	62
Figure 2.2 Changes across representative SBR cycles of concentrations of key compounds (COD sources (propionate/acetate), PHAs, NO ₂ ⁻ , N ₂ O and PO ₄ ³⁻) in the CANDO+P SBR system using different external electron donors: (a) propionate (phase III, day 163) and (b) acetate (phase IV, day 203).	67
Figure 2.3 Sustained high-rate reduction of nitrite and high-yield production of N ₂ O during CANDO+P reactor operation.	68
Figure 2.4 Overall bacterial community structure over 4 months of reactor operation (phase I and II).	70
Figure 2.5 Circular representation of co-occurrence and co-exclusion network between flanking OTUs and the “core” CANDO+P microbiome (<i>Accumulibacter</i> and <i>Zoogloea</i>) during the start-up period (phase I and II).	73

	18
Figure S2.1 Conceptual schematic of CANDO+P SBR operation.....	78
Figure S2.2 Dynamics in alpha diversity metrics over time: (a) chao1, (b) Shannon index and (c) observed OTUs.....	79
Figure 3.1 Concentration profiles of key substrates (NO_3^- , NO_2^- , N_2O , PO_4^{3-} and COD) in selected ex situ batch tests during the anoxic period with decoupled or coupled feeding of COD as electron donor.....	92
Figure 3.2 (a) N removal rates ($\text{mg-N/h}\cdot\text{gVSS}$) and (b) denitrifying P uptake rates ($\text{mg-P/h}\cdot\text{gVSS}$) by DPAO-enriched biomass with different dosing schemes (scenarios D_a,b,c_ $\text{NO}_3^-/\text{NO}_2^-/\text{N}_2\text{O}$ and D_a_ $\text{NO}_3^-+\text{NO}_2^-+\text{N}_2\text{O}$ in Table 3.1 in decoupled feeding mode.....	94
Figure 3.3 Electron consumption rates for different denitrification enzymes (NAR: nitrate reductase, NIR: nitrite reductase, NOR: nitric oxide reductase, NOS: nitrous oxide reductase) under decoupled (a) and coupled (b) feeding modes.....	102
Figure S3.1 A typical SBR cycle profiling the transformation of key C, N and P components (acetate as COD, NO_2^- , dissolved N_2O and PO_4^{3-}).....	105
Figure S3.2 (a) N removal rate ($\text{mg-N/h}\cdot\text{gVSS}$) and (b) denitrifying P uptake rate ($\text{mg-P/h}\cdot\text{gVSS}$) by DPAO-enriched biomass with different dosing schemes in coupled feeding mode (simultaneous addition of COD [acetate] and nitrogen oxide(s) with 40 mg-N/L of nitrogen oxides).....	106
Figure S3.3 Electron distribution for different denitrification enzymes (NAR: nitrate reductase, NIR: nitrite reductase, NOR: nitric oxide reductase, NOS: nitrous oxide reductase) under (a) decoupled and (b) coupled feeding modes.....	107

- Figure 4.1 Initial NO_2^- concentration (green) at the start of the anoxic period and percent conversion to N_2O (purple) in the lab-scale SBR throughout the operational period (from May to November 2015).118
- Figure 4.2 *Accumulibacter* maximum likelihood phylogenetic tree based on *ppk1* gene sequences (including *Accumulibacter ppk1* gene sequences downloaded from NCBI, *ppk1* genes extracted from four currently available type I genomes and the two draft genomes obtained in this study (in green), and *ppk1* gene fragments obtained via cloning and sequencing from two sampling dates (05/19/2015 in orange and 10/15/2015 in purple).121
- Figure 4.3 (a): Temporal change in relative abundance (%) of all extracted *Accumulibacter* phylotypes based on partial *ppk1* sequences from raw reads (IA-1 to IA-4 and IC-1 to IC-3) and two *ppk1* sequences from draft genomes (CANDO_1_IA and CANDO_2_IC). A phylogenetic tree based on figure 4.3 on top of the heatmap illustrates the phylogeny of these nine partial *ppk1* gene fragments. (b): Comparison of relative abundance of *Accumulibacter* clades IA (circle) and IC (square) based on average coverage for draft genomes (green) and based on the sum of the relative abundance of all IA and IC *ppk1* phylotypes (in purple). The sum of all IA and IC phylotypes are calculated by summing the relative abundance of all 4 IA phylotypes and 3 IC phylotypes, respectively.124
- Figure 4.4 Key denitrification gene loci in all available type I *Accumulibacter* draft genomes including four publicly available genomes and two (CANDO_1_IA and CANDO_2_IC) assembled from this study.128
- Figure 4.5 (a) Dynamics in relative abundance of 39 flanking bacterial genome bins (lower layer), the presence of different denitrification structural genes (*narG*, *nirK*, *nirS*, *nor* (*qnorB* or *cnorB*), and *nosZ* clade II) (middle layer), and the assigned taxonomy for each genome bin at the phylum level (upper layer). *nosZ* clade I is not represented in the middle layer because it was

not identified in any of the draft genome bins. (b) Sum of relative abundance of putative N ₂ O consumers, putative N ₂ O producers, and nondenitrifiers identified within the 39 flanking bacterial genomes.....	132
Figure S4.1 Extraction of CANDO_1_IA genome bin from metagenome scaffolds using differential coverage binning (x-axis: coverage for sample taken on 10/15/2015, y-axis: coverage for sample taken on 11/13/2015).....	153
Figure S4.2 Extraction of CANDO_2_IC genome bin from metagenome scaffolds (longer than 1.5 kbp) using differential coverage binning.	154
Figure S4.3 Comparison of the average nucleotide identity (ANI) and percent alignment for all 15 publicly available <i>Accumulibacter</i> genomes. CANDO_1_IA and CANDO_2_IC draft genomes were recovered in this study.	155
Figure S4.4 Comparison of relative abundance of different <i>Accumulibacter</i> clades (IA-IC, IIC) based on qPCR and metagenomic analysis.....	156
Figure S4.5 Reference <i>ppk1</i> gene phylogenetic tree based on 781 <i>ppk1</i> gene sequences (1007 bp) and 68 clone sequences in this study. Clades IA to IE and IIA to II-I are labeled.....	158
Figure S4.6 The temporal change of distribution of all 7 <i>Accumulibacter</i> phylotypes extracted from metagenomic reads (IA: IA-1-4, IC: IC-1-3) from 5/19/2015 (bottom row) to 11/13/2015 (top row).....	159
Figure S4.7 The relative abundance (%) of the sum of two <i>Accumulibacter</i> genome bins and the sum of 39 extracted flanking (non- <i>Accumulibacter</i>) bacterial genome bins from 05/19/2015 to 11/13/2015.	160
Figure S4.8 (a). Dynamics in relative abundance of 7 flanking (non-PAO) bacterial genome bins assembled from shotgun metagenomic sequencing of an aerobic EBPR system ²²⁰ (bottom),	

the presence and copy number per genome of different denitrification structural genes (*narG*, *nirK*, *nirS*, *norB* (*qnorB* or *cnorB*), and *nosZ*) (middle), and the assigned taxonomy for each genome bin at the phylum level (top). (b). Sum of relative abundance of putative N₂O consumers and producers, and putative nondenitrifiers.....161

Figure 5.1 The average relative abundance (%) of the 15 most abundant bacterial taxa at the genus level in the mother SBR via 16S rRNA gene amplicon sequencing. Left: Overall microbial community structure in biomass over time range when batch assays were conducted (9 samples between day 490 to 600) and within two months of SBR inoculation (4 samples between day 0 to 48); Right: Microbial community structure in different aggregate size fractions of biomass (day 591 and 626, right).169

Figure 5.2 (a): Average relative abundance (%) of five denitrification genes (*narG*, *nirS*, *nirK* and clade I and II *nosZ*) and *Accumulibacter* 16S rRNA (*Accumulibacter*) normalized to universal bacterial 16S rRNA gene abundance, as quantified by qPCR assays. (b): Comparison of the relative abundance (%) of the key NO₂⁻ reduction genes (*nirS* + *nirK*) and the key N₂O reduction genes (clade I+II *nosZ*) in both bulk biomass and different size fractions of biomass.174

Figure S5.1 Relative abundance for the 15-most abundant microbial taxa at the genus level in the mother SBR via 16S rRNA gene amplicon sequencing.....185

Figure S5.2 Correlation network between the top 15 most abundant bacterial taxa at the genus level detected in the nitrite-fed denitrifying EBPR bioreactor via 16S rRNA gene sequencing (colored circles) and the abundance of denitrification and *Accumulibacter* 16S rRNA (gray circles; *nirK*, *narG*, *Accumulibacter* 16S rRNA, and clade II *nosZ*) measured via qPCR...186

Figure S5.3 Average differences in functional gene relative abundance (%) between each biomass size fraction calculated based on post-hoc test. Error bar represents the 95% confidence interval. A positive number on the y-axis indicates higher abundance in the larger size fraction.....187

Figure 6.1 Two potential operational regimes proposed for CANDO+P application to mainstream municipal wastewater.....193

LIST OF TABLES

Table 2.1 N and P removal rates and efficiencies during anoxic and aerobic phases in two typical SBR cycles with different external electron donors (acetate and propionate).	68
Table 2.2 Comparison of overall NO_2^- removal efficiencies, specific N_2O production rates and N_2O conversion efficiencies between this (CANDO+P, phase III and IV) and previous CANDO studies.	75
Table 2.3 Comparison of specific NO_x ($\text{NO}_3^-/\text{NO}_2^-$) and P removal rates in this and other lab-scale DPAOs studies.	75
Table S2.1 Operational parameters and phases of the CANDO+P reactor operation.....	77
Table 3.1a Summary of substrate (COD, NO_3^- , NO_2^- and N_2O) addition schemes employed in <i>ex situ</i> batch assays in the absence of exogenous COD (decoupled feeding strategy: COD (acetate) dosing prior to NO_x feed).	86
Table 3.2b Summary of substrate (COD, NO_3^- , NO_2^- and N_2O) addition schemes employed in <i>ex situ</i> batch assays in the presence exogenous COD (coupled feeding strategy: simultaneous COD (acetate) and NO_x dosing).	86
Table 3.2 Comparison of N and P transformation rates.	98
Table 4.1 Summary statistics for two extracted <i>Accumulibacter</i> draft genomes.....	119
Table S4.1 Summary statistics for metagenome sequencing, assembly and annotation.....	142
Table S4.2 Denitrification genes and inference of HGT in available <i>Accumulibacter</i> genomes (a) : Identification of presence and absence of orthologous denitrification gene families in 15 <i>Accumulibacter</i> (type I and II) genomes obtained from PROTEINORTHO. (b) : ORFs identified as denitrification genes for 6 type I <i>Accumulibacter</i> draft genomes. A total of four	

are publicly available genomes (BA-92, BA-93, UW-3 and HKU_1) and two genomes assembled in this study (CANDO_1_IA and CANDO_2_IC) are shown. (c): HGT inference for denitrification genes from CANDO_1_1A and CANDO_2_IC.	143
Table S4.3 Summary statistics for 39 draft flanking (non-Accumulibacter) bacterial genomes extracted from our study (a) and the 8 draft bacterial genomes (including 7 flanking bacterial genomes and 1 Accumulibacter IB genome) extracted from an aerobic EBPR study (b)	150
Table S4.4 <i>ppk1</i> gene qPCR primers and performance statistics.....	152
Table S5.1 The relative abundance (%) and standard deviation of the top 15 bacterial taxa at the genus level in the denitrifying EBPR biomass, based on 16S rRNA gene sequencing. Taxonomy is shown at the phylum level (1 st column) and at the lowest level of taxonomic assignment (p: phylum, c: class, o: order, f: family, and g: genus; 2 nd column).	180
Table S5.2 qPCR primers and thermal cycling conditions used in this study.	181
Table S5.3 Quality control parameters for qPCR assays.	183
Table S5.4 Relative abundance (%) of Accumulibacter 16S rRNA (Accumulibacter) and five denitrification genes (<i>narG</i> , <i>nirS</i> , <i>nirK</i> and clade I and II <i>nosZ</i>) normalized to universal bacterial 16S rRNA gene abundance quantified by qPCR assays.	184

CHAPTER 1

Introduction

The discussion of low-energy nitrogen removal processes is adapted from a publication in *Environmental Science Process & Impacts*: Gao, H., Scherson, Y.D. and Wells, G.F. (2014) Towards energy neutral wastewater treatment: methodology and state of the art. *Environmental Science Process & Impacts* 16(6), 1223-1246.

1.1 Problem Statement

Nutrient pollution associated with excess reactive nitrogen (N) and phosphate (P) is responsible for a rash of negative environmental and public health problems, including eutrophication of nutrient limited natural water bodies, vast dead zones in the ocean margins, stratospheric ozone depletion, and ammonia toxicity to aquatic life^{1, 2}. In addition, reactive N pollution is linked to the emission of the potent greenhouse gas (GHG) nitrous oxide (N₂O), which has a global warming potential 310 times that of carbon dioxide (CO₂) and accounts for ~6.9% of total GHG emissions worldwide³. Biological wastewater treatment processes play a critical role in preventing the release of N and P from municipal and industrial wastewater to natural water bodies. Unfortunately, such biological nutrient removal processes are typically energy-intensive, and are characterized by substantial emissions of N₂O via incomplete microbial nitrogen transformations⁴⁻⁶. A paradigm shift is thus now underway that is transforming conventional energy-intensive nutrient removal bioprocesses to energy neutral or even energy-generating treatment bioprocesses. A novel nutrient removal process, CANDO (Coupled Aerobic-anoxic Nitrous Decomposition Operation) was recently introduced for N removal along with energy recovery via microbial N₂O generation. Despite its promise, the CANDO process does not currently target the removal of P, a critical area of concern in many parts of the world. Simultaneous biological N and P removal has been previously demonstrated in bioreactors that selected for a little understood group of microbes termed denitrifying polyphosphate accumulating organisms (DPAOs)⁷, but this variation on Enhanced Biological Phosphorus Removal (EBPR) systems is largely considered impractical due to its apparent capacity for high N₂O production⁷⁻⁹. Conditions leading to N₂O formation are not well understood, and knowledge of the microbial groups involved in P accumulation under

denitrifying conditions is lacking. However, in the context of N_2O as a bioenergy source, such high rates of production are promising. **In this dissertation, I developed and characterized a novel microbial bioprocess, herein termed CANDO+P, for simultaneous bioenergy recovery via high-rate microbial N_2O production and nutrient (N and P) removal from wastewater.**

Figure 1.1 shows a potential treatment configuration in which CANDO+P and anaerobic processes are used for treatment of sewage to recover energy and resources from both biodegradable organic carbon and waste N and P¹⁰. Two-stage anaerobic treatment of sewage produces methane (CH_4) that is combusted with O_2 and N_2O as co-oxidant. CH_4 capture from anaerobic digestion can also feed directly into this process. Volatile fatty acids (VFAs) produced in an upstream acidogenic reactor serves as the electron donors for the CANDO+P process. CANDO+P involves three steps: (1) nitrification of ammonium (NH_4^+) to NO_2^- ; (2) partial anoxic reduction of NO_2^- to N_2O accompanied by denitrifying P uptake; and (3) N_2O conversion to N_2 with energy recovery. Compared with traditional N removal processes, CANDO+P combines energy recovery via N_2O generation along with biological P removal and potential recovery. It also results in decreased O_2 and energy requirements, retains more organic carbon in sewage for energy generation via anaerobic digestion, and generates a novel bioenergy source (N_2O) directly from waste N. My work focusses specifically on the reduction of NO_2^- to N_2O coupled to uptake of P by DPAOs.

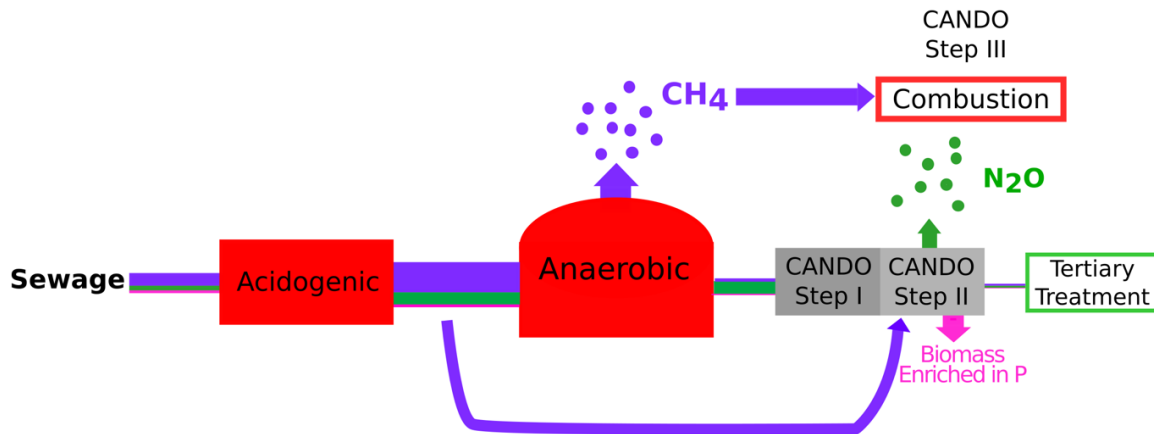


Figure 1.1 Schematic of a potential configuration employing the proposed CANDO+P process coupled to upstream anaerobic digestion for sustainable wastewater treatment targeting resource recovery.

Flows of organic carbon are shown in purple; flows of N are shown in green; flows of P are shown in pink¹⁷.

1.2 Technical Background

1.2.1 Nutrient Pollution in the Environment

Besides the removal of chemical oxygen demand (COD), the control of reactive N and P in wastewater via biological nutrient removal processes is of increasing concern during wastewater treatment. In 2008, the US National Academy of Engineering included management of the N cycle as one of fourteen grand challenges facing the engineering community in the 21st Century¹¹. Indeed, of nine “planetary boundaries” identified by Rockstrom and colleagues delimiting unacceptable environmental change², human interference with the N cycle was one of three boundaries to have already been exceeded. Additionally, we are approaching the boundary of P cycle².

As the world population is increasing, the demand for food supply and fertilizer required to grow crops will continue increasing. Fertilizer production uses about two thirds of the produced ammonia (NH_4^+) and more than 80% of the phosphorus mined to meet our demand for food^{12, 13, 14}. The improper use of reactive N (NH_4^+) generates N- and P-rich wastewater into groundwater, rivers, and coastal water. Excess nutrients cause the over-growth of algal, depletion of oxygen, and finally the spreading of “dead zone”. Today, over 400 systems have been reported as dead zones with a total area of more than 245,000 square kilometers¹⁵ (Figure 1.2). As a result, more cost-effective nutrient (N and P) management strategies and nutrient removal processes are required to solve issues related to nutrient pollution. Today, biological nutrient removal during wastewater management has widely used as an efficient way to alleviate nutrient pollution.

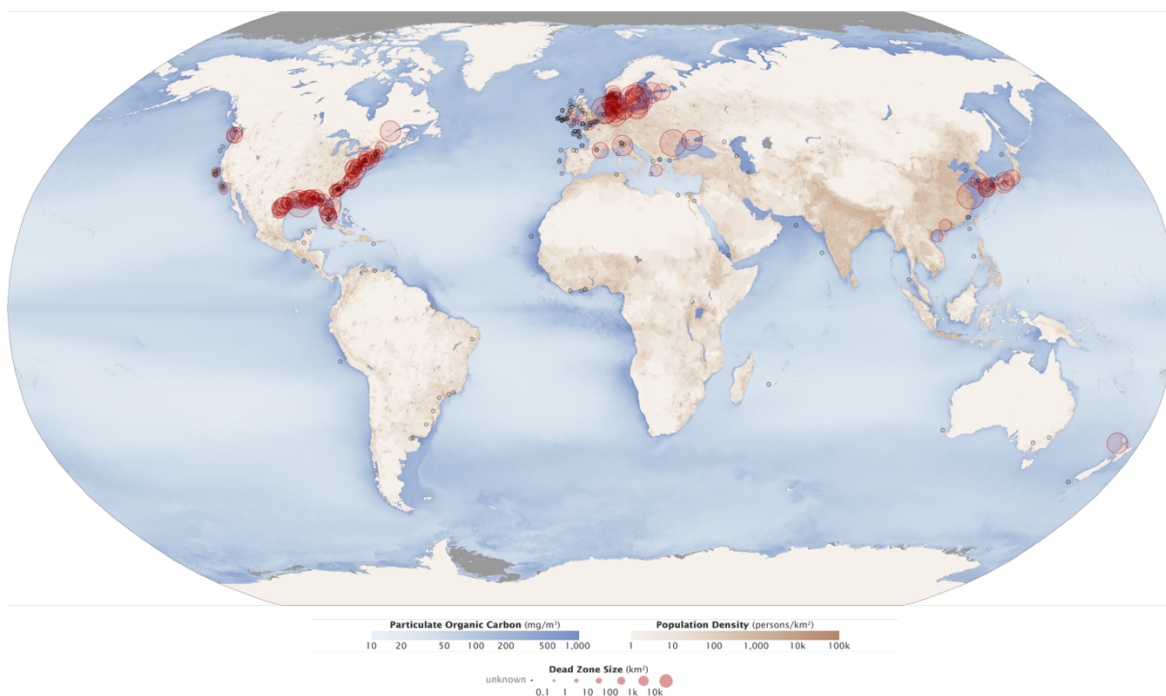


Figure 1.2 Global distribution of the size and number of marine dead zones in 2008. Figure from NASA Earth Observatory, by Robert Simmon and Jesse Allen (<https://earthobservatory.nasa.gov/IOTD/view.php?id=44677>).

Anthropogenic production of reactive nitrogen has significantly disrupted the natural nitrogen cycle. Naturally, N cycles at a rate of approximately 290 Tg-N/yr via bacteria N fixation (nitrogen gas $[N_2]$ to NH_4^+) in terrestrial and marine ecosystems¹⁶. The discovery of an industrial route for N fixation to NH_4^+ by the Haber-Bosch process enabled anthropogenic production of reactive N, and today this process produces 125 Tg-N/yr, nearly half of the natural N fixation¹⁶. However, the global removal rate of reactive N (production of N_2) from terrestrial and marine systems via anaerobic ammonium oxidation (anammox) and denitrification is only ~350 Tg-N/yr (Figure 1.3). In addition, 16 Tg-N/yr is released back to atmosphere in the form of nitrous oxide (N_2O), leaving ~50 Tg-N/yr reactive N remaining in the environment. This disruption of the natural biogeochemical N cycle and the release of excess reactive N to the environment has led to an array of environmental and public health problems, including ammonia toxicity to aquatic life;

eutrophication of nutrient-limited water bodies; increasing atmospheric concentrations of the potent greenhouse gas N_2O ; stratospheric ozone depletion; and direct adverse effects to human health (e.g. methemoglobinemia caused by nitrates)¹¹.

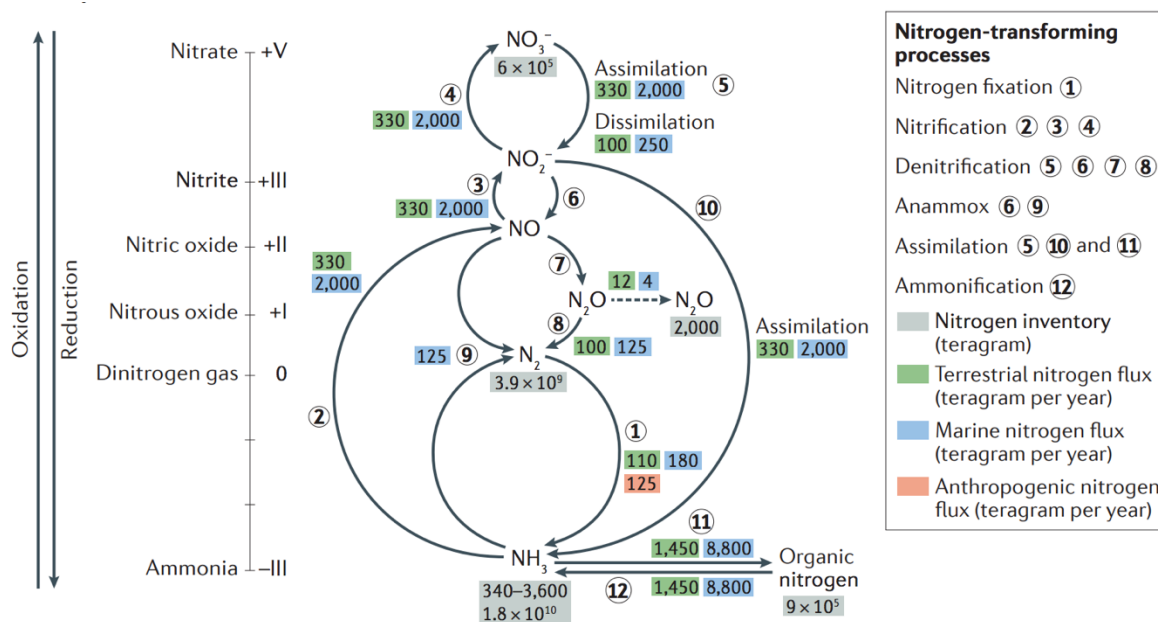


Figure 1.3 Biogeochemical N transformation processes and the annual nitrogen fluxes for these processes, modified from Kuypers et al.¹⁷.

Humankind is also devastating ecosystems to mine geological phosphate reserves. Unlike N that can be produced by the Haber-Bosch process, phosphate derives predominantly from non-renewable, mineable deposits of phosphate rock. As of 2013, 17.5 Tg-P/yr is produced¹⁸. The resulting P is used for fertilizer manufacturing, cattle-feed supplements, food preservatives, and the production of detergents. The uncertainty of global phosphate supply increases concerns about this essential but limited nutrient element. The prediction made by Dana Cordell and colleagues argued that ‘peak phosphorus’ production would occur around 2030¹⁴. The estimated amount of readily accessible P increased after this publication when new P reserves were discovered. However, the resource of P reserves is unevenly distributed globally, and three countries (Morocco,

USA and China) control over 85% of the known global phosphorus reserves^{19, 20}. In this context, P recovery and reuse from different waste streams becomes critical in sustainable P management and pollution prevention.

Nutrient-polluted (N and P) wastewater can be collected from point or non-point sources. The removal of N and P from wastewater via biological treatment processes is one of the major strategies currently applied to control nutrient pollution. Sewage sludge is also a significant sink for P²¹. Efficient P recovery and recycling from sewage sludge could decrease the current demand for the limited nonrenewable P resources²².

1.2.2 Low Energy or Energy Positive Approaches for NOD Removal

Efficient removal of N during wastewater treatment process is critical to prevent the release of excess reactive N to the environment. Nitrification/denitrification (Figure 1.4), which is the most common biological nitrogen removal (BNR) method in conventional wastewater treatment plants (WWTPs), is an energy intensive process that couples COD and nitrogenous oxygen demand (NOD) removal. High NOD increases the need for oxygen supply and aeration, which is the dominant energy consuming process ($\sim 50\%$) in typical WWTPs with N removal^{23, 24}. Therefore, it is unlikely that energy-positive wastewater treatment can be achieved without innovative management of nutrient removal processes.

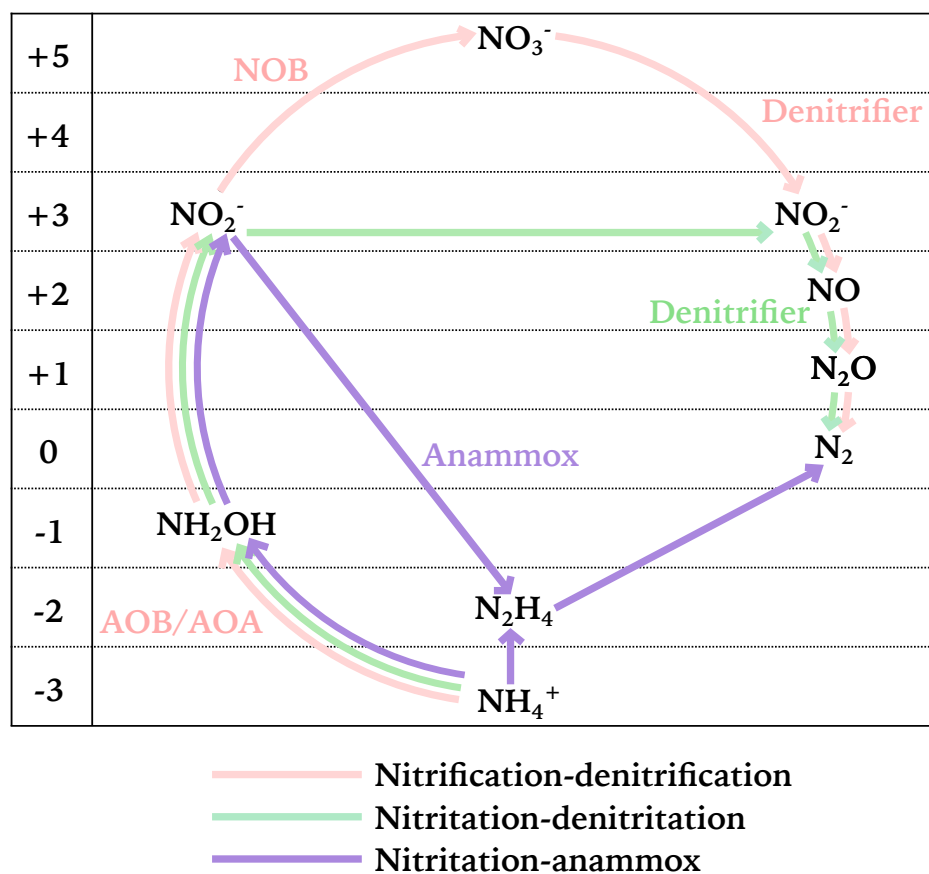


Figure 1.4 Nitrogen flow for nitrification-denitrification, nitritation-denitritation, and nitritation-anammox. Different colors represent different BNR processes. Numbers on the left denote the oxidation state of the chemical N-species. Figure modified based on Gao et al. (2014)²⁵ and Schreiber et al. (2012)²⁶.

Decoupling COD and NOD removal is a promising strategy to decrease energy demand for nutrient removal and divert carbon sources to energy production²⁷. Three emerging and energy-efficient strategies for NOD management have been applied at large scale or under investigation. In this dissertation, I will focus on energy generation and recovery from NOD (the 3rd strategy below).

1. **Nutrient recovery or direct reuse:** This is potentially the most sustainable, yet challenging future strategy for N management. Direct irrigation of crops or landscapes with nutrient-rich

effluent from anaerobic secondary treatment of municipal wastewater may be particularly attractive in rural, water-scarce locales²⁸, but is challenging in urban environments where transport distances to agricultural lands are long. Another promising option is source separation of urine, the dominant reservoir of nutrients in domestic wastewater, and treatment specifically for N and P recovery^{29, 30}.

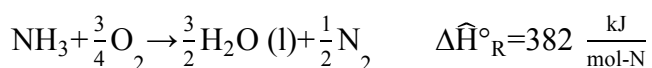
2. **Low-energy NOD removal:** Innovative N removal bioprocesses that “short-circuit” the conventional nitrification-denitrification paradigm offer the opportunity to dramatically decrease aeration and COD requirements for N removal, thereby conserving energy and offering the opportunity to route additional COD to energy production. Likely the most promising short-circuit N removal process leverages the combined microbial processes of nitritation and anammox.

First reported in 1995 by Mulder et al.³¹, the application of anammox during BNR is considered a promising way to reduce energy consumption. In conventional nitrification-denitrification processes, oxygen is consumed by aerobic ammonium oxidizing bacteria (AerAOB), ammonium-oxidizing archaea (AOA), and nitrite oxidizing bacteria (NOB), thereby oxidizing all NH_4^+ to NO_3^- . NO_3^- is then reduced to N_2 by heterotrophic denitrifiers, with organic carbon as the electron donor. With the suppression of NOB, nitritation-denitrification (also called the nitrite shunt), a short-cut process compared with nitrification-denitrification that involves NH_4^+ oxidation only to NO_2^- , becomes possible³². However, nitritation-denitrification still involves completely aerobic NH_4^+ oxidation, as well as substantial COD for NO_2^- reduction. In contrast, anammox can directly oxidize NH_4^+ to nitrogen gas using NO_2^- as the electron acceptor. By combining nitritation (oxidation of NH_4^+

to NO_2^- by AerAOB or AOA) and anammox, a shortcut BNR scheme is possible that reduces the requirement for O_2 by 60%^{33, 34} (with associated saving in electrical power need for aeration). In addition, organic carbon requirements for heterotrophic denitrification are reduced by ~90%, thereby eliminating the need for often-costly external organic electron donor supply (such as methanol) or allowing a rerouting of wastewater COD to anaerobic digestion for methane production^{34, 35}. Moreover, waste biomass production decreases substantially due to the lower biomass yield of anammox compared to heterotrophic denitrifiers³⁶. Based on stoichiometry, a ratio of 1.32:1 of NO_2^- to NH_4^+ is necessary for anammox metabolism³⁷, and partial nitritation of NH_4^+ to NO_2^- by AerAOB or AOA is a common way to produce the requisite nitrite³⁸. Till now, the three pathways of conventional nitrification-denitrification, nitritation-denitritation (or nitrite-shunt) and nitritation-anammox are the major practical nitrogen removal processes (Figure 1.4).

3. **Energy recovery from NOD:** NOD bound in reactive forms of N can be converted into renewable energy. But for this to occur, the N must be in a form that can be removed from water and usable for energy production. Two N species that fit these requirements are NH_3 and N_2O ³⁹. NH_3 is an energy source that releases electrons when oxidized or heat when combusted with oxygen (**Eq. 1.1**). NH_3 in wastewater can potentially generate power with electrochemical fuel cells⁴⁰.

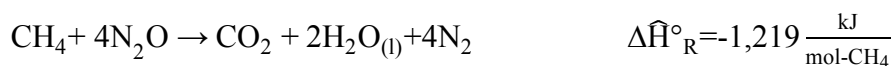
Eq. 1.1: The reaction of NH_3 with O_2 .



N_2O , derived from reactive forms of N, can also be removed from wastewater and used to recover energy. Recently, Scherson and colleagues⁴¹ introduced a new N removal

process that recovers energy from NOD nitrogen as N₂O. The process is called the Coupled Aerobic-anoxic Nitrous Decomposition Operation (CANDO) and converts reactive N to N₂O, then captures the gas and recovers energy from it by using it as a co-oxidant in CH₄ combustion or decomposing the N₂O over a metal oxide catalyst with the end product of N₂. The innovation is utilizing N₂O as a renewable energy source. Traditionally, N₂O has been viewed as an unwanted by-product of wastewater treatment because it is a GHG 310 times more powerful than CO₂ and is a dominant ozone-depleting substance⁴². For this reason, studies have generally focused on understanding the pathways for N₂O production in order to minimize its production. But, N₂O is like CH₄: both are harmful if released to the atmosphere, or sources of renewable energy if captured and combusted. In fact, N₂O is a powerful oxidant - commonly used in propulsion and automotive applications - that can increase energy recovery from methane⁴³⁻⁴⁵. Combustion of CH₄ with N₂O releases roughly 30% more heat as compared to O₂ (**Eq 1.2**), and, mitigates the release of N₂O to the atmosphere.

Eq 1.2 Comparison of the heat of reactions of CH₄ with N₂O (top) and CH₄ with O₂ (bottom).



CANDO involves three steps: (1) nitritation of NH₄⁺ to NO₂⁻; (2) partial anoxic reduction of NO₂⁻ to N₂O; and (3) N₂O conversion to N₂ with energy recovery. Step 1 has been demonstrated at full-scale with over 95% efficiency by the (SHARON) process⁴⁶, and step 3 is well documented⁷¹⁻⁷³. Step 2, NO₂⁻ reduction to N₂O, was demonstrated by partial heterotrophic denitrification. A feeding strategy in which acetate (electron donor) and NO₂⁻ (electron acceptor) delivered as alternating pulses selected for organisms that store

polyhydroxybutyrate (PHB) after the acetate pulse, and produce N_2O after the NO_2^- pulse. Reducing equivalents for NO_2^- reduction were derived from the stored PHB. High N_2O conversion (62% NO_2^- to N_2O) over long-term operation (>200 cycles) with 98% N-removal was reported in a lab-scale study treating synthetic wastewater (250 mg-N/L)⁴¹. CANDO is currently being evaluated at pilot-scale for sidestream (digester centrate) wastewater treatment.

Alternative methods for N_2O production have potential to improve energy generation in CANDO. At present, CANDO relies on heterotrophic organisms that consume biodegradable COD to reduce NO_2^- to N_2O . In some applications, the COD that is consumed could otherwise be used for energy recovery as CH_4 or electricity. But, autotrophic denitrification to N_2O with, for example H_2 , CH_4 , or NH_4^+ , does not consume biodegradable COD and produces less biomass than heterotrophic denitrification. If NH_4^+ is the source of reducing equivalents, then only a fraction of the influent NH_4^+ is oxidized to NO_2^- , with the balance oxidized for NO_2^- reduction, thus reducing aeration energy (like nitrification-anammox). Autotrophic production of N_2O with NH_4^+ oxidation has been reported by both AerAOB and AOA. AerAOB are capable of N_2O production by either oxidation of hydroxylamine, or by so-called nitrifier-denitrification, in which NO_2^- is sequentially reduced via NO to N_2O ⁴⁷⁻⁴⁹. However, further studies are needed to evaluate this strategy.

Energy recovery from NOD nitrogen as N_2O offers several benefits. First, N_2O is a dissolved gas that, like CH_4 , can be stripped or outgassed from solution, although N_2O is less readily stripped than CH_4 because of a higher solubility limit. Second, N_2O is already produced, albeit unintended, by conventional denitrification and short-circuit nitrogen

removal processes, contributing negatively to the carbon footprint of many WWTPs. Using N_2O as an oxidant in combustion destroys the gas, and maximizing its production increases energy recovery. Finally, converting reactive nitrogen to N_2O , instead of N_2 , shortens the treatment steps for denitrification. This results in fewer reducing equivalents consumed, less biomass produced, energy from nitrogen recovered, and possibly shorter SRT. The capture of N_2O during wastewater treatment can be a win-win strategy that offers the possibility of energy generation, cost reductions, and mitigation of climate change and stratospheric ozone depletion.

Figure 1.5 shows a comparison in terms of performance metrics for five N treatment processes, including CANDO, that are in different development stages (existing, emerging, future). Conventional nitrification-denitrification is the least efficient: the most oxygen and reducing equivalents are consumed, and the greatest quantity of biosolids is produced. Nitritation-denitrification offers a moderate improvement with reductions in oxygen, organics, and biosolids. Nitritation-anammox, as detailed in the previous section, offers the most dramatic improvement with reductions in oxygen demand by 60%, reducing equivalents by 90%, and biosolids by 75%. While various nitritation-anammox based processes are commercially available, concerns related to process stability, robustness, sensitivities to a variety of inhibitors⁵⁰⁻⁵⁶, and the slow growth rate of anammox have impeded broader adoption^{57, 53, 55}. Compared to nitritation-anammox, CANDO is less efficient, but does recover energy from NOD and offers other benefits not associated directly with energy. CANDO selects for heterotrophic bacteria with faster growth rates than anammox. The fast growth rates may improve process stability with short SRT. Also, CANDO may enable phosphorus (P) recovery through alternating anaerobic/anoxic cycling with stored PHB. This

operation is similar to conventional Enhanced Biological Phosphorus Removal (EBPR) where anaerobic/aerobic cycling selects for organisms that oxidize stored PHB to drive phosphate uptake. Combining CANDO with P removal and recovery optimize the use of organic matter by combining N and P removal. In this dissertation, CANDO+P process was evaluated by lab-scale study. The final process, CANDO autotrophic, represents a future concept that is the most efficient, but has yet to be demonstrated with high conversion to N_2O and over long-term operation. CANDO autotrophic is similar to nitritation-anammox in terms of oxygen, reducing equivalents, and biosolids to nitritation-anammox, but differs because energy is recovered from NOD. It is likely that existing and developing nitritation-anammox based processes, CANDO, and CANDO variants will be complementary, offering a unique treatment process that is ideal for each application.

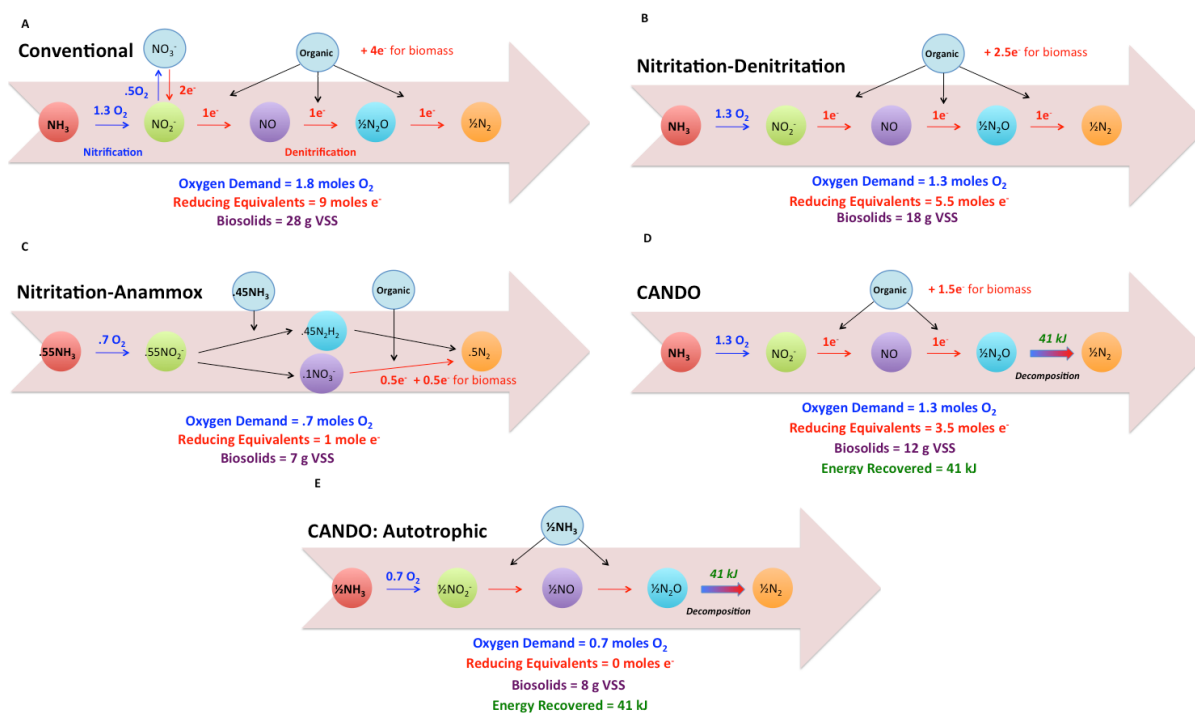


Figure 1.5 Comparison of four processes for nitrogen removal in terms of oxygen and reducing equivalents from organics consumed, biosolids produced, and energy recovered.

(A) Conventional Nitrification-Denitrification, (B) Nitritation-Denitrification, (C) Nitritation-Anammox, (D) CANDO, and (E) a possible future variation of CANDO, here termed CANDO

autotrophic. All calculations based on reported biomass yield and typical solids residence time for each unit operation⁵⁸. Figure from Han Gao et al. 2014²⁵.

A comparison was made recently by Scherson and Criddle to evaluate the energy requirement as well as GHG emission during wastewater management using both conventional and innovative wastewater treatment configurations (Figure 1.6)⁵⁹. Based on the calculations, emerging N removal technologies could potentially produce 0.03-0.13 kWh/m³ net power during BOD and nitrogen removal. Among all the 11 configurations analyzed in their study, mainstream CANDO with anaerobic digestion is the second promising technology for N removal from the mainstream in terms of energy production and the top promising configuration with respect to GHG emission.

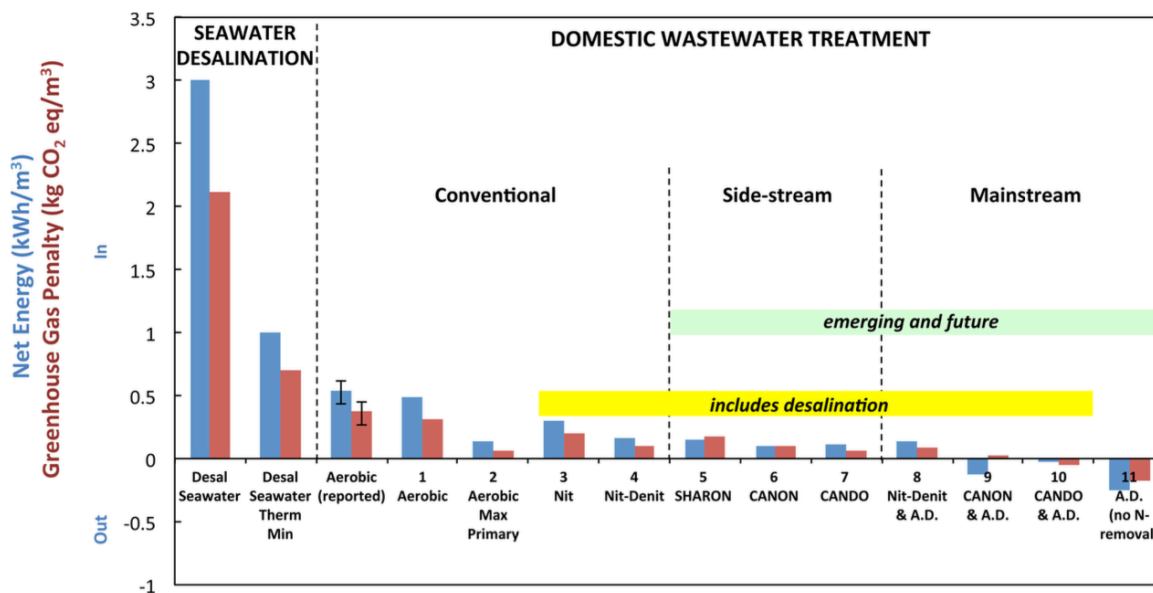


Figure 1.6 Net energy consumed or produced (blue) and associated GHG emissions as CO₂ equivalents (red) for removal of bCOD, nitrogen and salt from 1m³ of domestic wastewater and seawater.

11 different configurations were included: (1) conventional primary aerobic, (2) enhanced primary anaerobic digestion, (3) mainstream nitrification, (4) mainstream nitrification and denitrification, (5) side-stream SHARON, (6) side-stream CANON, (7) side-stream CANDO, (8) mainstream nitrification and denitrification with anaerobic digestion, (9) mainstream CANON with anaerobic

digestion, (10) mainstream CANDO with anaerobic digestion, and (11) anaerobic digestion with no N removal. Figure from Scherson and Criddle (2014)⁵⁹.

1.2.3 Enhanced Biological Phosphorus Removal (EBPR) and Polyphosphate Accumulating Organisms (PAOs)

In addition to reactive N, P was also a leading factor causing surface water eutrophication. To prevent P release to receiving water bodies, EBPR processes are increasingly used to remove soluble P during wastewater treatment. These processes rely on a group of bacteria known as polyphosphate accumulating organisms (PAOs)^{60, 61}. When subjected to dynamic anaerobic and aerobic conditions, PAOs remove P by releasing and then uptaking and storing more inorganic phosphate (P_i) than their metabolic demand. More specifically, under anaerobic conditions, PAOs degrade intercellular polyphosphate (polyP) to generate ATP and provides energy for organic substrate uptake (such as volatile fatty acids [VFAs]). VFAs are converted to polyhydroxyalkanoates (PHAs) with the reducing power provided by the degradation of intracellular glycogen and/or the tricarboxylic acid (TCA) cycle. Under the subsequent aerobic conditions, PHAs are oxidized and P_i is taken up to form polyP and replenish glycogen (Figure 1.7b). A traditional EBPR configuration (Figure 1.7a) starts with an anaerobic zone, followed by an aerobic zone to create conditions for PAOs to uptake and store soluble P as polyP. P is ultimately removed from influent wastewater by wasting sludge with high polyP content⁶⁰. In practice, an anaerobic/anoxic/aerobic configuration is typically applied in many WWTPs to combine nitrification-denitrification and EBPR for carbon (C), N and P removal.

A subset of PAOs, termed denitrifying PAOs (DPAOs), are also capable of using NO_3^- and/or NO_2^- as an electron acceptor to drive anoxic P uptake⁶²⁻⁶⁴. When accompanied by nitrification or full nitrification to produce NO_2^- and/or NO_3^- , DPAOs provide a potential pathway for coupling

biological P (Bio-P) removal and N removal^{25, 65}. Many recent studies focused on using NO_2^- instead of NO_3^- as the alternate electron acceptor to combine N and P removal. Emerging NO_2^- based N removal processes including nitritation/denitritation (nitrite shunt) and nitritation/anammox have received more attention as these processes promise to lower more than 30% of oxygen demand compared to conventional nitrification/denitrification based N removal processes utilizing NO_3^- ²⁵. Thus, a NO_2^- driven denitrifying phosphorus removal process would be more promising compared with a NO_3^- driven process. However, the inhibition of denitrifying P removal by NO_2^- and the accumulation of N_2O has been observed in several studies, increasing the challenge of implementing NO_2^- driven denitrifying P removal^{66, 67}.

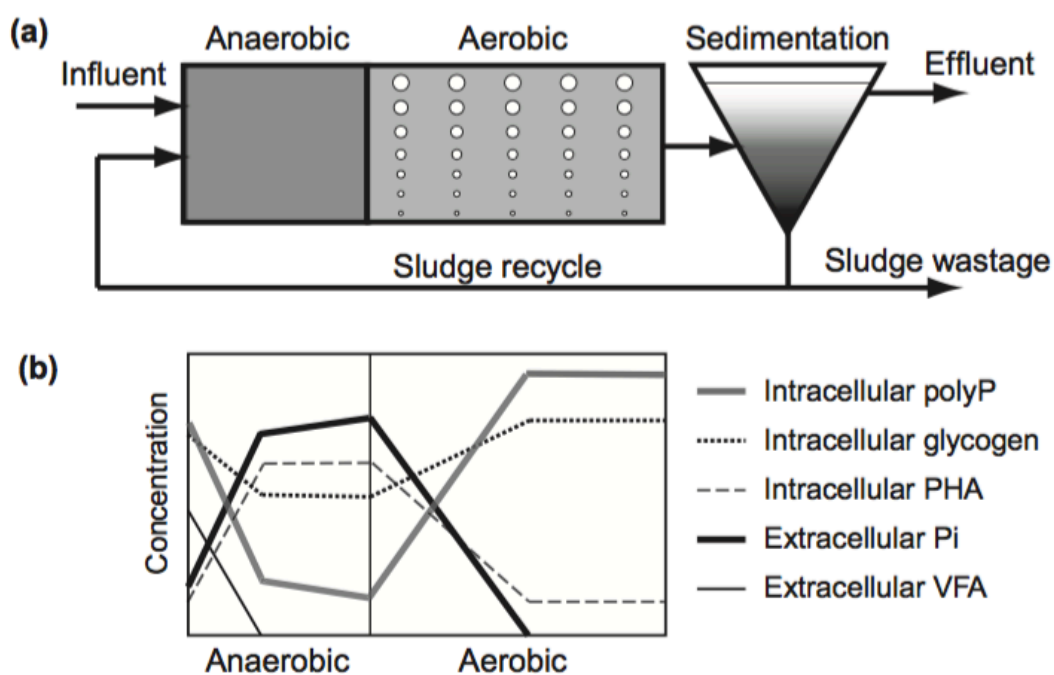


Figure 1.7 Schematic representation of the configuration a traditional anaerobic-aerobic EBPR process (A), and the profiling of key intracellular and extracellular chemicals (B). Figure from Shaomei He and Katherine D. McMahon 2011⁶⁰.

The advent of molecular methods has greatly expanded our knowledge of EBPR microbiology. Several bacterial genera have so far been proposed to function as PAOs including “*Candidatus Accumulibacter*”, *Tetrasphaera* spp., *Microthrix* spp., *Dechloromonas* spp., *Pseudomonas* spp., and “*Candidatus Accumulimonas*” (Figure 1.8)⁶⁸⁻⁷². Among all potential PAOs, *Candidatus Accumulibacter* and *Tetrasphaera* spp. are commonly identified in lab- and full-scale wastewater treatment systems^{60, 68, 73}. The major competitor in the EBPR process is glycogen accumulating organisms (GAOs), a group of microorganisms with similar C metabolism to PAOs but that do not exhibit P release and uptake⁷⁴. Glycogen, instead of PHAs, is used as both energy source and reducing power under anaerobic condition for GAOs. Similar to PAOs, the GAOs phenotypes have been confirmed for several bacterial genera, including those associated with “*Candidatus Competibacter*” in *Alphaproteobacteria*, *Propionivibrio* in *Betaproteobacteria* and tetrad-forming organisms (TFOs) affiliated with *Defluviicoccus* in *Gammaproteobacteria*⁷⁵⁻⁷⁷. As GAOs compete with PAOs directly for carbon sources without contributing to P removal, their proliferation is usually accompanied by the deterioration of EBPR performance^{61, 78}.

Several control strategies have been demonstrated to help *Accumulibacter*-related PAOs (herein *Accumulibacter*) to out-compete GAOs, including (1) pH, (2) substrate, and (3) temperature⁷⁹⁻⁸². *Accumulibacter* has been observed to out-compete GAOs with increasing pH from 7 to 8 due to higher substrate transport rate⁸³. Proton efflux in symport with Pi by Pit transporters has been considered as the primary controller of the proton gradient for acetate transport for *Accumulibacter*. *Defluviicoccus* and *Competibacter* appear to maintain the proton gradient by fumarate reductase (FRD) activity and by F₁F₀-ATPase. As more energy is required for substrate uptake under higher pH, the bioenergetic differences in substrate transport may provide

Accumulibacter a competitive advantage⁶⁰. Switching between acetate and propionate has also been observed to be an efficient strategy for enriching Accumulibacter rather than GAO groups due to variations on substrate utilization⁸⁴. Accumulibacter has no obvious preference on substrate such that it can maintain similar substrate utilization rates when immediately switching between acetate and propionate⁸⁵. In contrast, different GAO groups seem to only favor one substrate (acetate or propionate), and a slower substrate uptake rate was observed for GAO groups after switching from a previous substrate⁸⁶. Lower temperature was also reported by Lopes-Vazquez and colleagues as a control parameter for enriching Accumulibacter⁸⁷. Accumulibacter was selected under lower temperature possibly due to higher substrate uptake rate compared with Competibacter-related GAO⁸⁰.

broadly distribute into two groups: Type I (clades IA-IE) and Type II (clades IIA-[II-I]) (Figure 1.9, left). Several comparative genomic studies have indicated that each genome contains a substantial number of unique genes (>700 genes)⁹⁰⁻⁹² (Figure 1.9, right). Sequence variations, metabolic and physiological differences have been observed among *Accumulibacter* clades, including differentiations in capacity for denitrification and other N transformation⁹³⁻⁹⁵. Some discrepancies shown in genomic content are helpful to explain variations in metabolisms. For instance, the differentiated nitrate removal capability in some EBPR systems could be explained by the different abundance of nitrate reductase (NAR)-harboring or NAR-lacking *Accumulibacter*⁹⁵. Investigation of *Accumulibacter* gene expression and protein complement also suggested that metabolic regulation could partially play a role in explaining some discrepancies in the dynamics of *Accumulibacter* populations and versatility in their metabolism capabilities^{32, 96}. *Accumulibacter* strains capable of denitrifying P uptake is of particular interest when trying to combine P and N removal. However, a comprehensive comparison of genomic denitrification potential among all currently available *Accumulibacter* genomes is missing, which limits our understanding of the denitrifying *Accumulibacter*.

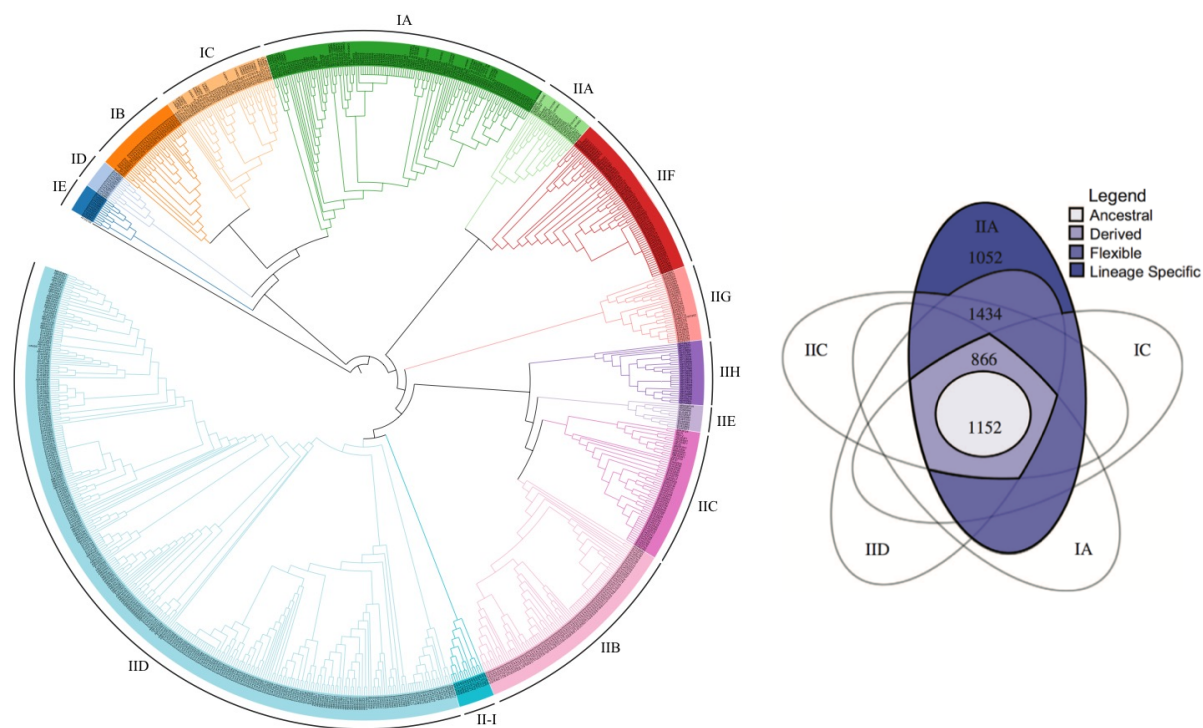


Figure 1.9 Figure at left: Phylogenetic tree for 749 available *Accumulibacter ppk1* sequences built in MEGA 7.0.18 using the maximum likelihood method with Tamura-Nei model. A total of 1007bp *Accumulibacter*-specific *ppk1* gene fragment was included for analysis. Figure at right: Five-way venn diagram depicting shared and unique genes for five *Accumulibacter* clades (IA, IC, IIA, IIC and IID) from Oyserman et al. 2016⁹².

1.2.4 Microbial N_2O production

Reactive N pollution has intensified the emission of N_2O , a potent GHG with a global warming potential 310 times that of CO_2 . Atmospheric N_2O concentration has increased ~30% in the last century (Figure 1.10). The impact of atmospheric N_2O could last for a long period of time since N_2O is very stable and may persist in the atmosphere for over 120 years^{26, 97}. Based on estimates from U.S. Environmental Protection Agency (EPA), U.S. wastewater treatment plants emit around 5.2 Tg N_2O as CO_2 equivalents⁹⁸. N_2O emission can account for as much as 78.4% of the overall CO_2 footprint of municipal wastewater treatment plants⁹⁹.

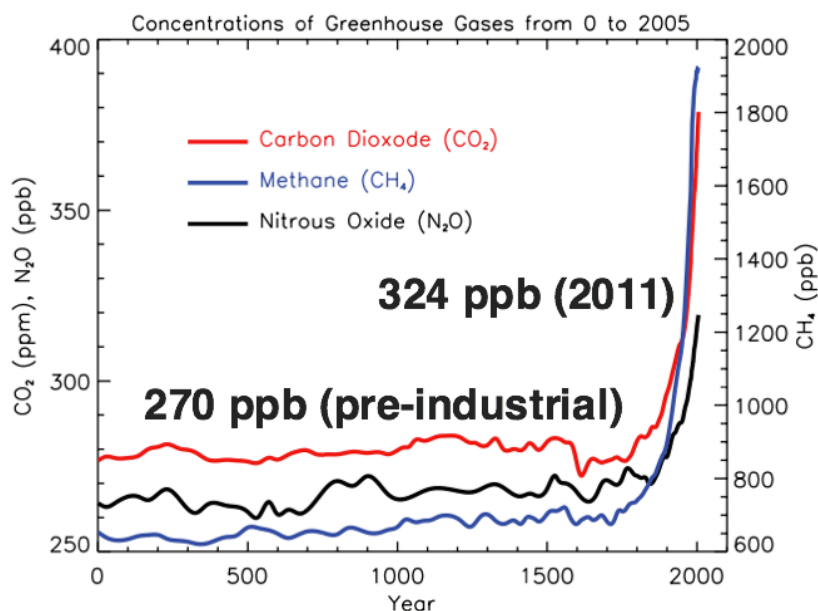


Figure 1.10 Changes in N₂O, CO₂ and CH₄ concentrations in the atmosphere over the past two centuries¹⁰⁰. Numbers in the figure denote the baseline pre-industrial atmospheric N₂O concentration and the increased N₂O concentration in 2011.

N₂O can be produced by two microbial bioprocesses during BNR processes: incomplete nitrification and heterotrophic denitrification²⁶ (Figure 1.10). Two main sources of N₂O in AOB driven nitrification are: (1) nitrifier denitrification: microbial reduction of NO₂⁻ to NO and N₂O by nitrite reductase (NIR) and nitric oxide reductase (NOR) and (2) the incomplete oxidation of hydroxylamine (NH₂OH) (NH₄⁺ → NH₂OH → NO → N₂O) with N₂O as a final product by hydroxylamine oxidoreductase (HAO) and NOR (Figure 1.10). During nitrification, N₂O can also be produced abiotically by N-nitrosation hybrid reactions when NH₂OH is oxidized to N₂O by NO₂⁻, HNO₂ or NO¹⁰¹⁻¹⁰⁴. The level of DO concentrations determines which pathway will be the dominant one during nitrification. Decreasing DO level will shift the major N₂O formation pathway from NH₂OH pathway to nitrifier denitrification^{105, 106}. Switching between anoxic to aerobic, or aerobic to anoxic conditions or intermittent aeration have been reported with increasing of N₂O production^{107, 108}. N₂O formation in nitrification is often caused by a combination of

multiple pathways, particularly in biofilms or granular systems due to the oxygen gradient within the systems.

Complete ammonia oxidation (Comammox) bacteria within the genus *Nitrospira* harbors gene clusters encoding AMO (ammonia monooxygenase), HAO and NXR (nitrite oxidoreductase), and can oxidize NH_3 directly to NO_3^- ^{109, 110}. N_2O emission from Comammox enrichment has not been reported yet. However, Comammox draft genomes indicate the genomic potential for N_2O production via hydroxylamine oxidation pathway¹¹⁰. The lack of NOR in Comammox clades A and B draft genomes suggests that they might be incapable of nitrifier denitrification.

Heterotrophic denitrification is another important source of N_2O during wastewater management. Heterotrophic denitrification is a four-step process that reduces NO_3^- to N_2 via NO_2^- , NO and N_2O . Each step is catalyzed by a specific enzyme: nitrate reductase (respiratory nitrate reductase [NAR] or periplasmic nitrate reductase [NAP]), nitrite reductase (NIR: cytochrome cd₁-type nitrite reductase [encoded by *nirS*], and copper-containing nitrite reductase [encoded by *nirK*]), nitric oxide reductase (NOR encoded by *norB*), and nitrous oxide reductase (NOS encoded by *nosZ*). Two phylogenetically distinct groups of the *nosZ* gene that catalyze N_2O reduction (clade I and II *nosZ*) have been identified recently¹¹¹. Currently, several hypotheses have been stated in existing literatures to explain the formation of N_2O by heterotrophic denitrification: (1) electron donor limitation and electron competition among the four key denitrification enzymes NAR, NIR, NOR and NOS¹¹²⁻¹¹⁴ (Figure 1.11). Electron competition between nitrogen oxide reductases in denitrification is thought to be particularly prevalent under electron donor limitations, including low COD/N ratio conditions or when the electron donor is intracellular compounds (e.g. PHAs); (2) microorganisms with limited (or absent) capability for using of N_2O as the terminal electron

acceptor due to the lack of genomic capacity for N₂O reduction (e.g. lack of NOS); and (3) the selective inhibition of the *nos* gene expression^{26, 67, 115-118}.

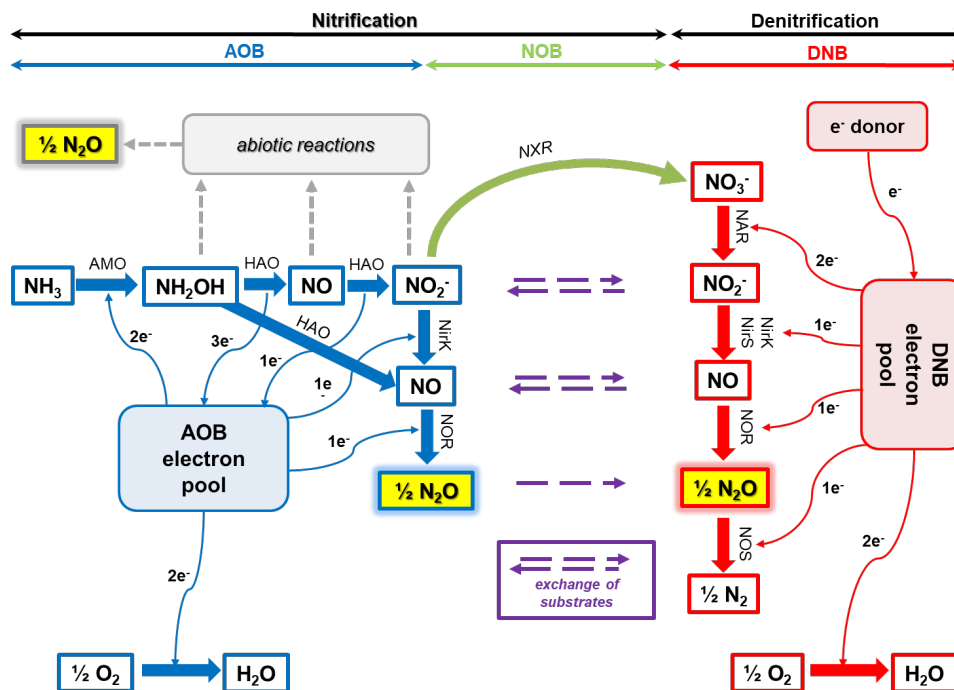
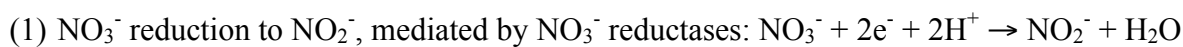


Figure 1.11 N transformation and N₂O formation pathways in nitrification (blue) and denitrification (red). Figure from Sabba et al. 2018.

Denitrification involves four sequential reduction reactions (**Eq. 1.3**). Elections produced by electron donors flow through electron pools (quinone pool [Q/QH₂] and the cytochrome bc₁ [Cyt bc₁] complex) and are then used by denitrification enzymes (Figure 1.11). Electron competition may occur when limited electron donor is supplied under circumstances such as low COD/N conditions. The lower affinity of nitrous oxide reductase for internal electron carriers compared with the other three enzymes may cause the decline of N₂O consumption rate, and thus the accumulation of N₂O.

Eq. 1.3 Four sequential steps and reactions of denitrification:



(2) NO_2^- reduction to NO, mediated by NO_2^- reductases: $\text{NO}_2^- + \text{e}^- + 2\text{H}^+ \rightarrow \text{NO} + \text{H}_2\text{O}$

(3) NO reduction to N_2O , mediated by NO reductases: $2\text{NO} + 2\text{e}^- + 2\text{H}^+ \rightarrow \text{N}_2\text{O} + \text{H}_2\text{O}$

(4) N_2O reduction to N_2 , mediated by N_2O reductases: $\text{N}_2\text{O} + 2\text{e}^- + 2\text{H}^+ \rightarrow \text{N}_2 + \text{H}_2\text{O}$

Denitrification is a taxonomically widespread trait and it has been considered as a modular process that can be split over multiple taxa in a shared environment. The existence of complete or partial denitrifiers in diverse of environments has been revealed by draft genomes recovered via shotgun metagenomic sequencing^{119, 120}. Depending on the genomic potential and environmental constraints, the reduction of nitrogen oxides can consist of different steps that can either act in concert or be performed individually. Of particular importance to this dissertation, incomplete denitrifiers lacking *nosZ* have been identified as potential source of N_2O as they are incapable of N_2O reduction. Nearly 40% of the complete or draft genomes available from National Center for Biotechnology Information (NCBI) that harbor NIR also lack NOS¹¹⁹. In addition to gene absence, down-regulation of *nosZ* may result in the loss of N_2O reduction related genes during evolution^{121, 122}. Moreover, interactions between N_2O producers (microorganisms harboring upstream denitrification gene clusters, e.g. *nar*, *nap*, *nir*, and *nor*) and consumers (bacteria with *nos* gene cluster) via cross-feeding could potentially eliminate the net accumulation of N_2O ¹²³. The correlation between microbes with truncated denitrification pathway and N_2O formation via denitrification pathway in complex microbial communities is little understood and needs further investigation.

The diversity of the *nosZ* gene was expanded recently into two groups (clade I and clade II, also known as typical and atypical *nosZ*)^{111, 124}. The differences between clade I and II *nosZ* genes were originally defined by, but are not limited to, phylogeny. Different *nos* gene cluster

organization, translocation pathway, and co-occurrence patterns with other denitrification genes also distinguish the two types of *nosZ*^{111, 124-126}. Co-occurrence of *nirS* or *nirK* with clade I *nosZ* was discovered in nearly 83% of genomes. In contrast, 51% of clade II *nosZ* containing genomes miss upstream denitrification genes (*nar/nap*, *nir*, and *nor*) and are termed as nondenitrifying N₂O reducers¹¹⁹. Differences between clade I and II *nosZ* in half-saturation constant and maximum N₂O reduction rates were also reported in pure culture studies¹²⁷. However, little is known about their contributions in natural and engineered ecosystems including wastewater treatment systems when the diversity and community structure of N₂O reducers are more complex¹²⁰. Nitrous oxide reductase has been reported to be sensitive to multiple factors, including DO, pH, NO₂⁻ (free nitrous acid, FNA) concentrations, carbon source and concentrations^{66, 67, 128-130}. A deeper understanding about clade I and clade II *nosZ* gene (or gene cluster) regulation under varying conditions including nutrient status, for example, N and C flux, will not only provide insight on the mechanism of N₂O formation but also shed light on niche differentiation between and within the two clades of N₂O reducers.

Large variations of N₂O emission were reported from BNR process due to the variation of operational conditions. N₂O emission from full-scale wastewater treatment plants could account for 0-15% of the total N loading, while 0-95% conversion of N₂O was observed in lab-scale systems^{10, 65, 97}. Elevated N₂O generation in denitrifying EBPR processes has been reported in several studies under different conditions, including (1) oxidation of endogenous COD in pulsed fed systems (switching between anaerobic/anoxic conditions); (2) limited availability of COD relative to NO₂⁻ or NO₃⁻ (low COD/N ratio); and (3) high concentrations of NO₂⁻ or FNA¹³¹⁻¹³³. Without a comprehensive study of both kinetics and microbial community structure and function,

the understanding of mechanisms for N₂O generation in denitrifying EBPR processes is still limited.

1.3 Research Objectives

Based on the knowledge gaps identified above, this dissertation focusses on the following specific research objectives:

OBJECTIVE I: IMPLEMENT A PROOF-OF-CONCEPT LAB-SCALE BIOREACTOR FOR SIMULTANEOUS N AND P REMOVAL AS WELL AS N₂O GENERATION.

In this objective, we targeted the following specific research questions:

- Can we extend the current high-yield N₂O generation CANDO process with P removal?
- Can we select a particular clade or clades of “Accumulibacter” enrichment culture for high rate of N₂O accumulation as well as P removal?

OBJECTIVE II: UNDERSTAND DENITRIFYING CAPABILITY OF THE MICROBIAL CONSORTIUM VIA REACTOR KINETIC ANALYSIS AND BATCH ASSAYS.

In this objective, we targeted the following specific research questions:

- Did the microbial consortia adapt to incomplete denitrification (NO₂⁻ to N₂O) coupled to P uptake and have different NO₃⁻, NO₂⁻ and N₂O reduction capabilities during long-term CANDO+P operation?
- What is the impact of different electron donors (external vs. internal) on denitrifying phosphate uptake and N₂O production?

OBJECTIVE III: EXPLORE THE MECHANISMS OF N₂O GENERATION IN CANDO+P.

The following hypotheses were tested to explore the mechanisms of N₂O generation in CANDO+P:

- Electron competition among different nitrogen oxide reductases
- Selection of “*Candidatus Accumolibacter*” (PAO) with truncated denitrification pathway missing *nos* gene
- Selection of flanking bacterial (non-PAO) organisms with truncated denitrification pathway and incapable for N₂O reduction

CHAPTER 2

Complete Nutrient Removal Coupled to Nitrous Oxide Production as a Bioenergy Source by Denitrifying Polyphosphate-accumulating Organisms

This chapter has been published in *Environmental Science and Technology*: Gao, H., Liu, M., Griffin, J.S., Xu, L., Xiang, D., Scherson, Y.D., Liu, W.T. and Wells, G.F. (2017) Complete Nutrient Removal Coupled to Nitrous Oxide Production as a Bioenergy Source by Denitrifying Polyphosphate-Accumulating Organisms. *Environmental Science & Technology* 51(8), 4531-4540.

ABSTRACT

Coupled Aerobic-anoxic Nitrous Decomposition Operation (CANDO) is a promising emerging bioprocess for wastewater treatment that enables direct energy recovery from nitrogen (N) in three steps: (1) ammonium oxidation to nitrite; (2) denitrification of nitrite to nitrous oxide (N₂O); and (3) N₂O conversion to N₂ with energy generation. However, CANDO does not currently target phosphorus (P) removal. Here, we demonstrate that denitrifying polyphosphate accumulating organism (PAO) enrichment cultures are capable of catalyzing simultaneous biological N and P removal coupled to N₂O generation in a 2nd generation CANDO process, CANDO+P. Over seven months (>300 cycles) of operation of a prototype lab-scale CANDO+P sequencing batch reactor treating synthetic municipal wastewater, we observed stable and near complete N removal accompanied by sustained high rate, high yield N₂O production with partial P removal. A substantial increase in abundance of the PAO “*Candidatus Accumulibacter phosphatis*” was observed, from 5% of the total bacterial community in the inoculum to over 50% after four months. Our work demonstrates the feasibility of combining high rate, high yield N₂O production for bioenergy production with combined N and P removal from wastewater, and it further suggests a putative denitrifying PAO niche for *Accumulibacter*.

2.1 Introduction

Conventional biological nutrient (nitrogen (N) and phosphorus (P)) removal processes, though generally reliable and efficiency, are energy intensive and do not target resource recovery or energy generation as a process goal¹. In addition, unintended emissions of nitrous oxide (N₂O) via incomplete nitrification (oxidation of ammonium (NH₄⁺) to nitrite (NO₂⁻)) or denitrification (reduction of nitrate (NO₃⁻) or NO₂⁻ to nitrogen gas (N₂) via nitric oxide (NO) and N₂O) is an emerging issue of concern for wastewater treatment processes targeting N removal. N₂O is a potent greenhouse gas with a global warming potential 310 times that of carbon dioxide (CO₂)². Thus, it is usually treated as an unwanted byproduct during wastewater treatment. Paradoxically, N₂O is also a powerful oxidant and a potential renewable energy source. Compared with stoichiometric combustion of 1 mole of methane (CH₄) with oxygen (O₂), roughly 30% more energy is produced via combustion of 1 mole of CH₄ with N₂O¹³⁴. Injections of N₂O with oxygen as a co-oxidant into a biogas-fed engine at flow rates simulating potential N₂O (from waste N) available from a full-scale wastewater treatment system were recently shown to increase power output by 5.7–7.3%¹³⁵. Due to its potential as an energy source, maximizing production, capture and use of N₂O for energy generation has emerged as a promising new concept for sustainable N removal and energy recovery from wastewater^{1,4}.

Recently, Scherson et al. introduced a novel biological N removal process, termed the Coupled Aerobic-anoxic Nitrous Decomposition Operation (CANDO), to remove NH₄⁺ from high-strength wastewater (digester supernatant) and convert it to N₂O for energy generation^{3,5}. Three steps are included: (1) microbial nitrification of NH₄⁺ to NO₂⁻; (2) microbial partial denitrification of NO₂⁻ to N₂O via cycling between anaerobic and anoxic conditions; and (3) N₂O

conversion to N_2 with energy production via co-combustion of CH_4 . Both steps 1 and 3, including measures to minimize NO_x emissions during co-combustion of N_2O with CH_4 , are well documented^{3,136-140}. In previous studies exploring high yield N_2O generation from waste N via microbial denitrification, a *Comamonas* enrichment culture and a type II *methanotrophic* enrichment have been shown to reduce NO_2^- to N_2O with high efficiencies using intracellular storage polymers (poly-3-hydroxybutyrate, PHB) as the primary electron donor^{3,5,11}. Pilot-scale testing of CANDO for N removal from high-strength sidestreams (anaerobic digester supernatant) is currently in progress.

Cyclic redox conditions in the 2nd step of CANDO is similar to operation of Enhanced Biological Phosphorus Removal processes (EBPR) widely used in wastewater treatment plants (WWTPs) for P removal¹⁴¹. The critical microbial functional group in EBPR processes is polyphosphate accumulating organisms (PAOs). When subjected to cyclic anaerobic-aerobic conditions, PAOs store endogenous carbon as polyhydroxyalkanoates (PHAs) and release P via polyphosphate (PolyP) hydrolysis in the anaerobic phase, and oxidize PHAs and uptake excess P to synthesis PolyP under aerobic conditions. Instead of using oxygen as the electron acceptor under aerobic condition, denitrifying PAOs (DPAOs) are able to couple NO_3^- or NO_2^- reduction to P uptake^{13,14}. “*Candidatus Accumulibacter phosphatis*” (herein Accumulibacter) has been identified as the primary PAO in most full-scale and lab-scale EBPR systems, and the ability to use NO_2^- as well as O_2 as the terminal electron acceptor has been demonstrated for selected Accumulibacter lineages^{60, 142}. This suggests that it may be possible to incorporate biological P removal and recovery into the CANDO process via selection for Accumulibacter-associated DPAOs. The primary objective of this study was thus to clarify feasibility of combining high rate, high

efficiency N and P removal from wastewater with high yield N_2O production as a novel bioenergy molecule. This 2nd generation process, termed CANDO+P, leverages a highly enriched denitrifying *Accumulibacter* community as a microbial biocatalyst.

2.2 Materials and Methods

2.2.1 CANDO+P Bioreactor Operation and Strategies for N_2O Production

Since steps 1 and 3 in CANDO have been demonstrated previously¹³⁶⁻¹⁴⁰, we focused on step 2 (microbial denitrification of NO_2^- to N_2O) in this study. A custom-built 14L (12L working volume, 50% decant per cycle) sequencing batch reactor (SBR) (Figure 2.1) was operated continuously for seven months under cyclic anaerobic/anoxic conditions, with a short aerobic polishing step. The SBR was operated with a “feast-famine” feeding strategy with synthetic municipal wastewater influent under the following conditions: HRT=12h, mixing speed of 123 rpm, temperature =22±1.5°C. No biomass was intentionally wasted during the operation. Biomass loss through the effluent or via decay was not quantified in the study. In the “feast-famine” feeding regime, biomass was alternated between chemical oxygen demand (COD) rich (anaerobic) and deplete conditions (anoxic followed by a short aerobic period). COD deplete conditions were accompanied by spiking with a high NO_2^- synthetic wastewater to mimic effluent from an upstream nitrification reactor. Electron donors (COD) were switched between acetate and propionate in the anaerobic phase every two cycles to enrich DPAOs⁸⁶. The reactor was inoculated with activated sludge from the Stickney Water Reclamation Plant (Chicago, USA). The synthetic wastewater medium (without COD and N) was prepared based on Smolders et al.¹⁴³. The synthetic wastewater medium (without COD and N) contained 66.79mg/L $MgSO_4$, 14mg/L $CaCl_2 \cdot 2H_2O$, 44.52 mg/L $NaH_2PO_4 \cdot H_2O$,

56.19mg/L K_2HPO_4 , 1mg/L yeast extract, and 0.1 g/L $NaHCO_3$. Each liter of mineral medium also contained 0.3mL of trace elements solution (1.5 g/L $FeCl_3 \cdot 6H_2O$, 0.15 g/L H_3BO_3 , 0.03 g/L $CuSO_4 \cdot 5H_2O$, 0.18 g/L KI, 0.06 g/L $Na_2MoO_4 \cdot 2H_2O$, 0.12 g/L $ZnSO_4 \cdot 7H_2O$, 0.15 g/L $CoCl_2 \cdot 6H_2O$ and 10g/L EDTA). Synthetic rather than real wastewater was employed in this study to maintain tight control and complete knowledge of influent constituents, so as to facilitate testing of feasibility (proof-of-concept) of combining high rate biological N and P removal with high yield N_2O generation. Organic carbon (acetate/propionate) and NO_2^- pulses were dosed separately to initiate anaerobic and anoxic periods, respectively. The initial COD level in the anaerobic period was set by adding a pulse of stock solution (128 g/L sodium acetate or sodium propionate as COD). Initial NO_2^- levels in the anoxic period were set by adding a pulse of nitrogen stock solution (138 g/L sodium nitrite). The SBR was operated in four phases to select DPAOs. Operational conditions are summarized in Table S2.1. In phase I (days 0-120, acclimation period), both COD and NO_2^- concentrations were kept low. To optimize the production of N_2O , in phase II (days 121-158), COD and NO_2^- concentrations were gradually increased to 100-120 mg/L as COD and 35-45 mg/L NO_2^- as N. Both COD and NO_2^- concentrations were kept stable and high in phases III (days 159-181) and IV (day 182-219). In phase IV, the COD/P ratio was increased to optimize P removal. In all the phases, COD/N (COD/ NO_2^- as N on a mass basis) ratio was maintained between 3-4 to facilitate maximum N_2O production via incomplete denitrification^{135, 144, 145}.

2.2.2 Bioreactor Performance Monitoring

The SBR operation was automatically controlled by a Programmable Logic Controller (PLC). The dissolved oxygen (DO) concentration and pH were continuously monitored online using a LDO sensor and a differential pH probe (Hach, USA), respectively. pH was automatically controlled at

8.0 ± 0.2 by addition of 0.3M hydrochloric acid and 0.3M sodium hydroxide stock solutions. Liquid phase N_2O in the reactor was also continuously monitored using a N_2O -WW sensor (Unisense, Denmark). Within-cycle SBR tests were conducted weekly to measure PO_4^{3-} , NO_2^- , volatile fatty acids (VFAs, including acetate and propionate) and intracellular storage polymers (PHAs) profiles throughout anaerobic, anoxic, and aerobic phases of reactor operation. Mixed liquor suspended solid (MLSS) and volatile MLSS (MLVSS) were measured periodically. MLSS and MLVSS were maintained at 4000 ± 400 mg/L and 3500 ± 350 mg/L, respectively, during stable operation.

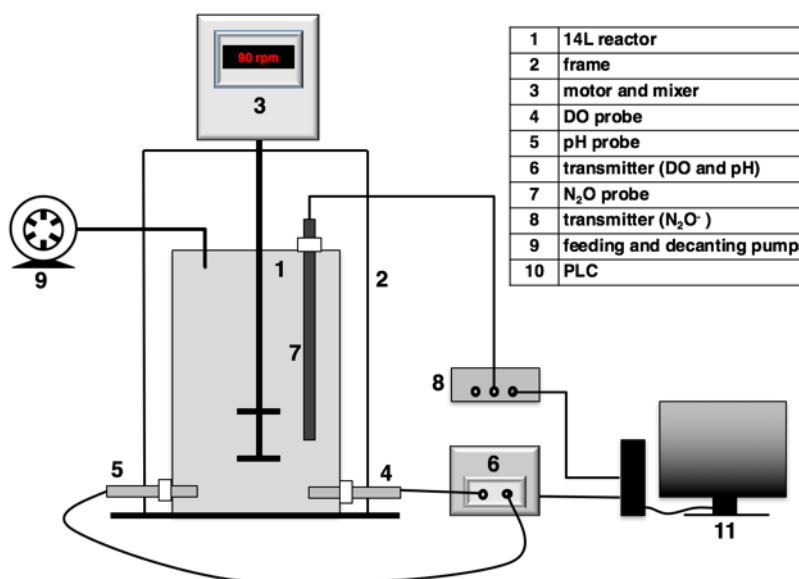


Figure 2.1 Schematic of the CANDO+P Sequencing Batch Reactor (SBR).

PO_4^{3-} , NO_2^- , and VFAs were assayed using an 881 Compact IC pro ion chromatograph (Metrohm, Swaziland) equipped with a Supp7 column with 0.36mM Na_2CO_3 as eluent. MLSS and MLVSS were measured according to standard methods¹⁴⁶. PHAs (including PHB, poly-3-hydroxyvalerate (PHV) and polyhydroxy-2-methylvalerate (PH2MV)) measurements were adapted from Song et al. and Oehmen et al.^{147,148}. 80-100 mg of freeze-dried biomass was placed

into PTFE-lined screw-topped glass tubes. Biomass was suspended in 2mL of acidic methanol solution (3% H₂SO₄) with 0.25 mg/ml benzoic acid as internal standard and 2mL of chloroform, and heated to 100 °C for 20h. After cooling to room temperature, 1mL of 1M NaCl solution was added, and the solution was shaken vigorously for 30s. 1mL of the bottom organic layer was transferred into a GC vial after settling for 15 minutes for phase separation. An Agilent 7890A GC-MS (Agilent Technologies, USA) with HP5-MS column was used for the analysis. A 0.2 µL sample was injected into the GC with 25:1 split ratio under constant pressure of 30.9 psi. The following temperature program was used: initial, 80°C for 2 mins, 8°C/min up to 176°C, 10°C/min up to 300°C, and holding at 300°C for 2.6 mins.

2.2.3 DNA Extraction and 16S rRNA Amplicon Sequencing

Community structure and PAO/DPAO enrichment were monitored over time via high-throughput amplicon-based DNA sequencing of 16S rRNA gene fragments. Biomass was sampled periodically from the SBR reactor. Genomic DNA was extracted from 1.5 mL of reactor biomass using the FastDNA SPIN Kit for Soil (MP Biomedicals, USA). The V4 region of the bacterial 16S rRNA gene was amplified using universal bacterial primers 515F and 806R from duplicate DNA extracts for each timepoint¹⁴⁹. Amplification and barcoding were performed using the Fluidigm Biomark multiplex PCR strategy, based on the protocol provided by the University of Illinois, Chicago DNA Services Facility. First, the V4 region of the bacterial 16S rRNA gene was amplified using forward primer CS1515f (5'-GTGCCAGCMGCCGCGGTAA) and reverse primer CS2806r (5'-GGACTACHVGGGTWTCTAAT)¹⁴⁹. A 20 µL PCR reaction was performed per DNA extract, using 2× Epicentre Premix F PCR mastermix (Epicentre, Madison, WI), 3.5U/µL Expand HiFidelity Taq (Roche Diagnostics, Indianapolis IN), 200 nM primer, and 1 µL genomic DNA.

PCR amplification followed a temperature profile of 95 °C for 5 minutes, followed by 28 cycles of: 95 °C (30 s), 55 °C (45 s), and 68 °C (30 s); and a final elongation step at 68°C for 7 minutes. For each timepoint, two DNA extracts were used for amplification. A second PCR step was then conducted using Fluidigm primers with sequencing adapters and a sample-specific barcode. Amplicons from replicate PCRs were pooled, and the PCR reaction was performed using 2× Accuprime Supermix (ThermoFisher, Carlsbad CA), 50 µM forward and reverse primers (Fluidigm, South San Francisco CA), and 1 µL of template from the first round of PCR using the following temperature program: 95 °C for 5 minutes, 95 °C for 30s, 60°C for 30s, and 68 °C for 30s in a total of 8 cycles. The resulting amplicons were processed with a Qiagen PCR purification kit and sequenced on the Illumina MiSeq V2 platform. Amplicon sequencing was performed on an Illumina MiSeq V2 at the University of Illinois Chicago DNA Services Facility.

USEARCH v8.1.1861 was used to remove singletons and chimeras, and to select representative OTUs based on 97% identity^{150, 151}. Phylogenetic affiliation was inferred for representative sequences from each OTU using the Greengenes sequence database in the Quantitative Insights Into Microbial Ecology (QIIME) platform^{152, 153}. Representative OTUs were also aligned via the SILVA Incremental Aligner (SINA) to identify ‘*Candidatus* Competibacter phasphatis’, one of the primary glycogen accumulating organisms (GAOs) that is often detected in lab-scale and full-scale reactors since Competibacter is not included in the Greengenes database^{154,74, 155, 156}. All the raw sequencing data in the study can be accessed through the NCBI SRA under the accession number SRP077722.

2.2.4 Statistical Analyses

To compare N₂O production efficiencies, Student's t-tests was performed in R v3.2.4¹⁵⁷. N₂O production efficiencies and maximum specific N₂O production rates were calculated based on the liquid phase N₂O concentration (mg/L as N). Gas phase N₂O was ignored due to the limited headspace and relatively high solubility of N₂O. N₂O has a high Henry's law constant of 24 mM/atm (at 25°C and 0% salinity) compared with 1.3 mM/atm for oxygen, indicating that high level of N₂O could accumulate in the liquid phase without active aeration¹³³. Performance characteristics and statistical analyses are reported for 13 weekly full SBR cycle profiles from day 127 to day 212 (phases II to IV) corresponding to the period of stable performance. Pairwise Pearson correlation coefficients between total *Accumulibacter* 16S rRNA gene, Clades IA and IIC *ppk1* genes and total *nirS* gene were also calculated and visualized using R v3.2.4. An association network was constructed to visualize the correlation between flanking OTUs and the two most abundant OTUs (assigned as *Accumulibacter* and *Zoogloea* at genus level in QIIME based on 16S rRNA sequencing results). OTUs with occurrence frequency less than 60% and less than 100 counts were excluded from the analysis. Both a pairwise nonmetric Spearman correlation matrix and Pearson correlation matrix were calculated in R v3.2.4. Network visualization was constructed using *circus*¹⁵⁸.

2.3 Results and Discussion

2.3.1 Bioreactor Performance and N_2O Production

To select for biomass capable of high rate incomplete denitrification for N_2O generation, a decoupled “feast-famine” feeding strategy was applied to the CANDO+P reactor via separate delivery of external COD (electron donor) during the anaerobic phase, and NO_2^- (electron acceptor) during the anoxic phase. NO_2^- removal via denitrification in the anoxic phase accompanied by production of N_2O (indicating incomplete denitrification) was observed immediately after reactor inoculation with activated sludge. After four months of operation (phase I), complete reduction of NO_2^- coupled to P uptake under anoxic conditions was observed. By controlling the influent COD/N ratio between 3-4 and completely removing external COD during the anaerobic period, N_2O rather than N_2 was the primary denitrification product, with stable conversion efficiencies of 70-80% throughout the operational period (Figure 2.2a). After five months of operation (during phase III and IV), as high as 35-45 mg NO_2^- -N/L was dosed during anoxic feeding to promote selection for DPAOs. pH was maintained at 8.0 ± 0.2 to limit free nitrous acid (HNO_2) inhibition ($<0.94 \mu\text{g } HNO_2/\text{L}$)^{66, 159}. N_2O conversion efficiencies were not significantly impacted by use of different electron donors based on N_2O conversion efficiencies for 13 weekly cycle tests during phase III and IV (6 cycles for acetate and 7 cycles for propionate, acetate: $75.2 \pm 9.4\%$, propionate: $74.3 \pm 7.6\%$, Student’s t-test p-value = 0.8663) (Figure 2.2b). In addition, no significant differences were found between maximum specific N_2O production rates for different electron donors (acetate: $5.7 \pm 2.0 \text{ mg } N_2O\text{-N/gVSS/h}$, propionate: $4.9 \pm 2.1 \text{ mg } N_2O\text{-N/gVSS/h}$, Student’s t-test p-value = 0.3244).

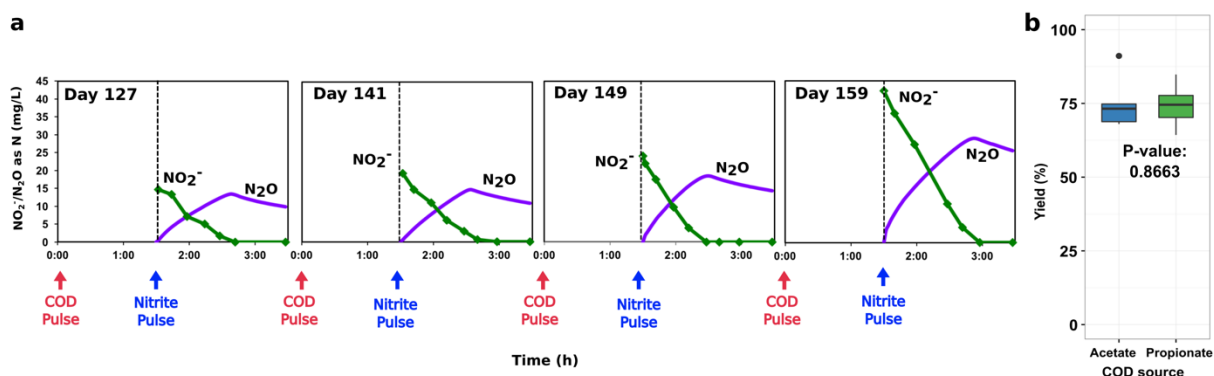


Figure 2.2 Changes across representative SBR cycles of concentrations of key compounds (COD sources (propionate/acetate), PHAs, NO₂⁻, N₂O and PO₄³⁻) in the CANDO+P SBR system using different external electron donors: (a) propionate (phase III, day 163) and (b) acetate (phase IV, day 203).

Profiles of substrates and products during two typical CANDO+P SBR cycles are shown in Figure 2.3a and 2.3b. These profiles originate from operational phases III (day 163) and IV (day 203) and illustrate bioreactor performance using propionate and acetate as the external COD source. The “feast-famine” feeding strategy led to COD uptake and accumulation of intracellular PHAs during the anaerobic phase, followed by employment of PHAs as electron donors for NO₂⁻ reduction and N₂O production in the anoxic phase. Apparent PHA consumption continued during the anoxic phase in some reactor cycles after complete depletion of NO₂⁻ (see, for example, figure 2.3), but with minimal impact on N₂O. The mechanism for this PHA consumption after NO₂⁻ depletion is not known, and warrants further investigation. Table 2.1 summarizes N and P removal rates and efficiencies during anoxic and aerobic phases of CANDO+P reactor operation using different external COD sources for the two typical cycles in Figure 2.3. Both NO₂⁻ reduction rates and N₂O conversion efficiencies were comparable when alternating between acetate and propionate. Complete NO₂⁻ removal were achieved in both cycles, and the maximum specific NO₂⁻ reduction rates were 6.2 mg NO₂⁻-N/gVSS•h and 7.9 mg NO₂⁻-N/gVSS•h for acetate and propionate, respectively. N₂O conversion efficiencies were around 70% in the two selected cycles.

For both electron donors, P uptake rates during anoxic and aerobic phases were similar, with anoxic and aerobic specific P uptake rates of 4.5 and 4.3 mg PO₄³⁻-P/gVSS•h, respectively, for acetate and 9.0 and 7.2 mg PO₄³⁻-P/gVSS•h for propionate. Partial P removal was observed in both cycles. Interestingly, minimal P was removed in the anoxic phase of operation once NO₂⁻ was fully consumed and N₂O was the sole available external electron acceptor, despite the fact that the electron donors, PHAs, were not completely depleted (see, for example, Figure 2.3). Based on this observation, it's tempting to speculate that DPAOs selected in this system may not be capable of reducing N₂O to N₂.

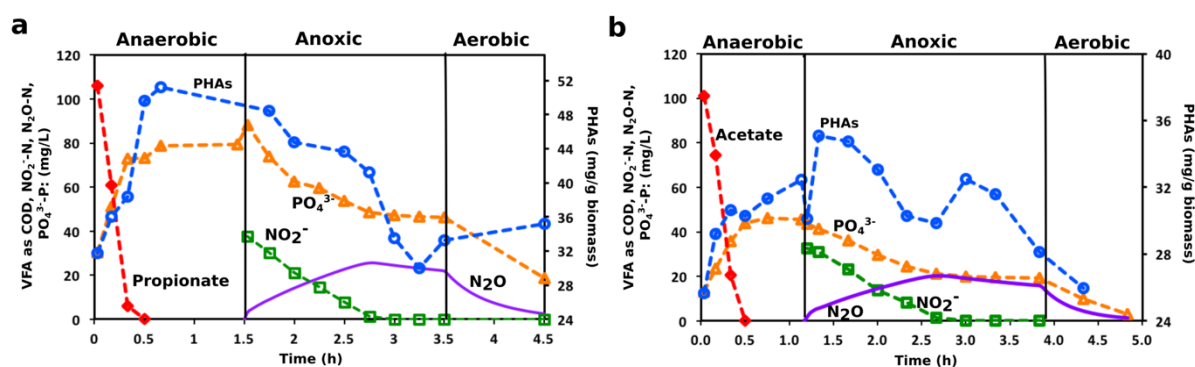


Figure 2.3 Sustained high-rate reduction of nitrite and high-yield production of N₂O during CANDOP reactor operation.

(a) Representative SBR profiles (phase II and III, days 127, 141, 149, and 159) demonstrating high rate NO₂⁻ reduction and N₂O generation under different initial NO₂⁻ concentrations (short aeration period was not shown in the figures). Carbon source for each cycle: day 127: acetate, day 141: propionate, day 149: acetate, day 159: propionate. (b) Comparison of N₂O yield with different external COD sources (acetate and propionate) based on 13 weekly full SBR cycle profiles from phases II to IV.

Table 2.1 N and P removal rates and efficiencies during anoxic and aerobic phases in two typical SBR cycles with different external electron donors (acetate and propionate).

External electron donor	COD/N ratio ^a	Specific NO ₂ ⁻ reduction rate (mg NO ₂ ⁻ -N/gVSS/h) ^b	N ₂ O conversion efficiency (%) ^c
Propionate	2.8	7.9	68.4
Acetate	3.1	6.2	74.8

External electron donor	Anoxic specific phosphorus uptake rate (mg PO ₄ ³⁻ -P/gVSS/h) ^b	Aerobic specific phosphorus uptake rate (mg PO ₄ ³⁻ -P/gVSS/h) ^b	Phosphorus removal efficiency (%)
Propionate	9.0	7.2	40
Acetate	4.5	4.3	76.1

- Units: (mgCOD/L)/ (mg NO₂⁻-N/L)
- Maximum specific NO₂⁻ and PO₄³⁻ utilization rates were calculated based on the first 60 minutes of the react period.
- Values were calculated based on dissolved N₂O.

2.3.2 Overall Microbial Diversity and Population Dynamics

To characterize structure and dynamics of the underlying microbial consortia during adaptation to CANDO +P conditions, shifts in overall microbial community composition were characterized using high-throughput 16S rRNA gene amplicon sequencing during operational phases I and II. The top 9 most abundant bacterial families as well as the distribution of five genera within the most abundant bacterial family *Rhodocyclaceae* are shown in Figure 2.4. Richness of the bacterial community in the reactor declined after two months of operation, as evidenced by the decline of both alpha diversity (Shannon and chao1 indexes) and numbers of observed OTUs (Figure S2.2). During operation, the relative abundance of 16S rRNA gene sequences associated with *Accumulibacter*, the primary PAOs in most full- and lab-scale bioreactors, gradually increased from 1.8% to 56.7% over 4 months of operation, at which point the reactor reached stable denitrification performance. The most abundant genus *Zoogloea* (26.2%) in the inoculum was replaced by *Accumulibacter* during this time period. GAOs that commonly compete with PAOs in EBPR processes comprised only a minor fraction of the overall bacterial community, based on low relative abundance (<2%) of gene sequences affiliated with the candidate genus *Competibacter*.

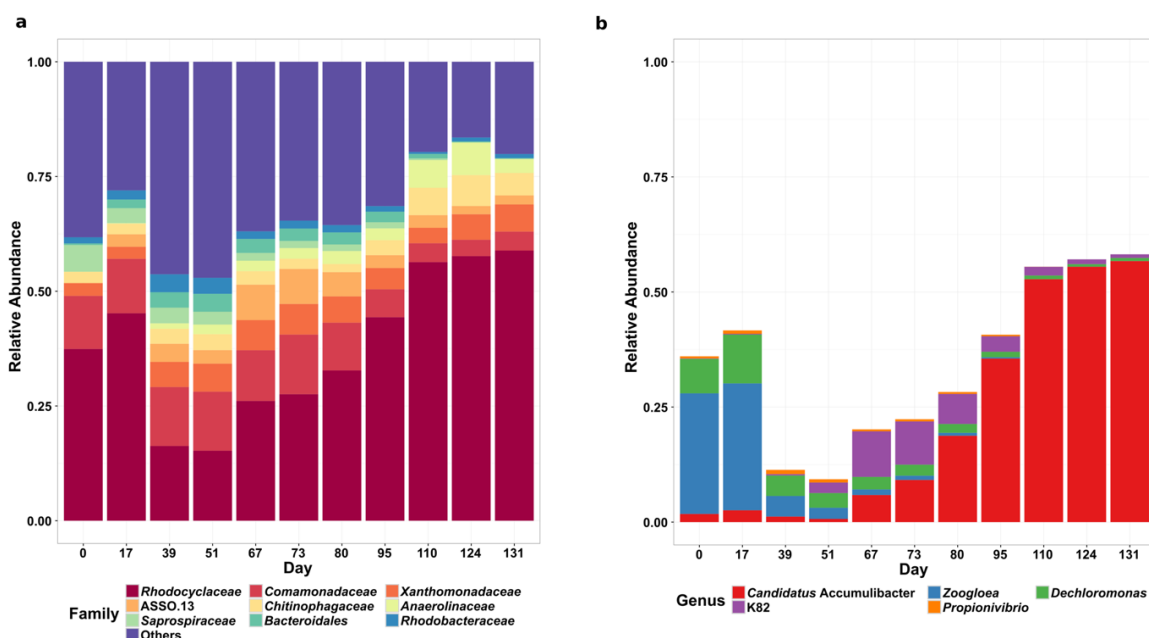


Figure 2.4 Overall bacterial community structure over 4 months of reactor operation (phase I and II).

(a) Relative abundance based on high-throughput 16S rRNA gene sequencing of the 9 most abundant bacterial families, with the remaining detected families as well as sequences unassigned at the family level included in the category “others”. (b) Relative abundance of the 5 genera detected in the CANDO+P reactor within family *Rhodocyclaceae* (normalized by total universal 16S rRNA gene).

We constructed a correlation-based network to explore the co-occurrence and co-exclusion patterns of flanking bacterial community members with the two most abundant genera, *Accumulibacter* (relative abundance 1.8%~56.7%) and *Zoogloea* (relative abundance 0%~26.2%) during CANDO+P reactor operation. Only correlations that were statistically significant (Spearman rank and Pearson correlation coefficient, p -value < 0.05) and strong (Spearman rank and Pearson correlation coefficient ≥ 0.6 or ≤ -0.6) are shown in Figure 2.5. The network consisted of 14 positive interactions and 81 negative interactions between flanking OTUs and *Accumulibacter*, and 31 positive interactions and 12 negative interactions between flanking OTUs and *Zoogloea*. 11 of the top 20 most abundant OTUs besides *Accumulibacter* and *Zoogloea* (average relative abundance > 0.8%, average accumulated relative abundance of the top 20 OTUs=

31.7%) were found to either strongly and significantly co-occur or co-exclude with *Accumulibacter* or *Zoogloea*. Only 3 out of the 11 OTUs, *Longilinea* in the family *Anaerolinaceae*, *Sediminibacterium* in the family *Chitinophagaceae* and class *SJA-28*, were positively associated with *Accumulibacter*. OTUs with putative phenotypes compatible with CANDO+P operational conditions were more likely to be positively correlated with *Accumulibacter*. In particular, taxa associated with the genus *Longilinea* (phylum: *Chloroflexi*) have been shown to be anaerobic filamentous bacteria capable of utilizing both acetate and propionate¹⁶⁰. *Longilinea* could thus potentially become a competitor of *Accumulibacter* and negatively impact settling behavior of the sludge¹⁶⁰. Besides *Zoogloea*, other OTUs within the family *Rhodocyclaceae* were out-selected during operation, including *Dechloromonas*. *Dechloromonas* enrichment was previously observed in an A₂O (anaerobic/anoxic/aerobic) process with NO₃⁻ as the electron acceptor¹⁶¹. Some putative heterotrophic denitrifiers, such as OTUs from families *Comamonadaceae* and *Xanthomonadaceae*, were also out-selected during operation.

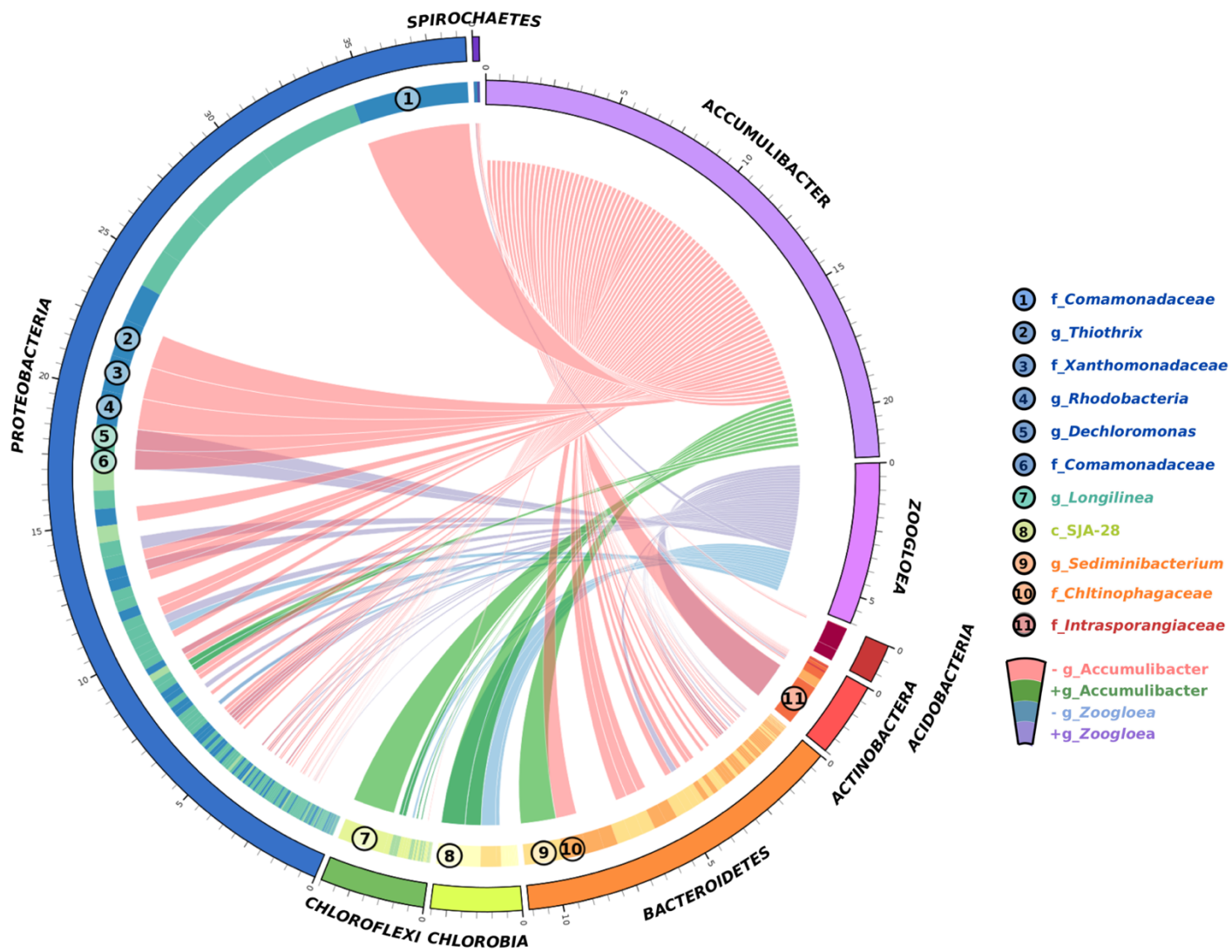


Figure 2.5 Circular representation of co-occurrence and co-exclusion network between flanking OTUs and the “core” CANDO+P microbiome (*Accumulibacter* and *Zoogloea*) during the start-up period (phase I and II).

OTUs were clustered at the 97% identity level. The inner circular diagram shows the relative abundance of 114 OTUs. Of the 20 most abundant flanking OTUs (average relative abundance > 0.8%), 11 that significantly co-occurred or co-excluded with *Accumulibacter* or *Zoogloea* are numbered and labeled based on the lowest level of taxonomic assignment in QIIME using the Greengenes reference database. The outer circular diagram shows the relative abundance of different phyla (phyla with relative abundance < 1% or contained <3 OTUs significantly correlated with either *Accumulibacter* or *Zoogloea* are excluded from the diagram).

Legend:

c_ : bacterial class; f_ : bacterial family; g_ : bacterial genus.

- g_*Accumulibacter*: negatively correlated with *Accumulibacter*; + g_*Accumulibacter*: positively correlated with *Accumulibacter*; -

g_*Zoogloea*: negative correlated with *Zoogloea*; + g_*Zoogloea*: positive correlated with *Zoogloea*.

2.4 Conclusions

Previous CANDO work focused on N removal alone, and suggested that both a *Comamonas* enrichment culture and a type II methanotrophic enrichment culture could efficiently generate N₂O for energy recovery while also promoting near-complete N removal from synthetic wastewater and anaerobic digester centrate^{3,5,11}. The results we present here indicate that a different microbial community dominated by taxa affiliated with *Accumulibacter* also support high-rate microbial N₂O production with concurrent N removal. Importantly, our work demonstrates that this activity can be combined with P removal for mainstream wastewater treatment, sequestered P in biomass that is then potentially amenable to P recovery. The proposed CANDO+P system is similar in layout to existing EBPR systems, suggesting that upgrading existing WWTP infrastructure (for example, with addition of a step feed system and nitrification reactor) may be possible. It should be noted, however, that a key remaining challenge to CANDO development is high efficiency collection of produced N₂O, as fugitive emissions of this potent greenhouse gas are highly undesirable. Our work to-date has focused on characterizing operational conditions and microbial mechanisms that enable high-rate, high yield N₂O production as a novel bioenergy source coupled to N, C, and P removal. Future efforts are needed to clarify approaches to N₂O collection. One appealing route is direct capture of off-gas from the short aerobic polishing step already present in CANDO+P for co-combustion with digester derived methane. The feasibility of this approach remains to be investigated.

Overall N removal efficiency and N₂O yield in this study were comparable with the previous CANDO studies focused on N removal alone (Table 2.2). In addition, both N and P removal rates were also comparable with other recent studies assessing the capacity of DPAOs to

use NO_3^- or NO_2^- as the terminal electron acceptor (Table 2.3). Compared with conventional lab-scale EBPR processes with COD/P ratios typically between 15:1 to 30:1, a lower COD/P (<10:1) ratio was used in our study^{143, 162}. COD limitations may be the cause of decreased P removal efficiency. Our future efforts will focus on optimizing P removal by employing batch tests under different COD/P ratios. In addition, our results demonstrate that both acetate and propionate are efficient feedstocks in the 2nd step of CANDO+P, with comparable NO_2^- removal rate and N_2O conversion efficiency. Future efforts are warranted to clarify treatment efficiency and stability with additional electron donors (glucose, methanol etc.) in the CANDO+P process, and in particular with more complex waste streams including real wastewater at both the lab-scale and pilot-scale.

Table 2.2 Comparison of overall NO_2^- removal efficiencies, specific N_2O production rates and N_2O conversion efficiencies between this (CANDO+P, phase III and IV) and previous CANDO studies.

Study	Overall NO_2^- removal efficiency	Specific N_2O production rate (mg-N/gVSS•h)*	N_2O conversion efficiency
Scherson et al. ³	>98%	25.2	75-80%
Scherson et al. ⁵	>98%	5.6	60-65%
Myung et al. ¹⁶³	72%	2.1 ± 0.4	65-75%
This study	>98%	5.1 ± 1.6 ^a	70-80%

* Specific N_2O production rate was calculated based on average maximum specific N_2O production rate for acetate and propionate in 13 weekly cycle tests in phase III and IV.

Table 2.3 Comparison of specific NO_x ($\text{NO}_3^-/\text{NO}_2^-$) and P removal rates in this and other lab-scale DPAOs studies.

Study	Electron Acceptor	Initial NO_3^- or NO_2^- concentration (mg-N/L)	Specific NO_3^- or NO_2^- reduction rate (mg NO_x^- -N/gVSS•h)	Specific phosphorus uptake rate (mg-P/gVSS•h)
This work	NO_2^-	38	6.8 ^a	5.7 ^a
Wang et al. ¹⁶⁴	NO_2^-	40	6.7 ^b	9.3 ^b
Zhang et al. ¹⁶⁵	NO_2^-	45	10.9 ^c	14.4 ^c
Zhou et al. ¹⁶⁶	NO_2^-	40	5.1 ^c	5.3 ^c
Zhou et al. ¹⁶⁶	NO_3^-	60	12.9 ^c	8.4 ^c
Wang et al. ¹⁶⁴	NO_3^-	34	3.6 ^b	4.3 ^b

- a. Values were calculated based on the average of anoxic reactions of 13 weekly cycle tests in phase III and IV during first 60 mins.
- b. Values were calculated based on anoxic reactions during first 15 mins.
- c. Values were calculated based on anoxic reactions during first 30 mins.

Taken together, the work we report here provides proof-of-concept of a novel microbial bioprocess, termed CANDO+P, for combined nutrient removal and energy and resource recovery from wastewater. Operational monitoring demonstrated complete N removal and partial P removal from synthetic wastewater coupled to high rate and high efficiency N₂O generation. In parallel, the system selected for biomass highly enriched in *Accumulibacter*, with a strong shift in *Accumulibacter* community structure from a Clade IIC dominated community in the inoculum to one co-dominated by putative DPAOs affiliated with Clade IA after several months of operation.

2.5 Supporting Information

2.5.1 Supporting Information - Tables

Table S2.1 Operational parameters and phases of the CANDO+P reactor operation.

	SBR operation				Initial COD (mg/L)	Initial NO ₂ ⁻ (mg-N/L)	Initial PO ₄ ³⁻ (mg- P/L)	COD/ P ratio
	Anaerobic (min)	Anoxic (min)	Aerobic (min)	Total cycle (h)				
phase I (acclimation period, day 0 to 120)	280	300	60	12	<80	<20	25	<3
phase II (day 121 to 158)	90	120	60	6	45 - 120	15 - 45	25	<5
phase III (day 159 to 181)	90	120	60	6	120 - 160	35 - 45	25	~5
phase IV (day 182 to 219)	70	160	60	6	120 - 160	34 - 45	15	~10

2.5.2 Supporting Information - Figures

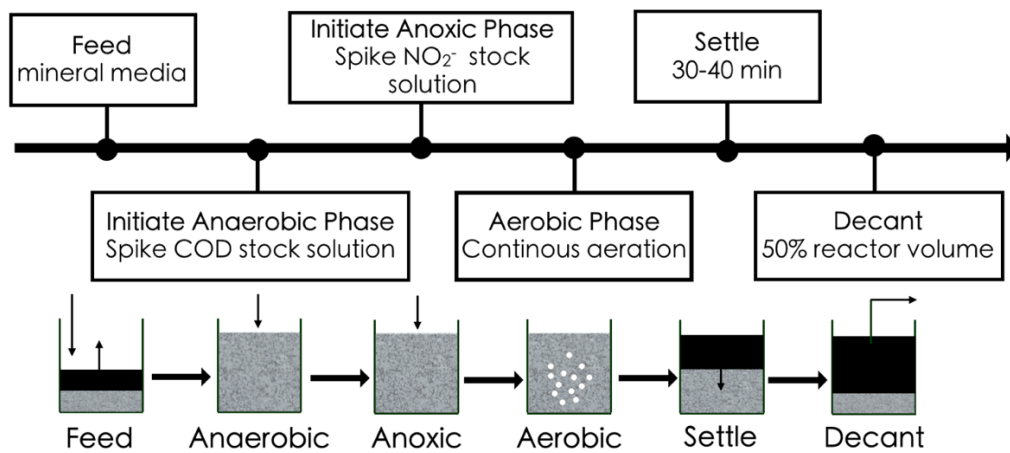


Figure S2.1 Conceptual schematic of CANDO+P SBR operation.

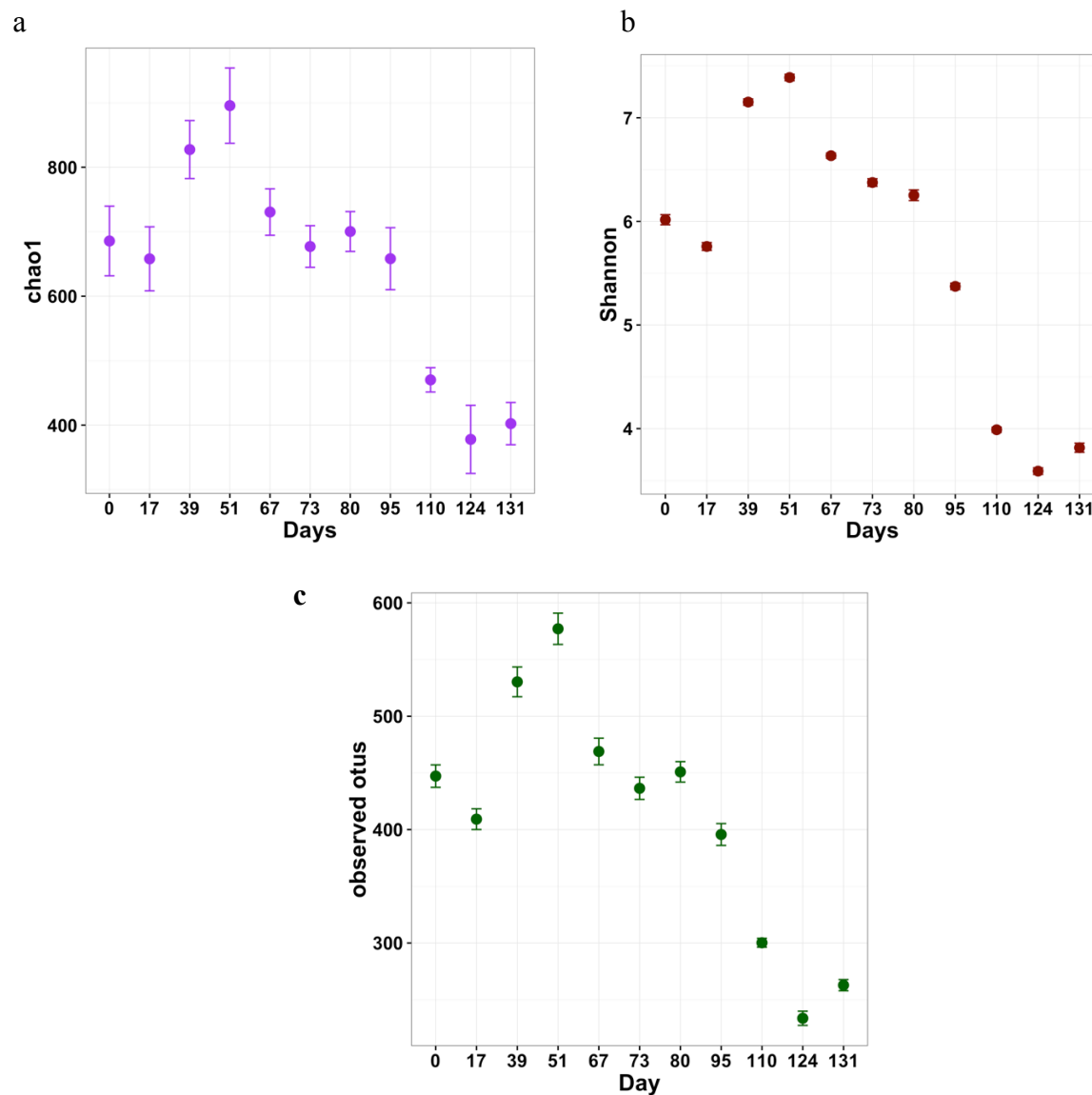


Figure S2.2 Dynamics in alpha diversity metrics over time: (a) chao1, (b) Shannon index and (c) observed OTUs.

All metrics were calculated after rarefying 10 times to the lowest sampling depth, and error bars indicate standard deviations. Samples were rarefied to the lowest sequencing depth 10 times and averaged to calculate Shannon and chao1 alpha diversity indexes and numbers of observed OTUs.

CHAPTER 3

Differential Kinetics of Nitrogen Oxides Reduction Leads to Elevated N₂O Production by a Nitrite Fed Denitrifying EBPR Bioreactor

This chapter has been submitted for review: Gao, H., Zhao, X., Zhou, L., Sabba, F., and Wells, G.F. Differential Kinetics of Nitrogen Oxides Reduction Leads to Elevated N₂O Production by a Nitrite Fed Granular Denitrifying EBPR Reactor (*In review*).

ABSTRACT

Denitrifying polyphosphate accumulating organisms (DPAOs) are capable of nitrate (NO_3^-) and/or nitrite (NO_2^-) reduction coupled to phosphorus (P) uptake when subjected to alternating anaerobic/anoxic conditions. However, accumulation of the denitrification intermediate nitrous oxide (N_2O), a potent greenhouse gas, has been previously observed in DPAO enrichments exposed to high NO_2^- concentrations. To date, denitrification capability and denitrifying P uptake rates of DPAOs using different electron acceptors after long-term exposure and adaptation to elevated concentrations of NO_2^- characteristic of shortcut N removal systems have not been examined. To address this knowledge gap, we operated a lab-scale sequencing batch reactor (SBR) under alternating anaerobic/anoxic conditions with high NO_2^- feed for over a year to obtain an enrichment of “*Candidatus Accumulibacter phosphatis*” putatively capable of denitrification. *Ex situ* batch assays were performed to clarify capacity for reduction of various nitrogen oxides and simultaneous P uptake by the DPAO enrichment culture under both decoupled (internal COD as electron donor) and coupled (external COD as electron donor) feeding conditions. These batch assays revealed distinct nitrogen oxides reduction and denitrifying P uptake capabilities, with significantly elevated kinetics when NO_2^- was supplied as the electron acceptor for P uptake and a strong propensity for N_2O accumulation in the presence of NO_2^- under both decoupled and coupled scenarios.

3.1 Introduction

Anthropogenic activities have greatly impacted the balance of many natural biogeochemical cycles, including nitrogen (N) and phosphorus (P)². Biological nutrient removal processes have long been considered a sustainable and economical way to remove N and P from wastewater. While these processes are largely successful, conventional routes for biological N removal are highly energy intensive and in some cases are linked to emissions of the potent greenhouse gas, nitrous oxide (N₂O). Emerging N removal processes including nitrification/denitrification (nitrite shunt) and partial nitrification/anammox promise to lower energy demand compared to conventional nitrification/denitrification based N removal processes²⁵. These processes rely on nitrite (NO₂⁻), rather than nitrate (NO₃⁻), as a key intermediate.

Enhanced biological phosphorus removal (EBPR) is increasingly used to remove P during wastewater treatment. EBPR processes rely on a group of bacteria known as polyphosphate accumulating organisms (PAOs). PAOs remove P by releasing and then uptaking excess P when subjected to dynamic anaerobic and aerobic conditions. A subset of PAOs, termed denitrifying PAOs (DPAOs), are also capable of using NO₃⁻ and/or NO₂⁻ as an electron acceptor to drive anoxic P uptake^{62, 64}. When accompanied by nitrification or full nitrification to produce NO₂⁻ and/or NO₃⁻, DPAOs provide a potential pathway for coupling biological P (Bio-P) removal and N removal^{25, 65}. However, inhibition of denitrifying P removal by NO₂⁻ and accumulation of N₂O has been observed in several studies, increasing the challenge of implementing NO₂⁻ driven denitrifying P removal^{66, 67}.

Several bacterial genera have so far been proposed to function as PAOs. Among all potential PAOs, *Candidatus Accumulibacter* (herein refer as Accumulibacter) is commonly

identified in lab and full-scale wastewater treatment systems^{60, 73}. The major competitor in the EBPR process is glycogen accumulating organisms (GAOs), a group of microorganisms with similar carbon (C) metabolism to PAOs but that do not exhibit P release and uptake⁷⁴. The GAO phenotype has been confirmed for several bacterial genera, including those associated with *Candidatus Competibacter* and tetrad-forming organisms (TFOs) affiliated with *Deftuviicoccus*⁷⁵.⁷⁶ The phylogenetic diversity of both putative PAOs and GAOs has been expanded recently⁷⁰.

The accumulation of N₂O has been observed during denitrification in DPAOs and DGAOs (denitrifying GAOs) enrichments. N₂O is an obligate denitrification intermediate when NO₃⁻ and/or NO₂⁻ is microbially reduced to nitrogen gas (N₂) via a series of enzymatic reactions. N₂O generation by denitrifiers appears to be particularly problematic under (1) low COD/N conditions (COD/N≤3), (2) high NO₂⁻ concentrations (and associated high free nitrous acid, FNA, concentrations), and (3) when only an intracellular organic carbon source (e.g. polyhydroxyalkanoates, PHAs) is available as an electron donor under dynamic feast-famine feeding strategies or decoupled feeding modes^{65, 134, 167}. Several hypotheses have been proposed to explain the accumulation of N₂O during denitrification. One possible explanation is electron competition among the four key denitrification enzymes nitrate reductase (NAR), nitrite reductase (NIR), nitric oxide reductase (NOR) and nitrous oxide reductase (NOS)^{112-114, 168}. Electron competition between terminal reductases in denitrification is thought to be particularly prevalent under electron donor limitations, including under low COD/N ratios or when the electron donor is intracellular (e.g. PHAs). A second possible explanation for N₂O accumulation during denitrification is the presence of microorganisms with truncated denitrifications pathways that lack genomic capacity for N₂O reduction (e.g. lack NOS)^{26, 169}. So far, the role of electron competition

and microorganisms with truncated denitrification pathways in explaining N_2O emissions by a DPAO enriched biomass adapted to denitrification is not known.

The overall objectives of this study were to (1) quantify denitrification and denitrifying P uptake kinetics using different electron acceptors (NO_3^- , NO_2^- and N_2O), and (2) assess electron competition among four denitrification enzymes (NAR, NIR, NOR, and NOS) of a DPAO enrichment culture adapted to elevated levels of NO_2^- . *Ex situ* batch assays were conducted to quantify DPAO kinetics and electron competition under both coupled and decoupled feeding conditions.

3.2 Materials and Methods

3.2.1 Bioreactor Setup and Operation

A 12L lab-scale sequencing batch reactor (SBR) was operated under anaerobic/anoxic conditions with an aerobic polishing phase for over a year for enrichment of DPAOs and simultaneous N and P removal. Reactor operation, monitoring, and performance are described elsewhere⁶⁵. Briefly, the reactor was fed under a feast-famine feeding regime, with COD (switching between acetate and propionate, 120-150 mg as COD/L) dosed during the anaerobic phase and NO_2^- dosed during anoxic conditions. A high NO_2^- (40-50 mg-N/L, COD/N=3) feed stream was used to simulate effluent from an upstream nitrification reactor treating municipal wastewater. Complete N and near complete P removal were achieved during long-term operation. N removal was accompanied by substantial accumulation of aqueous N_2O (~65-75% of NO_2^- removed, measured by an online N_2O -WW sensor [Unisense, Denmark])⁶⁵.

3.2.2 Batch Experiments Design

To quantify kinetics of denitrification and P uptake by DPAO enriched biomass, *ex situ* batch experiments were conducted in duplicate after stable N and P removal performance was achieved (days 460 to 630 of reactor operation). Two liters of biomass were withdrawn from the parent SBR at the beginning of a new cycle before COD was fed (anaerobic phase), purged with N₂ for 5 min to create anaerobic conditions, and transferred to a 2.5L sealed reactor vessel (2L working volume with 0.5L headspace). A pH meter (Mettler Toledo, USA) was used to monitor pH, and 0.3M hydrochloride acid was manually added to control pH to 7.8±0.2.

Two sets of batch assays were designed to explore nitrogen oxides reduction and denitrifying P uptake capabilities and kinetics: (1) addition of a single nitrogen oxide (NO₃⁻, NO₂⁻ or N₂O) as the sole electron acceptor under different COD/N ratios (COD/N from 3 to 12); and (2) addition of a combination of nitrogen oxides (NO₃⁻, NO₂⁻ and N₂O) as electron acceptors under COD/N=3. For each set of tests, both decoupled and coupled feeding strategies were investigated. Under decoupled feeding, COD (acetate) and nitrogen oxides were dosed sequentially, with nitrogen oxides only added after complete removal of exogenous COD (as in anaerobic/anoxic reactor cycling). Thus, an internal carbon source (PHAs) served as electron donor during denitrification. Under coupled feeding, acetate and nitrogen oxides were added simultaneously, and acetate was used directly as the electron donor. Details of batch tests, including substrate addition schemes and naming convention for batch test scenarios, are summarized in Table 3.1. 29 different batch tests were carried out (15 in decoupled feeding mode [Table 3.1a], and 14 in coupled feeding mode [Table 3.1b]).

Table 3.1a Summary of substrate (COD, NO_3^- , NO_2^- and N_2O) addition schemes employed in *ex situ* batch assays in the absence of exogenous COD (decoupled feeding strategy: COD (acetate) dosing prior to NO_x feed).

Feeding strategy	Nitrogen oxides	COD (mg/L)	NO_3^- (mg-N/L)	NO_2^- (mg-N/L)	N_2O (mg-N/L)	COD/N	Batch Test Scenario*
<i>Decoupled</i>	Single	120	10	0	0	12	D_a_ NO_3
	Single	120	20	0	0	6	D_b_ NO_3
	Single	120	40	0	0	3	D_c_ NO_3
	Single	120	0	10	0	12	D_a_ NO_2
	Single	120	0	20	0	6	D_b_ NO_2
	Single	120	0	40	0	3	D_c_ NO_2
	Single	120	0	60	10	2	D_d_ NO_2
	Single	120	0	0	10	12	D_a_ N_2O
	Single	120	0	0	20	6	D_b_ N_2O
	Single	120	0	0	40	3	D_c_ N_2O
	Combination	120	0	10	30	3	D_a_ $\text{NO}_2+\text{N}_2\text{O}$
	Combination	120	0	20	20	3	D_b_ $\text{NO}_2+\text{N}_2\text{O}$
	Combination	120	0	30	10	3	D_c_ $\text{NO}_2+\text{N}_2\text{O}$
	Combination	120	20	20	0	3	D_a_ NO_3+NO_2
	Combination	120	13	13	13	3	D_a_ $\text{NO}_3+\text{NO}_2+\text{N}_2\text{O}$

Table 3.2b Summary of substrate (COD, NO_3^- , NO_2^- and N_2O) addition schemes employed in *ex situ* batch assays in the presence exogenous COD (coupled feeding strategy: simultaneous COD (acetate) and NO_x dosing).

Feeding Strategy	Nitrogen Oxides	COD (mg/L)	NO_3^- (mg-N/L)	NO_2^- (mg-N/L)	N_2O (mg-N/L)	COD/N	Batch Test Scenario*
<i>Coupled</i>	Single	320	40	0	0	8	C_a_ NO_3
	Single	200	40	0	0	5	C_b_ NO_3
	Single	120	40	0	0	3	C_c_ NO_3
	Single	320	0	40	0	8	C_a_ NO_2
	Single	200	0	40	0	5	C_b_ NO_2
	Single	120	0	40	0	3	C_c_ NO_2
	Single	320	0	0	40	8	C_a_ N_2O
	Single	200	0	0	40	5	C_b_ N_2O
	Single	120	0	0	40	3	C_c_ N_2O
	Combination	120	0	10	30	3	C_a_ $\text{NO}_2+\text{N}_2\text{O}$
	Combination	120	0	20	20	3	C_b_ $\text{NO}_2+\text{N}_2\text{O}$
	Combination	120	0	30	10	3	C_c_ $\text{NO}_2+\text{N}_2\text{O}$
	Combination	120	20	20	0	3	C_a_ NO_3+NO_2
	Combination	120	13	13	13	3	C_a_ $\text{NO}_3+\text{NO}_2+\text{N}_2\text{O}$

* Batch test type notation is as follows: feeding strategy (decoupled: D or coupled: C), different feeding scenarios (COD/N or ratio of electron acceptors where these were supplied in combination) labeled by letters (a, b, c, or d), and electron acceptor present (NO_3^- , NO_2^- , N_2O , or combinations). Batch test scenarios are used in subsequent figures to differentiate dosing schemes.

3.2.3 Chemical Analysis

For each set of batch assays, NO_3^- , NO_2^- and phosphate (PO_4^{3-}) were measured with an automated Continuous Flow Analyzer (CFA) (Skalar, Netherlands) based on standard colorimetric methods¹⁴⁶. Acetate and N_2O were measured using a GC-FID and GC-ECD (Thermo Fisher Scientific, USA), respectively. A detailed description for these measurements is provided in the supporting information (SI). The mass transfer coefficient within the reactor vessel used for batch assays was modeled to calculate the total and dissolved N_2O produced¹⁷⁰. MLSS and MLVSS were measured using standard methods for each batch test¹⁴⁶.

3.2.4 Calculation of Electron Consumption and Electron Distribution Among Different Steps of Denitrification

The maximum NO_3^- , NO_2^- and N_2O reduction rates were calculated through linear regression of the NO_3^- , NO_2^- and N_2O profile in batch assays. The observed biomass-specific NO_3^- , NO_2^- and N_2O ($r_{\text{NO}_3^-,0}$, $r_{\text{NO}_2^-,0}$, and $r_{\text{N}_2\text{O},0}$, [mg N/(gVSS•h)]) were determined by dividing the maximum NO_3^- , NO_2^- and N_2O reduction rates by the MLSS concentration measured based on standard methods. With the assumption of minimal accumulation of NO, the reduction rate of NO is assumed to be equal to the reduction rate of NO_2^- . Calculations for electron consumption rate and electron distribution are based on methods reported previously^{112, 113}.

The true reduction rate of each nitrogen oxide was calculated based on the observed reduction rate:

$$r_{\text{NO}_3^-} = r_{\text{NO}_3^-,0}$$

$$r_{\text{NO}_2^-} = r_{\text{NO}_2^-,0} + r_{\text{NO}_3^-}$$

$$r_{\text{NO}} = r_{\text{NO}_2^-,0}$$

$$r_{\text{N}_2\text{O}} = r_{\text{N}_2\text{O},0} + r_{\text{NO}}$$

where $r_{\text{NO}_3^-}$, $r_{\text{NO}_2^-}$, r_{NO} , and $r_{\text{N}_2\text{O}}$ (mg N/(gVSS•h)) are the true reduction rate of NO_3^- , NO_2^- , NO and N_2O , respectively.

The electron consumption rate by each denitrification enzyme (NAR, NIR, NOR, and NOS) was calculated as follow:

$$r_{\text{NAR},e} = \frac{r_{\text{NO}_3^-}}{14} \times 2$$

$$r_{\text{NIR},e} = \frac{r_{\text{NO}_2^-}}{14} \times 1$$

$$r_{\text{NOR},e} = \frac{r_{\text{NO}}}{14} \times 1$$

$$r_{\text{NOS},e} = \frac{r_{\text{N}_2\text{O}}}{14} \times 1$$

where $r_{\text{NAR},e}$, $r_{\text{NIR},e}$, $r_{\text{NOR},e}$, and $r_{\text{NOS},e}$ (mmol e^- /(gVSS•h)) are the electron consumption rate of NAR, NIR, NOR, and NOS, respectively.

The distribution of electron among different denitrification enzyme is determined with the following equation:

$$\text{Electron distribution (\%)} = \frac{r_{\text{NOX},e}}{r_{\text{NAR},e} + r_{\text{NIR},e} + r_{\text{NOR},e} + r_{\text{NOS},e}} \times 100\%$$

where $r_{\text{NOX},e}$ is the electron consumption rate of NAR or NIR or NOR or NOS.

3.3 Results and Discussion

3.3.1 *Ex situ* Batch Assays Reveal Distinctive Kinetics with Different Nitrogen Oxides as Electron Acceptors

Prior to *ex situ* batch assays, the parent SBR was inoculated with biomass from a full-scale EBPR process and operated for over a year as a denitrifying EBPR process (alternating anaerobic/anoxic conditions) followed by a short aerobic polishing phase. 40-50 mg-N/L NO_2^- was fed at the start of the anoxic phase to simulate effluent from an upstream nitrification process and to select for reactor biomass adapted to elevated NO_2^- . Stable and complete COD and N removal accompanied by P uptake under anoxic conditions was achieved. A representative SBR cycle is shown in Figure S3.1. To compare denitrification kinetics of DPAO-enriched biomass using different electron acceptors, *ex situ* denitrifying P uptake tests were conducted with various nitrogen oxides species and concentrations under decoupled and coupled feeding strategies. We highlight qualitative trends in this section from these batch assays, and provide quantitative metrics for denitrification and P uptake kinetics in subsections 3.3.1.1 and 3.3.1.2.

Figure 3.1a shows the transformation of key substrates when a single electron acceptor (NO_3^- , NO_2^- , or N_2O , 40 mg-N/L) was dosed (COD/N ratio=3) under decoupled (Figure 3.1a, top figures) and coupled (Figure 3.1a, bottom figures) feeding strategies. Under the decoupled strategy, acetate was first consumed under anaerobic conditions for PHA synthesis and P release (data not shown). The average P-release/acetate-uptake ratio in decoupled feeding batch assays ($D_c \text{NO}_3/\text{NO}_2/\text{N}_2\text{O}$) of exogenous electron donor (acetate, anaerobic phase) was 0.3 ± 0.1 P-mol/C-mol. The expected value for a highly enriched PAO culture is 0.5 P-mol/C-mol, which suggests that part of the acetate provided was consumed by other non-PAO bacteria^{171, 172}. When

acetate was completely depleted after one hour anaerobic period (confirmed by GC measurement, data not shown), nitrogen oxide(s) was supplied as electron acceptor(s) (anoxic conditions), and intracellular PHAs served as electron donor for nitrogen oxide(s) reduction and P uptake by DPAOs (Figure 3.1a, D_c_NO₃/NO₂/N₂O). In contrast, under the coupled feeding strategy, instead of using PHAs as an internal electron donor, acetate was supplied with nitrogen oxide(s), and was used directly as an external electron donor (Figure 3.1a, C_c_NO₃/NO₂/N₂O). P release accompanied acetate consumption under anoxic conditions in the coupled feeding parallels previous observations, and P uptake was only observed after acetate was completely consumed. P release in the presence of both acetate and nitrogen oxides likely derives from the utilization of acetate for both PHAs production (accompanied by P release) and denitrification¹⁷³. The P-release/COD-uptake ratios under anoxic conditions in the coupled feeding assays using NO₃⁻, NO₂⁻ and N₂O as the terminal electron acceptor were 0.2±0.0, 0.1±0.0 and 0.2±0.0 P-mol/C-mol, respectively. This further suggests activity of both PAOs and non-PAOs in consuming acetate, based on comparison to PAO stoichiometry¹⁷⁴.

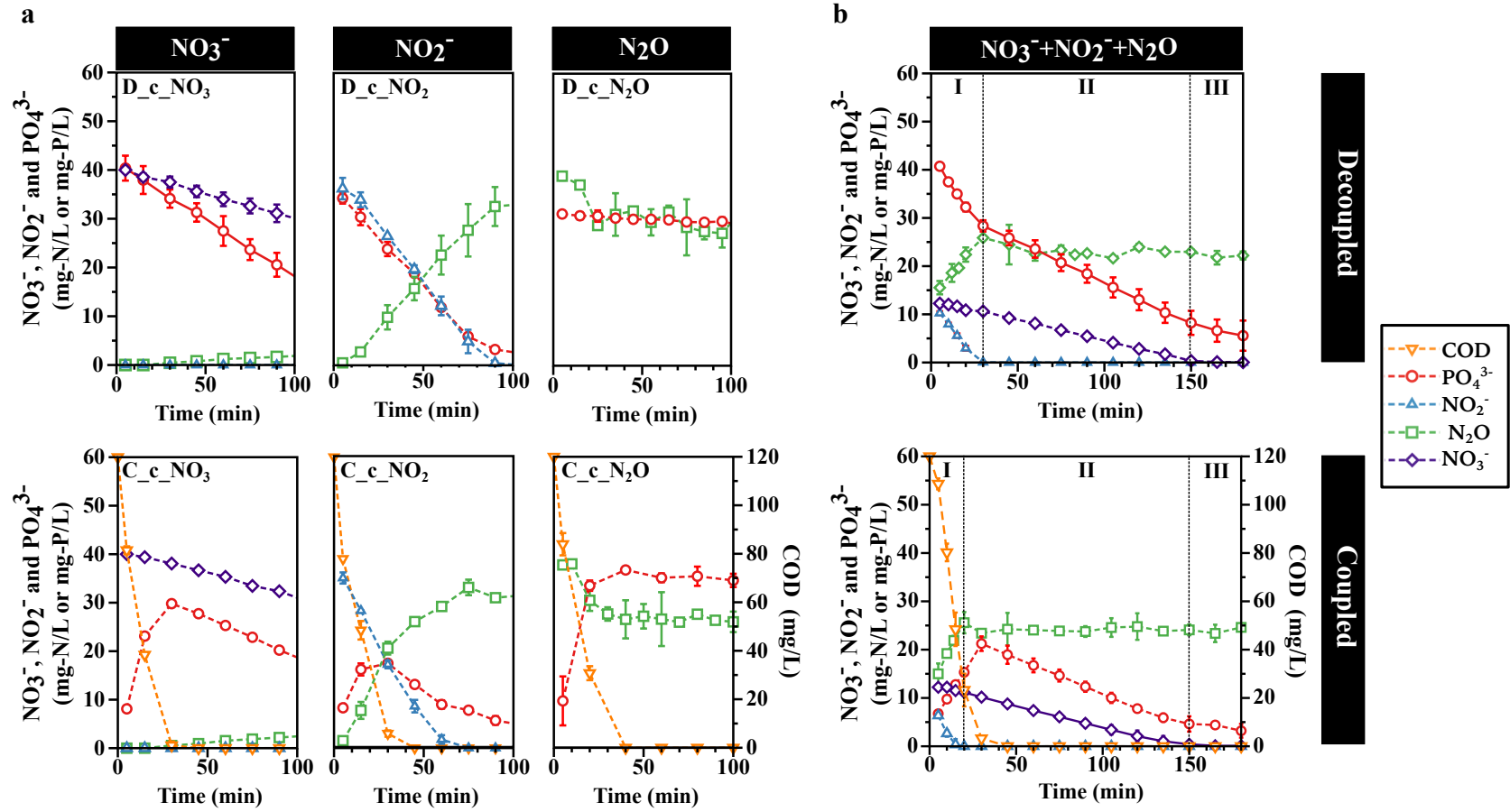


Figure 3.1 Concentration profiles of key substrates (NO_3^- , NO_2^- , N_2O , PO_4^{3-} and COD) in selected ex situ batch tests during the anoxic period with decoupled or coupled feeding of COD as electron donor.

(a): a single nitrogen oxide was used as electron acceptor (top figures: decoupled feeding, bottom figures: coupled feeding). Dosing schemes in the figure correspond to batch test scenario in Table 3.1. In all assays, the initial concentrations of nitrogen oxide and COD (acetate) were 40 mg-N/L and 120 mg COD/L, respectively. For decoupled feeding ($\text{D_c_NO}_3/\text{NO}_2/\text{N}_2\text{O}$), the conversion of COD (acetate) to intracellular PHAs during the preceding anaerobic period (prior to NO_x dosing) is not shown. The initial P concentration in decoupled feeding assays ($\text{D_c_NO}_3/\text{NO}_2/\text{N}_2\text{O}$) is the concentration of P after anaerobic P release. In the coupled feeding mode ($\text{C_c_NO}_3/\text{NO}_2/\text{N}_2\text{O}$), P concentration equals the initial P concentration in the parent reactor (measured 5 min after adding acetate and nitrogen oxide). Error bars in the figures are standard deviations based on duplicate experiments. (b): a combination of three nitrogen oxides was used as electron acceptor (top figure: decoupled feeding ($\text{D_a_NO}_3+\text{NO}_2+\text{N}_2\text{O}$), bottom figure: coupled feeding ($\text{C_a_NO}_3+\text{NO}_2+\text{N}_2\text{O}$)). The batch assay was separated into three different phases corresponding to different combinations of electron acceptors: I: $\text{NO}_3^-+\text{NO}_2^-+\text{N}_2\text{O}$; II: $\text{NO}_3^-+\text{N}_2\text{O}$; III: N_2O .

To better understand the behavior and interactions among different nitrogen oxides, a combination of all three N species (NO_3^- , NO_2^- and N_2O) was applied under both decoupled and coupled strategies, and distinct dynamics of these three species was observed (Figure 3.1b). In both cases, NO_2^- was rapidly used up within 30 minutes (phase I). This did not affect the NO_3^- reduction rate, as it stayed approximately constant throughout the reaction time. Interestingly, N_2O accumulation was only observed in the presence of NO_2^- (phase I). Accumulation ceased once NO_2^- was depleted, but denitrification with NO_3^- continued (phase II). Indeed, the N_2O concentration was approximately constant after NO_2^- was depleted, and remained nearly constant even after NO_3^- was depleted and N_2O was the sole available electron acceptor for denitrification. P uptake rate decreased when NO_2^- was depleted (Figure 3.1b, top, phase I to II) under the decoupled feeding strategy. Based on the limited number of measurements after NO_3^- was fully depleted (phase II to III), it was not possible to elucidate a change in P uptake rate.

3.3.1.1 Differential denitrification capabilities using different electron acceptors

As shown in Figure 3.1a, the nitrogen oxide(s) concentration in all *ex situ* batch assays was continuously reduced (except for N_2O , where reduction appeared to cease after ~40 minute of reaction) under both decoupled (Figure 3.1a, D_c_ $\text{NO}_3^-/\text{NO}_2^-/\text{N}_2\text{O}$) and coupled (Figure 3.1a, C_c_ $\text{NO}_3^-/\text{NO}_2^-/\text{N}_2\text{O}$) feeding strategies. After long-term NO_2^- feeding in the mother reactor, both NO_3^- and N_2O reduction rates were limited compared with the NO_2^- reduction rate. This pattern held when only a single electron acceptor (nitrogen oxide) was added, and when all three nitrogen oxides were added together in both coupled and decoupled feeding strategies (Figure 3.2a and Figure S3.2a). For instance, based on single electron acceptor addition feeding scenarios (scenarios D_c and C_c in Table 3.1), the NO_3^- and N_2O reduction rates were 1.6 ± 0.0 and 2.9 ± 0.6 mg-

N/(gVSS•h), respectively, in coupled feeding assays, and 1.5 ± 0.2 and 0.8 ± 0.2 mg-N/(gVSS•h) in decoupled feeding assays. In contrast, the NO_2^- reduction rate was 8.9 ± 0.9 mg-N/(gVSS•h) and 6.4 ± 1.4 mg-N/(gVSS•h) under coupled and decoupled feeding modes, respectively. The negligible accumulation of NO_2^- during NO_3^- reduction (Figure 3.1a, D and C_c_ NO_3) also indicated a rapid NO_2^- reduction rate. Reduction rates for NO_2^- and N_2O were consistently higher under coupled feeding compared to decoupled feeding (ANOVA $p<0.05$), suggesting that an exogenous electron donor (acetate) was better suited for heterotrophic NO_2^- and N_2O driven denitrification than intracellular PHAs. No significant differences in terms of nitrogen oxide reduction rates were observed using different concentrations of nitrogen oxides (ANOVA $p>0.05$) (Figure 3.2a).

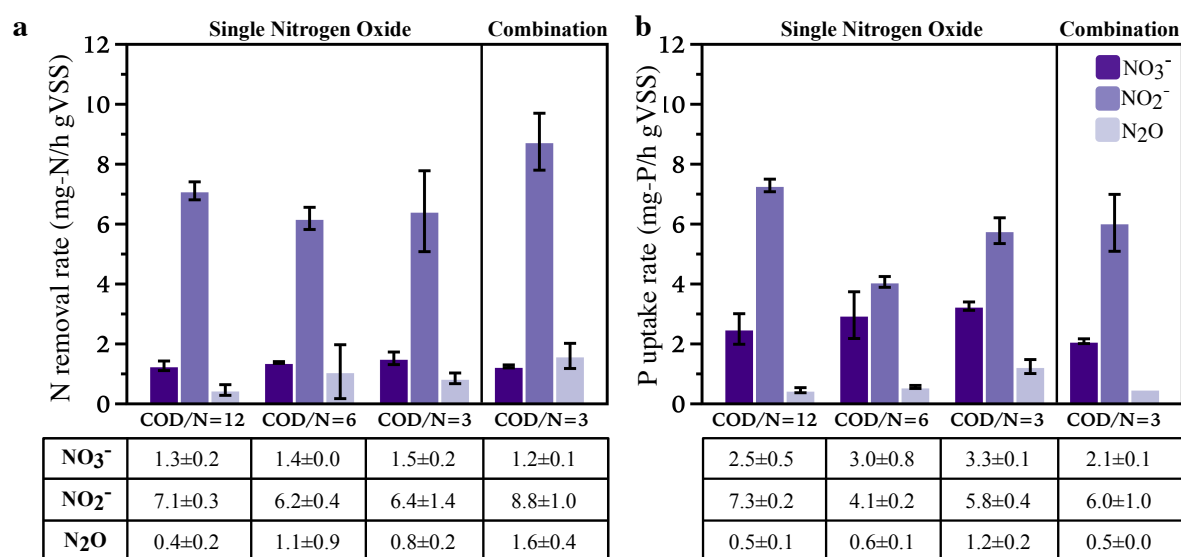


Figure 3.2 (a) N removal rates (mg-N/h•gVSS) and (b) denitrifying P uptake rates (mg-P/h•gVSS) by DPAO-enriched biomass with different dosing schemes (scenarios D_a,b,c_ $\text{NO}_3/\text{NO}_2/\text{N}_2\text{O}$ and D_a_ $\text{NO}_3+\text{NO}_2+\text{N}_2\text{O}$ in Table 3.1 in decoupled feeding mode.

Results for batch assays in coupled feeding mode are shown in Figure S3.2. Dosing schemes vary by nitrogen oxide (electron acceptor) concentrations, and therefore also by COD/N ratio. x-axis labels refer to the following conditions: single nitrogen oxide: COD/N=12 (10 mg-N/L, D_a), COD/N=6 (20 mg-N/L, D_b), and COD/N=3 (40 mg-N/L, D_c); combination: COD/N=3, combination of 13 mg-N/L of each nitrogen oxide (NO_3^- , NO_2^- and N_2O , D_a_ $\text{NO}_3+\text{NO}_2+\text{N}_2\text{O}$).

3.3.1.2 Distinctive P uptake kinetics with different electron acceptors

We observed similar differences in kinetics for P uptake as for denitrification in *ex situ* batch assays with different nitrogen oxides supplied as terminal electron acceptors. In decoupled feeding mode, significantly lower denitrifying P uptake rates were observed when NO_3^- or N_2O was supplied as the electron acceptor than when NO_2^- was supplied (Figure 3.2b). For example, when the initial nitrogen oxide concentration was 40 mg-N/L (Figure 3.2b, COD/N=3), the denitrifying P uptake rates were 3.3 ± 0.1 , 5.8 ± 0.4 and 1.2 ± 0.2 mg-P/(gVSS•h) for NO_3^- , NO_2^- and N_2O , respectively. Varying the concentration of NO_3^- did not substantially vary P uptake rate (ANOVA $p > 0.05$). However, varying the initial concentration of NO_2^- and N_2O significantly impacted the P uptake rate (ANOVA $p < 0.05$). Taken together, these results suggest that the DPAO-enriched biomass strongly favors NO_2^- as the electron acceptor for denitrifying P uptake, putatively due to long-term exposure and adaptation to a high NO_2^- feed. Interestingly, under coupled feeding conditions, a significant decrease in the P uptake rate was observed relative to decoupled feeding, particularly for NO_2^- driven P uptake (Figure S3.2b). This suggests that the non-PAO denitrifying population was better suited to use acetate rather than an internal electron donor (PHAs) for denitrification, and more COD (acetate) was routed towards direct denitrification by non-PAOs under the coupled feeding mode.

3.3.1.3 NO_3^- and NO_2^- driven N_2O production

Batch assays revealed that N_2O production during denitrifying P uptake depended strongly on type of nitrogen oxide available as electron acceptor (ANOVA $p < 0.001$), but did not vary significantly with feeding strategy (coupled vs. decoupled feeding) or COD/N ratio (ANOVA $p > 0.05$). In the presence of different concentrations of NO_2^- , high levels of N_2O accumulation were

observed under both coupled ($77.0 \pm 6.0\%$) and decoupled ($71.7 \pm 10.6\%$) feeding modes. This observation held even under high COD/N conditions ($\text{COD/N} > 3$) and coupled feeding conditions when lower N_2O accumulation was reported in other studies^{112, 134, 175}, demonstrating a strong propensity for generation of N_2O via incomplete denitrification even in the presence of excess electron donor. However, substantially lower accumulation of N_2O was observed when NO_3^- instead of NO_2^- was added as electron acceptor (coupled mode: $20.7 \pm 3.1\%$ and decoupled mode: $13.3 \pm 3.1\%$, average across different COD/N).

This strong propensity for NO_2^- driven N_2O accumulation was also supported when all three nitrogen oxides were simultaneously present in the anoxic period (Figure 3.1b). In this case, N_2O accumulation was only observed when NO_2^- was present in both decoupled and coupled feeding modes. 23 mg-N/L ($\sim 60\%$ of the total N loading) remained in the form of N_2O at the end of the tests. Very little production of denitrification intermediates (NO_2^- and N_2O) was detected after the dosed NO_2^- was fully consumed and NO_3^- reduction was still observed.

A diversity of *Accumulibacter* ecotypes have so far been discovered^{89, 176}. However, the diverse metabolic capabilities of *Accumulibacter*-enriched biomass to utilize different electron acceptors, including oxygen (O_2), NO_3^- and NO_2^- , are still little understood, particularly after long-term adaptation to NO_3^- and/or NO_2^- . In Table 3.2, we summarize N and P transformation kinetics reported in this study and in the literature for selected PAO/DPAO enriched biomass from reactors operated with different electron acceptors (aerobic, O_2 , or anoxic, NO_2^- or NO_3^-) and for heterotrophic denitrifiers. The intent of this table is to clarify long-term impact of reactor redox conditions on the capability (and kinetics) for utilizing different nitrogen oxides (NO_2^- and NO_3^-) for denitrification and denitrifying P uptake by PAO/DPAO enriched biomass, and compare NO_2^-

and NO_3^- reduction rates with heterotrophic denitrifiers. Taken together, results in Table 3.2 suggest that DPAO-enriched biomass exposed during long-term reactor operation to elevated levels of NO_2^- (as in this study) is better adapted (e.g. displays faster kinetic) to NO_2^- than NO_3^- for both denitrification and denitrifying P uptake. Conversely, in PAO-enriched biomass from reactors operated for NO_3^- or O_2 driven P removal, higher NO_3^- than NO_2^- driven denitrification and P uptake rates were observed. It is possible that the observed strong differences in NO_2^- versus NO_3^- utilization kinetics by PAO enriched biomass in Table 3.2 are due to the selection for EBPR biomass enriched with distinct *Accumulibacter* ecotypes and/or non-PAO denitrifiers with differential genomic capacities for different steps in the denitrification pathway. However, higher or comparable maximum NO_2^- reduction rate compared to NO_3^- was also observed by heterotrophic denitrifying biomass^{114,177}. A more extended list of kinetic values for pure and mixed culture heterotrophic denitrifiers can be found in Read-Daily et al.¹⁷⁸. A further understanding of these metabolic differences requires additional investigation on both typical denitrification and DPAO-enriched systems.

Table 3.2 Comparison of N and P transformation rates.

Reactor Description	Short-term electron acceptor	Initial NO ₃ ⁻ or NO ₂ ⁻ concentration (mg-N/L)	Specific NO ₃ ⁻ or NO ₂ ⁻ reduction rate (mg-N/(gVSS•h))	Specific P uptake rate (mg-N/(gVSS•h))	Enrichment culture	Reference
SBR fed with NO ₂ ⁻	NO ₂ ⁻	40	6.4±1.4	5.8 ± 0.4	DPAO	This study
	NO ₃ ⁻	40	1.6±0.0	3.3 ± 0.1		
SBR fed with NO ₂ ⁻	NO ₂ ⁻	11	6.8 ± 0.2	9.3 ± 0.3	DPAO	164
	NO ₃ ⁻	34	4.0 ± 0.2	4.8 ± 0.1		
SBR fed with NO ₃ ⁻	NO ₂ ⁻	20	13.9 ± 0.2	-	DPAO	113
	NO ₃ ⁻	20	15.9 ± 2.4	-		
SBR fed with NO ₃ ⁻	NO ₂ ⁻	75	8.7	-	DGAO	179
	NO ₃ ⁻	60	16.6	-		
SBR with anaerobic /aerobic period	NO ₂ ⁻	40	5.1	5.3	PAO	166
	NO ₃ ⁻	60	12.9	8.4		
SBR with anaerobic/ micro-aerobic period	NO ₂ ⁻	25	2.8 ± 1.0	5.6 ± 1.0	PAO	176
	NO ₃ ⁻	25	5.5 ± 0.1	11 ± 1.7		
SBR fed with methanol and NO ₃ ⁻	NO ₂ ⁻	30	5.3	-	Heterotrophic denitrifier	112
	NO ₃ ⁻	30	3.2	-		
SBR fed with acetate and NO ₃ ⁻	NO ₂ ⁻	-	10.8	-	Heterotrophic denitrifier	177
	NO ₃ ⁻	-	12.9	-		
Step feed reactor with acetate and NO ₃ ⁻	NO ₃ ⁻	40	9.1 ± 0.5 (NO ₂ ⁻)	-	Heterotrophic denitrifier	180*
			11.7 ± 0.5 (NO ₃ ⁻)	-		

* NO₃⁻ and NO₂⁻ reduction rates were calculated when NO₃⁻ was supplied as electron acceptor and NO₂⁻ accumulation was observed.

3.3.2 Electron Competition and Distribution under Coupled and Decoupled Feeding Strategies

In denitrification, the reduction of nitrogen oxides consumes electrons supplied by the oxidation of an electron donor. Competition for electrons (reducing equivalents from intracellular electron carriers, such as NADH) among four denitrification enzymes (NAR, NIR, NOR and NOS) has been hypothesized to be partly responsible for N₂O accumulation during denitrification^{112, 113, 168}. We thus assessed the role of electron competition in driving N₂O production in the DPAO enrichment culture under both coupled and decoupled feeding modes in response to (1) presence of a single nitrogen oxide as electron acceptor (NO₃⁻, NO₂⁻ or N₂O alone); (2) presence of concurrent nitrogen oxides (NO₃⁻ and NO₂⁻, NO₂⁻ and N₂O); and (3) presence of three nitrogen oxides. Due to the lower observed reduction rates and thus putative less intense electron competition, the combination of NO₃⁻ and N₂O was not tested. Electron consumption rate and electron distribution were calculated based on half reactions for different nitrogen oxides and nitrogen species profiles during the *ex situ* batch tests, following methods reported by Pan et al. (2013) and Ribera-Guardia et al. (2016).

Figure 3.3a and S3.3a illustrate electron consumption rate and electron distribution among NAR, NIR, NOR, and NOS in decoupled and coupled feeding tests. When NO₃⁻ was the only nitrogen oxide dosed as electron acceptor (Scenarios D_a,b,c_NO₃ in Figure 3.3), the total electron consumption rate (sum of electron consumption rates of all four nitrogen reductases) slightly increased as the concentration of initial NO₃⁻ increased (from 10 mg-N/L to 40 mg-N/L). The electron distributions among the 4 different denitrification enzymes were indistinguishable among all three scenarios (Scenarios D_a,b,c_NO₃, ANOVA p>0.05). The addition of NO₂⁻ together with NO₃⁻ (Scenarios D_a_NO₃+NO₂ and D_a_NO₃+NO₂+N₂O) significantly increased the total

electron consumption rate as well as the proportion of electrons consumed by NIR and NOR. The strong stimulation of electron consumption rate by NO_2^- suggests that a portion of the biomass microbial community could only utilize (or was far better adapted to utilizing) NO_2^- , but not NO_3^- , for denitrification.

Substantially different patterns of electron distribution and consumption rates were observed when NO_2^- rather than NO_3^- was used instead as the sole electron acceptor for the decoupled feeding tests (Scenarios D_a,b,c,d_ NO_2 , Figure 3.3a and S3.3a). The electron consumption rate was substantially higher compared with NO_3^- feeding, suggesting that electron supply did not limit NO_3^- reduction. However, when varying NO_2^- concentration (different COD/N ratios), the total electron consumption rates for NIR, NOR and NOS were nearly identical (scenarios D_a,b,c,d_ NO_2 , ANOVA $p > 0.05$). Electron equivalents were unevenly distributed among these three enzymes, with the majority distributed to NIR and NOR (~40% to 50%), and minority distributed to NOS (<20%) (Figure S3.3a, D_a,b,c,d_ NO_2). Even with the addition of N_2O (Figure 3.3a and S3.3a, Scenarios D_a,b,c_ $\text{NO}_2 + \text{N}_2\text{O}$), the majority of electrons (>80%) were still utilized by NIR and NOR.

We also calculated the electron consumption rate and electron distribution for batch assays with a coupled feeding strategy (Figure 3.3b and S3.3b). Electron consumption rates with coupled feeding for each scheme (scheme C_c_ $\text{NO}_3/\text{NO}_2/\text{N}_2\text{O}$, C_a_ $\text{NO}_3 + \text{NO}_2$, C_a_ $\text{NO}_3 + \text{N}_2\text{O} + \text{N}_2\text{O}$, and C_a,b,c_ $\text{NO}_2 + \text{N}_2\text{O}$) are slightly higher than those under decoupled mode when COD/N=3 (ANOVA $p < 0.05$). This could be due to the more diverse microbial consortia capable of utilizing acetate directly compared to uptake of acetate under anaerobic conditions and subsequent use of intracellular PHAs as the electron donor for denitrification⁸. Regardless of the differences in

electron consumption rates, the electron distribution between denitrification enzymes under both feeding modes was statistically indistinguishable (ANOVA $p > 0.05$). The nearly identical electron distribution pattern across multiple COD/N ratios under both decoupled and coupled feeding conditions provides additional evidence that the four denitrification enzymes (NAR, NIR, NOR and NOS) did not compete for electrons in this system. This result agrees with our observation that the electron consumption rate by NOS (for N_2O reduction) in both feeding schemes was slow even when only N_2O was present as a terminal electron acceptor (scenario c_ N_2O).

If patterns in rates of electron consumption and distribution were due primarily to electron competition between denitrification structural enzymes, higher N_2O reduction rates would be expected in the absence of competing electron acceptors. The electron consumption rate by NOS was not statistically significantly different (ANOVA $p > 0.05$) when N_2O was supplied alone (Figure 3.3, D_c_ N_2O and C_c_ N_2O) compared to when it was supplied with NO_2^- or NO_3^- (Figure 3.3, D/C_a,b,c_ NO_2+N_2O , D/C_a_ $NO_3+NO_2+N_2O$). This result indicates that electron competition alone does not limit the reduction rate of N_2O . Importantly, it further suggests that competition for reducing equivalents between NAR, NOR, NIR, and NOS cannot by itself explain the unusually high observed levels of N_2O generation we observed in this study when NO_2^- is present.

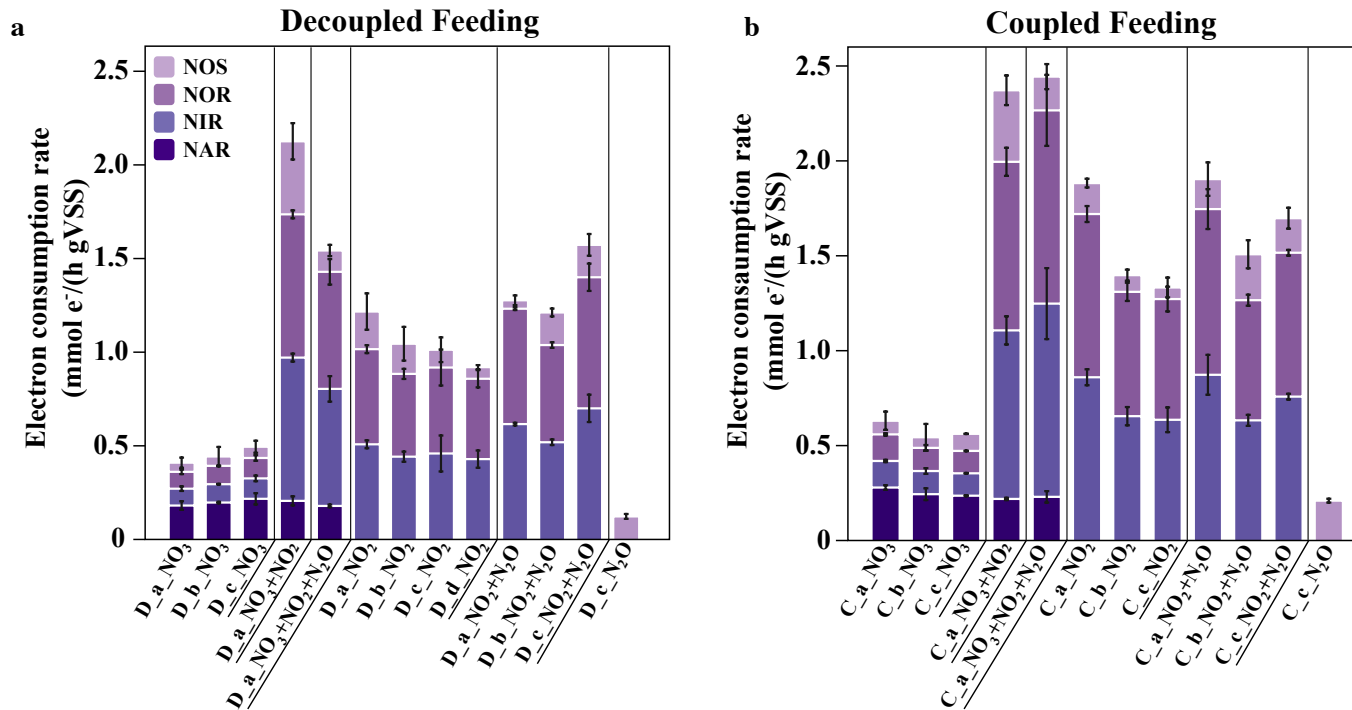


Figure 3.3 Electron consumption rates for different denitrification enzymes (NAR: nitrate reductase, NIR: nitrite reductase, NOR: nitric oxide reductase, NOS: nitrous oxide reductase) under decoupled (a) and coupled (b) feeding modes.

Dosing schemes in x-axes correspond to batch test scenario in Table 3.1, and vary based on concentration and type of nitrogen oxides supplied as electron acceptor(s) (NO_3^- , NO_2^- , and/or N_2O). Dosing scheme: a,b,c_ NO_x : varying concentrations of NO_x (10 mg-N/L, 20 mg-N/L and 40 mg-N/L); a_ $\text{NO}_3+\text{NO}_2+\text{N}_2\text{O}$: 13 mg-N/L each of NO_3^- , NO_2^- and N_2O ; a,b,c_ $\text{NO}_2+\text{N}_2\text{O}$: different combinations of NO_2^- and N_2O ; a_ NO_3+NO_2 : 20 mg-N/L NO_3^- and NO_2^- ; D_d_ NO_2 : 60 mg N/L NO_2^- . Complete details of nitrogen oxide dosing concentrations can be found in Table 3.1.

3.4 Conclusions

Accumulation of N_2O during denitrification by DPAOs could be affected by several environmental factors, including using an internal carbon source as electron donor. Electron competition has been proposed to explain the formation of N_2O under carbon limiting conditions (low COD/N ratio). Our results suggested that long-term exposure to elevated NO_2^- (40-50 mg-N/L) selected for a microbial consortium with distinctive nitrogen oxides reduction capabilities. More specifically, *ex situ* batch tests demonstrated a strong kinetic advantage for DPAOs in this system to use NO_2^- rather than NO_3^- , and further demonstrated extremely slow kinetics for N_2O reduction, even in the absence of other potentially competing electron acceptors. Moreover, a strong propensity for incomplete denitrification and consequent accumulation of N_2O was observed when NO_2^- served as electron acceptor. Electron competition was investigated by exploring electron consumption rates and electron distribution among four denitrification enzymes NAR, NIR, NOR and NOS. Results suggested that electron competition between core denitrification enzymes could not by itself explain unusually the high levels of N_2O production in our CANDO+P process after long term NO_2^- fed.

Two additional hypotheses for N_2O generation, *Accumulibacter* (PAO) with truncated denitrification pathways and flanking bacterial (non-PAO) organisms with truncated denitrification pathways lacking nitrous oxide reductase warrant further investigation. Genome-resolved metagenomic sequencing was employed to explore these two hypotheses in the next chapter.

3.5 Supporting Information

3.5.1 Supporting Information - Methods

Chemical analyses

Acetate and N₂O were measured using a GC-FID (Fisher-Thermo scientific, USA) with a TR-FFAP column. A 1 μL sample was injected into the GC with 50:1 split ratio with constant flow rate of 1 ml/min. Helium was used as carrier gas. The following temperature program was used: initial, 70 °C for 1 min, 10 °C/min up to 180°C, and holding at 180 °C for 6 min. Gas phase N₂O was measured by GC-ECD with a TG-BOND Q column. 100 μL of gas sample was injected with a split ratio of 50:1 and column flow of 5 ml/min using helium as carrier gas. An isothermal temperature program was used with oven temperature setpoint of 35°C with backflush started 3 min after injection. The detector temperature was 250 °C and N₂ was used as makeup gas.

3.5.2 Supporting Information - Figures

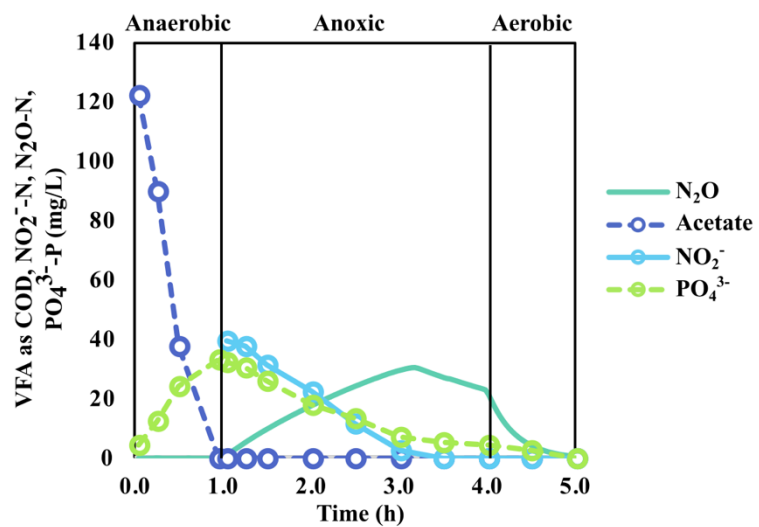


Figure S3.1 A typical SBR cycle profiling the transformation of key C, N and P components (acetate as COD, NO₂⁻, dissolved N₂O and PO₄³⁻).

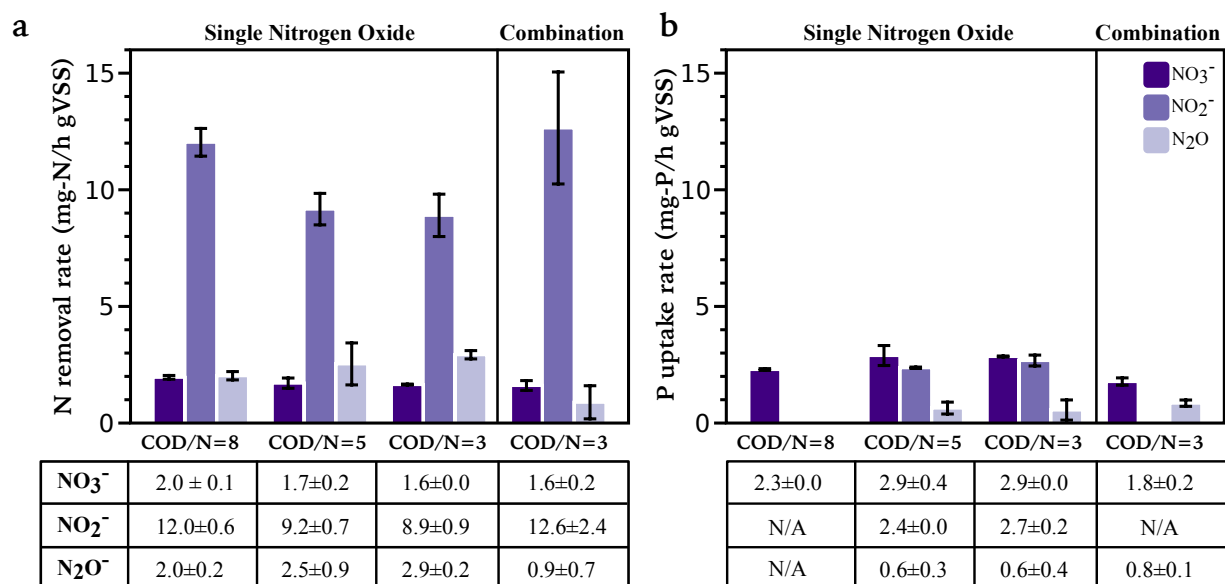


Figure S3.2 (a) N removal rate (mg-N/h·gVSS) and **(b)** denitrifying P uptake rate (mg-P/h·gVSS) by DPAO-enriched biomass with different dosing schemes in coupled feeding mode (simultaneous addition of COD [acetate] and nitrogen oxide(s) with 40 mg-N/L of nitrogen oxides).

x-axis labels refer to following conditions: single nitrogen oxide: COD/N=8 (320mg COD/L, C_a), COD/N=5 (200 mg COD/L, C_b), and COD/N=3 (120mg COD/L, C_c); combination: COD/N=3 (39 mg-N/L, combination of 13mg-N/L of each nitrogen oxide (NO_3^- , NO_2^- and N_2O), C_a_ $\text{NO}_3+\text{NO}_2+\text{N}_2\text{O}$). The NO_2^- driven P uptake rate is unavailable (when COD/N = 8 and 5) due to the rapid reduction rate of NO_2^- and lack of electron acceptor after COD was completely consumed. The P uptake rate for N_2O when COD/N=3 is not shown due to the large standard deviation for the duplicate experiments.

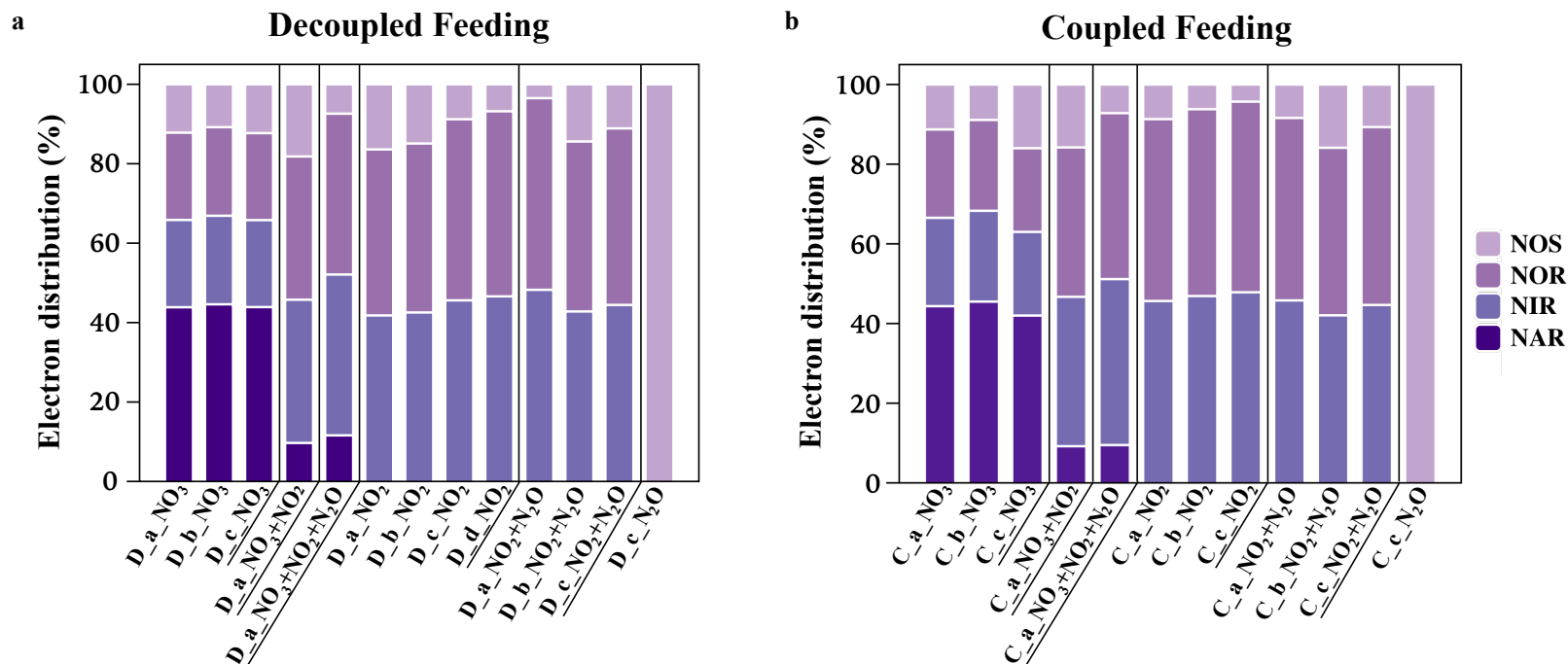


Figure S3.3 Electron distribution for different denitrification enzymes (NAR: nitrate reductase, NIR: nitrite reductase, NOR: nitric oxide reductase, NOS: nitrous oxide reductase) under (a) decoupled and (b) coupled feeding modes.

Dosing schemes in x-axes in the figure correspond to batch test scenario in Table 3.1, and vary based on concentration and type of nitrogen oxides supplied as electron acceptor(s) (NO₃⁻, NO₂⁻, and/or N₂O). Dosing scheme: a,b,c_NOx: varying concentrations of NOx (10 mg-N/L, 20 mg-N/L and 40 mg-N/L); a_NO₃+NO₂+N₂O: 13 mg-N/L each of NO₃⁻, NO₂⁻ and N₂O; a,b,c_NO₂+N₂O: different combinations of NO₂⁻ and N₂O; a_NO₃+NO₂: 20 mg-N/L NO₃⁻ and NO₂⁻; D_d_NO₂: 60 mg N/L NO₂⁻. Complete details of nitrogen oxide dosing concentrations can be found in Table 3.1.

CHAPTER 4

Metagenomics Analysis Reveals Potential N₂O Producers in a Nitrite-fed Denitrifying Biological Phosphorus Removal Process Enriched in *Candidatus Accumulibacter*

This chapter has been submitted for review: Gao, H., Mao, Y., Zhao, X., Liu, W., Zhang T. and Wells, G.F. Metagenomic Analysis Reveals Potential N₂O Producers in a Nitrite-fed Denitrifying Biological Phosphorus Removal Process Enriched in *Candidatus Accumulibacter* (*In review*).

ABSTRACT

Nitrous oxide (N_2O) is a potent greenhouse gas and an obligate intermediate in denitrification. Substantial N_2O accumulation has been reported in denitrifying enhanced biological phosphorus removal (EBPR) bioreactors enriched in denitrifying polyphosphate accumulating organisms (DPAOs), but little is known about underlying mechanisms for N_2O generation nor the long-term impact of NO_2^- feed on DPAO-enriched consortia. To address this knowledge gap, we employed genome-resolved metagenomics to investigate nitrogen transformation potential in a denitrifying EBPR bioreactor enriched in *Candidatus Accumulibacter* and prone to N_2O accumulation. Our analysis yielded 41 near-complete draft genomes, including two co-occurring *Accumulibacter* strains affiliated with clades IA and IC (the first published genome from this clade) and a diverse flanking denitrifying community. The dominant *Accumulibacter* clade IA encoded genes for complete denitrification, while the lower abundance *Accumulibacter* clade IC harbored all denitrification genes except for nitric oxide reductase. An evaluation of denitrification machinery in all publicly available *Accumulibacter* genomes suggested that type I *Accumulibacter* harbored more complete denitrification pathways compared to type II *Accumulibacter*, indicating that type I *Accumulibacter* may be better adapted to denitrifying systems. Analysis of 39 flanking bacterial genomes revealed a prevalence of taxa harboring incomplete denitrification pathways, and an increasing abundance of putative N_2O producers that lack N_2O reductase. Our results suggest that the unusually high levels of N_2O production observed in this *Accumulibacter*-enriched consortium is linked in part to the selection for flanking microorganisms with truncated denitrification pathways.

4.1 Introduction

Enhanced biological phosphorus removal (EBPR) processes are widely used as an efficient method for phosphorus (P) removal and recovery during wastewater treatment. The key functional group in EBPR processes is known as polyphosphate accumulating organisms (PAOs)⁶⁰. When subjected to alternating anaerobic/oxic conditions, PAOs take up dissolved P under oxic conditions, and removal of microbial biomass can then lead to effective P removal. A subset of PAOs, termed denitrifying PAOs (DPAOs), are also capable of P uptake under anoxic (denitrifying) conditions. When integrated nitrogen (N) and P removal from wastewater is desired, such anoxic P removal via DPAO activity is considered advantageous compared to oxic P removal, as both oxygen (and therefore aeration energy) and organic carbon requirements are curbed¹⁷³. DPAO activity over nitrite (NO₂⁻) rather than nitrate (NO₃⁻) is of particular interest when integrating EBPR with shortcut N removal systems such as nitrification-denitrification (nitrite shunt) that promise oxygen (and energy) savings relative to conventional N removal systems²⁵.

The predominant PAO in most EBPR processes is affiliated with the as-yet-uncultivated “*Candidatus Accumulibacter phosphatis*” (herein *Accumulibacter*)^{181, 182}. Phylogenetic analyses of the polyphosphate kinase gene (*ppkI*) have resolved the *Accumulibacter* genus into two major divisions (type I and II) and 14 clades (clades IA-IE and clades IIA-II-I)^{89, 95, 176, 183, 184}. Denitrifying capabilities of these different *Accumulibacter* clades are not fully understood, and only specific *Accumulibacter* clades are thought to be capable of denitrification^{95, 176, 185}. An evolutionary model of *Accumulibacter* clade IIA was constructed recently to investigate the evolution of metabolic traits that discriminate non-PAO from PAO through ancestral genome construction and the identification of horizontal gene transfer (HGT)⁹². The identification of

laterally derived genes provides insights into the basis for evolution from non-PAO to PAO. However, the evolution of denitrification traits within *Accumulibacter* genotypes has not been well studied, limiting the understanding of N transformations in denitrifying EBPR processes.

The relative abundance of *Accumulibacter* in PAO-enriched systems can vary from 20% to 80%, even in well-controlled lab-scale EBPR bioreactors with stable P removal^{97, 186, 187}. The function of the diverse non-*Accumulibacter* “flanking” community in PAO enrichment cultures is not well studied due to the limited number of metagenomic sequencing studies and the difficulty in extracting genomes for minority community members (below 1% relative abundance) from complex microbial ecosystems from shotgun metagenomes¹⁸⁸. The ability to reconstruct complete or near-complete genomes of rare taxa in microbial communities has greatly expanded with increasing sequencing depth and the development of new automated binning algorithms and softwares¹⁸⁹⁻¹⁹¹.

Wastewater treatment processes, including EBPR processes, have been identified as a potential source of N₂O emissions^{97, 187, 192}. N₂O is a potent greenhouse gas with a global warming potential 310 times higher than that of carbon dioxide (CO₂). It also catalyzes the destruction of stratospheric ozone¹⁹³⁻¹⁹⁵. Microbial denitrification is known to be one of the primary biotic N₂O producing processes^{111, 196}. Complete microbial denitrification involves four enzymatic reactions catalyzed by nitrate reductase (NAP or NAR, NO₃⁻ to NO₂⁻), nitrite reductase (NIR, NO₂⁻ to NO), nitric oxide reductase (NOR, NO to N₂O) and nitrous oxide reductase (NOS, N₂O to N₂)¹⁶⁹. Denitrification is a modular pathway, and the four nitrogen oxide reductases can be activated and regulated with a certain degree of independence¹⁶⁹. Moreover, microbes harboring incomplete (truncated) denitrification pathways that lack one or more of the core nitrogen oxide reductases

have been revealed by genomic analyses^{93, 115, 197-199}. Indeed, a subset of currently available denitrifier genomes lack the gene for NOS, and are therefore indicative of putative N₂O producers¹²⁰. Other denitrifier genomes harboring NOS with or without upstream structural denitrification genes indicate genomic capacity for N₂O consumption. In addition, the presence of NO₂⁻ or its conjugated acid nitrous acid (HNO₂) has been demonstrated to affect the accumulation of N₂O by denitrifiers, and several studies have explored short-term effects of NO₂⁻ during denitrification^{118, 134, 164, 200}. However, the long-term impact of NO₂⁻ (rather than NO₃⁻) on denitrifying microbial community structure and function has seen little exploration. Understanding impacts of NO₂⁻ driven denitrification is particularly important for emerging “shortcut N removal” microbial bioprocesses that employ NO₂⁻ as a key intermediate and offer the possibility for substantial energy savings relative to conventional nitrification/denitrification processes²⁵.

Accumulation of N₂O has been reported in several DPAO enrichment cultures and bioreactors^{8, 187, 201}. However, the specific taxa responsible for N₂O production as well as mechanisms underlying N₂O generation are not clear due to the complexity of the associated microbial consortia⁶⁵. Furthermore, while recent studies have compared genomic potential for denitrification among currently available *Accumulibacter* genomes^{93, 94}, none of these genomes derive from DPAOs enriched under long-term anaerobic/anoxic conditions with NO₂⁻ supplied as the terminal electron acceptor, and none derive from reactors or enrichments in which N₂O is the dominant product of denitrification.

The aim of this study was to investigate both denitrifying *Accumulibacter* and non-PAO microbial community structure and function under cyclic anaerobic/anoxic conditions, and to identify specific *Accumulibacter* clades or strains as well as other flanking microbial populations

as potential sinks and sources of N_2O when a high NO_2^- feed was supplied. To this end, we applied genome-resolved metagenomic analysis to study the composition and functional potential of a denitrifying *Accumulibacter* enrichment culture previously shown to generate unusually high levels of N_2O ⁶⁵. We hypothesized that the N_2O generation in this DPAO enriched denitrifying EBPR process could potentially be caused by two pathways: (1) selection for DPAOs (*Accumulibacter*) with truncated denitrification pathways that lack genomic capacity for N_2O reduction; and/or (2) selection for non-PAO denitrifiers in the flanking microbial community that are putative N_2O producers. Our results demonstrate that an *Accumulibacter* clade IA genome encoding a complete denitrification pathway is specialized for simultaneous N and P removal, and is accompanied by a low abundance but stably co-occurring novel clade IC *Accumulibacter* (the first published genome from this clade). Furthermore, our results elucidate a prevalence of non-PAO N_2O producers with truncated denitrification pathways in the flanking microbial consortia.

4.2 Materials and Methods

4.2.1 DNA Extraction and Metagenome Sequencing, Assembly and Gene Annotation

A lab-scale sequencing batch reactor (SBR) was operated as described previously for 7 months as a denitrifying P removal reactor⁶⁵. Further details of reactor operation are supplied in the Supporting Information (SI). Genomic DNA was extracted in duplicate from 2ml reactor biomass at five different time points (05/19/2015, 08/07/2015, 09/17/2015, 10/15/2015 and 11/13/2015) using the Fast DNA SPIN Kit for soil (MP Biomedicals, OH). Duplicate DNA extracts were pooled for library preparation and metagenomic sequencing at the Beijing Genomics Institute (BGI) (Shenzhen, China) using a 2x150bp paired end run on the Illumina HiSeq 4000

platform, with an average library insert size of 380bp. In total, 81.9 Gbp of raw sequencing data was produced. Adaptor trimming and quality control was done by BGI with Q20>90% and Q30>85%, generating roughly 75.8 Gbp of clean data. The quality of metagenomic sequencing data for each sample was checked by FastQC²⁰². Metagenomic reads in each individual sample were *de novo* assembled in the CLC Genomics Workbench v6.0.2 (CLCBio, Qiagen) using a kmer of 63, minimal contig length of 500bp and scaffolding enabled. The quality for each assembled scaffold was checked by QUAST²⁰³. Sequence coverage for each assembled scaffold was calculated by mapping raw reads from the sample to assembled contigs using Bowtie2 with default parameters²⁰⁴. Open reading frame (ORF) calling and annotation were performed for each sample using the DOE Joint Genome Institute's Integrated Microbial Genome database tool with biosample ID of Gb0150360-0150364²⁰⁵.

4.2.2 *Accumulibacter* Genome Binning, Annotation and Comparative Genome Analysis

Differential coverage binning was performed as previously described to bin metagenomic contigs into two draft *Accumulibacter* genomes¹⁸⁸. A detailed description of the methodology for assembly, ORF calling, and binning can be found in the SI. CheckM was applied to validate the quality of assembled genomes²⁰⁶. A pair-wise average nucleotide identity (ANI) (in percentage) and the percentage of alignment between 13 publicly available *Accumulibacter* genomes and genomes extracted in this study was calculated with the JSpecies WS online server using BLAST (ANiB)²⁰⁷. All predicted ORFs in type I *Accumulibacter* genomes, including the two draft genomes obtained in this study and four additional reference genomes, were BLAST searched against the NCBI nr database for gene annotation with an e-value cut-off of 10^{-5} . Annotation and functional analysis were performed in MEGAN using the SEED, eggNOG and KEGG databases²⁰⁸⁻²¹⁰. ORFs

assigned as genes related to denitrification processes were extracted (Table S4.2). LALIGN/PLALIGN was applied to find internal duplications and similarity scores between protein sequences²¹¹.

4.2.3 Orthologous Gene Family Detection and Gene Flux Analysis

24 draft genomes within the *Rhodocyclales* order (including 13 genomes within *Accumulibacter*) were downloaded from NCBI and used with the two draft *Accumulibacter* genomes extracted from our study for orthologous gene family detection and gene flux analysis. Orthologous gene families were identified using PROTEINORTHO V5.15 with 75% coverage and 70% of identity²¹². A phylogenetic analysis was then performed based on 59 aligned pan single-copy genes, as described previously⁹². Identified orthologous gene families and the phylogeny of these 26 *Rhodocyclales* genomes was used to conduct a gene flux analysis using Count²¹³. Orthologous gene family abundance with a gene gain/loss pattern related to the denitrification pathway were extracted in order to study the evolution of the denitrification trait in *Accumulibacter*. A phylogenetic approach was applied to infer HGT²¹⁴. Ancestral, derived, lateral derived, flexible genes, lineage-specific as well as the core genome of the overall *Accumulibacter* and the type I *Accumulibacter* genomes were defined, following methods in Oyserman et al.⁹². More detailed information related to downloaded *Rhodocyclales* genomes, core genome determination and HGT inference is provided in the SI.

4.2.4 *ppk1* Clone Library Construction and Sequencing

To characterize *Accumulibacter* population structure, the *Accumulibacter*-specific *ppk1* gene was PCR amplified from bioreactor samples 05/19/2015 and 10/15/2015 with primers Acc_ppk1-254f and Acc_ppk1-1376r⁸⁹. Detailed information about PCR conditions can be found

in the SI. PCR products were cloned using the pGEM-T Easy Vector System (Promega, USA), and resulting plasmids were purified with the Purelink Quick Plasmid Miniprep kit (Invitrogen, USA), per the manufacturer's instructions. Cloned inserts in a total of 48 isolated plasmids from each sample were sequenced by ATGC Inc. (Wheeling, IL) with an ABI 3730 DNA analyzer (Applied Biosystems, USA). The forward and reverse reads were trimmed and merged in the DECIPHER "R" package²¹⁵, and 68 *ppk1* fragments (1123bp) were generated.

4.2.5 *ppk1* Gene Screening and Phylogenetic Analysis

To screen *ppk1* from assembled metagenomic scaffolds, a BLASTX search was performed in DIAMOND using ORFs predicted from co-assembled scaffolds as a query and an e-value cut-off of 10^{-5} ²¹⁶. The obtained ORFs, 68 cloned *ppk1* sequences, and 781 reference *ppk1* sequences were aligned using MAFFT and trimmed to 1007bp²¹⁷. All trimmed sequences were used to construct a maximum likelihood phylogenetic tree using FastTree 2.1 with the GTR model (Figure S4.5). Because *ppk1* genes extracted from assembled metagenomics contigs derive from composite genome bins that likely mask genomic microdiversity, unassembled metagenomic sequence data was used to screen for *Accumulibacter ppk1*-like fragments and resolve microdiversity of *Accumulibacter*. Detailed methods for *ppk1* screening from raw reads are described in SI.

4.2.6 Flanking Bacterial Genome Binning and Metabolic Potential Analysis

Scaffolds assembled from individual sample were binned using CONCOCT with a minimal scaffold length of 1500bp¹⁸⁹. The quality of genome bins was analyzed by CheckM²⁰⁶. Only genomes with completeness greater than 80% and contamination less than 10% were retained for downstream analysis. All the flanking bacterial genomes were deposited in Kbase narrative "CANDO_flanking_genome" (<https://narrative.kbase.us/narrative/ws.25540.obj.1>). Phylosift was

used to taxonomically classify all extracted genome bins from different samples²¹⁸. ANI was calculated between genomes within the same bacterial family, and genome bins with ANI greater than 95% were considered to be the same species. Genome coverage was calculated based on the average coverage of all associated scaffolds normalized by the average coverage of essential single copy genes. A summary of genome statistics can be found in Table S4.3. A combined BLAST and MEGAN approach was applied to determine the genome-specific metabolic potential for denitrification²¹⁹. This approach is described in detail in the SI.

To compare the genomic denitrification potential between a denitrifying and a conventional aerobic EBPR microbial system, raw metagenomic reads from an aerobic EBPR process were downloaded (SRA accession number: SRP038016)²²⁰. Metagenomic assembly, mapping and genome binning and annotation were performed following the protocol described above.

4.3 Results and Discussion

4.3.1 Reactor Characterization and Metagenomic Sequence Data Collection

A lab-scale SBR was operated continuously as a denitrifying EBPR process for seven months under cyclic anaerobic/anoxic conditions with a short aerobic polishing phase, as described previously⁶⁵. NO_2^- was fed as the sole external electron acceptor during anoxic periods, and 60%-80% of NO_2^- was converted to N_2O during the stable operational period (Figure 4.1). Near complete N removal was coupled to partial phosphate removal, with similar rates of phosphate uptake under anoxic and aerobic conditions, as described previously⁶⁵. 16S rRNA gene amplicon sequencing in our previous study demonstrated shifts in microbial community structure coupled to enrichment of *Accumulibacter* after several months of operation⁶⁵. To assess genomic potential

for N transformations and N₂O production and consumption in the bioreactor microbial consortium, five samples representing biomass in different phases of reactor operation (start-up, transition and stable phase) were taken from the SBR for shotgun metagenomic sequencing. Figure 4.1 shows the initial NO₂⁻ concentration (start of anoxic phase), percent conversion to N₂O during anoxic period, and the five corresponding sampling dates over 7 months of reactor operation. The first sample was taken within one month of inoculation, and the rest of the samples were taken after several months of NO₂⁻ feeding in which we also observed high N₂O accumulation. Metagenomic sequencing of genomic DNA from these samples yielded a total of 500 million reads (75.8 Gbp) after quality filtering. Each sample was assembled separately for genome binning and functional profiling (Table S4.1). Data from the last two sampling points (10/15 and 11/13) were also combined and co-assembled to obtain longer contigs and higher quality *Accumulibacter* genomes.

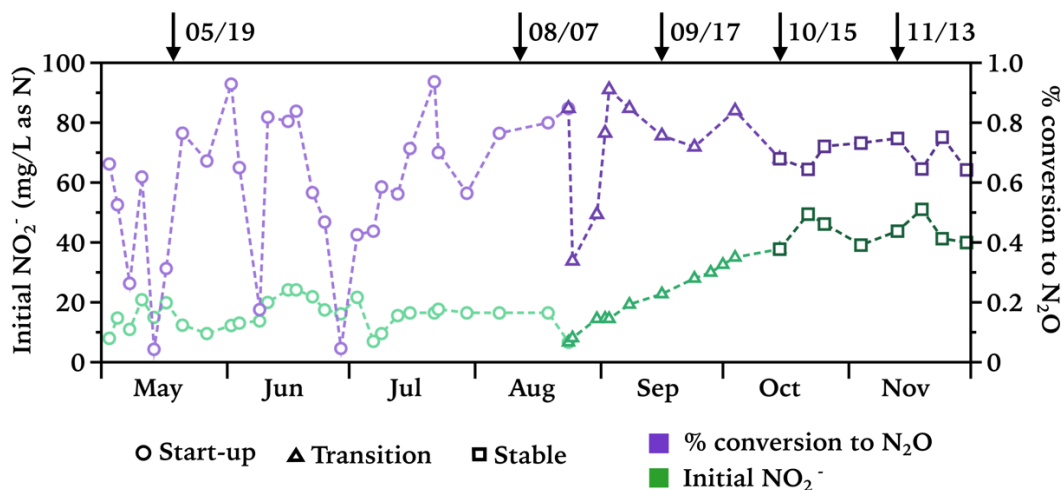


Figure 4.1 Initial NO₂⁻ concentration (green) at the start of the anoxic period and percent conversion to N₂O (purple) in the lab-scale SBR throughout the operational period (from May to November 2015).

The arrows represent sampling dates subjected to shotgun metagenome sequencing. Percent conversion to N₂O was calculated based on maximum measured N₂O concentration in aqueous phase and the amount of NO₂⁻ removed during the anoxic period.

4.3.2 *Accumulibacter* Genome Assembly, Population Characterization, and Assessment of Microdiversity

Two composite draft *Accumulibacter* genomes (CANDO_1_IA and CANDO_2_IC) were assembled via analysis of shotgun metagenome data. Summary statistics for these two draft genomes were assessed using checkM (Table 4.1). ANI scores (in percentage) between extracted genomes (CANDO_1_IA and CANDO_2_IC) and 13 *Accumulibacter* reference genomes were calculated to assess the whole sequence similarities of the extracted genomes (Figure S4.3). CANDO_1_IA, BA-92 and UW-3 genomes (the latter two were previously identified as clade IA genomes) share an average ANI of 99%, indicating that they represent the same species^{221, 222, 93, 94}. In contrast, CANDO_2_IC shows an ANI less than 90% with all the other *Accumulibacter* genomes. The BA-92 genome was previously identified as a clade IC genome based on *ppk1* gene phylogeny⁹³. However, phylogenetic analyses based on both a comprehensive *ppk1* reference database and on a selected subset of COG (Clusters of Orthologous Groups) families in *Accumulibacter* genomes indicate that BA-92 more likely affiliates with clade IB (Figure 4.2 and S4.3). These results suggest that the CANDO_2_IC draft genome represents a novel *Accumulibacter* strain distinct from currently available *Accumulibacter* genomes, and is the first published genome for *Accumulibacter* clade IC.

Table 4.1 Summary statistics for two extracted *Accumulibacter* draft genomes.

	# of scaffolds	Completeness (%)	Contamination (%)	Genome Size (Mbp)	N50 (bp)	Longest scaffold (bp)	GC content (%)
CANDO_1_IA	262	91.43	0.28	3.6	24148	129843	64
CANDO_2_IC	658	86.6	2.36	4.3	9230	43570	62

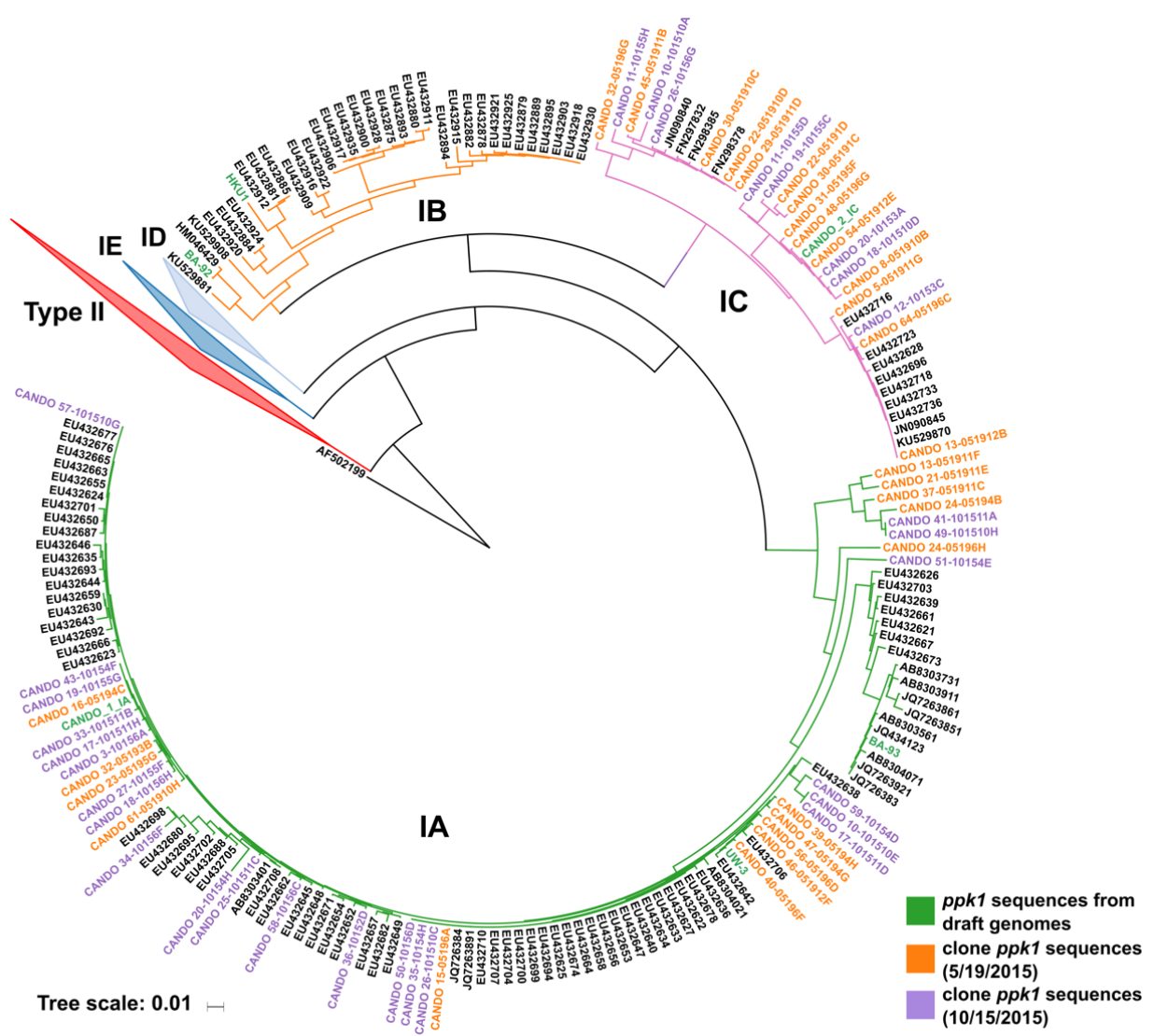


Figure 4.2 Accumulibacter maximum likelihood phylogenetic tree based on *ppk1* gene sequences (including Accumulibacter *ppk1* gene sequences downloaded from NCBI, *ppk1* genes extracted from four currently available type I genomes and the two draft genomes obtained in this study (in green), and *ppk1* gene fragments obtained via cloning and sequencing from two sampling dates (05/19/2015 in orange and 10/15/2015 in purple).

A total of 1007bp of aligned *ppk1* gene fragments were employed for reference phylogenetic tree construction. Type II (including the IIA (five clone sequences), IID (singleton) and IIG (singleton) sequences found in our clone sequences) and Type I clades IE and ID sequences are collapsed, and branches for clade IA-IC are colored in green, orange, and purple, respectively. A more complete reference *ppk1* phylogenetic tree with 781 reference sequences can be found in Figure S4.5. NCBI accession number for draft genomes BA-93, BA-92 and HKU1 are GCA_000585075.1, GCA_000585055.1, and GCA_000987395.1. The UW-3 genome was downloaded from JGI Integrated Microbial Genomes (IMG genome ID 2687453699).

Accumulibacter-specific *ppk1* gene amplification, cloning and sequencing for two different samples (05/19 and 10/15) was employed to profile strain-level diversity and community structure. Based on this analysis, we identified five different Accumulibacter clades (IA, IC, IIA, IID and IIG) in the reactor, with clades IA (37 clone sequences) and IC (24 clone sequences) being the two dominant Accumulibacter clades throughout the operational period (a phylogenetic analysis of clone sequences for the two major type I clades IA and IC is shown in Figure 4.2, and phylogenetic inference for sequences affiliating with all five clades is shown in Figure S4.5). Type II Accumulibacter showed low abundance shortly after reactor inoculation (5 sequences for IIA, and singletons for both IID and IIG on 05/19), and abundance declined further (singleton for IIA on 10/15) after six months of operation. Microdiversity within Accumulibacter clades IA and IC was observed based on cloned sequences (Figure 4.2, labeled in orange and purple). However, only two Accumulibacter-like *ppk1* sequences were screened from draft genomes (Figure 4.2, labeled in green). While the *ppk1* sequences recovered from draft genomes were nearly identical to *ppk1* gene sequences from clone libraries, the observed diversity in the clone libraries suggests that *ppk1* genes extracted from assembled metagenomic contigs derive from composite genome bins that likely mask genomic microdiversity.

To further assess strain-level microdiversity within Accumulibacter clade(s), Accumulibacter-like partial *ppk1* sequences were extracted directly (pre-assembly) from merged pair-end shotgun metagenome reads, then assembled and clustered into phylotypes at the 99% identity level. Phylogenetic analysis indicated that these phylotypes affiliated with clades IA (4 phylotypes, herein IA-1 to IA-4) and IC (3 phylotypes, herein IC-1 to IC-3). This metagenome-based *ppk1* sequence analysis corroborates Accumulibacter community structure and strain-level

microdiversity based on *ppk1* gene cloning and sequencing. The relative abundances of all seven partial *ppk1* phylotypes extracted from metagenomic sequencing data were calculated to explore the dynamics and diversity of *Accumulibacter* phylotypes in the DPAO enrichment reactor (Figure 4.3a). Among all *Accumulibacter* IA phylotypes, IA-1, IA-2, and IA-3 were nearly equally abundant initially (Figure S4.6). However, IA-1 was selectively enriched (from 3% to 15-35%) after three months of operation, while the abundance of the other clade IA phylotypes (IA-2 and IA-3) increased slightly. One IA phylotype, IA-4, was maintained at a low-levels (<0.3%) in all samples over the course of reactor operation. Only one IC phylotype, IC-1, was consistently present in the reactor over 7 months of operation (1.5-3% abundance), while the other two phylotypes (IC-2 and IC-3) almost disappeared (<0.5%) 4 months after inoculation. The strong enrichment of IA-1 (accounting for more than 60% of all *Accumulibacter*) suggests that this *Accumulibacter* strain may be adapted to utilization of NO_2^- as a terminal electron acceptor.

The two dominant phylotypes, IA-1 and IC-1, representing each *Accumulibacter* clade (IA and IC), were >99% identical to the two *ppk1* sequences from assembled *Accumulibacter* genomes (CANDO_1_IA and CANDO_2_IC; Figures 4.2 and 4.3), indicating that these two *Accumulibacter* phylotypes are representative of the two extracted composite genomes. The relative abundances of two *Accumulibacter* clades (IA and IC) were also calculated based on average coverage of the two composite genomes and the sum of IA and IC strains (based on *ppk1* phylotypes extracted from metagenomic sequence data prior to assembly) (Figure 4.3b). The relative abundance of the two clades (IA and IC) were comparable between these two quantification methods. We also evaluated *Accumulibacter* diversity and abundance via qPCR-based quantification with two sets of clade-specific *ppk1* gene primers (Figure S4.4 and SI). Taken

together, qPCR analyses coupled to phylogenetic analyses of *ppk1* gene sequences from clone libraries and from unassembled metagenomic reads demonstrate microdiversity within the *Accumulibacter* community in this reactor, but also demonstrate that the draft clade IA and IC composite genomes assembled from metagenomes in this study are representative of the dominant *Accumulibacter* phylotypes. However, the enrichment over time in this reactor of a single IA phylotype (IA-1) over 3 other IA phylotypes (IA-2 to IA-4) suggests the potential for niche differentiation at a phylogenetic scale finer than previously defined *Accumulibacter* clades. More high-resolution genome-targeted studies of *Accumulibacter* are warranted to provide deeper knowledge about the compositional structure and functional outcomes of microdiversity in *Accumulibacter*-enriched EBPR processes.

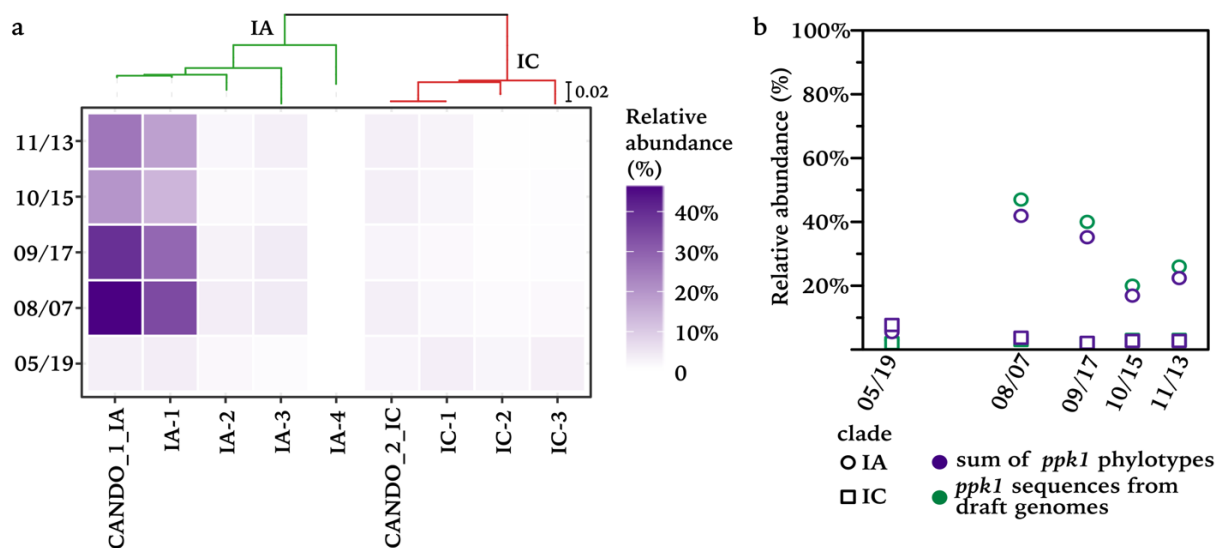


Figure 4.3 (a): Temporal change in relative abundance (%) of all extracted *Accumulibacter* phylotypes based on partial *ppk1* sequences from raw reads (IA-1 to IA-4 and IC-1 to IC-3) and two *ppk1* sequences from draft genomes (CANDO_1_IA and CANDO_2_IC). A phylogenetic tree based on figure 4.3 on top of the heatmap illustrates the phylogeny of these nine partial *ppk1* gene fragments. **(b):** Comparison of relative abundance of *Accumulibacter* clades IA (circle) and IC (square) based on average coverage for draft genomes (green) and based on the sum of the relative abundance of all IA and IC *ppk1* phylotypes (in purple). The sum of all IA and IC phylotypes are

calculated by summing the relative abundance of all 4 IA phylotypes and 3 IC phylotypes, respectively.

4.3.3 Comparative Genomics of Denitrification Machinery in Type I *Accumulibacter* Genomes.

To explore differences in genomic denitrification potential and the evolution of the denitrification trait within *Accumulibacter* clades, we compared denitrification-associated gene homologues by performing a gene flux analysis (Figure 4.4 and Table S4.2). The dominant CANDO_1_IA recovered in this study encoded genes for complete denitrification, while the lower abundance CANDO_2_IC harbored all denitrification genes except for *nor*.

Denitrification-associated gene homologues were classified as core (common to all *Accumulibacter* strains, including ancestral as well as laterally derived genes with phylogenetic evidence of HGT), flexible, and lineage-specific genes based on analysis of 26 *Rhodocyclales* genomes, following methods described in Oyserman et al.⁹². Among 28 denitrification-associated gene homologues, 11 were identified as core *Accumulibacter* genes, including one laterally derived gene (*napB*) and 10 ancestral genes (*nirLGH*, *nirS*, *nirNJ*, *nirBD*, NO₃⁻/NO₂⁻ transporter, and *napF*). Interestingly, one copy of a cytochrome cd₁ nitrite reductase (*nirS*) gene was found in CANDO_2_IC, while CANDO_1_IA and other type I *Accumulibacter* genomes contain two copies of *nirS*. The *nirS* shared by both CANDO_1_IA and CANDO_1_IC was classified as an ancestral gene, while the other copy was identified as a flexible gene with evidence of HGT. It is possible that the extra copy of *nirS* putatively acquired by HGT in CANDO_1_IA may provide a competitive advantage in terms of NO₂⁻ utilization. It should be noted, however, that the CANDO_2_IC draft genome reported here is incomplete, and additional *nirS* gene copies may be present in the 13% predicted to be missing. Furthermore, gene expression of the two *nirS* copies and the affinity of two expressed nitrite reductases in CANDO_1_IA requires further investigation.

Among the four steps of denitrification, only the *nir* gene cluster (linked to NO_2^- reduction) was identified as core to all Accumulibacter. However, periplasmic nitrate reductase (*napAGH*) and nitrous oxide reductase (*nosZDFL*) gene clusters were also identified as core to all type I Accumulibacter (Table S4.2-A). Both clusters *napAGH* and *nosZDF* are predicted to be present in the last common ancestor (LCA) of Accumulibacter, but were inferred as lost for some type II Accumulibacter genomes by gene flux analysis. The loss of *napAGH* and *nosZDF* for type II Accumulibacter genomes indicates potentially limited denitrifying P uptake capability for type II Accumulibacter and a potential niche in denitrifying systems for type I Accumulibacter. In support of this, very limited denitrifying P uptake rates were recently reported for a type II Accumulibacter dominated pilot-scale EBPR system¹⁷⁶. Interestingly, the membrane-bound nitrate reductase gene cluster (*nar*) was only present in clade IC (CANDO_2_IC), clade IIC (SK_01, SK_02 and HKU2) and clade IIA (Aalborgensis_IIA) genomes. The function and interactions of two distinct nitrate reductases (NAR and NAP) in Accumulibacter warrants further investigation.

Interestingly, nitric oxide reductase was classified as a flexible gene acquired by HGT for type I and II Accumulibacter, and it was not found in two of the six currently available type I Accumulibacter draft genomes (CANDO_2_IC and HKU_1). In addition, the complete genome UW-3_IA carries an incomplete *qnorB* gene⁹⁴. Generally, for a typical denitrifier, nitrite reductase and nitric oxide reductase gene clusters are located close together in the genome and are co-expressed to minimize the accumulation of NO ^{169, 223}. However, a *qnorB* homolog was not located upstream or downstream of the *nirS* genes in the CANDO_2_IC and BA-93_IA genomes. The mechanism and regulation of nitric oxide reduction in these Accumulibacter phylotypes warrants further investigation.

A core motivation of this study was to test the hypothesis that N₂O generation in this denitrifying EBPR reactor is caused by selection for DPAOs (*Accumulibacter*) that lack genomic capacity for N₂O reduction. However, *nosZ* was identified in our analysis as a core Type I *Accumulibacter* gene, and is present in both CANDO_1_IA and CANDO_2_IC draft genomes. Both draft genomes harbor clade II (atypical) *nosZ*, a recently discovered *nosZ* gene variant that is evolutionarily distinct from the typical clade I *nosZ*^{111, 124}. This finding indicates that *Accumulibacter* strains present in this N₂O generating reactor microbiome do in fact harbor the genomic potential for N₂O consumption, and therefore provides evidence against our hypothesis that N₂O generation in this system is caused by selection of DPAOs with truncated denitrification pathways. However, it is important to note that gene presence indicates functional potential but not necessarily a functional gene product, as gene regulation controls the expression of genomic content. Differential gene expression among denitrification genes, particularly the down-regulation of *nosZ*, has been observed in some EBPR studies even under anaerobic/aerobic conditions^{220, 224, 225}. In addition, stop codons were detected within the assembled CANDO_2_IC *nosZ*, which may indicate a nonfunctional *nosZ* in the CANDO_2_IC genome.

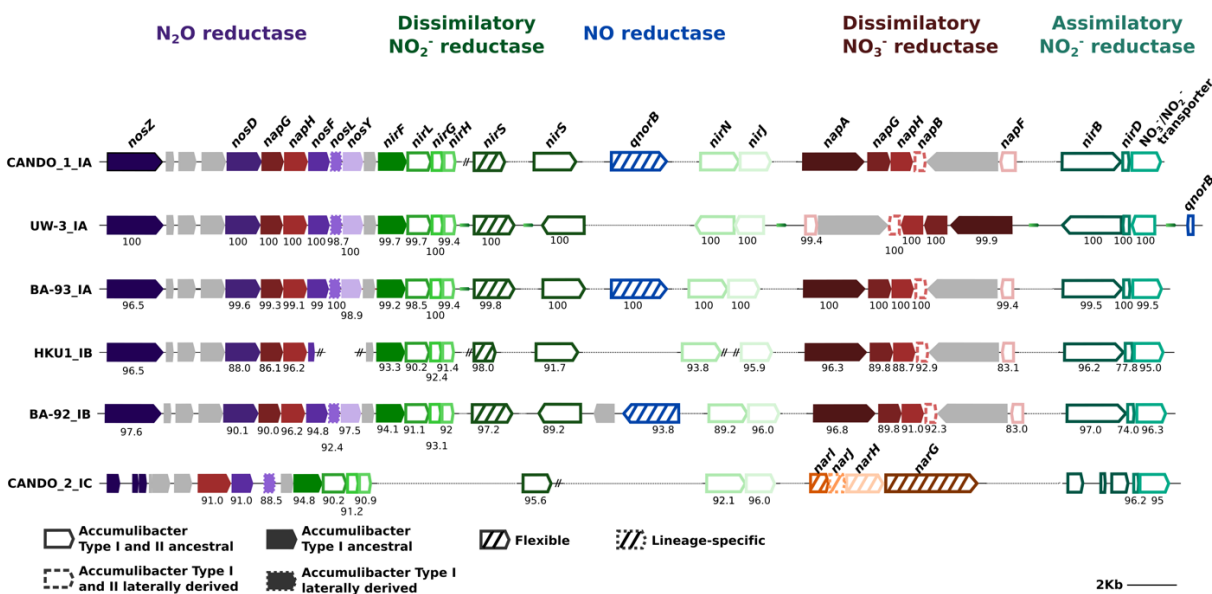


Figure 4.4 Key denitrification gene loci in all available type I *Accumulibacter* draft genomes including four publicly available genomes^{94, 220, 226} and two (CANDO_1_IA and CANDO_2_IC) assembled from this study.

The approximate size and transcriptional direction of genes are indicated by the arrow boxes. Colors identify homologous genes. Genes with unrelated functions or with unknown functions are in grey. Numbers below genes represent amino acid identities (in percentage) of the predicted genes compared to CANDO_1_IA. Solid outlines, dashed outlines, filled with solid outlines, filled with dashed outlines, slash pattern with solid outlines and slash pattern with dashed outlines indicate classification of gene loci as *Accumulibacter* type I and II ancestral genes, *Accumulibacter* type I and II laterally derived genes, *Accumulibacter* type I ancestral genes, *Accumulibacter* type I laterally derived genes, flexible, and lineage-specific genes, respectively, based on gene flux analysis. Genes identified on the same scaffold are connected by solid line and genes identified on different scaffolds are connected by dotted lines. Genes and noncoding regions are drawn to scale. The small green arrows after *nirH*, *nirS* and *napA* in the UW-3-IA genome and after *nirH* in the BA-93_IA genome represent a long gap between genes located on the same scaffold. Double slashes indicate beginning or ends of metagenomic scaffolds.

4.3.4 Diversity of Denitrification Pathways among Flanking Genomes.

Although *Accumulibacter* is the dominant bacterial functional group in this denitrifying EBPR reactor, non-PAO bacteria still account for over 50% of the overall microbial community. This non-PAO “flanking” bacterial community besides *Accumulibacter* could also be involved in N transformation pathways and act as a source of N₂O. In order to test the hypothesis that this

flanking community harbored a prevalence of putative N₂O producers lacking genomic capacity for N₂O reduction, we reconstructed individual flanking bacterial genomes for each time-series sample (excluding 05/19 due to low sequencing depth). Genome bins with <80% completeness and >10% contamination were removed from further analysis to ensure comprehensive and accurate characterization of microbial metabolic potential. Ultimately, 39 individual flanking bacterial genome bins were recovered with average completeness and contamination of 89.0±6.3% and 2.4±1.7%, respectively. Detailed information including taxonomic classification and summary genome quality statistics are shown in Table S4.3. The sum of all assembled genomes for both *Accumulibacter* and flanking non-PAO populations represents over 40% relative abundance of the overall microbial community in all samples, except for 05/19 (startup period) (Figure S4.7).

We further analyzed dynamics in abundance of each high-quality flanking genome bin during the operational period and assessed which denitrification steps are encoded in each genome (Figure 4.5). Sample 05/19, taken soon after reactor inoculation, was excluded from this analysis due to the relatively low abundance of recovered flanking genomes in this time point (Figure S4.7). Only structural genes for denitrification were included in the analysis¹⁹⁰. 69% of reconstructed genomes harbored at least one denitrification gene. Surprisingly, only one draft genome encoded genes for complete denitrification, demonstrating a high prevalence of truncated denitrification pathways. A similarly high prevalence of bacterial genomes with incomplete denitrification pathways was observed recently in an aquifer system and in a partial nitritation-anammox bioreactor, and has also been documented in complete genomes retrieved from public databases^{119, 120, 199, 227}. Dominance of incomplete denitrifiers has not previously been reported in a denitrifying wastewater treatment bioreactor.

Two phylogenetically distinct groups of the *nosZ* gene that catalyze N₂O reduction (clade I and II *nosZ*) have been identified recently¹¹¹. However, only clade II *nosZ* was identified in the reconstructed genomes in this study. We identified genomes with capacity for NO₂⁻ reduction (e.g. harboring *nirS* or *nirK*) but not for N₂O reduction (e.g. lacking *nosZ*) as putative N₂O producers, while genomes with *nosZ* were considered as putative N₂O consumers. A large proportion (6 out of 10) of the putative N₂O producers were assigned to the α -, β -, and γ -*Proteobacteria*. In particular, three N₂O producing genomes assigned to the bacterial family *Xanthomonadaceae* (bins 24-26) were highly abundant in reactor samples from October and November, suggesting that *Xanthomonadaceae*-affiliated taxa may be one of the sources of N₂O in this system. In agreement with this assessment, *Pseudoxanthomonas taiwanensis* sp. within the family *Xanthomonadaceae* was previously identified as a N₂O-producing species isolated from hot springs¹⁹⁸. In contrast, bacterial genomes carrying *nosZ*, the last step of denitrification, may be considered a sink for N₂O. We documented 17 draft genomes (bins 1-17) encoding *nosZ*. 14 of these genomes (82%) affiliated with the phyla *Bacteroidetes*, *Chloroflexi*, *Ignavibacteriae*, *Proteobacteria* and *Verrucomicrobia* appear to be nondenitrifying N₂O reducers with no capability for N₂O production.

One possible explanation for the prevalence of incomplete (truncated) denitrification pathways in this community is that denitrification intermediates, particularly N₂O, may be cross-fed between bacterial taxa. Cross-feeding has been hypothesized to be a useful adaptation to optimize enzyme concentrations and minimize the total concentration of intermediates^{123, 228}. Interestingly, 14 out of 17 putative N₂O consumers we discovered were incapable of NO₃⁻ or NO₂⁻ reduction, and can only obtain N₂O through cross-feeding under anoxic conditions. However, high N₂O accumulation was observed throughout the operational period, especially after the three-

month start-up period⁶⁵. As illustrated in Figure 4.5, the cumulative abundances of putative N₂O producers with no *nosZ* show a strong and statistically significant increasing trend during this period (relative abundance increased from 4.14% (09/17) to 9.04% (11/13), Spearman $\rho=1$, p-value=0.04). No clear pattern was discovered for abundance of putative N₂O reducers and nondenitrifiers (Spearman p-value>0.05).

In order to compare patterns of putative N₂O producers and consumers in this NO₂⁻ fed denitrifying EBPR system to more conventional processes, we also assembled 8 near-complete genomes from a previously described aerobic EBPR reactor (Figure S4.8)²²⁰. Analysis of the denitrification-associated gene complement in these genomes suggested a balanced distribution of putative N₂O consumers and producers on two selected operational days (day 75: 10.36% and 13.97%, and on day 180: 3.37% and 4.90%, respectively). Abundance for both potential N₂O consumers and producers declined in this aerobic EBPR system over time. Compared with this EBPR system where oxygen was supplied as the electron acceptor, the increasing abundance of putative N₂O producers in our denitrifying EBPR system suggests that long-term high NO₂⁻ feeding may select for microbes with truncated denitrification pathways as a source of N₂O.

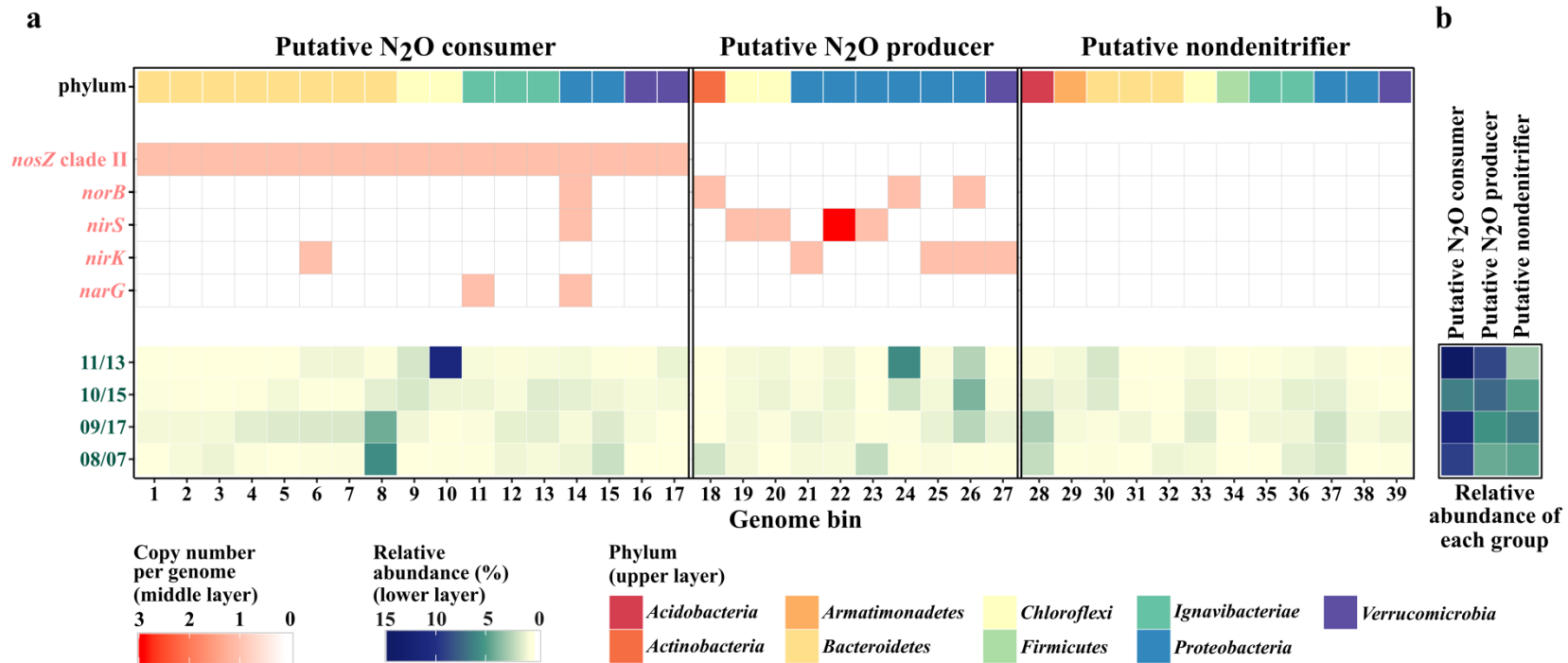


Figure 4.5 (a) Dynamics in relative abundance of 39 flanking bacterial genome bins (lower layer), the presence of different denitrification structural genes (*narG*, *nirK*, *nirS*, *nor* (*qnorB* or *cnorB*), and *nosZ* clade II) (middle layer), and the assigned taxonomy for each genome bin at the phylum level (upper layer). *nosZ* clade I is not represented in the middle layer because it was not identified in any of the draft genome bins. **(b)** Sum of relative abundance of putative N₂O consumers, putative N₂O producers, and nondenitrifiers identified within the 39 flanking bacterial genomes.

Putative N₂O consumers are bacterial genomes with a *nosZ* gene. Draft genomes with upstream denitrification genes but lacking *nosZ* genes are identified as putative N₂O producers. Genomes with no denitrification genes extracted are classified as nondenitrifiers.

4.4 Conclusions

Several mechanisms have been proposed to explain the accumulation of N₂O in both natural and engineered systems. One hypothesis for accumulation of denitrification intermediates (including N₂O) is that nitrogen oxide reductases compete for the same finite pool of intracellular electron donors^{112, 114}. Thus, the reduction of NO₂⁻ could suppress the reduction of N₂O via competition for electrons. However, our reactor monitoring data showed slow N₂O reduction rate even after NO₂⁻ was completely consumed and N₂O became the only available electron acceptor⁶⁵. This suggests that electron competition is unlikely to be the primary reason for N₂O accumulation in this DPAO-enriched bioprocess.

An additional potential explanation for elevated N₂O generation by bacterial taxa with complete denitrification pathways is high inhibitory NO₂⁻ (or HNO₂) concentrations or other environmental conditions that may have an impact on the expression and/or the activity of *nosZ*⁶⁶,⁶⁷. All type I *Accumulibacter* genomes, including the two recovered in this study, harbor clade II *nosZ* genes, which has a different *nos* gene cluster organization and translocation pathway compared to clade I *nosZ* genes¹¹¹. *Accumulibacter* clade II *nos* clusters lack *nosR* and *nosX*, which have been implicated in regulation of the expression of clade I *nosZ*. The clade I *nosZ* promoter was also not founded upstream of the assembled *nosZ* in the CANDO_1_IA or CANDO_2_IC genomes, suggesting that clade II *nosZ* might have a different regulatory mechanism compared with clade I *nosZ*. Thus, further investigation is required to explore the regulation and activation of *Accumulibacter* clade II *nosZ*, and to assess the impact of NO₂⁻ on clade II *nosZ* regulation and activation.

The modularity of the denitrification pathway and a non-random co-occurrence pattern between *nirS/nirK* and *nosZ* has been demonstrated^{119, 120}. The genome-centric metagenomic analysis presented here also highlights the diversity and modularity of denitrification pathways in a complex system, and an increasing abundance of denitrifiers with truncated denitrification pathways over the course of reactor operation. Both potential N₂O producers that lack *nosZ* and nondenitrifying N₂O reducers with clade II *nosZ* but no upstream structural denitrification genes were apparent in the reactor microbiome, whereas only a single genome bin (bin 14) harbored a complete denitrification pathway. The enrichment of NO₂⁻ reducers lacking the *nosZ* gene in the flanking bacterial community over time may partially explain the high N₂O production observed in this NO₂⁻-fed reactor.

In summary, in this study, we assembled two Type I *Candidatus* Accumulibacter genomes representing clades IA and IC, the latter of which is not currently represented in published genomes. These additional Accumulibacter genomes are invaluable for understanding niche adaptation and ecophysiology of this critically important functional group. Our results demonstrate variation in genomic denitrification capabilities among Accumulibacter strains, with a potential advantage in denitrifying EPBR systems for type I Accumulibacter clades based on a comprehensive comparison of denitrification gene clusters. In addition, we assessed potential sources of the unusually high levels of N₂O generated in this NO₂⁻-fed EBPR reactor by investigating the genomic denitrification potential for 39 flanking bacterial genomes. Overall, we discovered a substantial number of flanking bacterial genomes incapable of mediating all four denitrification steps. Our results suggest that N₂O production within this DPAO-enriched microbial consortium likely derives at least in part from flanking non-PAO denitrifying bacteria, particularly those in

the family *Xanthomonadaceae*, that harbor truncated denitrification pathways; lack genomic capacity for N₂O reduction; and were enriched over the course of denitrifying EBPR operation. It should be noted that it is possible that differential gene expression in addition to variations in gene content within the denitrification pathway in *Accumulibacter*, and in particular regulation of *nosZ* gene expression when exposed to elevated NO₂⁻ concentrations, may also lead to accumulation of N₂O. Follow up metatranscriptomic analysis and/or reverse transcription qPCR-based measurements targeting this DPAO enrichment culture are warranted, as these may elucidate variations in denitrification gene expression that may also partially underlie unusually high levels of N₂O observed here.

Data Availability

Raw sequencing data has been submitted to the National Center for Biotechnology Information (NCBI) Sequence Read Archive (SRA) database under BioSample accession number SAMN06957052-SAMN0695705256. Two *Accumulibacter* draft genomes were deposited in GenBank under accession number PHDR000000000 and PDHS000000000. GenBank accession numbers for the *ppk1* nucleotide sequences in this study are MF953887-MF953954.

4.5 Supporting Information

4.5.1 Supporting Information – Methods

Reactor operation

A 14L lab-scale SBR with 12L working volume was operated continuously as a denitrifying biological phosphorus removal system for 7 months under cyclic anaerobic and anoxic conditions, with a short aerobic polishing step, in order to enrich denitrifying PAOs. Detailed reactor operating conditions, performance, and experimental methods for key metabolite (acetate/propionate, PHAs, NO_2^- , N_2O and PO_4^{3-}) measurements were described previously⁶⁵. Briefly, acetate or propionate was dosed at the start of the anaerobic (COD rich) period as the electron donor. The electron donor was switched between acetate and propionate every two SBR cycles. In the anoxic (COD deplete) phase, high NO_2^- feed was dosed as a terminal electron acceptor for denitrification.

Accumulibacter genome binning

Raw reads from two different samples (10/15 and 11/13) were co-assembled using CLC Genomic Workbench v6.0.2 with a kmer of 37 and minimal scaffold length of 500bp. In order to estimate contig coverage, raw reads from each individual sample were then mapped to co-assembled scaffolds using Bowtie2. Open reading frames (ORFs) were predicted on assembled scaffolds using Prodigal 6.3.2²²⁹. A set of 107 hidden Markov models (HMMs) of essential single copy genes was searched against ORFs using HMMER3 using the `-cut_tc` option²³⁰. Taxonomic classification of the identified proteins was obtained via BLASTP against the RefSeq protein database with a maximum e-value cut-off of 10^{-5} ²³¹. MEGAN was used to visualize the taxonomic assignments, and phylum and class-level taxonomic assignments were extracted²³². The

mmgenome R package was used to manually extract *Accumulibacter* genome bins based on bicoverage plots, taxonomic classification, GC content and tetranucleotide frequency, with minimal scaffold length of 1500 bp²³³.

Accession numbers of all downloaded genomes

26 genomes within the *Rhodocyclales* order were downloaded for the study, including 13 *Accumulibacter* genomes (12 of the 13 *Accumulibacter* genomes were downloaded from NCBI : BA-93 (GCA_000585075.1), BA-92 (GCA_000585055.1), BA-91 (GCA_000585035.2), BA-94 (GCA_000585095.1), HKU1 (GCA_000987395.1), HKU2 (GCA_000987445.1), SK-01 (GCA_000584955.2), SK-02 (GCA_000584975.2), SK-11 (GCA_000584995.1, SK-12: GCA_000585015.1, UW-1: GCA_000024165.1, Aalborgensis: GCA_900089955^{77, 93, 94, 220, 226} . UW-3 was downloaded from JGI Integrated Microbial Genomes [IMG] with genome ID 2687453699⁹⁴), one *Azoarcus* genome (GCA_001682385.1), 3 *Dechloromonas* genomes (GCA_000519045.1, GCA_000012425.1, GCA_001551835.1), 8 *Thauera* genomes (GCA_000310185.1, GCA_001591165.1, GCA_001922305.1, GCA_001051995.2, GCA_000621305.1, GCA_000310225.1, GCA_000831325.1, GCA_000443165.1) and one *Zoogloea* genome (GCA_002028455.1).

Genome-based phylogenetic tree construction

A total of 13 publicly available *Accumulibacter* genomes were downloaded and deposited in a Kbase narrative “CANDO_genome” (<https://narrative.kbase.us/narrative/ws.22211.obj.1>) for further analysis. A genome tree was constructed in Kbase (www.kbase.us) using the Species Tree app by inserting *Accumulibacter* genomes into a subset of public KBase genomes closely related to the inserted genomes (<https://kbase.us/insert-genomes-into-species-tree-app/>). A select subset

of 49 COG domains was used to determine phylogenetic relationships between genomes. A maximum likelihood phylogenetic tree was then built with FastTree2²³⁴.

Accumulibacter core genome determination

Two criteria were used to determine genes within *Accumulibacter* (type I and II) and type I *Accumulibacter* core genome⁹²: (1) a gene family must exist in at least 8 *Accumulibacter* genomes and at least 5 type I *Accumulibacter* genomes. The genome-number cutoff was determined to identify approximately 99% of the core genome calculated based on draft genome completeness; (2) a core gene must be inferred in the last common ancestor of *Accumulibacter* (node 14 in Figure S4.3) (or type I *Accumulibacter* [node 12 in Figure S4.3]) and retained at each internal *Accumulibacter* (or type I *Accumulibacter*) node based on gene flux analysis.

Denitrification related genes HGT inference

A phylogenetic approach was used to infer whether denitrification related genes in CANDO_1_1A and CANDO_2_IC were laterally acquired by HGT⁹². All *Accumulibacter* derived genes with KEGG annotations and ORFs related to denitrification pathway were extracted (Table S4.2) and blasted against the NCBI nr database (Release April 12, 2018) with e-value of 1E-6 and max_target_seq of 150. Genes with less than 150 BLAST results were filtered and excluded from this analysis. The average percentage of non-*Rhodocyclaceae* hits in the top 150 BLAST results of all derived genes was calculated (8%) and used as the cutoff for HGT inference. A denitrification gene was considered to be derived by HGT if less than 8% of the BLAST hits was assigned to family *Rhodocyclaceae*.

ppk1 gene clone library

PCR amplification for *ppk1* gene cloning was conducted with the forward primer Acc-ppk1-254f (5'-TCA CCA CCG ACG GCA AGA C -3') and reverse primer Acc-ppk1-1376r (5'-ACG ATC ATC AGC ATC TTG GC -3')⁸⁹. PCR reactions were conducted in duplicate for duplicate genomic DNA extracts, generating a total of four 20 μ L PCR amplification reactions for each sample. Each PCR reaction contained 10 μ L 2 \times FailSafe premix F (Epicentre, USA), 0.35U expand HIFI taq enzyme (Roche, USA), 2 μ L genomic DNA, and 0.4 μ L of the 10 μ M forward and reverse primers. The following temperature program was used: initial denaturation at 95°C for 4min, followed by 30 cycles of denaturation at 95°C for 30s, annealing at 65°C for 1min and extension at 72°C for 2min; and a final extension step at 72°C for 12min.

ppk1 gene qPCR

Quantification of clades IA, IB, IC and IIC was carried out by qPCR using two distinct sets of primers targeting clade-specific *ppk1* gene variants. qPCR reactions using a widely used primer set first reported by He et al. were described previously^{65, 89}. qPCR-based quantification with a recently redesigned clade-specific *ppk1* primers that account for expanded database representation of *Accumulibacter* diversity was performed in a Biorad CFX thermal cycler (BioRad Laboratories, USA)¹⁷⁶. For clade IA and IC primers, each 20 μ L reaction contained 10 μ L iTaq SYBRGreen supermix (BioRAD Laboratories, USA), 1 μ L each of 10 μ M forward and reverse primer, and 2 μ L of sample genomic DNA. For the quantification of IB and IIC-specific *ppk1*, FailSafe premix F (Epicentre, USA) with 1 \times SYBRGreen 1 (Invitrogen, USA) was employed in place of the iTaq SYBRGreen Supermix. The qPCR reaction volume was 20 μ L with 10 μ L of qPCR premix, 0.35U expand HIFI taq enzyme (Roche, USA), 1 μ L each of 10 μ M forward and reverse primer and 2 μ L of genomic DNA. The thermal cycling protocol used for all clade-specific *ppk1* qPCR assays was

as follows: initial denaturation at 95°C for 4min, followed by 35 cycles of denaturation at 95°C for 30s, annealing at 65°C for 30s, and extension at 72°C for 30s. All the primers applied are listed in Table S5.

ppk1 screening from raw sequencing reads

Pair-end reads for each sample were merged first using Cope v1.2.5 before *ppk1* screening²³⁵. Unassembled merged sequences were then used as query sequences to search against a reference *ppk1* database with DIAMOND. All matched query sequences from each sample were recovered and reassembled with Velvet with a kmer of 127²³⁶. Assembled partial *ppk1* gene sequences were aligned against the reference alignment described previously (Figure S5.5) using MAFFT with the addfragments and adjustdirection options. The resulting multiple sequence alignment was manually inspected in MEGA7, and poorly aligned sequences were removed²³⁷. All extracted sequences from different samples were combined and dereplicated in USEARCH using the substring option¹⁵³. Sequences with greater than 99% nucleotide identity were combined. These Accumulibacter-like partial *ppk1* fragments were then inserted into the previously built phylogenetic tree based on maximum likelihood using pplacer v1.1²³⁸.

Screening denitrification structural genes

Denitrification structural genes encoding the large subunit of respiratory nitrate reductase (*narG*), cytochrome cd₁ nitrite reductase (*nirS*), copper-containing nitrite reductase (*nirK*), nitric oxide reductase (*norB*), and nitrous oxide reductase (*nosZ*) were first identified using BLAST against reference denitrification gene databases. Reference denitrification gene sequences were downloaded from the FunGene functional gene pipeline and repository²³⁹. The BLASTN search was performed using ORFs in a draft genome as a query, using e-value cut-off of 10⁻⁵ and similarity

cut-off of 70%. The candidate target sequences in the 1st BLAST search were then subjected to a 2nd BLAST search against the NCBI-nr database and annotated with MEGAN to filter out any potentially mismatched sequences.

4.5.2 Supporting Information – Tables

Table S4.1 Summary statistics for metagenome sequencing, assembly and annotation

Sample used for assembly	Clean reads (Gbp)	Assembled reads (Gbp)	# of Contigs	N50** (Contigs)	# of Scaffolds	N50 ** (Scaffolds)	Reads mapping to contigs*	# of ORFs	ORFs with COG	ORFs with KEGG
05/19	3.6	0.18	169192	1171	152549	1262	32.29%	290813	59.05%	24.06%
08/07	15.7	0.54	454862	1359	401511	1500	63.90%	818855	56.17%	21.94%
09/17	19.9	0.68	524488	1553	469398	1709	72.09%	992367	55.34%	21.35%
10/15	21.4	0.65	466309	1818	400686	2146	76.30%	920735	58.23%	22.55%
11/13	15.1	0.41	289846	1889	251479	2209	78.72%	588173	60.65%	23.43%
10/15 + 11/13	36.6	0.44	181673	3124	160467	3372	*	698254	*	*

*COG and KO annotations were not conducted for ORFs generated by co-assembly.

** N50 was calculated based on contigs (scaffolds) greater than 500bp.

Table S4.2 Denitrification genes and inference of HGT in available *Accumulibacter* genomes (**a**): Identification of presence and absence of orthologous denitrification gene families in 15 *Accumulibacter* (type I and II) genomes obtained from PROTEINORTHO. (**b**): ORFs identified as denitrification genes for 6 type I *Accumulibacter* draft genomes. A total of four are publicly available genomes (BA-92, BA-93, UW-3 and HKU_1^{94, 220, 226}) and two genomes assembled in this study (CANDO_1_IA and CANDO_2_IC) are shown. (**c**): HGT inference for denitrification genes from CANDO_1_IA and CANDO_2_IC.

a.

Gene	Total number of genes in all <i>Accumulibacter</i> genomes (out of 15) ‡	Core <i>Accumulibacter</i> gene (1=core, 0=non-core)	Total number of genes in type I <i>Accumulibacter</i> genomes (out of 6) ‡	Core type I <i>Accumulibacter</i> gene (1=core, 0=non-core)	Type I <i>Accumulibacter</i> genomes						Type II <i>Accumulibacter</i> genomes						
					IA		IC		IB		IIA		IIF		IIC		
					CANDO_1_IA	BA-93	UW-3/IA	CANDO_2_IC	HKU1	BA-92	Aalborgensis	UW-1-IIA	BA-94	SK-11	SK-12	BA-91	SK-01
Genome Completeness (%) **																	
<i>napF</i>	15	1	6	1	Acc bin1_41	BA-93-IA_213/UW-3_2003	Acc bin2_124	Accumulibacter	Accumulibacter_aalborgensis	310 UW-1-IIA-com	Accumulibacter	Accumulibacter	Accumulibacter	BA-91-IC_185	SK-01-IC_371	SK-02-IC_122	Candidatus_Accur
<i>nirJ</i>	15	1	6	1	Acc bin1_394	BA-93-IA_131 UW-3_829	Acc bin2_1396	Accumulibacter	Accumulibacter_aalborgensis	180 UW-1-IIA-com	Accumulibacter	Accumulibacter	Accumulibacter	BA-91-IC_184	SK-01-IC_371	SK-02-IC_122	Candidatus_Accur
<i>napB</i>	14	1	6	1	Acc bin1_40	BA-93-IA_213/UW-3_2005	Acc bin2_752	Accumulibacter	Accumulibacter_aalborgensis	220 UW-1-IIA-com	Accumulibacter*	Accumulibacter	Accumulibacter	BA-91-IC_400	SK-01-IC_100	SK-02-IC_903	Candidatus_Accur
<i>nirD</i>	14	1	6	1	Acc bin1_759	BA-93-IA_609 UW-3_2198	Acc bin2_1561	Accumulibacter	Accumulibacter_aalborgensis	128 UW-1-IIA-com	Accumulibacter	Accumulibacter	Accumulibacter*	SK-01-IC_356	SK-02-IC_755	Candidatus_Accur	
<i>nirF</i>	13	0	6	1	Acc bin1_93	BA-93-IA_299/UW-3_3157	Acc bin2_1597	Accumulibacter	Accumulibacter_aalborgensis	116 UW-1-IIA-com	*	Accumulibacter*	Accumulibacter	BA-91-IC_196	SK-01-IC_576	SK-02-IC_336	Candidatus_Accur
<i>nirG</i>	13	1	6	1	Acc bin1_95	BA-93-IA_299/UW-3_3155	Acc bin2_1595	Accumulibacter	Accumulibacter_aalborgensis	116 UW-1-IIA-com	*	*	Accumulibacter	BA-91-IC_160	SK-01-IC_578	SK-02-IC_335	Candidatus_Accur
<i>nirH</i>	13	1	5	1	Acc bin1_968	BA-93-IA_36 UW-3_3154	Acc bin2_1067	*	Accumulibacter_aalborgensis	309 UW-1-IIA-com	Accumulibacter*	Accumulibacter	Accumulibacter	BA-91-IC_186	SK-01-IC_368	SK-02-IC_336	Candidatus_Accur
<i>nirN</i>	13	1	5	1	Acc bin1_393	BA-93-IA_130 UW-3_830	Acc bin2_1397	*	Accumulibacter_aalborgensis	180 UW-1-IIA-com	Accumulibacter	Accumulibacter*	Accumulibacter	SK-01-IC_371	SK-02-IC_122	Candidatus_Accur	
<i>nirL</i>	12	1	6	1	Acc bin1_94	BA-93-IA_299/UW-3_3156	Acc bin2_1596	Accumulibacter	Accumulibacter_aalborgensis	116 UW-1-IIA-com	*	*	Accumulibacter*	SK-01-IC_577	SK-02-IC_336	Candidatus_Accur	
<i>nirS</i>	11	1	6	1	Acc bin1_1448	BA-93-IA_110/UW-3_2548	Acc bin2_2430	Accumulibacter	Accumulibacter_aalborgensis	226*	*	*	*	BA-91-IC_446	SK-01-IC_771	SK-02-IC_313	Candidatus_Accur
NO ₃ ⁻ /NO ₂ ⁻ transporter	11	1	6	1	Acc bin1_760	BA-93-IA_610 UW-3_2197	Acc bin2_1560	Accumulibacter	Accumulibacter_aalborgensis	128 UW-1-IIA-com	*	*	Accumulibacter*	*	*	SK-02-IC_754	Candidatus_Accur
<i>nirB</i>	11	1	5	1	Acc bin1_758	BA-93-IA_608 UW-3_2199	*	Accumulibacter	Accumulibacter_aalborgensis	128 UW-1-IIA-com	Accumulibacter*	*	*	SK-01-IC_356	SK-02-IC_754	Candidatus_Accur	
<i>napG</i>	8	0	5	1	Acc bin1_87	BA-93-IA_298/UW-3_3163	*	Accumulibacter	Accumulibacter*	UW-1-IIA-com	*	*	Accumulibacter	*	*	*	*
<i>napH</i>	8	0	5	1	Acc bin1_88	BA-93-IA_298/UW-3_3162	*	Accumulibacter	Accumulibacter*	UW-1-IIA-com	*	*	Accumulibacter	*	*	*	*
<i>napI</i>	8	0	5	1	Acc bin1_38	BA-93-IA_213/UW-3_2006	*	Accumulibacter	Accumulibacter*	UW-1-IIA-com	*	*	Accumulibacter	*	*	*	*
<i>napA</i>	7	0	5	1	Acc bin1_36	BA-93-IA_213/UW-3_2008	*	Accumulibacter	Accumulibacter*	UW-1-IIA-com	Accumulibacter*	*	*	*	*	*	*
<i>nosF</i>	7	0	5	1	Acc bin1_89	BA-93-IA_298/UW-3_3161	Acc bin2_1600	*	Accumulibacter*	UW-1-IIA-com	*	Accumulibacter*	*	*	*	*	*
<i>nosZ</i>	7	0	5	1	Acc bin1_82	BA-93-IA_298/UW-3_3168	*	Accumulibacter	Accumulibacter*	UW-1-IIA-com	*	Accumulibacter*	*	*	*	*	*
<i>nirS</i> (second copy)	7	0	4	0	Acc bin1_1995	BA-93-IA_317/UW-3_2971	*	Accumulibacter*	UW-1-IIA-com	*	Accumulibacter*	Accumulibacter*	*	*	*	*	*
ABC transporter, substrate binding periplasmic protein MalF	6	0	6	1	Acc bin1_1446	BA-93-IA_110/UW-3_2546	Acc bin2_2427	Accumulibacter	Accumulibacter*	*	*	*	*	*	*	*	*
<i>napG</i>	6	0	5	1	Acc bin1_37	BA-93-IA_213/UW-3_2007	*	Accumulibacter	Accumulibacter*	UW-1-IIA-com	*	*	*	*	*	*	*
<i>nosD</i>	6	0	5	1	Acc bin1_86	BA-93-IA_298/UW-3_3164	*	Accumulibacter	Accumulibacter*	UW-1-IIA-com	*	*	*	*	*	*	*
<i>narI</i>	6	0	1	0	*	*	Acc bin2_3397	*	aalborgensis_339*	*	*	*	*	BA-91-IC_447	SK-01-IC_773	SK-02-IC_313	Candidatus_Accur
<i>nosL</i>	5	0	5	1	Acc bin1_90	BA-93-IA_298/UW-3_3160	Acc bin2_1599	*	Accumulibacter*	*	*	*	*	*	*	*	*
Potassium efflux system Kfa protein	5	0	5	1	Acc bin1_1447	BA-93-IA_110/UW-3_2547	*	Accumulibacter	Accumulibacter*	*	*	*	*	*	*	*	*
<i>narG</i> (second copy)	5	0	1	0	*	*	Acc bin2_3400	*	aalborgensis_339*	*	*	*	*	SK-01-IC_776	SK-02-IC_312	Candidatus_Accur	
<i>narH</i> (second copy)	5	0	1	0	*	*	Acc bin2_3399	*	aalborgensis_339*	*	*	*	*	SK-01-IC_775	SK-02-IC_313	Candidatus_Accur	
Cytochrome c-type biogenesis protein ResA	4	0	4	0	Acc bin1_92	BA-93-IA_299/UW-3_3158	*	Accumulibacter*	*	*	*	*	*	*	*	*	*
<i>nosY</i>	4	0	4	0	Acc bin1_918	BA-93-IA_219/UW-3_3159	*	Accumulibacter*	*	*	*	*	*	*	*	*	*
<i>nosZ</i>	4	0	3	0	Acc bin1_1449	BA-93-IA_1317*	*	Accumulibacter*	UW-1-IIA-com	*	*	*	*	*	*	*	*
NO ₃ ⁻ /NO ₂ ⁻ transporter (second copy)	4	0	1	0	*	*	Acc bin2_3401	*	aalborgensis_339*	*	*	*	*	SK-01-IC_777	SK-02-IC_312*		
NO ₃ ⁻ /NO ₂ ⁻ transporter (third copy)	2	0	1	0	*	*	Acc bin2_3402	*	aalborgensis_339*	*	*	*	*	*	*	*	*
<i>narJ</i>	1	0	1	0	*	*	Acc bin2_3398	*	aalborgensis_339*	*	*	*	*	*	*	*	*

* not found in the genome

** pink bar represents the completeness of the *Accumulibacter* genome

‡ Green bar represents the percentage of *Accumulibacter* genomes that harbor the specific denitrification gene

Labels in the table refer to contig number in each *Accumulibacter* genome

b.

CANDO_1_IA					
Contig number	ORF number	Start position (bp)	End position (bp)	length	Gene
Contig_29	12	15433	17730	2298	<i>nosZ</i>
	13	17822	18136	315	
	14	18290	19021	732	
	15	19216	20205	990	
	16	20209	21633	1425	<i>nosD</i>
	17	21630	22532	903	<i>napG</i> (second copy)
	18	22532	23494	963	<i>napH</i> (second copy)
	19	23504	24376	873	<i>nosF</i>
	20	24390	24863	474	<i>nosL</i>
	21	24874	25701	828	<i>nosY</i>
	22	25715	26215	501	Cytochrome c-type biogenesis protein <i>ResA</i>
	23	26278	27444	1167	<i>nirF</i>
	24	27452	28432	981	<i>nirL</i>
	25	28425	28904	480	<i>nirG</i>
26	28901	29398	498	<i>nirH</i>	
Contig_11	36	40739	43264	2526	<i>napA</i>
	37	43366	44310	945	<i>napG</i>
	38	44307	45209	903	<i>napH</i>
	39	45263	45730	468	<i>napB</i>
	40	45711	48617	2907	
41	48699	49340	642	<i>napF</i>	
Contig_188	18	17924	20353	2430	<i>nirB</i>
	19	20378	20686	309	<i>nirD</i>
	20	20732	21943	1212	$\text{NO}_3^-/\text{NO}_2^-$ transporter
Contig_936	1	1	1290	1290	<i>nirS</i> (second copy)
Contig_93	64	66932	68530	1599	<i>nirN</i>
	65	68530	69804	1275	<i>nirJ</i>
Contig_530	30	29969	31264	1296	ABC transporter, substrate binding periplasmic protein <i>MalE</i>
	31	31428	32540	1113	Potassium efflux system Kfa protein
	32	32955	34694	1740	<i>nirS</i>
Contig_2616	1	109	2397	2289	<i>norZ</i>

NCIB Accession Number: PDHR00000000

CANDO_2_IC					
Contig number	ORF number	Start position	End position	length	Gene
Contig_3522	4	3571	4068	498	<i>nirH</i>
	5	4065	4544	480	<i>nirG</i>
	6	4537	5517	981	<i>nirL</i>
	7	5525	6697	1173	<i>nirF</i>
	8	6904	7038	135	

	9	7448	7921	474	<i>nosL</i>
	10	7935	8807	873	<i>nosF</i>
	11	9021	10367	1347	<i>napH</i>
	12	10513	11244	732	
	13	11389	11568	180	
	14	11568	11702	135	
	15	11784	12113	330	<i>nosZ</i>
	16	12110	12373	264	<i>nosZ</i>
	17	12847	13398	552	<i>nosZ</i>
	4	2317	3063	747	<i>narI</i>
	5	3060	3743	684	<i>narJ</i>
	6	3746	5269	1524	<i>narH</i>
	7	5266	9084	3819	<i>narG</i>
Congit_11833	8	9130	10785	1656	NO ₃ ⁻ /NO ₂ ⁻ transporter (second copy)
	9	10910	11941	1032	NO ₃ ⁻ /NO ₂ ⁻ transporter (third copy)
Contig_3155	3	2612	3805	1194	<i>nirJ</i>
	4	3805	5412	1608	<i>nirN</i>
	13	14470	15681	1212	NO ₃ ⁻ /NO ₂ ⁻ transporter
Congit_3388	14	15718	15957	240	<i>nirD</i>
	15	16155	16838	684	<i>nirB</i>
	16	17068	17259	192	<i>nirB</i>
	17	17961	18596	636	<i>nirB</i>
	5	3210	4505	1296	ABC transporter, protein <i>MalE</i>
Contig_6160	6	4679	5026	348	
	7	5023	5868	846	
	8	6405	7587	1183	<i>nirS</i>
	*	end of contig			

NCIB Accession Number: PDHS00000000

HKU1					
Contig number	ORF number	Start position	End position	length	Gene
	3	1108	3405	2298	<i>nosZ</i>
	4	3487	3801	315	
	5	3952	4674	723	
	6	4870	5859	990	
LBIU01000345.1	7	5864	7285	1422	<i>nosD</i>
	8	7282	8193	912	<i>napG</i> (second copy)
	9	8193	9155	963	<i>napH</i> (second copy)
	10	9165	9434	270	<i>nosF</i>
LBIU01000307.1	6	3697	4002	306	

	5	2443	3606	1164	<i>nirF</i>
	4	1455	2435	981	<i>nirL</i>
	3	983	1462	480	<i>nirG</i>
	2	498	986	489	<i>nirH</i>
LBIU01000366.1	4	3535	5274	1740	<i>nirS</i>
LBIU01000485.1	1	1	903	903	<i>nirS</i>
LBIU01000254.1	4	3136	4296	1161	<i>nirN</i>
LBIU01000715.1	1	35	1231	1197	<i>nirJ</i>
	16	14957	17386	2430	<i>nirB</i>
LBIU01000080.1	15	14579	14932	354	<i>nirD</i>
	14	13304	14515	1212	NO ₃ ⁻ /NO ₂ ⁻ transporter
	10	8433	10958	2526	<i>napA</i>
	11	11059	12003	945	<i>napG</i>
LBIU01000002.1	12	12000	12902	903	<i>napH</i>
	13	12957	13424	468	<i>napB</i>
	14	13462	16302	2841	
	15	16384	16884	501	<i>napF</i>

Genebank accession number: GCA_000987395.1

BA-92					
Contig number	ORF number	Start position	End position	length	Gene
	39	41038	43335	2298	<i>nosZ</i>
	38	40631	40945	315	
	37	39747	40478	732	
	36	38563	39552	990	
	35	37135	38559	1425	<i>nosD</i>
	34	36236	37138	903	<i>napG</i> (second copy)
	33	35274	36236	963	<i>napH</i> (second copy)
JEMX01000011.1	32	34392	35264	873	<i>nosF</i>
	31	33905	34378	474	<i>nosL</i>
	30	33067	33894	828	<i>nosY</i>
	29	32553	33053	501	
	28	31126	32292	1167	<i>nirF</i>
	27	30138	31118	981	<i>nirL</i>
	26	29666	30145	480	<i>nirG</i>
	25	29172	29669	498	<i>nirH</i>
JEMX01000009.1	50	53065	54735	1671	<i>nirS</i>
	24	36290	38029	1740	<i>nirS</i>
	23	34973	35818	846	
JEMX01000038.1	22	32388	34670	2283	<i>norZ</i>
					Nitrite-sensitive transcriptional repressor <i>nsrR</i>
JEMX01000052.1	21	31724	32206	483	
	16	45716	48145	2430	<i>nirB</i>

	17	48170	48541	372	<i>nirD</i>
	18	48623	49834	1212	NO ₃ ⁻ /NO ₂ ⁻ transporter
	37	51947	52444	498	<i>napF</i>
	38	52529	55369	2841	
	39	55479	55946	468	<i>napB</i>
JEMX01000018.1	40	55985	56899	915	<i>napH</i>
	41	56896	57840	945	<i>napG</i>
	42	58040	60565	2526	<i>napA</i>
	43	60567	60815	249	<i>napD</i>
JEMX01000061.1	102	100722	1023388	922667	<i>nirN</i>
JEMX01000061.1	103	102338	103531	1194	<i>nirJ</i>

Genebank accession number: GCA_000585055.1

BA-93					
Contig number	ORF number	Start position	End position	length	Gene
	17	12404	14701	2298	<i>nosZ</i>
	18	14793	15107	315	
	19	15261	15992	732	
	20	16187	17176	990	
	21	17180	18604	1425	<i>nosD</i>
	22	18601	19503	903	<i>napG</i> (second copy)
	23	19503	20465	963	<i>napH</i> (second copy)
JEMY01000044.1	24	20475	21347	873	<i>nosF</i>
	25	21361	21834	474	<i>nosL</i>
	26	21845	22672	828	<i>nosY</i>
	27	22686	23186	501	
	28	23249	24415	1167	<i>nirF</i>
	29	24423	25403	981	<i>nirL</i>
	30	25396	25875	480	<i>nirG</i>
	31	25872	26369	498	<i>nirH</i>
	213	226226	227896	1671	<i>nirS</i>
	217	230236	230571	336	<i>nirC</i>
JEMY01000010.1	32	34774	36513	1740	<i>nirS</i>
JEMY01000013.1	105	118056	120344	2289	<i>norZ</i>
JEMY01000001.1	132	153275	154873	1599	<i>nirN</i>
	133	154873	156147	1275	<i>nirJ</i>
	79	88055	89134	1080	<i>narH</i>
JEMY01000004.1					Nitric oxide - responding transcriptional regulator <i>dnr</i> (Crp/Fnr family)
	89	97502	98194	693	
	180	194142	196571	2430	<i>nirB</i>
	181	196596	196904	309	<i>nirD</i>

	182	196950	198161	1212	NO ₃ ⁻ /NO ₂ ⁻ transporter
	120	143021	143521	501	<i>napF</i>
	121	143603	146449	2847	
JEMY01000026.1	122	146490	146957	468	<i>napB</i>
	123	147011	147913	903	<i>napH</i>
	124	147910	148854	945	<i>napG</i>
	125	148956	151481	2526	<i>napA</i>

Genebank accession number: GCA_000585075.1

UW-3					
Contig number	ORF number	Start position	End position	length	Gene
	3168	476833	479131	2298	<i>nosZ</i>
	3167	476427	476742	315	
	3166	475542	476274	732	
	3165	474358	475348	990	
	3164	472930	474355	1425	<i>nosD</i>
	3163	472031	472934	903	<i>napG</i> (second copy)
	3162	471069	472032	963	<i>napH</i> (second copy)
Ga0131788_12	3161	470187	471060	873	<i>nosF</i>
	3160	469700	470174	474	<i>nosL</i>
	3159	468862	469690	828	<i>nosY</i>
	3158	468348	468829	501	
	3157	467119	468286	1167	<i>nirF</i>
	3156	466131	467112	981	<i>nirL</i>
	3155	465659	466139	480	<i>nirG</i>
	3154	465165	465663	498	<i>nirH</i>
	2971	278238	279909	1671	<i>nirS</i>
	2548	2672706	2674445	1740	<i>nirS</i>
	830	867033	868632	1599	<i>nirN</i>
	829	865840	867034	1194	<i>nirJ</i>
	2003	2107383	2107884	501	<i>napF</i>
	2004	2107965	2110812	2847	
	2005	2110851	2111319	468	<i>napB</i>
	2006	2111372	2112275	903	<i>napH</i>
Ga0131788_11	2007	2112271	2113216	945	<i>napG</i>
	2008	2113317	2115843	2526	<i>napA</i>
	2199	2305402	2307832	2430	<i>nirB</i>
	2198	2305069	2305378	309	<i>nirD</i>
	2197	2304061	2305024	963	NO ₃ ⁻ /NO ₂ ⁻ transporter
	2703	2833766	2834006	240	<i>norB</i>

IMG (Integrated Microbial Genomes) genome ID 2687453699

C.

CANDO_1_IA														
Contig number	ORF number	Gene	Most abundant class assigned	Number of most abundant class assigned	Most abundant order assigned	Number of most abundant order assigned	Most abundant family assigned	Number of most abundant family assigned	Number of Rhodocyclales assigned	% of Rhodocyclales assigned	HGT (<8%) (1= with phylogenetic evidence of HGT, 0= with no phylogenetic evidence of HGT)	Core Accumulibacter gene (1=core, 0=non-core)	Core type I Accumulibacter gene (1=core, 0=non-core)	
Contig_29	12	<i>nosZ</i>	Epsilonproteobacteria	63	Campylobacterales	58	Campylobacteraceae	57	6	0.04	1	0	1	
	16	<i>nosD</i>	Betaproteobacteria	50	Rhodocyclales	20	Rhodospirillaceae	15	13	0.087	0	0	1	
	17	<i>narG</i> (second copy)	Epsilonproteobacteria	59	Campylobacterales	54	Campylobacteraceae	41	8	0.053	1	0	1	
	18	<i>narH</i> (second copy)	Epsilonproteobacteria	61	Campylobacterales	53	Campylobacteraceae	39	8	0.053	1	0	1	
	19	<i>nosF</i>	Epsilonproteobacteria	61	Campylobacterales	50	Campylobacteraceae	36	8	0.053	1	0	1	
	20	<i>nosL</i>	Epsilonproteobacteria	54	Campylobacterales	40	Campylobacteraceae	21	8	0.053	1	0	Derived	
	21	<i>nosY</i>	Epsilonproteobacteria	60	Campylobacterales	48	Campylobacteraceae	33	8	0.053	1	0	0	
	22	Cytochrome c-type biogenesis proteinA	Betaproteobacteria	137	Nitrosomonadales	44	Nitrosomonadaceae	33	11	0.073	1	0	0	
	23	<i>nirF</i>	Betaproteobacteria	140	Burkholderiales	63	Zoogloeaceae	22	15	0.1	0	0	1	
	24	<i>nirL</i>	Betaproteobacteria	128	Rhodocyclales	42	Comamonadaceae	25	17	0.106	0	1	1	
25	<i>nirG</i>	Betaproteobacteria	84	Rhodocyclales	38	Zoogloeaceae	20	15	0.099	0	1	1		
26	<i>nirH</i>	Betaproteobacteria	75	Rhodocyclales	27	Methylococcaceae	18	12	0.08	0	1	1		
Contig_11	36	<i>napA</i>	Gammaproteobacteria	71	Enterobacteriales	46	Enterobacteriaceae	38	12	0.08	0	0	1	
	37	<i>napG</i>	Gammaproteobacteria	77	Aeromonadales	46	Aeromonadaceae	46	10	0.067	1	0	1	
	38	<i>napH</i>	Betaproteobacteria	58	Rhodocyclales	34	Rhodobacteraceae	31	13	0.087	0	0	1	
	39	<i>napB</i>	Gammaproteobacteria	62	Rhodobacterales	26	Rhodobacteraceae	26	10	0.067	1	Derived	1	
	41	<i>napF</i>	Betaproteobacteria	89	Enterobacteriales	44	Yersiniaceae	28	8	0.053	1	1	1	
Contig_188	18	<i>nirB</i>	Betaproteobacteria	122	Burkholderiales	68	Burkholderiaceae	65	13	0.087	0	1	1	
	19	<i>nirD</i>	Betaproteobacteria	86	Rhodocyclales	27	Bradyrhizobiaceae	20	14	0.093	0	1	1	
	20	NQ /NQ' transporter	Betaproteobacteria	87	Pseudomonadales	46	Pseudomonadaceae	46	9	0.06	1	1	1	
Contig_936	1	<i>nirS</i>	Betaproteobacteria	91	Burkholderiales	40	Pseudomonadaceae	30	10	0.067	1	0	0	
Contig_93	64	<i>nirN</i>	Betaproteobacteria	136	Burkholderiales	51	Comamonadaceae	38	17	0.113	0	1	1	
	65	<i>nirJ</i>	Betaproteobacteria	82	Rhodocyclales	38	Methylococcaceae	23	16	0.107	0	1	1	
Contig_530	30	ABC transporter, substrate binding periplasmic protein	Betaproteobacteria	123	Burkholderiales	113	Burkholderiaceae	101	2	0.013	1	0	1	
	31	Potassium efflux system Kfa protein	Gammaproteobacteria	105	Oceanospirillales	40	Oceanospirillaceae	19	3	0.02	1	0	1	
	32	<i>nirS</i>	Betaproteobacteria	133	Burkholderiales	56	Comamonadaceae	23	14	0.093	0	1	1	
Contig_465	1	Nitrite-sensitive transcriptional repressor	Betaproteobacteria	72	Neisseriales	41	Neisseriaceae	41	3	0.02	1	0	1	
Contig_2616	1	<i>qnorB</i>	Betaproteobacteria	147	Burkholderiales	127	Burkholderiaceae	90	5	0.033	1	0	0	
CANDO_2_IC														
Contig number	ORF number	Gene	Most abundant class assigned	Number of most abundant class assigned	Most abundant order assigned	Number of most abundant order assigned	Most abundant family assigned	Number of most abundant family assigned	Number of Rhodocyclales assigned	% of Rhodocyclales assigned	HGT (<8%) (1= with phylogenetic evidence of HGT, 0= with no phylogenetic evidence of HGT)	Core Accumulibacter gene (1=core, 0=non-core)	Core type I Accumulibacter gene (1=core, 0=non-core)	
Contig_3522	4	<i>nirH</i>	Betaproteobacteria	83	Rhodocyclales	31	Methylococcaceae	18	12	0.08	0	1	1	
	5	<i>nirG</i>	Betaproteobacteria	84	Rhodocyclales	38	Methylococcaceae	21	15	0.099	0	1	1	
	6	<i>nirL</i>	Betaproteobacteria	125	Rhodocyclales	43	Comamonadaceae	26	17	0.106	0	1	1	
	7	<i>nirF</i>	Betaproteobacteria	138	Burkholderiales	61	Zoogloeaceae	22	15	0.1	0	1	1	
	9	<i>nosL</i>	Epsilonproteobacteria	51	Campylobacterales	39	Campylobacteraceae	21	8	0.02	1	0	Derived	
	10	<i>nosF</i>	Epsilonproteobacteria	61	Campylobacterales	50	Campylobacteraceae	36	8	0.053	1	0	1	
	11	<i>napH</i>	Betaproteobacteria	53	Campylobacterales	28	Campylobacteraceae	15	15	0.1	0	0	1	
	15	<i>nosZ</i>	Epsilonproteobacteria	69	Campylobacterales	68	Campylobacteraceae	66	7	0.06	1	0	1	
	16	<i>nosZ</i>	Betaproteobacteria	30	Rhodocyclales	18	Rhodospirillaceae	15	9	0.047	1	0	1	
	17	<i>nosZ</i>	Epsilonproteobacteria	70	Campylobacterales	67	Campylobacteraceae	64	7	0.08	0	0	1	
Contig_11833	4	<i>narI</i>	Betaproteobacteria	149	Burkholderiales	121	Comamonadaceae	89	4	0.026	1	0	1	
	5	<i>narJ</i>	Betaproteobacteria	149	Burkholderiales	105	Comamonadaceae	87	5	0.033	1	0	1	
	6	<i>narH</i>	Betaproteobacteria	149	Burkholderiales	116	Comamonadaceae	87	4	0.027	1	0	1	
	7	<i>narG</i>	Betaproteobacteria	149	Burkholderiales	117	Comamonadaceae	93	4	0.027	1	0	1	
	8	NO ₃ ⁻ /NO ₂ ⁻ transporter (second copy)	Betaproteobacteria	108	Burkholderiales	48	Comamonadaceae	45	6	0.04	1	0	1	
	9	NO ₃ ⁻ /NO ₂ ⁻ transporter (third copy)	Betaproteobacteria	80	Pseudomonadales	50	Pseudomonadaceae	50	2	0.013	1	0	1	
	Contig_3155	3	<i>nirJ</i>	Betaproteobacteria	82	Rhodocyclales	38	Zoogloeaceae	20	16	0.107	0	1	1
		4	<i>nirN</i>	Betaproteobacteria	135	Burkholderiales	52	Comamonadaceae	39	17	0.113	0	1	1
Contig_3388	13	NO ₃ ⁻ /NO ₂ ⁻ transporter	Betaproteobacteria	83	Pseudomonadales	55	Pseudomonadaceae	55	9	0.06	1	1	1	
	14	<i>nirD</i>	Betaproteobacteria	72	Pseudomonadales	42	Pseudomonadaceae	42	12	0.08	0	1	1	
Contig_6160	8	<i>nirS</i>	Betaproteobacteria	126	Burkholderiales	62	Burkholderiaceae	30	12	0.08	0	0	1	

Table S4.3 Summary statistics for 39 draft flanking (non-Accumulibacter) bacterial genomes extracted from our study (a) and the 8 draft bacterial genomes (including 7 flanking bacterial genomes and 1 Accumulibacter IB genome) extracted from an aerobic EBPR study (b)

a.

Genome ID	Relative abundance (%)					N ₂ O producer or consumer or non-denitrifier	Phylogenetic affiliation					Completeness	Contamination	Mean GC content	Genome Size (bp)	Length of the longest contig	N50 of contigs	Number of contigs	Length of the longest scaffold	N50 of scaffolds	Number of scaffolds		
	CANDO_0519	CANDO_0807	CANDO_0917	CANDO_1015	CANDO_1113		phylum	class	order	family	genus											species	
1	0.04	1.27	0.01	0.01	0	N ₂ O producer	Actinobacteria	Actinobacteri	Actinomycetales	Micrococcales	Jambivibacter	95.51	8.13	0.53	3371348	69678	19658	426	69678	22285	378		
2	0.58	1.64	2.31	0.84	0.14	non-denitrifier	Acidobacteria					81.78	3.47	0.55	3600662	35471	3926	1388	40802	6328	732		
3	0.01	0.05	0.22	0.43	0.32	non-denitrifier	Armatimonadetes					87.35	0.93	0.59	3246610	80276	29504	207	105290	48291	125		
4	0.02	0.1	0.12	0.96	1.15	non-denitrifier	Bacteroidetes	Bacteroidetes	Cytophaga			96.45	2.19	0.46	4259813	134498	27759	282	147894	43124	181		
5	0.03	0.11	1.03	0.05	0.4	N ₂ O consumer	Bacteroidetes	Flavobacteriia	Flavobacteriales	Cryomorphaceae	Flavicola	98.1	0	0.30	3264396	153694	30138	211	153694	30138	192		
6	0.27	0.23	0.31	0.03	0	N ₂ O consumer	Bacteroidetes	Flavobacteriia	Flavobacteriales	Cryomorphaceae	Flavicola	81	2.15	0.60	3139790	40661	7517	608	40661	8262	540		
7	1.43	0.51	0.32	0.02	0	N ₂ O consumer	Bacteroidetes	Flavobacteriia	Flavobacteriales	Cryomorphaceae		83.43	4.57	0.59	3773280	43473	6770	799	44455	7596	671		
8	0	0.01	0.31	0.08	0.02	N ₂ O consumer	Bacteroidetes	Flavobacteriia	Flavobacteriales	Flavobacteriaceae	Flavobacterium	88.2	0.44	0.34	2687782	29213	5945	567	29213	6002	549		
9	0.02	0	0.4	0.04	0	non-denitrifier	Bacteroidetes	Flavobacteriia	Flavobacteriales			93.57	1.29	0.31	3457893	31422	9744	516	31422	9744	506		
10	0	0.48	0.03	0	0	non-denitrifier	Bacteroidetes	Flavobacteriia				98.1	1.95	0.43	3358587	79175	17497	291	79175	17576	280		
11	0.07	5.59	3.99	0.74	0.11	N ₂ O consumer	Bacteroidetes	Sphingobacteriia	Sphingobacteriales	Chitinophagaceae	Unassign	86.24	2.73	0.43	3063969	51456	5401	867	52508	9283	451		
12	0.01	0.1	0.81	0.03	0.01	N ₂ O consumer	Bacteroidetes	Sphingobacteriia	Sphingobacteriales	Saprosiraceae		99.01	0.99	0.42	5775792	82720	29442	311	82720	31697	282		
13	0.02	0.01	0.95	0.33	0.01	N ₂ O consumer	Bacteroidetes	Sphingobacteriia	Sphingobacteriales			96.7	1.48	0.39	3132491	112465	30299	192	112465	35421	162		
14	0.03	0.12	1.08	0.06	0.43	N ₂ O consumer	Bacteroidetes					91.96	1.22	0.30	3053313	41807	5621	663	41807	5663	651		
15	0.02	0.01	0.38	1.12	1.17	N ₂ O consumer	Chloroflexi	Anaerolineae	Anaerolineales	Anaerolineaceae	Anaerolinea	96.62	1.09	0.55	5396076	60025	14859	632	83024	17845	513		
16	0.01	0.01	0.13	0.52	0.36	N ₂ O producer	Chloroflexi	Anaerolineae	Anaerolineales	Anaerolineaceae	Anaerolinea	80.13	5.76	0.66	5935909	27580	6545	1251	27580	6752	1118		
17	0.02	0.32	0.87	0.55	0.25	N ₂ O producer	Chloroflexi	Anaerolineae	Anaerolineales	Anaerolineaceae		90.3	3.73	0.46	5484937	60071	11298	789	70515	14935	545		
18	0.05	0.31	0.35	0.3	0.28	non-denitrifier	Chloroflexi	Anaerolineae	Anaerolineales	Anaerolineaceae	Anaerolinea	80.45	4.55	0.57	2961439	28395	7299	565	29423	8073	472		
19	0.08	0.05	0.04	0.49	11.79	N ₂ O consumer	Chloroflexi	Caldilineae	Caldilineales	Caldilineaceae		89.51	0.36	0.60	3743371	99844	19273	318	99844	20229	290		
20	0	0	0	0.23	0	non-denitrifier	Firmicutes	Clostridia	Clostridiales			91.73	3.12	0.44	3329163	49938	7276	589	49938	7276	586		
21	0	0	0.4	0.25	0.05	non-denitrifier	Ignavibacteria	Ignavibacteriia	Ignavibacteriales	Ignavibacteriaceae	Ignavibacterium	86.33	2.98	0.39	3235906	28659	5233	856	32760	6184	650		
22	0.35	0.76	0.41	0.69	0.16	non-denitrifier	Ignavibacteria	Ignavibacteriia	Ignavibacteriales			90.69	3.32	0.35	3937146	59677	16544	390	76988	20692	279		
23	0.02	0.22	0.77	0.89	0.2	N ₂ O consumer	Ignavibacteria	Ignavibacteriia	Ignavibacteriales			83.54	0.63	0.40	3556809	63072	6806	808	63072	8373	583		
24	0.01	0.43	0.69	0.2	0.15	N ₂ O consumer	Ignavibacteria	Ignavibacteriia				91.35	1.09	0.39	3546363	40170	7728	616	40170	8196	583		
25	0.01	0.05	0.12	0.47	0.21	N ₂ O consumer	Ignavibacteria	Ignavibacteriia				89.33	3.55	0.40	4087077	54037	9145	681	64657	12145	491		
26	0.01	0.28	0.61	0.18	0.08	N ₂ O producer	Proteobacteria	Alphaproteobacteria	Rhodobacterales	Rhodobacteraceae	Rhodobacter	92.36	1.55	0.67	3919152	161819	17177	385	161819	18611	309		
27	0.07	1.1	1.28	0.71	0.41	non-denitrifier	Proteobacteria	Alphaproteobacteria				83.85	1.23	0.69	3244900	35056	4747	1016	36651	7554	541		
28	1.05	0.47	0.24	0.73	0.3	N ₂ O consumer	Proteobacteria	Betaproteobacteria	Burkholderiales	Comamonadaceae		80.55	3.29	0.64	3394846	28058	5361	1023	39756	9437	491		
29	0.12	1.5	0.95	0.43	0.07	N ₂ O consumer	Proteobacteria	Betaproteobacteria	Rhodocyclales	Rhodobacteraceae	Zoogloeaceae	Thaueria	Sp. N	82.02	1.4	0.39	3690028	27682	4189	1469	43108	7508	709
30	0.04	0.23	0.39	0.58	0.42	N ₂ O producer	Proteobacteria	Betaproteobacteria	Unassigned	betaproteobacteria		81.03	3.22	0.71	3959369	65093	8404	866	75135	12883	485		
31	2.84	1.69	0.05	0.01	0.01	N ₂ O producer	Proteobacteria	Betaproteobacteria				81.37	1.34	0.62	3957613	77586	10823	565	77586	16477	316		
32	0.01	0	0.26	0.1	0.01	non-denitrifier	Proteobacteria	Deltaproteobacteria	Bdellovibrionia	Bdellovibrionales	Bdellovibrionaceae		86.99	4.07	0.41	4469296	32573	5890	941	32573	5900	938	
33	0.05	0.03	0.08	1.35	5.63	N ₂ O producer	Proteobacteria	Gammaproteobacteria	Xanthomonadales	Xanthomonadales	PseudoXanthomonas	81.85	0.53	0.70	2639813	28682	5465	803	57569	20825	209		
34	0.09	0.18	0.61	0.34	0.18	N ₂ O producer	Proteobacteria	Gammaproteobacteria	Xanthomonadales	Xanthomonadales	Rudaea	85.67	1.37	0.62	3234480	36150	8024	567	41352	10273	422		
35	0.15	0.06	1.99	3.63	2.1	N ₂ O producer	Proteobacteria	Gammaproteobacteria	Xanthomonadales	Xanthomonadales		95.74	1.86	0.63	3550215	207744	40310	279	207746	48838	210		
36	0.01	0	0.01	0.33	0.58	N ₂ O consumer	Verrucomicrobia	Sphingobacteriia	Chthoniobacter			96.82	5.41	0.59	3567367	46973	11705	493	78398	12603	429		
37	0	0	0.19	0.2	0.03	N ₂ O consumer	Verrucomicrobia	Unassigned	Verrucomicrobia			81.11	1.4	0.61	4058141	23379	4313	1115	22379	4327	1092		
38	0.01	0.06	0.53	0.02	0.04	non-denitrifier	Verrucomicrobia	Verrucomicrobia	Verrucomicrobiales	Verrucomicrobiaceae	Verrucomicrobium	96.95	3.74	0.63	6374720	162322	42963	283	162322	45507	259		
39	0.01	0.07	0.6	0.13	0.01	N ₂ O producer	Verrucomicrobia					95.58	2.39	0.65	3750541	110138	38695	168	129579	44941	140		
Sum of relative abundance of N ₂ O consumers, producers and non-denitrifiers																							
3.1	9.36	11.96	5.51	3.66		N ₂ O consumer																	
3.26	4.14	5.34	7.3	9.04		N ₂ O producer																	
3.18	9.41	12.19	6.2	15.48		N ₂ O consumer																	
1.12	4.5	6.31	4.57	2.56		non-denitrifier																	

b.

Genome_ID	Relative abundance (%)			N ₂ O producer or non-denitrifier	Phylogenetic affiliation						Completeness	Contamination	Mean GC contc	Genome Size (bp)	Length of the longest contig	N ₅₀ of contigs	Number of contigs	Length of the longest scaffold	N ₅₀ of scaffold	Number of scaffolds
	Average	P1	P2		phylum	class	order	family	genus	species										
1	0.68	0.28	1.08	N ₂ O consumer	Bacteroidetes	Bacteroidetes	Bacteroidia				80.91	4.53	0.358000864	5358596	23087	4624	1488	23087	4624	1488
2	2.21	3.85	0.58	N ₂ O consumer	Bacteroidetes	Bacteroidetes					95.97	2.69	0.412831198	4771277	75800	14710	551	75800	14710	551
3	5.77	9.84	1.70	N ₂ O consumer	Bacteroidetes	Flavobacteriia	Flavobacteriales	Flavobacteriaceae	Aequorivita		98.72	0.39	0.376501861	3289418	177324	53450	139	177324	53450	139
4	5.30	10.07	0.54	N ₂ O producer	Bacteroidetes	Flavobacteriia	Flavobacteriales	Flavobacteriaceae			98.84	1.18	0.367491171	3743826	268748	103147	87	268748	103147	87
5	0.89	0.25	1.54	N ₂ O producer	Chloroflexi						92.73	0.91	0.524109912	6470679	293316	87050	195	293316	87050	195
6	1.43	0.04	2.83	N ₂ O producer	Proteobacteria	Alphaproteobacter	Sphingomonadales	Erythrobacteraceae	Erythrobacter	Erythrobacter Lito	98.57	1.95	0.634464205	3714509	167394	50589	181	167394	50589	181
7	5.32	0.00	10.65	non-denitrifier	Bacteroidetes						94.05	1.61	0.396549795	4165608	260247	156176	53	260247	156176	53
Sum of relative abundance of N ₂ O consumers, producers and non-denitrifiers																				
8.67	13.97	3.37	N ₂ O consumer																	
7.63	10.36	4.90	N ₂ O producer																	
5.32	0.00	10.65	non-denitrifier																	

Table S4.4 *ppk1* gene qPCR primers and performance statistics.

		Name	Forward Primer	Reverse Primer	Amplicon size (bp)	qPCR performance		Reference
						Std curve correlation coefficient	qPCR efficiency (%)	
IA	Old	Acc-ppk-974f/113r	TGATGCGCGACA ATCTCAAATTCAA	AATGATCGGATTG AAGCTCTGGTAG ATGGCCTCGAAGA	140	0.999	98.6	Zhang et al.
	New	AccIA-ppk1-978f/1058r	GCGCGACAATCT CAAATTCAA	GGTTGC TGGCCTCGAAAAC GTTGC	81	0.993	98.7	Camejo et al.
IB	Old	Acc-ppk-372f/653r	TGAAGGCATTTCG CTTCCT	AAGCAGTATTTCGC TGTC	282	0.994	105.1	Zhang et al.
	New	AccIB-ppk1-884f/1009r	TGCTTGGCCACTT CAACC	GCTTGAAGGGCTG GAACT	126	0.997	101.5	Camejo et al.
IC	Old	Acc-ppk1-362f/758r	AGCTGGCGAGTG AAGGCATTTCG GCGACACTTTGGT	AACAGGTTGCTGT TGCGCGTGA	397	0.999	89.0	Zhang et al.
	New	AccIC-ppk1-815f/911r	AATGCG CGACACTTTGGCA ATGCG	CGCTCGGTGAGGT CGAA	96	0.996	97.2	Camejo et al.
IIC	Old	Acc-ppk-254f/460r	TCACCACCGACG GCAAGAC	CCGGCATGACTTC GCGGAAG	207	0.999	97.2	He et al.
	New	AccIIC-ppk1-635f/794r	GCGACAGTGAGT ACGCCT	TTGGCGCGCAGAT TGGT	160	0.997	94.5	Camejo et al.

4.5.3 Supporting Information - Figures

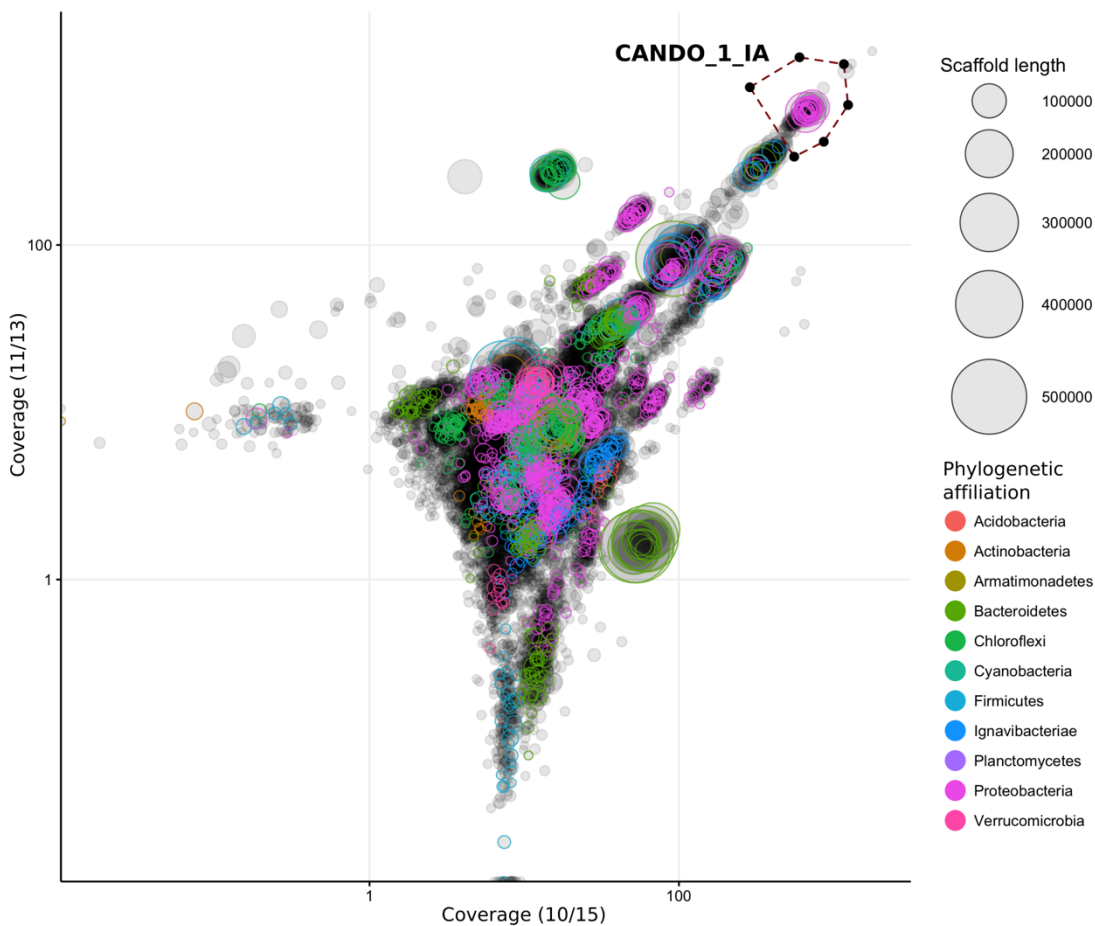


Figure S4.1 Extraction of CANDO_1_IA genome bin from metagenome scaffolds using differential coverage binning (x-axis: coverage for sample taken on 10/15/2015, y-axis: coverage for sample taken on 11/13/2015).

Circles represent scaffolds greater than 1.5 kbp and are colored by phylum level phylogenetic affiliation. The box in the figure encloses the scaffold bin for *Accumulibacter* clade IA. The *Accumulibacter* affiliation was confirmed by extracting *Accumulibacter*-specific *ppk1* gene sequences from the scaffolds.

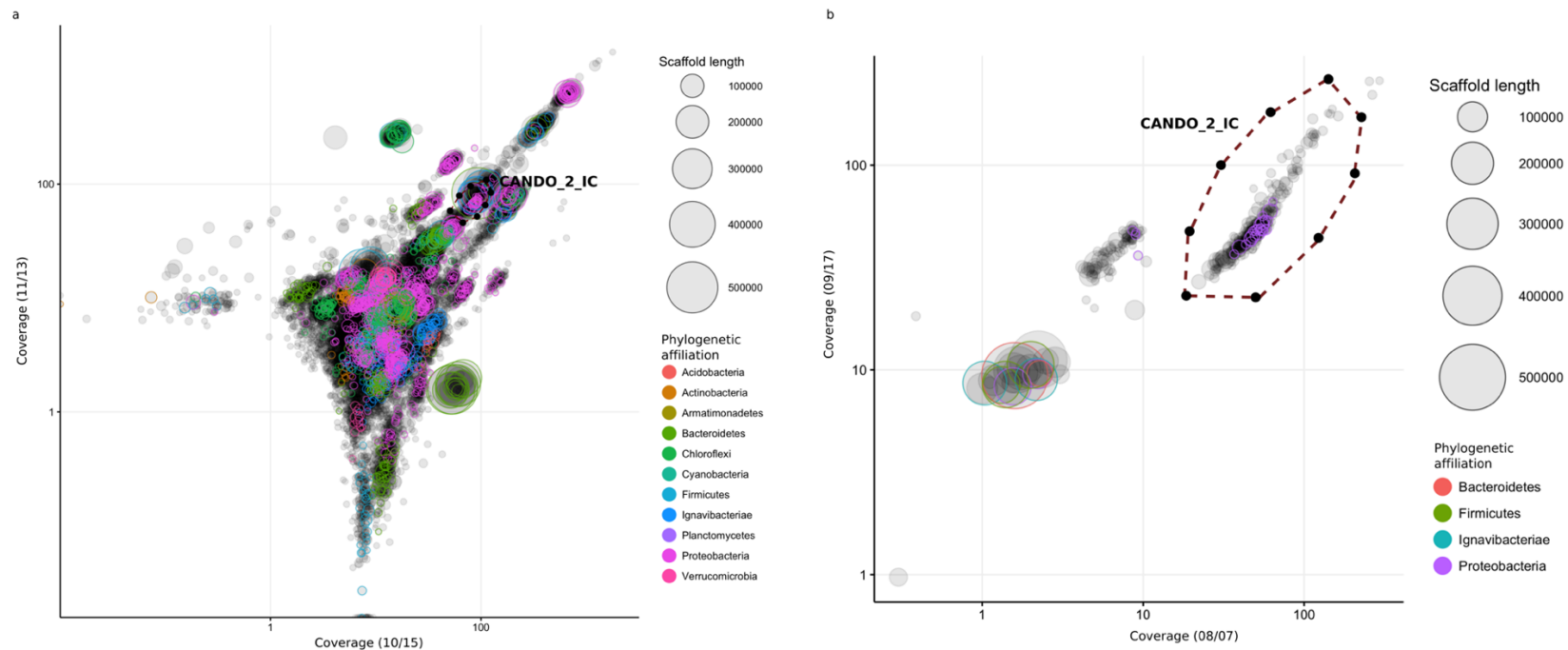


Figure S4.2 Extraction of CANDO_2_IC genome bin from metagenome scaffolds (longer than 1.5 kbp) using differential coverage binning.

(a): x-axis: coverage for sample taken on 10/15/2015, y-axis: coverage for sample taken on 11/13/2015. The box encloses the scaffold bin for *Accumulibacter* clade IC. Circles in figure S4.2b represent scaffolds enclosed by box in figure S4.2a. (b): x-axis: coverage for enclosed scaffolds based on sample taken on 08/07/2015, y-axis: coverage for enclosed scaffolds based on sample taken on 09/17/2015. Circles in both a and b are colored by phylum level phylogenetic affiliation and scaled by the length of scaffold.

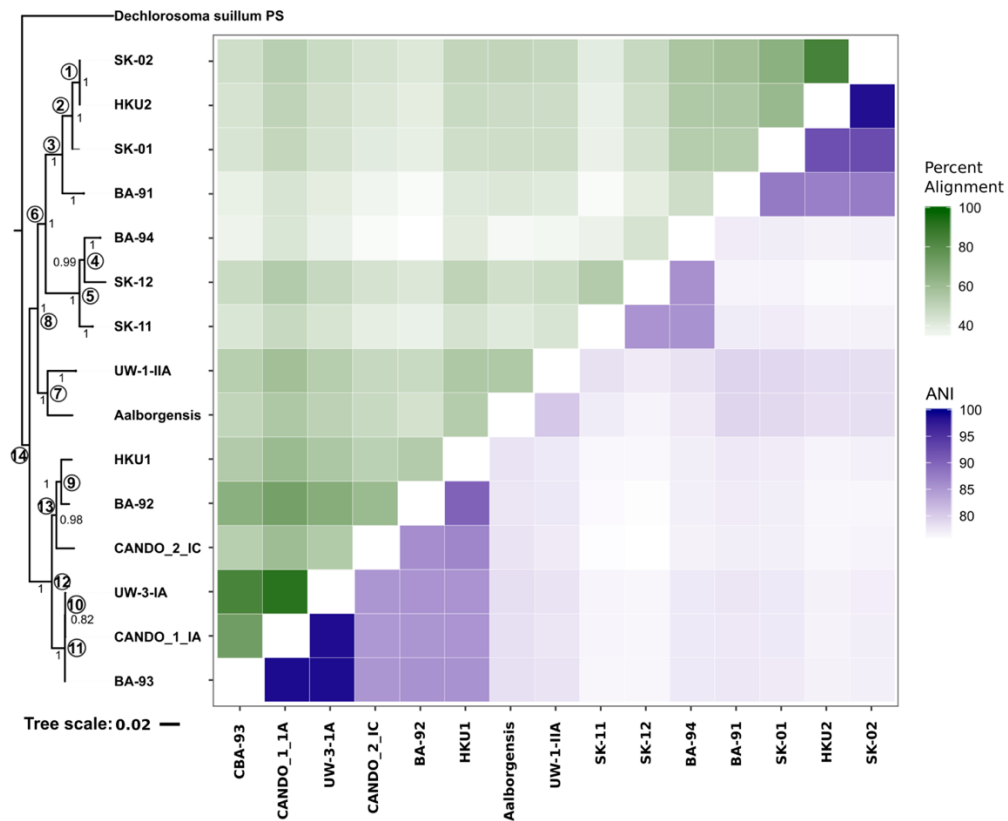


Figure S4.3 Comparison of the average nucleotide identity (ANI) and percent alignment for all 15 publicly available *Accumulibacter* genomes. CANDO_1_IA and CANDO_2_IC draft genomes were recovered in this study.

A total of 13 genome assemblies were downloaded from NCBI and JGI. The GenBank accession numbers for these genomes are listed in the methods of the SI. The phylogenetic tree in this figure was generated in Kbase using the Insert Genomes into Species Tree App, and nodes are labelled in order to map inferred gene gain/loss patterns for gene flux analysis. A total of 49 highly conserved COG domains was used for the alignment and the tree was built using FastTree2 with a maximum likelihood method. A detailed list of the 49 COG domains is described in the Kbase documentation (<https://kbase.us/insert-genomes-into-species-tree-app/>).

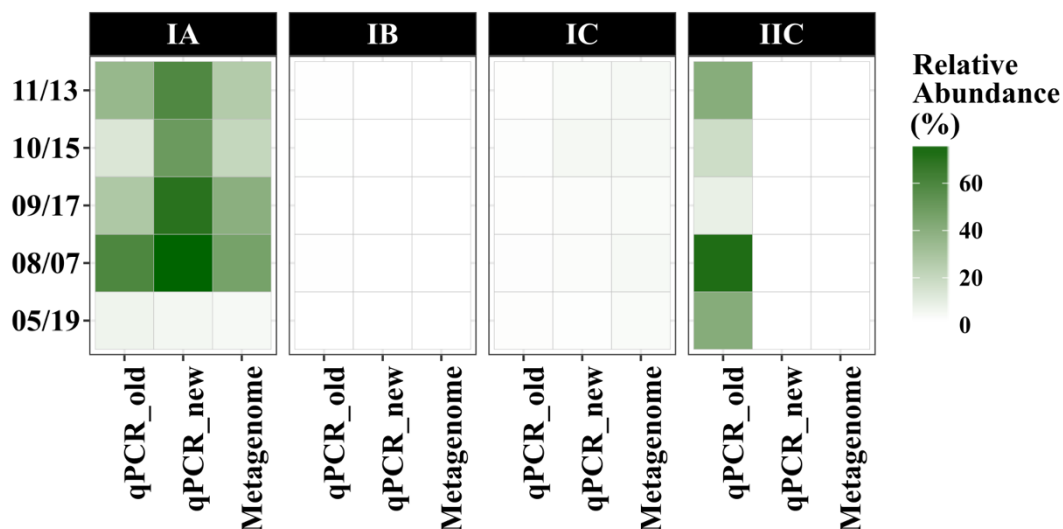


Figure S4.4 Comparison of relative abundance of different Accumulibacter clades (IA-IC, IIC) based on qPCR and metagenomic analysis.

For the qPCR assays, both an older primer set (qPCR_old) designed by He et al. and Zhang et al. and a recent reported primer set (qPCR_new) designed by Camejo et al. were used for comparison^{89, 176, 184}. Relative abundance was calculated by normalizing the *ppk1* gene copy number by universal bacterial 16S rRNA gene copy number.

Figure S4.5 Reference *ppk1* gene phylogenetic tree based on 781 *ppk1* gene sequences (1007 bp) and 68 clone sequences in this study. Clades IA to IE and IIA to II-I are labeled. The phylogenetic tree was built in FastTree using the maximum likelihood method. A *Rhodocyclus tenuis ppk1* gene (accession number: AF502199) was used as the outgroup. Only branching order, not tree branch length, is taken into account in the phylogenetic tree.

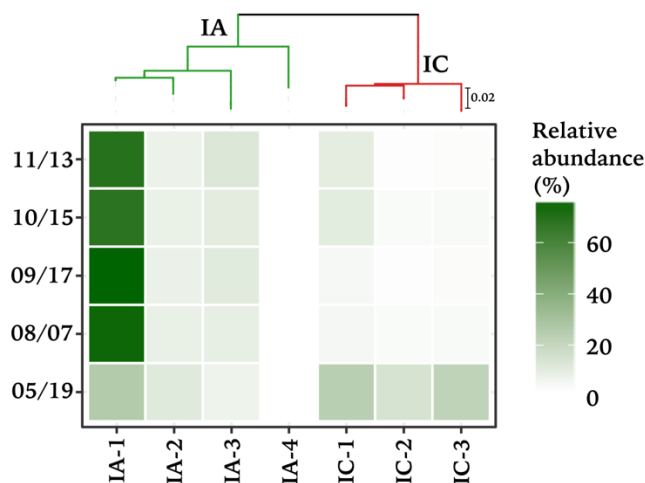


Figure S4.6 The temporal change of distribution of all 7 *Accumulibacter* phylotypes extracted from metagenomic reads (IA: IA-1-4, IC: IC-1-3) from 5/19/2015 (bottom row) to 11/13/2015 (top row).

Relative abundance was calculated by dividing coverage of individual *Accumulibacter* phylotype by the sum of coverage for all 7 *Accumulibacter* phylotypes. IA-1 and IC-1 *ppk1* phylotypes were >99% identical to the two *ppk1* sequences from assembled *Accumulibacter* composite genomes in this study.

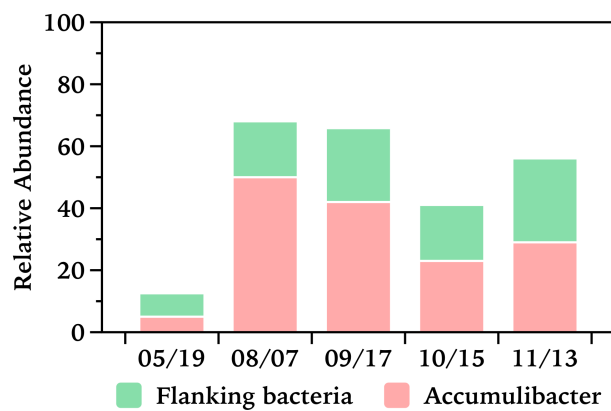


Figure S4.7 The relative abundance (%) of the sum of two *Accumulibacter* genome bins and the sum of 39 extracted flanking (non-*Accumulibacter*) bacterial genome bins from 05/19/2015 to 11/13/2015.

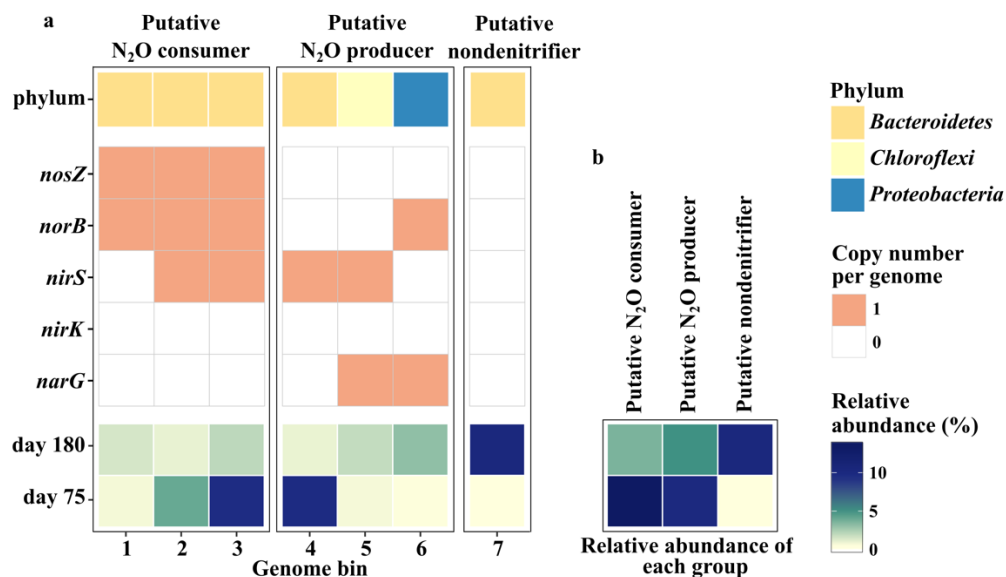


Figure S4.8 (a). Dynamics in relative abundance of 7 flanking (non-PAO) bacterial genome bins assembled from shotgun metagenomic sequencing of an aerobic EBPR system²²⁰ (bottom), the presence and copy number per genome of different denitrification structural genes (*narG*, *nirK*, *nirS*, *norB* (*qnorB* or *cnorB*), and *nosZ*) (middle), and the assigned taxonomy for each genome bin at the phylum level (top). **(b).** Sum of relative abundance of putative N₂O consumers and producers, and putative nondenitrifiers.

Bin_1-3 are identified as potential N₂O consumers as they harbor *nosZ*. Bin_4-6 are identified as putative N₂O producers.

CHAPTER 5

Segregation of Microbial Community Composition and Function in Granular Denitrifying EBPR Process

This chapter has been submitted for review: Gao, H., Zhao, X., Zhou, L., Sabba, F., and Wells, G.F. Differential Kinetics of Nitrogen Oxides Reduction Leads to Elevated N₂O Production by a Nitrite Fed Granular Denitrifying EBPR Reactor (*In review*).

ABSTRACT

The formation of granular microbial aggregates was observed without intentional granule selection in a denitrifying enhanced biological phosphorus removal (EBPR) reactor with constant nutrient removal and high-rate nitrous oxide (N₂O) formation. Sources of N₂O emission and the interactions among microbial populations from other granular nitrogen (N) removal processes, for example, nitrification-anammox, have been explored. However, little is known about N₂O formation in microbial aggregates for denitrifying EBPR process via denitrification pathway. Thus, we applied 16S rRNA gene amplicon sequencing and real-time quantitative PCR (qPCR) to determine denitrifying EBPR microbial community composition and genetic denitrification potential within different size fractions of biomass. High-throughput 16S rRNA gene sequencing revealed the segregation of microbial community in small floccular and large granular aggregates, and the selective enrichment of putative *Candidatus* Accumulibacter-associated denitrifying phosphate accumulating organisms (DPAOs) in large granular biomass. Genetic potential for N₂O accumulation has been reported to be connected to the relative abundance of nitrite reductase gene (*nir*) and nitrous oxide reductase gene (*nos*). qPCR-based profiling of denitrification functional genes demonstrated that smaller floccular aggregates had higher genetic potential for N₂O production rather than consumption, while large granular aggregates were more likely to be a putative sink for N₂O.

5.1 Introduction

Microbial granules are typically dense clusters of cells with diverse taxonomic origins²⁴⁰. Even though cell dispersion could occur at the edge of an aggregate, usually, a stable microbial aggregate is able to retain an approximately spherical shape even with high strength mechanical interruption²⁴⁰. Since the introduction of granular sludge for anaerobic treatment²⁴¹, several granular-sludge-based wastewater treatment techniques have been developed, including aerobic granular- and annamox granular-based treatment processes²⁴²⁻²⁴⁵. Due to their low cost and low footprint, these granular wastewater treatment processes become an alternative to the conventional floc-based treatment processes²⁴⁶. Compared with floc biomass-based processes, granular-based processes promise high rates of nutrient and organic carbon removal²⁴⁷. Besides, the higher density of biomass aggregates makes it easier and faster to be separated from clean water²⁴⁷. The system stability is also reported to increase probably due to the metabolic complementation and ecological interactions in these self-forming mesoscopic structures²⁴⁸.

Operationally, the successful development of granules can be controlled by seed sludge, substrate composition, organic loading rate, feeding strategy, reactor design and hydrodynamics, and settling time^{242, 243, 247, 249-251}. Gel-forming extracellular polymeric substances (EPS) have been hypothesized to act as a structural gel and bridge bacterial cells to form the precursor of a granule. And EPS have been reported to play an essential role in determining the stability of granules^{249, 252-254}. Although intentional selection for granules could shorten the granulation period, several recent studies have demonstrated that loose floccular biomass and dense granules can coexist, even in suspended growth reactors without intentional selection for granules^{240, 255, 256}.

Recently, several studies have focused on understanding the microbial community structure and N_2O emission in granular anammox reactors. By separating anammox granules into different size fractions, Luo and colleagues discovered that the abundance of key taxa, including anammox bacteria and ammonium oxidizing bacteria (AOB), varied with granular size²⁵⁷. Besides, the overall microbial community diversity as well as the anammox bacteria diversity increased in larger granules. Both nitrifiers and putative heterotrophic denitrifiers were proposed to be the source of N_2O in the oxic or anoxic zone within an anammox granule²⁵⁸. Polyphosphate accumulating organisms (PAOs) and denitrifying PAOs (DPAOs) enriched granules have been observed under cyclic anaerobic/aerobic or anaerobic/anoxic/aerobic conditions for phosphorus (P) (and N) removal^{79, 172, 259, 260}. However, little is known about how the microbial community (including PAOs/DPAOs and non-PAOs) and the genetic potential for denitrification varies in different biomass fractions in DPAO-enriched bioreactors. In particular, few studies have investigated the role of PAOs and flanking non-PAO community in different aggregate size fractions.

The overall objective of this study was to investigate the segregation of microbial populations and genetic potential for N transformations as well as N_2O accumulation by aggregate size (flocs versus granules). After separating biomass into different size fractions, we employed high-throughput 16S rRNA amplicon sequencing and quantitative PCR (qPCR) to assess the community structure and the function of both PAO and non-PAO fractions of the overall microbial consortium, and to reveal the segregation of putative N_2O producers and consumers by aggregate size fractions.

5.2 Materials and Methods

5.2.1 Biomass Separation by Particle Size

A sieve analysis was performed prior to DNA extraction to separate biomass aggregates with different sizes on two selected days (day 591 and day 626). A total of 50mL biomass was collected to obtain a representative amount of biomass for each size fraction. Three different sieve sizes were used to separate aggregates into four size ranges: <150 μ m, 150-350 μ m, 350-600 μ m and >600 μ m. In this work, for comparison purposes, we defined aggregates smaller than 600 μ m in diameter as small floccular aggregates (flocs) and greater than 600 μ m as large granular aggregates (granules).

5.2.2 DNA Extraction and 16S rRNA Gene Amplicon Sequencing

High-throughput amplicon-based 16S rRNA gene sequencing was used to characterize the microbial community structure in the total biomass from nine samples between days 490 to 600 and eight samples representing four size ranges of biomass on days 591 and 626. 2 mL of biomass was sampled from the mother bioreactor for DNA extraction representing total biomass during the period when batch assays were conducted. Duplicate DNA extractions were performed using the FastDNA SPIN Kit for soil (MP Biomedicals, USA), following the manufacturer's instructions. A detailed description of PCR amplification, library preparation for Illumina MiSeq Sequencing, and bioinformatics analysis is provided in the SI^{152, 261, 262}.

5.2.3 Quantifying Denitrification Genes via Quantitative PCR (qPCR)

qPCR assays were employed to quantify the abundance of the key denitrification functional genes: nitrate reductase (*narG*), cytochrome cd₁-type nitrite reductase (*nirS*), copper-containing

nitrite reductase (*nirK*), and nitrous oxide reductase (*nosZ*) (clades I and II). The abundance of *Accumulibacter* was also quantified based on *Accumulibacter*-specific 16S rRNA gene qPCR analyses. qPCR analyses of universal bacterial 16S rRNA genes were used to normalize all targeted genes. gDNA extracts were diluted 100-fold before performing qPCR to remove potential PCR inhibition. Two biological replicates were employed for each sample. Details of qPCR assays, including primers used in the study, reaction reagents, temperature programs and quality control parameters are provided in the SI.

5.2.4 Statistical Analysis

Analysis of variance (ANOVA) and post-hoc tests as well as Spearman correlation analysis were performed in R 3.3.2¹⁵⁷. To study co-occurrence and co-exclusion patterns between the most abundant bacteria taxa in genus level, Spearman correlation analyses between the top 15 microbial taxa (at the genus level) were conducted based on relative abundance of taxa in different size fractions. Strong and significant correlations (Spearman $|\rho| > 0.7$, $p < 0.05$) were visualized by R package *igraph*²⁶³. Analysis of similarities (ANOSIM) and permutation analysis of variance (PERMANOVA) were performed in the R package *Vegan* based on a Bray-Curtis dissimilarity matrix with 1000 permutations²⁶⁴.

5.3 Results and Discussion

5.3.1 Microbial Community Analyses Reveal Predominant PAOs and GAOs and Segregation of Key Functional Guilds in EBPR Biomass Aggregates

5.3.1.1 Enrichment of PAOs and GAOs after long-term NO_2^- feeding

The overall microbial composition and dynamics in this denitrifying EBPR bioreactor was investigated by applying high-throughput 16S rRNA gene amplicon sequencing to samples which were taken shortly after inoculation (day 0-50) and during the period when batch assays were conducted (day 490-600). The average relative abundances of the 15 most abundant bacterial taxa at the genus level when batch assays were conducted are summarized in Figure 5.1. Taxa names are given at the lowest possible assignment based on the Greengenes database. The relative abundances of these genera across all sampling dates are shown in Figure S5.1. The top 15 bacterial genera correspond to over 75% of the overall microbial community after ~500 days of operation. The abundances of the same genera in biomass samples taken shortly after inoculation are also shown, where they account for less than 25% of the overall microbial community. Several relatively high abundance putative PAOs and GAOs are apparent in the reactor biomass after >1 year of operation, including the canonical PAO affiliated with *Accumulibacter* ($13.5 \pm 4.2\%$) and putative GAOs affiliated with *Candidatus* *Competibacter* ($12.6 \pm 7.8\%$) (herein referred to as *Competibacter*) and *Defluviicoccus* ($9.2 \pm 6.0\%$). In addition to putative PAOs and GAOs, the genus affiliated with the family *Xanthomonadaceae* were also detected with high abundance ($19.9 \pm 3.0\%$). These results demonstrate the development of a distinct microbial community structure and the proliferation of several dominant bacterial genera under anaerobic/anoxic cycling (with a short aerobic polishing phase) and high NO_2^- concentrations in feed.

5.3.1.2 Microbial population segregation by aggregate size fraction

The inoculum for the parent SBR was predominantly floccular. During SBR operation, despite the fact that granule selection was not an explicit goal of reactor operation, formation of white granules was observed. Granule formation was particularly evident during the period when

batch assays were conducted. We characterized differences in microbial community composition based on 16S rRNA gene sequencing between different size fractions of biomass in order to assess variations by aggregate size fractions (Figure 5.1). Based on permutation analysis of variance (PERMANOVA), differences in community structure based on all aggregate size fractions were marginally significant (PERMANOVA, $p=0.054$). However, when only the floccular aggregates (<600 μm) and granular aggregates (>600 μm) were compared, strong and statistically significant variations in community structure were observed (PERMANOVA, $p=0.03$).

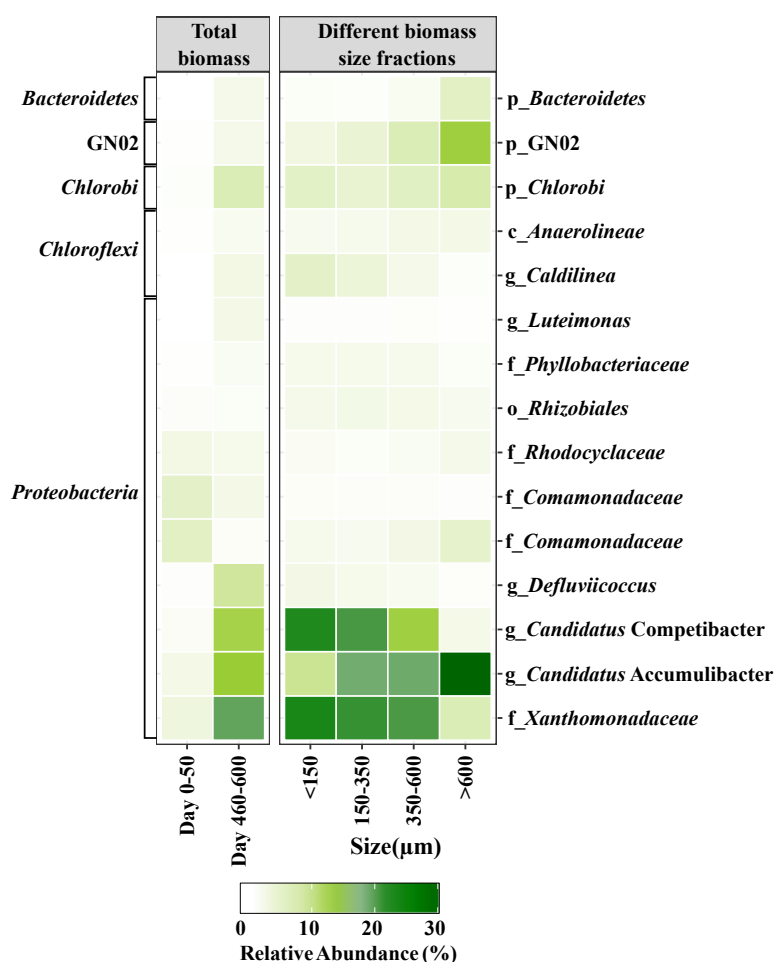


Figure 5.1 The average relative abundance (%) of the 15 most abundant bacterial taxa at the genus level in the mother SBR via 16S rRNA gene amplicon sequencing. Left: Overall microbial community structure in biomass over time range when batch assays were conducted (9 samples

between day 490 to 600) and within two months of SBR inoculation (4 samples between day 0 to 48); Right: Microbial community structure in different aggregate size fractions of biomass (day 591 and 626, right).

Average and standard deviation for the relative abundance (%) of all 15 bacterial taxa are listed in Table S5.1, and a complete profile in all sampling time points is shown in Figure S5.1. Taxonomy is shown at the phylum level (left label) and at the lowest level of taxonomic assignment (p: phylum, c: class, o: order, f: family and g: genus; right label).

ANOVA and post-hoc tests were performed to compare the relative abundance of highly abundant bacterial genera in different size fractions. Among the top 15 most abundant taxa at genus level, five affiliated with *Xanthomonadaceae*, *Bacteroidetes*, *Competibacter*, *Accumulibacter*, and *Defluviococcus* showed at least marginally significant ($p < 0.1$) overall divergence in relative abundance among biomass within the 4 different size classes (ANOVA $p < 0.05$ for *Xanthomonadaceae*, *Bacteroidetes* and *Competibacter*, $p = 0.063$ for *Accumulibacter* and $p = 0.072$ for *Defluviococcus*). Post-hoc tests were then conducted for these genera to test for significant differences in abundance between specific size fractions. Among the five genera showing divergent abundance among biomass with different sizes, higher abundance in large granules ($>600\mu\text{m}$) were found for *Accumulibacter* and the bacterial taxon in the phylum *Bacteroidetes*, while the opposite was found for putative GAOs associated with the genera *Competibacter* and *Defluviococcus*, as well as the most abundant microbial taxon in bulk biomass affiliated with the family *Xanthomonadaceae* (ANOVA $p < 0.05$). The observed evidence for enrichment of *Accumulibacter* in large granules ($>600\mu\text{m}$) suggests that selection for large granular aggregates may play a key role in retaining *Accumulibacter* and promoting denitrifying P uptake, despite the lack of explicit operational strategies in this study to select for granular biomass.

Based on the correlation analysis between the most abundant bacterial genera, each microbial genus was correlated (negatively or positively) with at least four other bacterial taxa

(Figure S5.2), indicating potential biological interactions between the dominant microbial taxa in the system. Biological interactions have been proposed to be the dominant driver of population structure and dynamics, particularly within microscale biomass aggregates²⁴⁸. Co-aggregations can occur within bacterial genera that exploit interspecific interactions, potentially promoting metabolite utilization and population growth²⁶⁵⁻²⁶⁷. However, the ecological interactions in granules become more complicated as the cell-cell interactions are physically highly dynamic (cells attaching and detaching dynamically)²⁵⁹. Ecological interactions likely play an important role in shaping the microbial community and aggregate architecture in our system, and may explain segregation of microbial genera by aggregate size and associations between dominant bacterial genera within multiple aggregate size fractions. A clearer understanding how local interactions influence the microscale spatial microbial assembly in denitrifying EBPR systems and the function of other non-PAO organisms warrants further investigation.

5.3.2 Genetic Denitrification Potential in Biomass

The denitrification pathway has a modular genetic organization, and different microorganisms have been shown to harbor genomic potential for complete or truncated (e.g. incomplete, where one or more of the core nitrogen oxide reductases is lacking) denitrification. N_2O production (NO_2^- reduction when assuming no or little net production of NO)¹¹⁴ and consumption rates (N_2O reduction) are controlled in denitrifying environments by two sets of enzymes: NIR, (either cytochrome cd_1 containing NO_2^- reductase encoded by *nirS*) or copper containing NO_2^- reductase encoded by *nirK*), and NOS, (encoded by *nosZ*). *nosZ* gene variants have in turn been recently classified into two phylogenetically distinct groups, termed clades I and II (also known as typical and atypical *nosZ*)^{111, 124}. The relative abundance and importance of these

two key N₂O reduction genes in wastewater treatment bioreactors has so far received little attention¹²⁰. Denitrifiers harboring truncated pathways that lack *nosZ* (and thus produce N₂O as a catabolic end product) could potentially be the source of N₂O in the environment²⁶. It has been suggested that quantification of NIR abundance relative to NOS may allow testing of genomic capacity for N₂O production^{124, 268, 269}.

We have demonstrated that electron competition does not fully explain the distinct nitrogen oxide reduction capabilities we observed in *ex situ* batch assays (Chapter 3). We aimed to further explore the possibility that N₂O accumulation is associated with genetic denitrification potential, namely an imbalance in functional genes related to denitrification, within the microbial community. We used qPCR assays to measure abundance of the key denitrification genes *narG*, *nirS*, *nirK*, and *nosZ* (clade I and II) as well as *Accumulibacter*-specific 16S rRNA gene abundance in reactor biomass during the period when batch assays were performed (day 490-600) (Figure 5.2a). By quantifying denitrification-related genes as well as *Accumulibacter*-specific 16S rRNA gene in different fractions of biomass, we aimed to also quantify segregation by aggregate size of *Accumulibacter* and of genetic potential for denitrification, and N₂O production and consumption.

The relative abundances of key denitrification genes (*narG*, *nirS*, *nirK* and clade I and II *nosZ*) in overall (non-size segregated) biomass are shown in Figure 5.2a. The relative abundance (in percentage) is calculated based on normalizing the measured copies of the target gene to copies of total bacterial 16S rRNA genes. By comparing the abundance of denitrification functional genes in universal biomass, we found that the relative abundance of *nirS* (9.5±2.8%) was the highest. *nirS* relative abundance was almost ten times higher than the relative abundance of *narG* (relative abundance: 1.9±0.7%, paired t-test p<0.001) and *nirK* (relative abundance: 0.7±0.2%, paired t-test

$p < 0.001$) after long-term NO_2^- feeding. The imbalance between *nirS* + *nirK* (key controls on NO_2^- reduction) and *narG* (key control on NO_3^- consumption) could potentially explain the slower NO_3^- rate compared with NO_2^- reduction rate in *ex situ* batch assays (Figure 5.2a). Importantly, *nosZ* genes from both clades (clade I [$3.3 \pm 0.1\%$] or clade II [$1.6 \pm 0.8\%$]) were present at significantly lower abundance than *nirS* in total biomass (paired t-test $p < 0.05$).

We next compared *Accumulibacter* abundance and genetic denitrification potential among different size classes of biomass aggregates ($<150\mu\text{m}$, $150\text{-}350\mu\text{m}$, $350\text{-}600\mu\text{m}$ and $>600\mu\text{m}$). In agreement with our 16S rRNA gene sequencing, qPCR results demonstrated that *Accumulibacter* was strongly and significantly enriched (higher abundance) in large aggregate size classes ($>600\mu\text{m}$ and $350\text{-}600\mu\text{m}$) compared to small floccular aggregates ($<350\mu\text{m}$) assays (ANOVA $p < 0.05$). The relative abundances of the four denitrification genes (*narG*, *nirS*, *nirK* and clade II *nosZ*) within different size fractions of biomass were also statistically significantly different (ANOVA $p < 0.05$), with the exception of clade I *nosZ*. Post-hoc pairwise comparison further revealed that significant differences primarily existed between biomass fractions $<150\mu\text{m}$ and $>350\mu\text{m}$ (size classes $350\text{-}600\mu\text{m}$ and $>600\mu\text{m}$) (Figure S5.3) for *nirS* and *nirK* gene abundances.

A correlation analysis was conducted to explore co-occurrence or co-exclusion patterns within different size fractions of biomass between relative abundance of denitrification functional genes and the top 15 most abundant bacterial taxa (based on 16S rRNA gene sequencing data) (Figure S5.2). Only a few genera were significantly correlated with *narG* (bacterial genera belonging to *Xanthomonadaceae*, *Chlorobi*, *Comamonadaceae* and *Rhodocyclaceae*) and clade II *nosZ* gene (bacteria genera belonging to *Competibacter*, *Defluviicoccus*, *Accumulibacter* and

Bacteroidetes). The lack of strong associations between denitrification genes and highly abundant bacteria genera could provide some indications that denitrification, particularly NO_2^- reduction, is not controlled by a single dominant taxon but by a diverse microbial consortium selected in our study. *Accumulibacter* (quantified by qPCR assay) is strongly and significantly correlated with clade II *nosZ* gene abundance. This finding agrees with the discovery in previous study that some currently available *Accumulibacter* genomes contain a clade II *nosZ* gene⁹³.

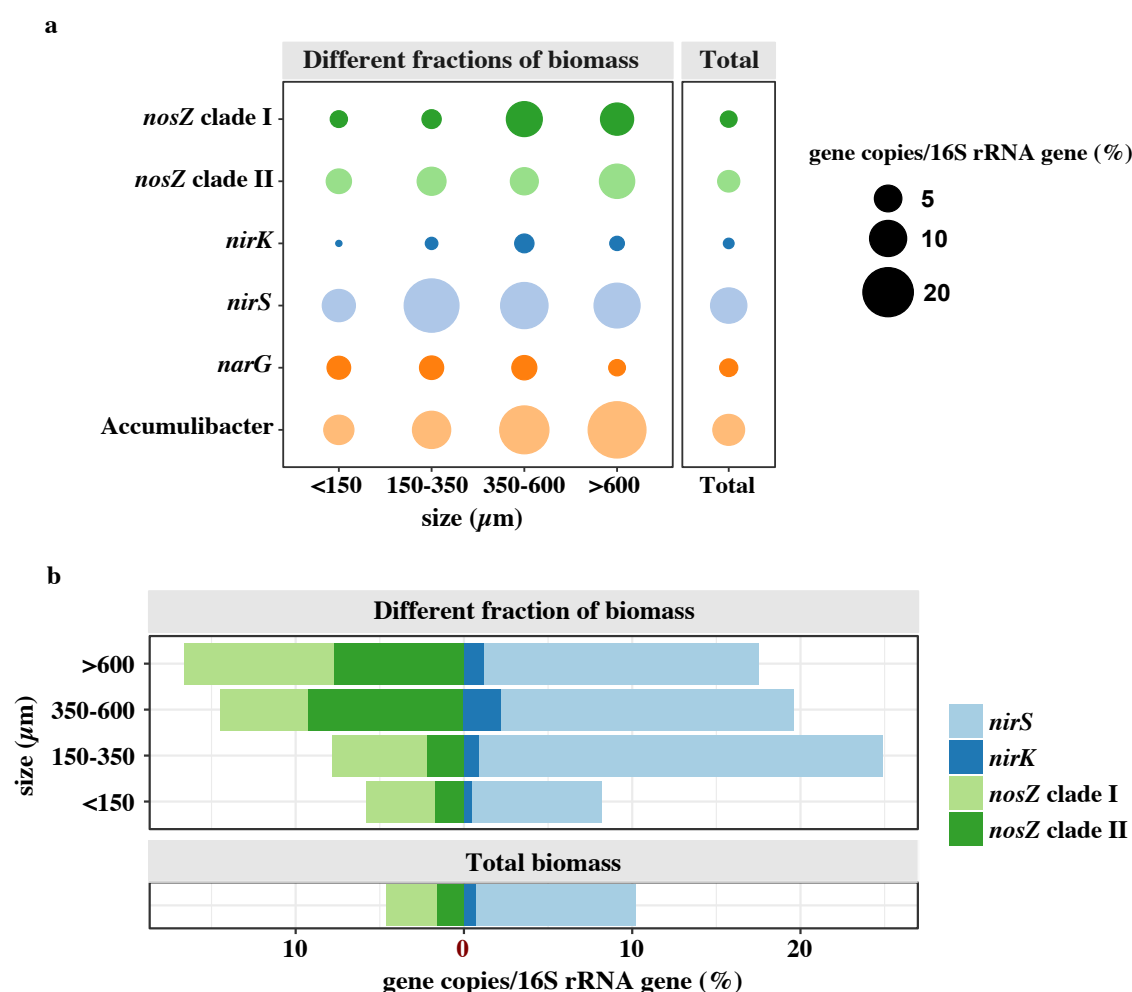


Figure 5.2 (a): Average relative abundance (%) of five denitrification genes (*narG*, *nirS*, *nirK* and clade I and II *nosZ*) and *Accumulibacter* 16S rRNA (*Accumulibacter*) normalized to universal bacterial 16S rRNA gene abundance, as quantified by qPCR assays. **(b):** Comparison of the relative abundance (%) of the key NO_2^- reduction genes (*nirS* + *nirK*) and the key N_2O reduction genes (clade I+II *nosZ*) in both bulk biomass and different size fractions of biomass.

Average relative gene abundance (%) for each gene in total biomass was calculated based on total biomass samples taken on 10 different days during batch tests (day 490 to day 625 of reactor operation, Table S5.4). Relative abundance (%) for different biomass size fractions was averaged by samples from two days (day 591 and 625). Normalized copy number (%) was calculated based on copy numbers for targeted genes divided by copy number of universal bacterial 16S rRNA gene.

5.3.3 Potential N₂O Producers and Consumers in Granular Sludge

To further explore the genetic potential for N₂O accumulation in this DPAO enrichment culture, we compared the relative abundance of the key NO₂⁻ reduction genes (*nirS+nirK*) and the key N₂O reduction genes (clade I and II *nosZ*) in both bulk biomass and different size fractions of biomass (Figure 5.2b). A significant difference in abundance between *nirS+nirK* (10.2±2.8%) and clade I+II *nosZ* genes (4.9±0.2%) was identified in the bulk biomass (paired t-test, p<0.001). This significant imbalance between *nirS/nirK* (nitrite reductase) and *nosZ* genes suggests that microbes with truncated denitrification pathways lacking *nosZ* gene, and therefore lacking genomic capacity to act as N₂O consumers, were selected after this long-term elevated NO₂⁻ feeding^{26, 120}.

We next compared the abundance of NO₂⁻ and N₂O reductases in the four biomass size fractions to explore whether different size fractions harbor differential genetic potential to act as N₂O sources and sinks. Interestingly, we discovered significant higher relative abundance of NO₂⁻ reductase (*nirK* and *nirS*) compared to N₂O reductase (*nosZ*) genes in floccular aggregates (<600µm) (paired t-test, p<0.05), but no statistically significant difference in abundance in larger granular aggregates (>600µm) (paired t-test, p>0.05), mainly due to increasing abundance of clade II *nosZ* (Figure 5.2b). This higher abundance of clade II *nosZ* in large granules was associated with the enrichment of several bacterial genera, including *Accumulibacter* and a genus in the phylum *Bacteroidetes*, as indicated by the strong positive correlation (p<0.05) between these two genera and clade II *nosZ* (Figure S5.2).

Taken together, our results suggest that the lower abundance of genes encoding N₂O reductase compared to NO₂⁻ reductase in this complex microbial consortium enriched in DPAOs may be responsible for the unusually high propensity for N₂O accumulation that we observed in this system in the presence of NO₂⁻. It further suggests that the floccular aggregates (<600µm) may act as N₂O sources (enriched in potential N₂O producers that lack *nosZ*), particularly compared to larger *Accumulibacter* enriched granular aggregates (>600µm). However, it should be noted that genetic potential alone cannot fully explain the reduced N₂O production rate or extent we observed with the addition of NO₃⁻ rather than NO₂⁻ to *ex situ* batch assays (See Figures 3.2 and 2.3). Another possible explanation for the patterns of N₂O production that we observed could be the presence in reactor biomass of both microbial populations harboring genes for complete denitrification (NO₃⁻ to N₂) and populations that are only capable of incomplete denitrification (e.g. that lack genomic capacity for NO₃⁻ or N₂O reduction). When NO₂⁻ is not available for incomplete denitrification, NO₃⁻ may be consumed by bacterial species with genes encoding for the full denitrification pathway. Furthermore, selective inhibition of the NOS enzyme has been reported, particularly with high FNA concentrations^{106, 129 66, 67}. The FNA concentrations in our batch assays were between 0.4 (10 mg NO₂⁻-N/L at pH 7.8) and 2 µg HNO₂-N/L (60 mg NO₂⁻-N/L at pH 7.8), which previous work has suggested may inhibit up to 80% and 40% of nitrite reductase and nitrous oxide reductase activities, respectively⁶⁷, thereby potentially leading to N₂O accumulation. Additional work is warranted to quantify transcriptional patterns and to better understand gene regulation of different steps of denitrification in this type of complex denitrifying EBPR consortia.

5.4 Conclusions

- A diverse microbial consortium with distinctive nitrogen oxides reduction capabilities, including a strong propensity under some conditions for incomplete denitrification and consequent production of N_2O , was selected after long-term exposure to elevated NO_2^- (40-50 mg-N/L) in a DPAO-enriched EBPR reactor. Besides putative DPAOs and other heterotrophic denitrifiers were also selected under anaerobic/anoxic conditions.
- qPCR-based functional gene quantification demonstrated a significant imbalance in genetic potential for nitrite reduction (*nirS+nirK*) compared to nitrous oxide reduction (clade I and II *nosZ*). This suggests the presence of abundant denitrifiers with truncated denitrification pathways that lack genomic capacity for N_2O reduction after long-term feeding with NO_2^- .
- Strong segregation of putative DPAOs, GAOs, and genetic potential for reduction of NO_2^- and N_2O in different aggregate size fractions was also observed. The higher abundance of DPAOs and clades I and II *nosZ* in large granular size fractions indicates that intentional selection of these aggregates could potentially be applied to promote DPAO enrichment and activity while also providing a robust biological sink for N_2O .

5.5 Supporting Information

5.5.1 Supporting Information - Methods

PCR amplification for amplicon sequencing

For each sample, we prepared duplicate DNA extracts. A two-step PCR amplification and barcoding were performed using the Fluidigm Biomark multiplex PCR strategy as previously described²⁷⁰. First, forward primer 515f (5'-GTG CCA GCM GCC GCG GTA A) and reverse primer 806r (5'-GGA CTA CHV GGG TWT CTA AT) were used to amplify the V4 region of the universal bacterial 16S rRNA gene¹⁴⁹. A 20 μ L PCR reaction was performed per DNA extract, using 2 \times Epicentre Premix F PCR mastermix (Epicentre, USA), 3.5 U/ μ L Expand HiFidelity Taq (Roche Diagnostics, USA), 200 nM of each primer, and 1 μ L gDNA. The following PCR amplification temperature program was used: 95 °C for 5 minutes, followed by 28 cycles of 95 °C for 30 s, 55 °C for 45 s, and 68 °C for 30 s with a final elongation step at 68°C for 7 minutes. Amplicons from replicate first PCR runs were pooled before the second PCR amplification. Fluidigm primers with sequencing adapters and a sample-specific barcode were used to perform the second PCR step. The PCR reaction was performed using 2 \times Accuprime Supermix (ThermoFisher, USA), 50 μ M forward and reverse primers (Fluidigm, USA), and 1 μ L of template from the combined first round PCR products using the following temperature program: 95 °C for 5 minutes, 95 °C for 30s, 60°C for 30s, and 68 °C for 30s in a total of 8 cycles. The resulting amplicons were then send to the University of Illionis Chicago DNA Service Facility for further purification with a Qiagen PCR purification kit and sequence on the Illumina MiSeq V2 platform.

16S rRNA gene amplicon sequencing data processing

After removing barcodes, filtering for low-quality sequences (sequences with more than 1 error per 100 bases were removed), and merging reverse and forward paired end sequences, USEARCH v8.1.1861 was used to remove singletons and chimeras and to select representative OTUs based on a 97% identity cutoff^{150, 151}. The Greengenes sequence database was employed for phylogenetic inference for representative sequences from each OTU in the Quantitative Insights Into Microbial Ecology (QIIME) platform^{152, 153}. Representative OTUs were also aligned via the SILVA Incremental Aligner (SINA) database to identify ‘*Candidatus* Competibacter phasphatis’ and *Defluviicoccus*, candidate glycogen accumulating organisms (GAOs), since neither is included in the Greengenes database¹⁵⁴. Samples were rarefied to the lowest sequencing depth for further diversity analysis.

Quantitative PCR (qPCR)

All qPCR assays except *nirK* and clade II *nosZ* were performed on a CFX Connect thermocycler (Bio-rad, USA) in a 20 μ L reaction volume containing 10 μ L of 2 \times SsoAdvanced Universal SYBR Green Supermix (Bio-rad, USA), 0.5 μ M of primers and 2 μ L of diluted DNA extracts. To quantify the abundance of clade II *nosZ*, the iTaq Universal SYBR Green Supermix (Biorad, USA) was used. For the quantification of *nirK*, FailSafe Green premix was made by mixing 2 \times FailSafe premix F (Epicentre, USA) with 10,000 \times SYBR Green 1 nucleic acid stain (Invitrogen, USA). The qPCR reaction volume for *nirK* was 20 μ L with 10 μ L of FailSafe Green premix, 0.5 U/reaction Expand HiFidelity taq enzyme (Roche Diagnostics, USA), 0.5 μ M of primers and 2 μ L of diluted gDNA. Each qPCR reaction was performed in triplicate.

5.5.2 Supporting Information - Tables

Table S5.1 The relative abundance (%) and standard deviation of the top 15 bacterial taxa at the genus level in the denitrifying EBPR biomass, based on 16S rRNA gene sequencing. Taxonomy is shown at the phylum level (1st column) and at the lowest level of taxonomic assignment (p: phylum, c: class, o: order, f: family, and g: genus; 2nd column).

Phylum	Lowest level of taxonomic assignment *	Total biomass (%)		Size fractions (µm) (%)			
		Day 0-48	Day 490-600	<150	150-350	350-600	>600
Proteobacteria	f_ <i>Xanthomonadaceae</i>	3.0±1.1	19.9±3.0	24.1±5.5	21.7±1.2	20.9±1.6	6.9±1.9
Proteobacteria	g_ <i>Candidatus</i> Accumulibacter	2.2±0.9	13.5±4.2	9.6±2.4	19.1±9.2	19.3±4.0	31.2±2.1
Proteobacteria	g_ <i>Candidatus</i> Competibacter	0.9±0.9	0.126±0.078	22.9±1.2	21.0±2.4	12.9±0.1	2.0±0.5
Chlorobi	p_ <i>Chlorobi</i>	0.5±0.6	6.9±2.0	5.1±1.9	4.0±1.9	5.5±2.5	7.8±1.5
Proteobacteria	g_ <i>Defluviicoccus</i>	0.3±0.1	9.2±6.0	2.3±0.9	1.7±0.2	1.3±0.5	0.4±0.0
GN02	p_GN02	0.2±0.1	1.9±3.0	2.6±3.0	3.7±4.6	6.9±8.4	13.0±11.0
Proteobacteria	f_ <i>Comamonadaceae</i>	5.4±1.2	0.8±0.4	1.6±0.9	1.4±0.9	2.3±1.6	4.6±1.9
Chloroflexi	g_ <i>Caldilinea</i>	0.1±0.1	2.4±0.3	4.9±2.6	3.5±2.5	1.9±0.9	0.5±0.2
Proteobacteria	f_ <i>Comamonadaceae</i>	4.9±1.9	2.2±1.2	0.8±0.6	0.6±0.5	0.6±0.4	0.3±0.1
Proteobacteria	f_ <i>Rhodocyclaceae</i>	2.4±0.9	1.7±1.3	1.0±0.3	0.7±0.2	1.1±0.7	1.9±1.4
Bacteroidetes	p_ <i>Bacteroidetes</i>	0.0±0.0	1.9±0.4	0.7±0.4	0.5±0.3	1.2±0.0	5.3±0.9
Chloroflexi	f_ <i>Anaerolineae</i>	0.2±0.1	1.3±0.3	1.4±0.7	1.6±1.0	2.2±1.5	2.2±0.9
Proteobacteria	o_ <i>Rhizobiales</i>	0.6±0.4	0.7±0.4	1.9±1.0	2.1±1.5	2.0±1.3	1.4±0.8
Proteobacteria	f_ <i>Phyllobacteriaceae</i>	0.2±0.2	1.1±0.4	1.8±0.8	1.8±1.2	1.6±0.9	0.7±0.2
Proteobacteria	g_ <i>Luteimonas</i>	0.1±0.0	2.2±1.4	0.3±0.2	0.3±0.1	0.4±0.0	0.2±0.1

Table S5.2 qPCR primers and thermal cycling conditions used in this study.

Gene	Primers	Size	Step	Temperature	Time	Reference
Universal 16S	519f: CAG CMG CCG CGG TAA NWC 907r: CCG TCA ATT CMT TTR AGT T	393bp	Initial Denaturation	95°C	5min	271
			30 cycles	95°C	30s	
				60°C	30s	
				68°C	30s	
Accumulibacter 16S	518f: CCA GCA GCC GCG GTA AT 846r: GTT AGC TAC GGC ACT AAA AGG	351bp	Initial Denaturation	95°C	3min	89
			35 cycles	95°C	30s	
				59°C	60s	
				72°C	30s	
<i>narG</i>	narG-f TCG CCS ATY CCG GC S ATG TC narG-r GAG TTG TAC CAG TCR GCS GAY TCS G		Initial Denaturation	95°C	15min	272
			5 cycles	95°C	30s	
				63°C Decrease 1°C per cycle	30s	
			35 cycles	95°C	30s	
63°C	30s					
<i>nirS</i>	cd3aF: GT(C/G) AAC GT(C/G) AAG GA(A/G) AC(C/G) GG R3cd: GA(C/G) TTC GG(A/G) TG(C/G) GTC TTG A	387bp	Initial Denaturation	95°C	10min	273
			35 cycles	95°C	30s	
				56°C	30s	
				72°C	30s	
<i>nirK</i>	nirK5R: GCC TCG ATC AGR TTR TGG nirK583FdegCF: TCA TGG TGC TGC CGC GYG ANG G	~430bp	Initial Denaturation	94°C	2min	274 275
			35 cycles	94°C	30s	
				60°C	60s	
				72°C	60s	
Clade I <i>nosZ</i>	NosZ1840f: CGC RAC GGC AAS AAG GTS MSS GT NosZ2090r: CAK RTG CAK SGC RTG GCA GAA	267bp	Initial Denaturation	95°C	15min	276
			6 cycles	95°C	15s	
				65°C Decrease 1°C per cycle	30s	
			35 cycles	95°C	30s	
				59°C	15s	
				72°C	30s	
80°C	15s					

Gene	Primers	Size	Step	Temperature	Time	Reference
Clade II <i>nosZ</i>	nosZ-II-f: CTI GGI CCI YTK CAY AC nosZ-II-r: GCI GAR CAR AAI TCB GTR C	745bp	Initial Denaturation	95°C	5min	124
			35cycles	95°C	30s	
				55°C	60s	
				72°C	45s	
				80°C	30s	

Table S5.3 Quality control parameters for qPCR assays.

Gene	Efficiency	R²
Universal 16S	92.2%	0.999
Accumulibacter 16S	100.3%	0.997
<i>narG</i>	88.6%	0.992
<i>nirS</i>	96.2%	0.999
<i>nirK</i>	97.6%	0.997
Clade I <i>nosZ</i>	92.0%	0.998
Clade II <i>nosZ</i>	96.2%	0.993

Table S5.4 Relative abundance (%) of *Accumulibacter* 16S rRNA (*Accumulibacter*) and five denitrification genes (*narG*, *nirS*, *nirK* and clade I and II *nosZ*) normalized to universal bacterial 16S rRNA gene abundance quantified by qPCR assays.

	Operation days	<i>Accumulibacter</i>	<i>narG</i>	<i>nirS</i>	<i>nirK</i>	<i>nosZ</i> clade I	<i>nosZ</i> clade II
Total biomass	Day 458	6.1±0.5	1.1±0.2	7.5±1.0	0.6±0.2	3.0±0.4	0.5±0.2
	Day 472	8.0±2.1	1.9±0.0	13.3±5.7	1.1±0.3	4.4±0.7	1.2±0.1
	Day 486	7.5±1.9	2.9±1.1	11.5±4.6	0.5±0.3	4.8±3.3	0.7±0.2
	Day 507	8.7±2.4	1.7±0.7	12.5±3.2	0.5±0.0	2.2±0.8	2.2±1.7
	Day 521	8.2±2.1	1.2±0.1	7.5±6.6	0.9±0.5	3.1±1.1	2.1±1.2
	Day 535	5.5±1.3	1.4±0.8	5.2±0.9	0.7±0.0	2.6±0.4	1.8±0.3
	Day 549	4.2±1.2	2.3±0.5	9.7±1.7	0.9±0.5	4.2±1.7	2.1±0.4
	Day 563	8.1±2.5	2.9±0.6	8.7±1.5	0.7±0.0	1.9±0.4	2.4±1.3
Different fraction of biomass (µm)	Day 591 <150	5.2±0.6	3.1±0.8	9.0±4.8	0.5±0.2	3.6±0.1	1.4±0.4
	Day 591 150-350	6.6±4.7	2.9±0.7	26.4±17.5	0.8±0.6	7.1±5.4	2.6±1.3
	Day 591 350-600	16.3±7.1	3.5±2.0	18.2±8.2	2.9±0.6	4.7±0.4	11.8±8
	Day 591 >600	27.5±14.4	1.5±0.6	17.0±5.3	1.6±1.1	12.9±4.5	8.7±6.4
	Day 626 <150	7.1±0.6	3.9±0.1	6.4±0.9	0.6±0.1	4.7±0.1	1.9±0.3
	Day 626 150-350	14.9±2.5	4.5±0.8	21.5±1.7	0.9±0.1	4.0±0.4	1.9±0.0
	Day 626 350-600	21.5±4.5	4.5±2.4	16.6±8.3	1.5±0.7	5.8±0.4	6.7±0.2
	Day 626 >600	26.4±4.2	1.7±0.1	15.6±7.5	0.7±0.2	4.9±0.4	6.7±5.7

5.5.3 Supporting Information - Figures

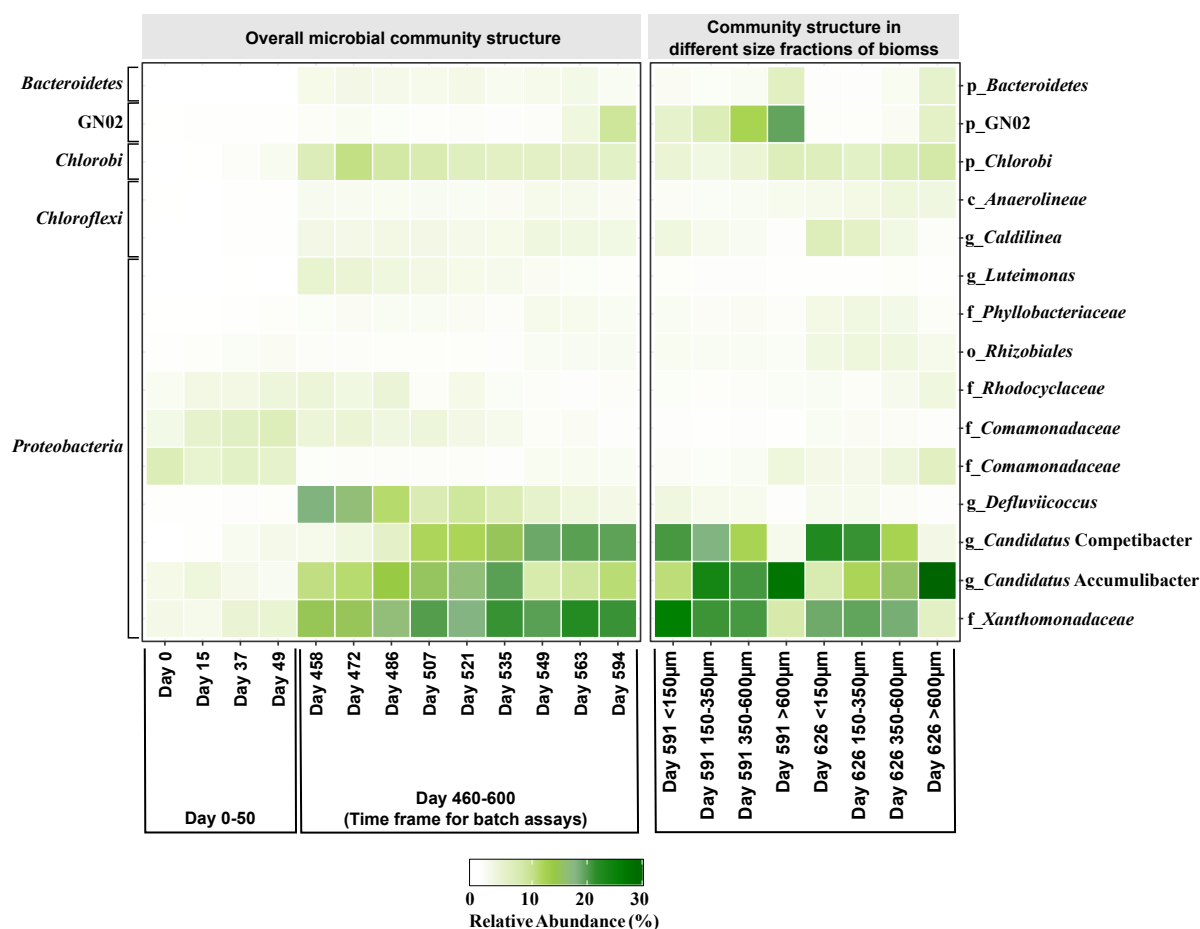


Figure S5.1 Relative abundance for the 15-most abundant microbial taxa at the genus level in the mother SBR via 16S rRNA gene amplicon sequencing.

Left: Overall microbial community structure in biomass over time range when batch assays were conducted (day 460 to day 600) and within two months of SBR inoculation (day 0 to day 50); Right: Microbial community structure in different size fractions (<150 µm, 150-350 µm, 350-600 µm, and >600 µm) of biomass in two selected days (day 591 and 626). Taxonomy is shown at the phylum level (left label) and at the lowest level of taxonomic assignment (p: phylum, c: class, o: order, f: family, and g: genus; right label).

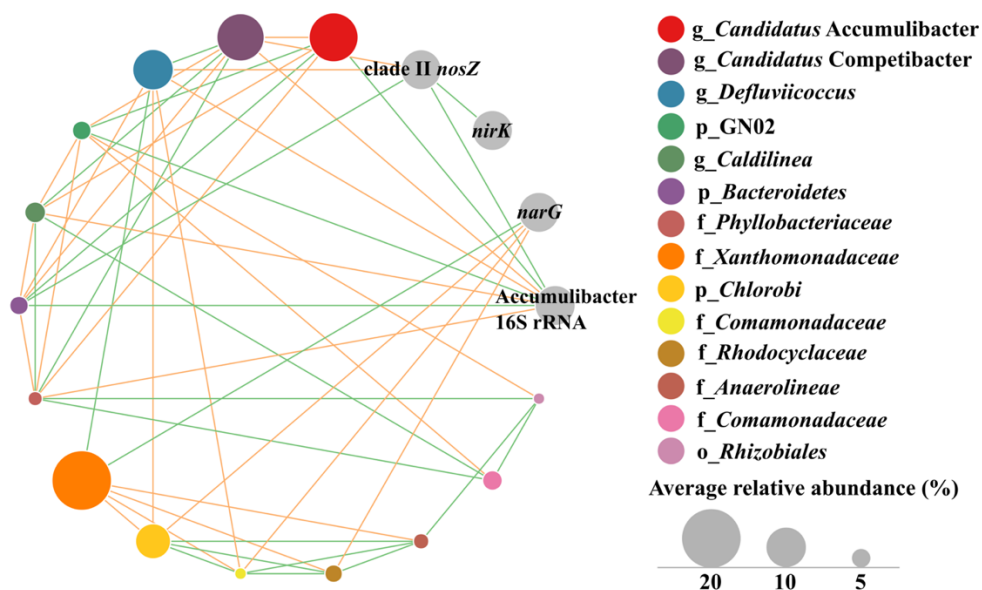


Figure S5.2 Correlation network between the top 15 most abundant bacterial taxa at the genus level detected in the nitrite-fed denitrifying EBPR bioreactor via 16S rRNA gene sequencing (colored circles) and the abundance of denitrification and *Accumulibacter* 16S rRNA (gray circles; *nirK*, *narG*, *Accumulibacter* 16S rRNA, and clade II *nosZ*) measured via qPCR.

Spearman correlation analysis between the top 15 bacterial genera was conducted based on the relative abundance of these bacterial genera in different biomass size fractions. Taxa names are given at the lowest level of taxonomic assignment (p: phylum, c: class, o: order, f: family, and g: genus). *nirS* and clade I *nosZ* are not shown in the figure because they were not correlated with any bacterial taxon or denitrification genes. A positive correlation (Pearson correlation $\rho > 0.8$, $p < 0.05$) between nodes is indicated by a green edge, and negative correlation (Pearson correlation $\rho < -0.8$, $p < 0.05$) is indicated by an orange edge. The size for each colored circle represents the average relative abundance (%) of the bacterial genus in reactor biomass between day 486 and day 625 (time frame when batch assays occurred).

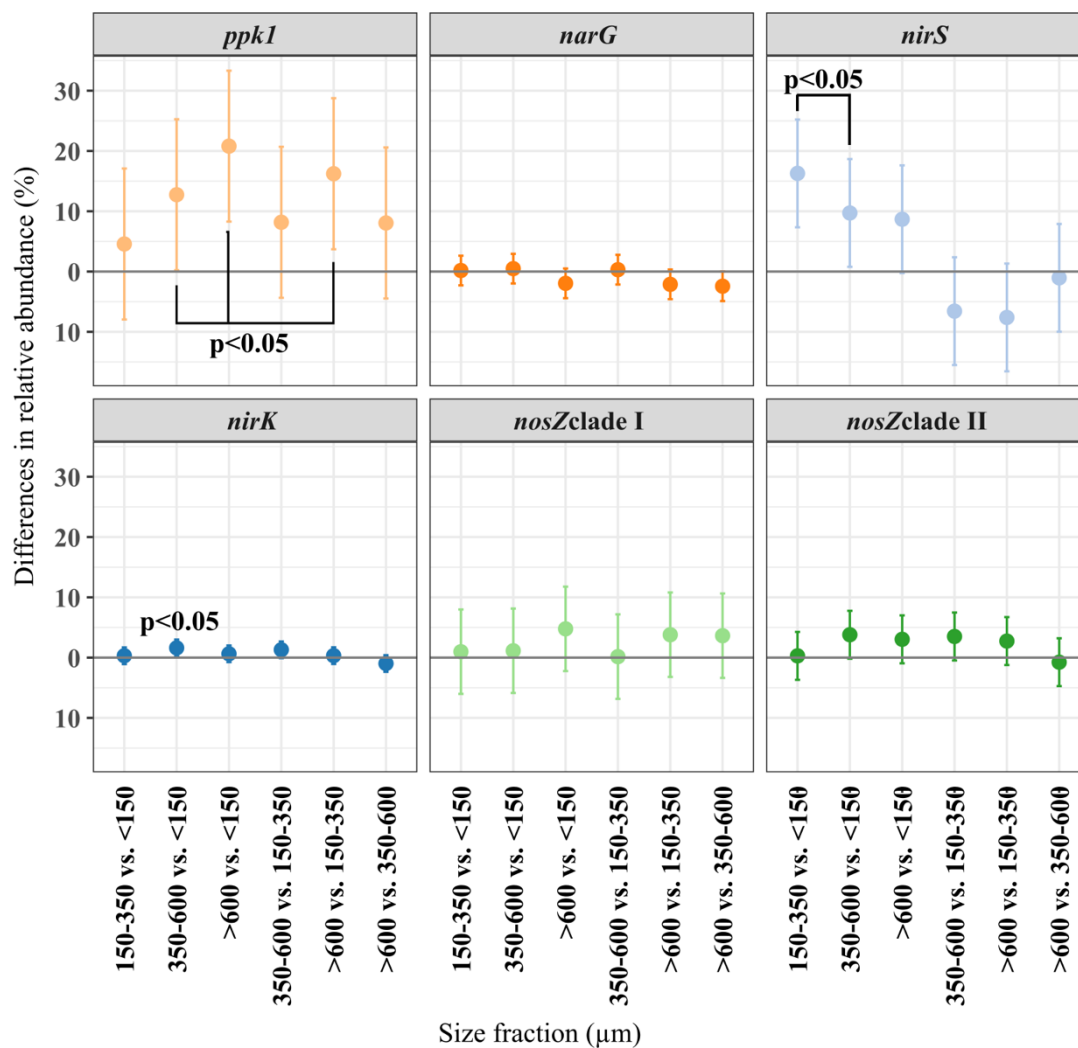


Figure S5.3 Average differences in functional gene relative abundance (%) between each biomass size fraction calculated based on post-hoc test. Error bar represents the 95% confidence interval. A positive number on the y-axis indicates higher abundance in the larger size fraction.

CHAPTER 6

Conclusions and Future Work

6.1 Summary

The Coupled Aerobic-anoxic Nitrous Decomposition Operation with Phosphorus removal (CANDO+P) is a new concept of wastewater treatment that combines the removal of nutrients with both energy recovery via N_2O and resource recovery through P-enriched biomass removal. It leverages a currently unwanted byproduct with a high global warming potential, N_2O , as a novel source of energy. Indirect energy benefits and cost savings relative to conventional N and P removal processes also derive from the decrease in COD needed for N removal relative to denitrification; oxygen savings via anoxic P removal and the selection for nitrification rather than complete nitrification; and the reduction in waste biomass production, thereby decreasing costs of downstream sludge treatment. Furthermore, the selection for P-enriched biomass allows for P recovery as a fertilizer. CANDO+P thus represents a new approach for bioenergy production, nutrient recovery, and protection of the water environment. Besides domestic wastewater treatment, the proposed system has the potential to influence a range of activities associated with nutrient pollution and N_2O emission, including industrial wastewater treatment, management of landfill leachate and food waste, biomass production for biofuels.

The feasibility of CANDO+P was demonstrated in a lab-scale SBR operated for almost three years. Stable nutrient (N and P) removal accompanied by high-rate and high-efficiency N_2O production was observed during the long-term operation (**Chapter 2 and Chapter 3**). Compared with other (denitrifying) EBPR or heterotrophic denitrifying systems, a specific microbial consortium was selected with distinct denitrification capabilities utilizing different nitrogen oxides (NO_3^- , NO_2^- and N_2O) (**Chapter 3**). The selected microbial community has a strong kinetic preference for utilizing NO_2^- as an electron acceptor rather than NO_3^- and N_2O for denitrification

and denitrifying P uptake. Surprisingly, the strong accumulation of N₂O (70-90%) during NO₂⁻ reduction was observed under low COD/N or high FNA conditions, where limited N₂O formed in other studies (**Chapter 3**). The continuous N₂O formation under low COD/N or low FNA conditions indicates that the application of CANDO or CANDO+P is not limited to sidestream treatment with high N loading. Results presented here demonstrate that CANDO+P application for dilute mainstream municipal wastewater treatment is also promising.

Even though stable performance was observed during three years of operation, the bioreactor harbored a dynamic microbial community, with co-existing *Accumulibacter*-associated PAOs, *Competibacter* and *Defluviicoccus*-associated GAOs, and diverse flanking organisms (**Chapter 3, 4, and 5**). Granulation occurred in the SBR without intentional selection for granules. Microbial community segregation with the enrichment of *Accumulibacter* in larger aggregates was demonstrated by investigating the microbial community structure in different size fractions of the biomass aggregates (**Chapter 5**). Currently, all CANDO studies focus on floccular (suspended growth) systems. Our observations suggest the possibility of developing a granular or biofilm-based CANDO (or CANDO+P) system.

Three potential mechanisms underlying the formation of N₂O in our system were tested by combining kinetic studies and genome resolved metagenomic analysis (**Chapter 3 and Chapter 4**): (1) the competition for electrons between four denitrification enzymes (NAR, NIR, NOR and NOS); (2) the selection of denitrifying *Accumulibacter* (PAO) with a truncated denitrification pathway (lacking *nosZ*); and (3) the selection of flanking organisms (non-PAO) with incomplete denitrification pathways. As electron consumption rates and electron distribution among denitrification enzymes did not change significantly by varying nitrogen oxides concentrations,

electron competition does not seem to be the major driver for N₂O production in our system (**Chapter 3**). Deep sequencing and genome resolved metagenomic analysis enable the recovery of draft bacterial genomes from diverse microbial communities (**Chapter 4**). Two *Accumulibacter* and 39 flanking microorganism draft genomes were extracted from the SBR. A high prevalence of flanking bacterial populations with incomplete denitrification pathways was discovered. The selection of putative N₂O producers missing the *nosZ* gene indicated that those flanking organisms could potentially contribute to N₂O production in the system. However, both *Accumulibacter* genomes (clade IA and IC) appear to harbor genomic potential for N₂O reduction (**Chapter 4**). A comprehensive phylogenetic analysis of denitrification gene clusters among *Accumulibacter* clades suggested that type I *Accumulibacter* clades might have a potential advantage in denitrifying EPBR system. The observed reduced N₂O driven phosphate uptake rate in both the mother CANDO+P reactor and kinetic studies suggested that the expression or activation of *Accumulibacter nosZ* gene might be suppressed (**Chapter 4**), although this requires further investigation. In summary, multiple sources of N₂O could co-exist in the complex CANDO+P microbial community, and it is likely that denitrification driven N₂O formation is probably not controlled by a single mechanism.

6.2 Future study

6.2.1 Potential implications of CANDO+P for mainstream treatment

CANDO+P has been demonstrated to be feasible in lab-scale with synthetic wastewater. Pilot studies treating real wastewater are warranted to determine whether this new nutrient removal and recovery process can be implemented in full-scale. Two hypothetical mainstream CANDO+P

treatment schemes appear promising (Figure 6.1). The first operational regime (Figure 6.1A) couples an anaerobic phase for P release by DPAOs to a low DO aerobic phase for P uptake and simultaneous nitrification/denitrification via NO_2^- . Previous reports suggested promising P and N removal in this operational mode, but also highlighted the propensity for high N_2O emissions²⁷⁷. The second operational regime (Figure 6.1B) combines anaerobic/anoxic phases with aerobic polishing for P uptake and N_2O production (SBR1) with a downstream nitrification reactor (SBR2). An internal recycle doses NO_2^- to the anoxic phase of SBR1 to drive DPAO activity. Besides municipal wastewater treatment, a broader application of CANDO+P to industrial wastewater treatment, management of landfill leachate, food waste, and waste streams generated during biofuel production also warrants testing. In addition to testing more realistic feed streams, the efficiency of N_2O collection and the downstream utilization of N_2O as a biogas also need further investigation when scaling-up the system. A life cycle assessment coupled to a techno-economic analysis should then be performed to quantify risks and benefits of CANDO+P relative to other process alternatives, including conventional EBPR, denitrifying EBPR without energy recovery, and other N removal processes.

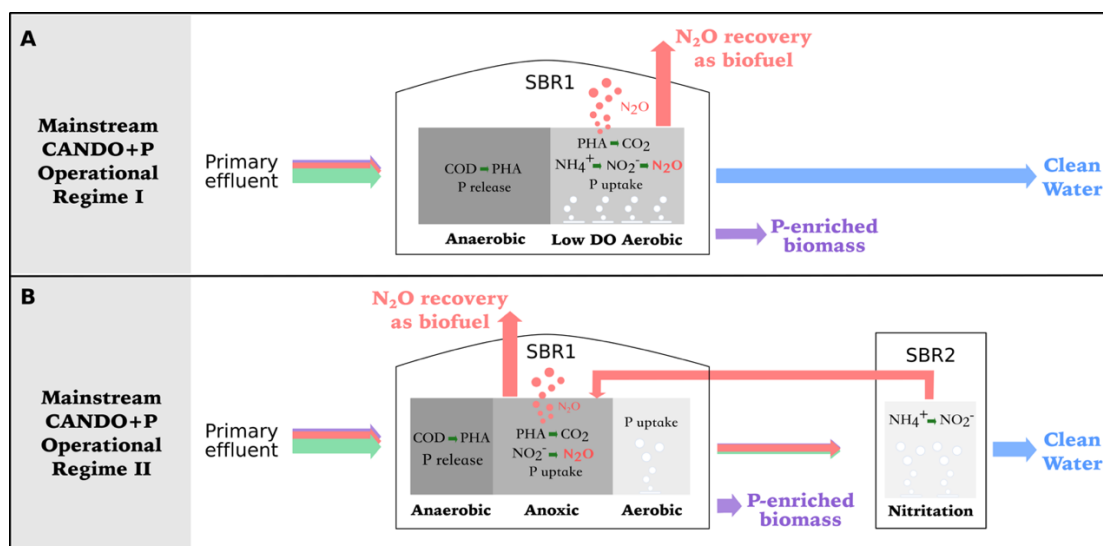


Figure 6.1 Two potential operational regimes proposed for CANDO+P application to mainstream municipal wastewater.

A) Alternating anaerobic and low DO aerobic phases (simultaneous nitrification, denitrification, and P uptake) in a single SBR; **B)** Alternating/ anoxic phases with an aerobic polishing phase in SBR1, followed by nitrification in SBR2.

6.2.2 Mechanisms of N_2O formation at multiple scales

In chapter 4, the presence of potential N_2O producers in the flanking CANDO+P microbial community was demonstrated by shotgun metagenomic analysis. The production of N_2O by *Accumulibacter* and this flanking community, and the interactions and competition for C and N between PAOs and non-PAOs, require further investigation. The response of the denitrifying bacteria community to varied biotic and abiotic factors can be reflected by changes in gene expression and in pools of primary metabolites^{32, 278, 279}. Further exploration of gene expression and the actual physiology of cells by metatranscriptomic and metabolomic analyses will provide more insights into the mechanisms of N_2O accumulation. As N_2O accumulation during denitrification is also closely related to carbon metabolism, energy production, and electron equivalents, the development of a comprehensive metabolic model would extend our understanding of N_2O production by linking all C and N metabolisms. Combining metagenomic, metatranscriptomic and metabolomic data and building a metabolic model for flux prediction could reveal the role of PAOs and flanking organisms under dynamic conditions and their contribution to N_2O production, providing a more profound understanding of N_2O generation in CANDO+P and other denitrifying EBPR systems²⁸⁰.

The accumulation of N_2O by an *Accumulibacter* enriched culture was investigated in this study. However, a diverse suite of alternative candidate PAOs has also been reported in other EBPR or denitrifying EBPR systems, including *Tetrasphaera*. Assessing the production of N_2O

and revealing the mechanisms of N₂O formation by other PAOs will expand our understanding of N₂O formation mechanisms in denitrifying EBPR processes. This will not only benefit CANDO+P which aims to maximize the production of N₂O for energy recovery, but also provide insight into denitrifying EBPR processes that try to reduce N₂O formation and lower the carbon footprint during treatment.

6.2.3 Linking microbial community dynamics to system performance

Microbial community assembly is critical to emergent function for many biological engineering systems including wastewater treatment. The selection for desired functional groups and a diverse microbial community determine the efficiency and stability of the treatment process, though in ways that are still only partially understood²⁸¹⁻²⁸³. In the research presented in this dissertation, selective pressures imposed by the anaerobic/anoxic/aerobic conditions and high NO₂⁻ feed caused dramatic shifts in microbial community structure, with associated shifts in specific denitrification capabilities (**Chapter 3 and Chapter 5**). Understanding the processes structuring microbial communities can provide insight into designing control strategies to improve the efficiency and robustness of the engineered systems. Niche-selection and neutral theory are the two popular ecological theories explaining microbial community assembly by deterministic and stochastic processes, respectively^{282, 284-286}. Even with a fluctuating microbial community in the CANDO+P system (variations with respect to PAO abundance), stable performance was achieved. The relationship between functional redundancy and microbial community structure is still poorly understood²⁸⁷. Follow-up replicate long-term CANDO+P experiments would increase our understanding of the relative role of niche and neutral microbial community assembly mechanisms and the selection of a core microbiome in denitrifying EBPR processes, and would aid in linking

community dynamics to system performance. Combined with draft genomes recovered from metagenomic sequencing, microbial function and functional redundancy can be evaluated by exploring the dynamics and patterns of both functional gene-centric structure and taxonomic composition.

REFERENCES

1. *NAE Grand Challenges for Engineering; National Academy of Engineering*, Washington, DC, 2008.
2. Rockstrom, J.; Steffen, W.; Noone, K.; Persson, A.; Chapin, F. S.; Lambin, E. F.; Lenton, T. M.; Scheffer, M.; Folke, C.; Schellnhuber, H. J.; Nykvist, B.; de Wit, C. A.; Hughes, T.; van der Leeuw, S.; Rodhe, H.; Sornlin, S.; Snyder, P. K.; Costanza, R.; Svedin, U.; Falkenmark, M.; Karlberg, L.; Corell, R. W.; Fabry, V. J.; Hansen, J.; Walker, B.; Liverman, D.; Richardson, K.; Crutzen, P.; Foley, J. A., A safe operating space for humanity. *Nat* **2009**, *461*, (7263), 472-475.
3. US-EPA, Global anthropogenic non-CO₂ greenhouse gas emissions: 1990-2030; *Office of Atmospheric Programs*, Climate Change Division.: Washington, DC, 2012.
4. EPRI, Water & Sustainability: US Electricity Consumption for Water Supply and Treatment- the Next Half Century; Palo Alto, CA, 2002.
5. Kampschreur, M. J.; Temmink, H.; Kleerebezem, R.; Jetten, M. S. M.; van Loosdrecht, M. C. M., Nitrous oxide emission during wastewater treatment. *Water Res* **2009**, *43*, (17), 4093-4103.
6. Le Corre, K. S.; Valsami-Jones, E.; Hobbs, P.; Parsons, S. A., Phosphorus recovery from wastewater by struvite crystallization: a review. *Crit. Rev. Environ Sci Technol* **2009**, *39*, (6), 433-477.
7. Zhou, Y.; Lim, M.; Harjono, S.; Ng, W. J., Nitrous oxide emission by denitrifying phosphorus removing culture using polyhydroxyalkanoates as carbon source. *J Environ Sci* **2012**, *24*, (9), 1616-1623.
8. Meyer, R. L.; Zeng, R. J.; Giugliano, V.; Blackall, L. L., Challenges for simultaneous nitrification, denitrification, and phosphorus removal in microbial aggregates: mass transfer limitation and nitrous oxide production. *FEMS Microbiol. Ecol.* **2005**, *52*, (3), 329-338.
9. Lemaire, R.; Meyer, R. L.; Taske, A.; Crocetti, G. R.; Keller, J.; Yuan, Z., Identifying causes of N₂O accumulation in a lab-scale sequencing batch reactor performing simultaneous nitrification, denitrification, and phosphorus removal. *J Biotechnol* **2006**, *122*, 62-72.
10. Scherson, Y. D.; Woo, S.-G.; Criddle, C. S., Production of nitrous oxide from anaerobic digester centrate and its use as a co-oxidant of biogas to enhance energy recovery. *Environ Sci Technol* **2014**, *48*, (10), 5612-5619.
11. Committee, G. C. f. E. Grand Challenges for Engineering; *National Academy of Engineering of the national academies*: 2012.
12. Gruber, N.; Galloway, J. N., An Earth-system perspective of the global nitrogen cycle. *Nat.* **2008**, *451*, (7176), 293-6.
13. Fryzuk, M. D., Inorganic chemistry: ammonia transformed. *Nat.* **2004**, 427.
14. Cordell, D.; Drangert, J.O.; White, S., The story of phosphorus: Global food security and food for thought. *Glob Environ Change* **2009**, *19*, (2), 292-305.
15. Diaz, R. J.; Rosenberg, R., Spreading dead zones and consequences for marine ecosystems. *Science* **2008**, *321*, (5892), 926-929.
16. Galloway, J. N.; Townsend, A. R.; Erisman, J. W.; Bekunda, M.; Cai, Z.; Freney, J. R.; Martinelli, L. A.; Seitzinger, S. P.; Sutton, M. A., Transformation of the nitrogen cycle: recent trends, questions, and potential solutions. *Science* **2008**, 320.
17. Kuypers, M. M. M.; Marchant, H. K.; Kartal, B., The microbial nitrogen-cycling network. *Nat Rev Microbiol* **2018**, *16*, (5), 263-276.

18. Lu, C.; Tian, H., Global nitrogen and phosphorus fertilizer use for agriculture production in the past half century: shifted hot spots and nutrient imbalance. *Earth System Science Data* **2017**, *9*, (1), 181-192.
19. Elser, J.; Bennett, E., A broken biogeochemical cycle. *Nat* **2011**, *478*, 29-31.
20. Elser, J. J., Phosphorus: a limiting nutrient for humanity? *Curr Opin Biotechnol* **2012**, *23*, (6), 833-8.
21. Petzet, S.; Peplinski, B.; Cornel, P., On wet chemical phosphorus recovery from sewage sludge ash by acidic or alkaline leaching and an optimized combination of both. *Water Res* **2012**, *46*, (12), 3769-80.
22. Reijnders, L., Phosphorus resources, their depletion and conservation, a review. *Resour, Conserv Recy* **2014**, *93*, 32-49.
23. Zessner, M.; Lampert, C.; Kroiss, H.; Lindtner, S., Cost comparison of wastewater treatment in Danubian countries. *Water Sci Technol* **2010**, *62*, (2), 223-30.
24. Stinson, B.; Murthy, S.; Bott, C.; Wett, B.; Al-Omari, A.; Bowden, G.; Mokhyerie, Y.; Clippeleir, H. D. Roadmap towards energy neutrality & chemical optimization at enhanced nutrient removal facilities, *WEFTEC*, Chicago, IL, USA, 2013; Chicago, IL, USA, 2013.
25. Gao, H.; Scherson, Y. D.; Wells, G. F., Towards energy neutral wastewater treatment: methodology and state of the art. *Environ Sci Process Impacts* **2014**, *16*, (6), 1223-46.
26. Schreiber, F.; Wunderlin, P.; Udert, K. M.; Wells, G. F., Nitric oxide and nitrous oxide turnover in natural and engineered microbial communities: biological pathways, chemical reactions, and novel technologies. *Front Microbiol* **2012**, *3*, 1-24.
27. Wett, B.; Nyhuis, G.; Podmirseg, S. M.; Gomez-Brandon, M.; Muik, M.; Puempel, T.; Hell, M.; Omari, A.; Declippeleir, H.; Pusker, R.; Bott, C.; Akintayo, O.; Bunce, R.; Chandran, K.; Desta, M.; Dockett, N.; Han, M.; Fredericks, D.; Holgate, B.; Jimenez, R.; Keswani, H.; Kinnear, D.; Ma, Y.; Michealis, M.; Miller, M. W.; Neethling, J. B.; O'Shaughnessy, M.; Park, H.; Shaw, A.; Stinson, B.; DeBarbadillo, C.; Takacs, I.; Welling, C.; Murthy, S. In Oral Presentation: Application of mainstream deammonification, *WEFTEC*, Chicago, IL, USA, **2013**
28. McCarty, P. L.; Bae, J.; Kim, J., Domestic wastewater treatment as a net energy producer-can this be achieved? *Environ Sci Technol* **2011**, *45*, (17), 7100-7106.
29. Guest, J. S.; Skerlos, S. J.; Barnard, J. L.; Beck, M. B.; Daigger, G. T.; Hilger, H.; Jackson, S. J.; Karvazy, K.; Kelly, L.; Macpherson, L.; Mihelcic, J. R.; Pramanik, A.; Raskin, L.; Van Loosdrecht, M. C. M.; Yeh, D.; Love, N. G., A new planning and design paradigm to achieve sustainable resource recovery from wastewater. *Environ Sci Technol* **2009**, *43*, (16), 6126-6130.
30. Larsen, T. A.; Gujer, W., Implementation of source separation and decentralization in cities. *Source Separation and Decentralization for Wastewater Management*, *IWA Publishing*: New York, NY, 2013; pp 135-150.
31. Mulder, A.; Van De Graaf, A. A.; Robertson, L. A.; Kuenen, J. G., Anaerobic ammonium oxidation discovered in a denitrifying fluidized bed reactor. *FEMS Microbiol Ecology* **1995**, *16*, 177-185.
32. Oyserman, B. O.; Noguera, D. R.; del Rio, T. G.; Tringe, S. G.; McMahon, K. D., Metatranscriptomic insights on gene expression and regulatory controls in *Candidatus Accumulibacter phosphatis*. *The ISME J* **2015**, *10*, (4), 810-822.

33. Vlaeminck, S. E.; De Clippeleir, H.; Verstraete, W., Microbial resource management of one-stage partial nitrification/anammox. *Microb biotechnol* **2012**, *5*, (3), 433-448.
34. Kuai, L.; Verstraete, W., Ammonium removal by the oxygen-limited autotrophic nitrification-denitrification system. *Appl Environ Microbiol* **1998**, *64*, (11), 4500-4506.
35. Siegrist, H.; Salzgeber, D.; Eugster, J.; Joss, A., Anammox brings WWTP closer to energy autarky due to increased biogas production and reduced aeration energy for N-removal. *Water Sci and Technol* **2008**, *57*, (3), 383-388.
36. Sun, S. P.; Nacher, C. P.; Merkey, B.; Zhou, Q.; Xia, S. Q.; Yang, D. H.; Sun, J. H.; Smets, B. F., Effective biological nitrogen removal treatment processes for domestic wastewater with low C/N ratios: a review. *Environ Engineering Sci* **2010**, *27*, (2), 111-125.
37. Strous, M.; Heijnen, J. J.; Kuenen, J. G.; Jetten, M. S., The sequencing batch reactor as a powerful tool for the study of slowly growing anaerobic ammonium-oxidizing microorganisms. *Appl Microbiol Biotechnol* **1998**, *50*, 589-596.
38. Galí, A.; Dosta, J.; van Loosdrecht, M. C. M.; Mata-Alvarez, J., Two ways to achieve an anammox influent from real reject water treatment at lab-scale: Partial SBR nitrification and SHARON process. *Process Biochem* **2007**, *42*, (4), 715-720.
39. Foundation, W. E. R., Energy production and efficiency research-the roadmap to net-zero energy. *WERF*, **2011**.
40. Rees, N. V.; Compton, R. G., Carbon-free energy: a review of ammonia- and hydrazine-based electrochemical fuel cells. *Energy Environ Sci* **2011**, *4*, 1255-1260.
41. Scherson, Y. D.; Wells, G. F.; Woo, S.-G.; Lee, J.; Park, J.; Cantwell, B. J.; Criddle, C. S., Nitrogen removal with energy recovery through N₂O decomposition. *Energy Environ Sci* **2013**, *6*, (1), 241.
42. Office of Atmospheric Programs Climate Change Division, U. E., Summary Report: Global Anthropogenic Non-CO₂ Greenhouse Gas Emissions: 1990-2030. **2012**.
43. Pfahi, U. J.; Ross, M. C.; Shepherd, J. E., Flammability Limits, Ignition Energy, and Flame Speeds in H₂-CH₄-NH₃-N₂O-O₂-N₂ Mixtures. *Combust Flame* **2000**, *123*, (1-2), 140-158.
44. Powell, O. A.; Miller, J. E.; Dreyer, C.; Papas, P. Characterization of Hydrocarbon/Nitrous Oxide Propellant Combinations, *46th AIAA Aerospace Science Meeting and Exhibit, Reno* **2008**; pp 1-7.
45. Scherson, Y. D.; Lohner, K. A.; Cantwell, B.; Kenny, T. Small-scale planar nitrous oxide monopropellant thruster for "green" propulsion and power generation, *46th AIAA/ASME/SAE/ASEE Joint Propulsion Conference & Exhibit*, American Institute of Aeronautics and Astronautics: Nashville, TN, **2010**.
46. U. van Dongen, M. S. M. J. a. M. C. M. v. L., The SHARON®-Anammox® process for treatment of ammonium rich wastewater. *Water Sci Technol* **2001**, *44*, (1), 153-160.
47. Chandran, K.; Stein, L. Y.; Klotz, M. G.; van Loosdrecht, M. C., Nitrous oxide production by lithotrophic ammonia-oxidizing bacteria and implications for engineered nitrogen-removal systems. *Biochem Soc trans* **2011**, *39*, (6), 1832-7.
48. Frame, C. H.; Casciotti, K. L., Biogeochemical controls and isotopic signatures of nitrous oxide production by a marine ammonia-oxidizing bacterium. *Biogeosciences* **2010**, *7*, (9), 2695-2709.

49. Schreiber, F.; Wunderlin, P.; Udert, K. M.; Wells, G. F., Nitric oxide and nitrous oxide turnover in natural and engineered microbial communities: biological pathways, chemical reactions, and novel technologies. *Front in microbiol* **2012**, *3*, 1-24.
50. Aktan, C. K.; Yapsakli, K.; Mertoglu, B., Inhibitory effects of free ammonia on Anammox bacteria. *Biodegradation* **2012**, *23*, (5), 751-762.
51. Carvajal-Arroyo, J. M.; Sun, W.; Sierra-Alvarez, R.; Field, J. A., Inhibition of anaerobic ammonium oxidizing (anammox) enrichment cultures by substrates, metabolites and common wastewater constituents. *Chemosphere* **2013**, *91*, (1), 22-27.
52. Jensen, M. M.; Thamdrup, B.; Dalsgaard, T., Effects of specific inhibitors on anammox and denitrification in marine sediments. *Appl Environ Microbiol* **2007**, *73*, (10), 3151-3158.
53. Wunderlin, P.; Siegrist, H.; Joss, A., Online N₂O measurement: the next standard for controlling biological ammonia oxidation? *Environ Sci Technol* **2013**, *47*, (17), 9567-9568.
54. Jin, R.-C.; Yang, G.-F.; Yu, J.-J.; Zheng, P., The inhibition of the Anammox process: A review. *J Chem Eng* **2012**, *197*, 67-79.
55. Joss, A.; Derlon, N.; Cyprien, C.; Burger, S.; Szivak, I.; Traber, J.; Siegrist, H.; Morgenroth, E., Combined nitrification-anammox: advances in understanding process stability. *Environ Sci Technol* **2011**, *45*, (22), 9735-9742.
56. Lotti, T.; van der Star, W. R.; Kleerebezem, R.; Lubello, C.; van Loosdrecht, M. C., The effect of nitrite inhibition on the anammox process. *Water Res* **2012**, *46*, (8), 2559-2569.
57. Kartal, B.; Kuenen, J. G.; van Loosdrecht, M. C., Sewage treatment with anammox. *Science* **2010**, *328*, (5979), 702-703.
58. Rittmann, B. E.; McCarty, P. L., *Environmental Biotechnology: Principles and Applications*. Tata McGraw-Hill Education: 2012.
59. Scherson, Y. D.; Criddle, C. S., Recovery of freshwater from wastewater: upgrading process configurations to maximize energy recovery and minimize residuals. *Environ Sci Technol* **2014**, *48*, (15), 8420-32.
60. He, S.; McMahan, K. D., Microbiology of 'Candidatus Accumulibacter' in activated sludge. *Microb Biotechnol* **2011**, *4*, (5), 603-619.
61. Seviour, R. J.; Mino, T.; Onuki, M., The microbiology of biological phosphorus removal in activated sludge systems. *FEMS Microbiol Reviews* **2003**, *27*, (1), 99-127.
62. Hu, Z.-r.; Wentzel, M. C.; Ekama, G. A., Anoxic growth of phosphate-accumulating organisms (PAOs) in biological nutrient removal activated sludge systems. *Water Res* **2002**, *36*, 1-11.
63. Adams, R. I.; Bateman, A. C.; Bik, H. M.; Meadow, J. F., Microbiota of the indoor environment: a meta-analysis. *Microbiome* **2015**, *3*, 49.
64. Carvalho, G.; Lemos, P. C.; Oehmen, A.; Reis, M. A. M., Denitrifying phosphorus removal: Linking the process performance with the microbial community structure. *Water Res* **2007**, *41*, (19), 4383-4396.
65. Gao, H.; Liu, M.; Griffin, J. S.; Xu, L.; Xiang, D.; Scherson, Y. D.; Liu, W. T.; Wells, G. F., Complete nutrient removal coupled to nitrous oxide production as a bioenergy source by denitrifying polyphosphate-accumulating organisms. *Environ Sci Technol* **2017**, *51*, (8), 4531-4540.

66. Zhou, Y.; Pijuan, M.; Yuan, Z., Free nitrous acid inhibition on anoxic phosphorus uptake and denitrification by poly-phosphate accumulating organisms. *Biotechnol Bioeng* **2007**, *98*, (4), 903-912.
67. Zhou, Y.; Pijuan, M.; Zeng, R. J.; Yuan, Z., Free nitrous acid inhibition on nitrous oxide reduction by a denitrifying-enhanced biological phosphorus removal sludge. *Environ Sci Technol* **2008**, *42*, 8260-8265.
68. Nguyen, H. T. T.; Le, V. Q.; Hansen, A. A.; Nielsen, J. L.; Nielsen, P. H., High diversity and abundance of putative polyphosphate-accumulating Tetrasphaera-related bacteria in activated sludge systems. *FEMS Microbiol Ecol* **2011**, *76*, (2), 256-267.
69. Nguyen, H. T. T.; Nielsen, J. L.; Nielsen, P. H., 'Candidatus Halomonas phosphatis', a novel polyphosphate-accumulating organism in full-scale enhanced biological phosphorus removal plants. *Environ Microbiol* **2012**, *14*, (10), 2826-2837.
70. Stokholm-Bjerregaard, M.; McIlroy, S. J.; Nierychlo, M.; Karst, S. M.; Albertsen, M.; Nielsen, P. H., A critical assessment of the microorganisms proposed to be important to enhanced biological phosphorus removal in full-scale wastewater treatment systems. *Front Microbiol* **2017**, *8*, 718.
71. Kristiansen, R.; Nguyen, H. T. T.; Saunders, A. M.; Nielsen, J. L.; Wimmer, R.; Le, V. Q.; McIlroy, S. J.; Petrovski, S.; Seviour, R. J.; Calteau, A.; Nielsen, K. a. r. L.; Nielsen, P. H. a. r., A metabolic model for members of the genus Tetrasphaera involved in enhanced biological phosphorus removal. *The ISME J* **2012**, *7*, (3), 543-554.
72. Kong, Y.; Xia, Y.; Nielsen, J. L.; Nielsen, P. H., Structure and function of the microbial community in a full-scale enhanced biological phosphorus removal plant. *Microbiol* **2007**, *153*, (Pt 12), 4061-73.
73. McMahon, K. D.; Yilmaz, S.; He, S.; Gall, D. L.; Jenkins, D.; Keasling, J. D., Polyphosphate kinase genes from full-scale activated sludge plants. *Appl Microbiol Biotechnol* **2007**, *77*, (1), 167-173.
74. Oehmen, A.; Yuan, Z.; Blackall, L. L.; Keller, J., Comparison of acetate and propionate uptake by polyphosphate accumulating organisms and glycogen accumulating organisms. *Biotechnol Bioeng* **2005**, *91*, (2), 162-8.
75. Wong, M. T.; Liu, W. T., Ecophysiology of *Defluviicoccus*-related tetrad-forming organisms in an anaerobic-aerobic activated sludge process. *Environ Microbiol* **2007**, *9*, (6), 1485-96.
76. Kong, Y.; Xia, Y.; Nielsen, J. L.; Nielsen, P. H., Ecophysiology of a group of uncultured Gammaproteobacterial glycogen-accumulating organisms in full-scale enhanced biological phosphorus removal wastewater treatment plants. *Environ Microbiol* **2006**, *8*, (3), 479-89.
77. Albertsen, M.; McIlroy, S. J.; Stokholm-Bjerregaard, M.; Karst, S. M.; Nielsen, P. H., "Candidatus Propionivibrio aalborgensis": A novel glycogen accumulating organism abundant in full-scale enhanced biological phosphorus removal plants. *Front Microbiol* **2016**, *7*, 1033.
78. Oehmen, A.; Lemos, P. C.; Carvalho, G.; Yuan, Z.; Keller, J.; Blackall, L. L.; Reis, M. A., Advances in enhanced biological phosphorus removal: from micro to macro scale. *Water Res* **2007**, *41*, (11), 2271-300.
79. Weissbrodt, D. G.; Schneiter, G. S.; Furbringer, J. M.; Holliger, C., Identification of trigger factors selecting for polyphosphate- and glycogen-accumulating organisms in aerobic granular sludge sequencing batch reactors. *Water Res* **2013**, *47*, (19), 7006-18.

80. Lopez-Vazquez, C. M.; Oehmen, A.; Hooijmans, C. M.; Brdjanovic, D.; Gijzen, H. J.; Yuan, Z.; van Loosdrecht, M. C., Modeling the PAO-GAO competition: effects of carbon source, pH and temperature. *Water Res* **2009**, *43*, (2), 450-62.
81. Smolders, G. J. F.; Loosdrecht, M. C. M. v.; Heijnen, J. J., pH: Key factor in the biological phosphorus removal process. *Water Sci Tech* **1994**, *29*, (7), 71-74.
82. Winkler, M. K.; Bassin, J. P.; Kleerebezem, R.; de Bruin, L. M.; van den Brand, T. P.; van Loosdrecht, M. C., Selective sludge removal in a segregated aerobic granular biomass system as a strategy to control PAO-GAO competition at high temperatures. *Water Res* **2011**, *45*, (11), 3291-9.83.
83. Oehmen, A.; Teresa Vives, M.; Lu, H.; Yuan, Z.; Keller, J., The effect of pH on the competition between polyphosphate-accumulating organisms and glycogen-accumulating organisms. *Water Res* **2005**, *39*, (15), 3727-37.
84. Carvalheira, M.; Oehmen, A.; Carvalho, G.; Reis, M. A. M., The effect of substrate competition on the metabolism of polyphosphate accumulating organisms (PAOs). *Water Res* **2014**, *64*, 149-159.
85. Oehmen, A.; Zeng, R. J.; Yuan, Z.; Keller, J., Anaerobic metabolism of propionate by polyphosphate-accumulating organisms in enhanced biological phosphorus removal systems. *Biotechnol Bioeng* **2005**, *91*, (1), 43-53.
86. Lu, H.; Oehmen, A.; Viridis, B.; Keller, J.; Yuan, Z., Obtaining highly enriched cultures of *Candidatus Accumulibacter* phosphates through alternating carbon sources. *Water Res* **2006**, *40*, (20), 3838-3848.
87. Lopez-Vazquez, C. M.; Song, Y. I.; Hooijmans, C. M.; Brdjanovic, D.; Moussa, M. S.; Gijzen, H. J.; van Loosdrecht, M. C., Temperature effects on the aerobic metabolism of glycogen-accumulating organisms. *Biotechnol Bioeng* **2008**, *101*, (2), 295-306.
88. Lasken, R. S.; McLean, J. S., Recent advances in genomic DNA sequencing of microbial species from single cells. *Nat Rev Genet* **2014**, *15*, (9), 577-84.
89. He, S.; Gall, D. L.; McMahon, K. D., "*Candidatus Accumulibacter*" population structure in enhanced biological phosphorus removal sludges as revealed by polyphosphate kinase genes. *Appl Environ Microbiol* **2007**, *73*, (18), 5865-74.
90. Flowers, J. J.; He, S.; Yilmaz, S.; Noguera, D. R.; McMahon, K. D., Denitrification capabilities of two biological phosphorus removal sludges dominated by different "*Candidatus Accumulibacter*" clades. *Environ microbiol reports* **2009**, *1*, (6), 583-588.
91. Flowers, J. J.; He, S.; Malfatti, S.; del Rio, T. G.; Tringe, S. G.; Hugenholtz, P.; McMahon, K. D., Comparative genomics of two '*Candidatus Accumulibacter* clades performing biological phosphorus removal. *The ISME J* **2013**, *7*, (12), 2301-2314.
92. Oyserman, B. O.; Moya, F.; Lawson, C. E.; Garcia, A. L.; Vogt, M.; Heffernan, M.; Noguera, D. R.; McMahon, K. D., Ancestral genome reconstruction identifies the evolutionary basis for trait acquisition in polyphosphate accumulating bacteria. *The ISME J* **2016**, 1-15.
93. Skennerton, C. T.; Barr, J. J.; Slater, F. R.; Bond, P. L.; Tyson, G. W., Expanding our view of genomic diversity in *Candidatus Accumulibacter* clades. *Environ Microbiol* **2014**, *17*, (5), 1574-1585.
94. Flowers, J. J.; He, S.; Malfatti, S.; del Rio, T. G.; Tringe, S. G.; Hugenholtz, P.; McMahon, K. D., Comparative genomics of two "*Candidatus Accumulibacter*" clades performing biological phosphorus removal. *The ISME J* **2013**, *7*, (12), 2301-2314.

95. Flowers, J. J.; He, S.; Yilmaz, S.; Noguera, D. R.; McMahon, K. D., Denitrification capabilities of two biological phosphorus removal sludges dominated by different *Candidatus Accumulibacter* clades. *Environ Microbiol Rep* **2009**, *1*, (6), 583-588.
96. Wexler, M.; Richardson, D. J.; Bond, P. L., Radiolabelled proteomics to determine differential functioning of *Accumulibacter* during the anaerobic and aerobic phases of a bioreactor operating for enhanced biological phosphorus removal. *Environ Microbiol* **2009**, *11*, (12), 3029-44.
97. Kampschreur, M. J.; Temmink, H.; Kleerebezem, R.; Jetten, M. S.; van Loosdrecht, M. C., Nitrous oxide emission during wastewater treatment. *Water Res* **2009**, *43*, (17), 4093-103.
98. Ritter, W. F.; Chitikela, S. R., Greenhouse gas emissions from wastewater treatment plants and by-product operations -a comprehensive review. *World Environmental and Water Resources Congress* **2014**.
99. Daelman, M. R.; van Voorthuizen, E. M.; van Dongen, U. G.; Volcke, E. I.; van Loosdrecht, M. C., Seasonal and diurnal variability of N₂O emissions from a full-scale municipal wastewater treatment plant. *Sci Total Environ* **2015**, *536*, 1-11.
100. Solomon, S.; Qin, D.; Manning, M.; Chen, Z.; Marquis, M.; Averyt, K. B.; Tignor, M.; Miller, H. L., Changes in Atmospheric Constituents and Radiative Forcing. In *Contribution of Working Group I to the Fourth Assessment Report of the Intergovernmental Panel on Climate Change, 2007*, Cambridge University Press: Cambridge, United Kingdom and New York, NY, USA, 2007.
101. Terada, A.; Sugawara, S.; Hojo, K.; Takeuchi, Y.; Riya, S.; Harper, W. F., Jr.; Yamamoto, T.; Kuroiwa, M.; Isobe, K.; Katsuyama, C.; Suwa, Y.; Koba, K.; Hosomi, M., Hybrid nitrous oxide production from a partial nitrifying bioreactor: hydroxylamine interactions with nitrite. *Environ Sci Technol* **2017**, *51*, (5), 2748-2756.
102. Harper, W. F.; Takeuchi, Y.; Riya, S.; Hosomi, M.; Terada, A., Novel abiotic reactions increase nitrous oxide production during partial nitrification: Modeling and experiments. *J Chem Eng* **2015**, *281*, 1017-1023.
103. Soler-Jofra, A.; Stevens, B.; Hoekstra, M.; Picioreanu, C.; Sorokin, D.; van Loosdrecht, M. C. M.; Pérez, J., Importance of abiotic hydroxylamine conversion on nitrous oxide emissions during nitrification of reject water. *J Chem Eng* **2016**, *287*, 720-726.
104. Spott, O.; Florian Stange, C., Formation of hybrid N₂O in a suspended soil due to co-denitrification of NH₂OH. *J Plant Nutrition Soil Sci* **2011**, *174*, (4), 554-567.
105. Ma, C.; Jensen, M. M.; Smets, B. F.; Thamdrup, B., Pathways and Controls of N₂O Production in Nitrification-Anammox Biomass. *Environ Sci Technol* **2017**, *51*, (16), 8981-8991.
106. Tallec, G.; Garnier, J.; Billen, G.; Gossiaux, M., Nitrous oxide emissions from secondary activated sludge in nitrifying conditions of urban wastewater treatment plants: effect of oxygenation level. *Water Res* **2006**, *40*, (15), 2972-80.
107. Domingo-Felez, C.; Mutlu, A. G.; Jensen, M. M.; Smets, B. F., Aeration strategies to mitigate nitrous oxide emissions from single-stage nitrification/anammox reactors. *Environ Sci Technol* **2014**, *48*, (15), 8679-87.
108. Yu, R.; Kampschreur, M. J.; Loosdrecht, M. C. M. V.; Chandran, K., Mechanisms and specific directionality of autotrophic nitrous oxide and nitric oxide generation during transient anoxia. *Environ Sci Technol* **2010**, *44*, 1313-1319.

109. van Kessel, M. A. H. J.; Speth, D. R.; Albertsen, M.; Nielsen, P. H.; den Camp, H. J. M. O.; Kartal, B.; Jetten, M. S. M.; Lüscher, S., Complete nitrification by a single microorganism. *Nat* **2015**, *528*, (7583), 555-559.
110. Daims, H.; Lebedeva, E. V.; Pjevac, P.; Han, P.; Herbold, C.; Albertsen, M.; Jehmlich, N.; Palatinszky, M.; Vierheilig, J.; Bulaev, A.; Kirkegaard, R. H.; von Bergen, M.; Rattei, T.; Bendinger, B.; Nielsen, P. H.; Wagner, M., Complete nitrification by *Nitrospira* bacteria. *Nat* **2015**, *528*, (7583), 504-509.
111. Sanford, R.; Wagner, D.; Wu, Q.; Chee-Sanford, J.; Thomas, S.; Cruz-Garcia, C.; Rodriguez, G.; Massol-Deya, A.; Krishnani, K.; Ritalahti, K.; Silke, N.; Konstantinidis, K.; Löffler, F., Unexpected nondenitrifier nitrous oxide reductase gene diversity and abundance in soils. *PNAS* **2012**, *109*, (48), 19709-19714.
112. Pan, Y.; Ni, B.; Bond, P. L.; Ye, L.; Yuan, Z., Electron competition among nitrogen oxides reduction during methanol-utilizing denitrification in wastewater treatment. *Water Res* **2013**, *47*, (10), 3273-3281.
113. Ribera-Guardia, A.; Marques, R.; Arangio, C.; Carvalheira, M.; Oehmen, A.; Pijuan, M., Distinctive denitrifying capabilities lead to differences in N₂O production by denitrifying polyphosphate accumulating organisms and denitrifying glycogen accumulating organisms. *Bioresour Technol* **2016**, *219*, (C), 106-113.
114. Pan, Y.; Ni, B.; Yuan, Z., Modeling electron competition among nitrogen oxides reduction and n₂o accumulation in denitrification. *Environ Sci Technol* **2013**, *47*, (19), 11083-11091.
115. Philippot, L.; Andert, J.; Jones, C. M.; Bru, D.; Hallin, S., Importance of denitrifiers lacking the genes encoding the nitrous oxide reductase for N₂O emissions from soil. *Global Change Biol* **2011**, *17*, (3), 1497-1504.
116. Oh, J.; Silverstein, J., Acetate limitation and nitrite accumulation during denitrification. *J Environ Eng* **1999**, *125*, (3), 234-242.
117. Zheng, J.; Doskey, P. V., Modeling nitrous oxide production and reduction in soil through explicit representation of denitrification enzyme kinetics. *Environ Sci Technol* **2015**, *49*, (4), 2132-2139.
118. Pan, Y.; Ye, L.; Ni, B.; Yuan, Z., Effect of pH on N₂O reduction and accumulation during denitrification by methanol utilizing denitrifiers. *Water Res* **2012**, *46*, (15), 4832-4840.
119. Graf, D. R.; Jones, C. M.; Hallin, S., Intergenomic comparisons highlight modularity of the denitrification pathway and underpin the importance of community structure for N₂O emissions. *PLoS One* **2014**, *9*, (12), e114118.
120. Hallin, S.; Philippot, L.; Löffler, F. E.; Sanford, R. A.; Jones, C. M., Genomics and ecology of novel N₂O-reducing microorganisms. *Trends Microbiol* **2017**, 1-13.
121. Koskineemi, S.; Sun, S.; Berg, O. G.; Andersson, D. I., Selection-Driven gene loss in bacteria. *Plos Genetics* **2012**, *8*, (6), 1-7.
122. Felgate, H.; Giannopoulos, G.; Sullivan, M. J.; Gates, A. J.; Clarke, T. A.; Baggs, E.; Rowley, G.; Richardson, D. J., The impact of copper, nitrate and carbon status on the emission of nitrous oxide by two species of bacteria with biochemically distinct denitrification pathways. *Environ Microbiol* **2012**, *14*, (7), 1788-800.
123. Lilja, E. E.; Johnson, D. R., Segregating metabolic processes into different microbial cells accelerates the consumption of inhibitory substrates. *The ISME J* **2016**, *10*, (7), 1568-78.

124. Jones, C. M.; Graf, D. R.; Bru, D.; Philippot, L.; Hallin, S., The unaccounted yet abundant nitrous oxide-reducing microbial community: a potential nitrous oxide sink. *The ISME J* **2013**, *7*, (2), 417-26.
125. Berks, B. C.; Sargent, F.; Palmer, T., The Tat protein export pathway. *Molecular Microbiol* **2000**, *35*, (2), 260-274.
126. Pohlschroder, M.; Hartmann, E.; Hand, N. J.; Dilks, K.; Haddad, A., Diversity and evolution of protein translocation. *Annual Review of Microbiol* **2005**, *59*, (91-111).
127. Yoon, S.; Nissen, S.; Park, D.; Sanford, R. A.; Löffler, F. E., Nitrous oxide reduction kinetics distinguish bacteria harboring clade I *nosZ* from those harboring clade II *nosZ*. *Appl Environ Microbiol* **2016**, *82*, (13), 3793-800.
128. Tallec, G.; Garnier, J.; Billen, G.; Gousailles, M., Nitrous oxide emissions from denitrifying activated sludge of urban wastewater treatment plants, under anoxia and low oxygenation. *Bioresour Technol* **2008**, *99*, (7), 2200-9.
129. Alinsafi, A.; Adouani, N.; Béline, F.; Lendormi, T.; Limousy, L.; Sire, O., Nitrite effect on nitrous oxide emission from denitrifying activated sludge. *Process Biochem* **2008**, *43*, (6), 683-689.
130. Hanaki, K.; Hong, Z.; Matsuo, T., Production of nitrous oxide gas during denitrification of wastewater. *Water Sci Technol* **1992**, *26*, (5-6), 1027-1036.
131. Itokawa, H.; Hanaki, K.; Matsuo, T., Nitrous oxide production in high-loading biological nitrogen removal process under low COD/N ration condition. *Water Res* *35*, (3), 657-664.
132. Lu, H.; Chandran, K., Factors promoting emissions of nitrous oxide and nitric oxide from denitrifying sequencing batch reactors operated with methanol and ethanol as electron donors. *Biotechnol Bioeng* **2010**, *106*, (3), 390-8.
133. Law, Y.; Ye, L.; Pan, Y.; Yuan, Z., Nitrous oxide emissions from wastewater treatment processes. *Philos Trans R Soc Lond B Biol Sci* **2012**, *367*, (1593), 1265-77.
134. Scherson, Y. D.; Wells, G. F.; Woo, S.-G.; Lee, J.; Park, J.; Cantwell, B. J.; Criddle, C. S., Nitrogen removal with energy recovery through N₂O decomposition. *Energy Environ Sci* **2013**, *6*, (1), 241-248.
135. Scherson, Y. D.; Criddle, C. S., Recovery of Freshwater from Wastewater: Upgrading process configurations to maximize energy recovery and minimize residuals. *Environ Sci Technol* **2014**, *48*, (15), 8420-8432.
136. Hellinga, C.; Schellen, A. A. J. C.; Mulder, J. W.; Loosdrecht, M. C. M. v.; Heijnen, J. J., The sharon process: an innovative method for nitrogen removal from ammonium-rich waste water. *Wat Sci Tech* **1998**, *37*, 135-142.
137. Warakomski, A.; Kempen, R. v.; Kos, P. Microbiology and Biochemistry of the nitrogen cycle process applications: SHARON, ANAMMOX, and Nitritation, *Nutrient Removal Speciality Conference WEF IWA EPA Chesapeake WEA*, Baltimore, MD, USA, 2007; Baltimore, MD, USA, 2007.
138. Mulder, J. W.; Duin, J. O. J.; Goverde, J.; Poiesz, W. G.; van Veldhuizen, H. M.; van Kempen, R.; Roeleveld, P. Full-Scale Experience with the Sharon Process through the Eyes of the Operators, *WEFTEC*, 2006; Water Environment Federation: 2006; pp 5256-5270.
139. Bettella, A.; Moretto, F.; Geremia, E.; Bellomo, N.; Pavarin, D.; Petronio, D. Development and flight testing of a hybrid rocket booster for UAV assisted take off, *49th AIAA/ASME/SAE/ASEE Joint Propulsion Conference*, San Jose, CA, 2013; San Jose, CA, 2013.

140. Pfahl, U. J.; Orss, M. C.; Shepherd, J. E.; Pasamehmetoglu, K. O.; Unal, C., Flammability limits, ignition energy, and flame speeds in H₂-CH₄-NH₃-N₂O-O₂-N₂ mixtures. *Combust Flame* **2000**, *123*, (1-2), 140-158.
141. Mino, T.; Loosdrecht, M. C. M. v.; Heijnen, J. J., Microbiology and biochemistry of the enhanced biological phosphate removal process. *Water Res* **1998**, *32*, (11), 3193-3207.
142. Peterson, S. B.; Warnecke, F.; Madejska, J.; McMahon, K. D.; Hugenholtz, P., Environmental distribution and population biology of *Candidatus Accumilibacter*, a primary agent of biological phosphorus removal. *Environ Microbiol* **2008**, *10*, (10), 2692-2703.
143. Smolders, G. J. F.; Meij, J. v. d.; Loosdrecht, M. C. M. v.; Heijnen, J. J., Model of the anaerobic metabolism of the biological phosphorus removal process: stoichiometry and pH influence. *Biotechnol Bioeng* **1994**, *43*, 461-470.
144. Itokawa, H.; Hanaki, K.; Matsuo, T., Nitrous oxide production in high-loading biological nitrogen removal process under low COD/N ratio condition. *Water Res* **2001**, *35*, (3), 657-664.
145. Ahn, J. H.; Kim, S.; Park, H.; Rahm, B.; Pagilla, K.; Chandran, K., N₂O Emissions from Activated Sludge Processes, 2008-2009: Results of a National Monitoring Survey in the United States. *Environ Sci Technol* **2010**, *44*, 5405-5411.
146. APHA, Standard Methods for the Examination of Water and Wastewater, *20th ed.* Washington D.C., USA, 1998.
147. Song, J. H.; Jeon, C. O.; Choi, M. H.; Yoon, S. C.; Park, W., Polyhydroxyalkanoate (PHA) production using waste vegetable oil by *Pseudomonas* sp. Strain DR2. *J Microbiol Biotechnol* **2008**, *18*, (8), 1408-1415.
148. Oehmen, A.; Keller-Lehmann, B.; Zeng, R. J.; Yuan, Z.; Keller, J., Optimisation of poly-β-hydroxyalkanoate analysis using gas chromatography for enhanced biological phosphorus removal systems. *J Chromatogr A* **2005**, *1070*, (1-2), 131-136.
149. Caporaso, J. G.; Lauber, C. L.; Walters, W. A.; Berg-Lyons, D.; Huntley, J.; Fierer, N.; Owens, S. M.; Betley, J.; Fraser, L.; Bauer, M.; Gormley, N.; Gilbert, J. A.; Smith, G.; Knight, R., Ultra-high-throughput microbial community analysis on the Illumina HiSeq and MiSeq platforms. *The ISME J* **2012**, *6*, (8), 1621-4.
150. Edgar, R. C., UPARSE: highly accurate OTU sequences from microbial amplicon reads. *Nat Met* **2013**, *10*, (10), 996-998.
151. Edgar, R. C.; Haas, B. J.; Clemente, J. C.; Quince, C.; Knight, R., UCHIME improves sensitivity and speed of chimera detection. *Bioinformatics* **2011**, *27*, (16), 2194-200.
152. Caporaso, J. G.; Kuczynski, J.; Stombaugh, J.; Bittinger, K.; Bushman, F. D.; Costello, E. K.; Fierer, N.; Peña, A. G.; Goodrich, J. K.; Gordon, J. I.; Huttley, G. A.; Kelley, S. T.; Knights, D.; Koenig, J. E.; Ley, R. E.; Lozupone, C. A.; McDonald, D.; Muegge, B. D.; Pirrung, M.; Reeder, J.; Sevinsky, J. R.; Turnbaugh, P. J.; Walters, W. A.; Widmann, J.; Yatsunencko, T.; Zaneveld, J.; Knight, R., QIIME allows analysis of high-throughput community sequencing data. *Nat Met* **2010**, *7*, (5), 335-336.
153. Edgar, R. C., Search and clustering orders of magnitude faster than BLAST. *Bioinformatics* **2010**, *26*, (19), 2460-2461.
154. Pruesse, E.; Peplies, J.; Glockner, F. O., SINA: accurate high-throughput multiple sequence alignment of ribosomal RNA genes. *Bioinformatics* **2012**, *28*, (14), 1823-9.

155. Crocetti, G. R.; Banfield, J. F.; Keller, J.; Bond, P. L.; Blackall, L. L., Glycogen-accumulating organisms in laboratory-scale and full-scale wastewater treatment processes. *Microbiol* **2002**, *148*, 3353-3364.
156. Zeng, R. J.; van Loosdrecht, M. C.; Yuan, Z.; Keller, J., Metabolic model for glycogen-accumulating organisms in anaerobic/aerobic activated sludge systems. *Biotechnol Bioeng* **2003**, *81*, (1), 92-105.
157. Core R team, *R: A Language and Environment for Statistical Computing*. *R Foundation for Statistical Computing*: Vienna, Austria, 2014.
158. Krzywinski, M.; Schein, J.; Birol, I.; Connors, J.; Gascoyne, R.; Horsman, D.; Jones, S. J.; Marra, M. A., Circos: an information aesthetic for comparative genomics. *Genome Res* **2009**, *19*, (9), 1639-45.
159. Zhou, Y.; Pijuan, M.; Zeng, R. J.; Yuan, Z., Free nitrous acid inhibition on nitrous oxide reduction by a denitrifying-enhanced biological phosphorus removal sludge. *Environ Sci Technol* **2008**, *42*, (22), 8260-8265.
160. Yamada, T.; Imachi, H.; Ohashi, A.; Harada, H.; Hanada, S.; Kamagata, Y.; Sekiguchi, Y., *Bellilinea caldifistulae* gen. nov., sp. nov. and *Longilinea arvoryzae* gen. nov., sp. nov., strictly anaerobic, filamentous bacteria of the phylum Chloroflexi isolated from methanogenic propionate-degrading consortia. *Int J Syst Evol Microbiol* **2007**, *57*, (10), 2299-2306.
161. Kim, J. M.; Lee, H. J.; Lee, D. S.; Jeon, C. O., Characterization of the denitrification-associated phosphorus uptake properties of "*Candidatus Accumulibacter phosphatis*" Clades in sludge subjected to Enhanced Biological Phosphorus Removal. *Appl Environ Microbiol* **2013**, *79*, (6), 1969-1979.
162. Weissbrodt, D. G.; Neu, T. R.; Kuhlicke, U.; Rappaz, Y.; Holliger, C., Assessment of bacterial and structural dynamics in aerobic granular biofilms. *Front Microbiol* **2013**, *4*.
163. Myung, J.; Wang, Z.; Yuan, T.; Zhang, P.; Van Nostrand, J. D.; Zhou, J.; Criddle, C. S., Production of nitrous oxide from nitrite in stable type II methanotrophic enrichments. *Environ Sci Technol* **2015**, *49*, (18), 10969-10975.
164. Wang, Y.; Zhou, S.; Ye, L.; Wang, H.; Stephenson, T.; Jiang, X., Nitrite survival and nitrous oxide production of denitrifying phosphorus removal sludges in long-term nitrite/nitrate-fed sequencing batch reactors. *Water Res* **2014**, *67*, (C), 33-45.
165. Zhang, S. H.; Huang, Y.; Hua, Y. M., Denitrifying dephosphatation over nitrite: effects of nitrite concentration, organic carbon, and pH. *Bioresour Technol* **2010**, *101*, (11), 3870-5.
166. Zhou, S.; Zhang, X.; Feng, L., Effect of different types of electron acceptors on the anoxic phosphorus uptake activity of denitrifying phosphorus removing bacteria. *Bioresour Technol* **2010**, *101*, (6), 1603-10.
167. Liu, Y.; Peng, L.; Guo, J.; Chen, X.; Yuan, Z.; Ni, B. J., Evaluating the role of microbial internal storage turnover on nitrous oxide accumulation during denitrification. *Sci Rep* **2015**, *5*, 15138.
168. Sabba, F.; Picioreanu, C.; Nerenberg, R., Mechanisms of nitrous oxide (N₂O) formation and reduction in denitrifying biofilms. *Biotechnol Bioeng* **2017**, *114*, (12), 2753-2761.
169. Zumft, W. G., Cell biology and molecular basis of denitrification. *Microbiol Mol Biol Rev* **1997**, *62*, (4), 533-616.

170. Ye, L.; Ni, B. J.; Law, Y.; Byers, C.; Yuan, Z., A novel methodology to quantify nitrous oxide emissions from full-scale wastewater treatment systems with surface aerators. *Water Res* **2014**, *48*, 257-68.
171. Brdjanovic, D.; Loosdrecht, M. C. M. v.; Hooijmans, C. M.; Alaerts, G. J.; Heijnen, J. J., Temperature effects on physiology of biological phosphorus removal. *J Environ Eng* **1997**, *123*, (2), 144-153.
172. Bassin, J. P.; Winkler, M. K.; Kleerebezem, R.; Dezotti, M.; van Loosdrecht, M. C., Improved phosphate removal by selective sludge discharge in aerobic granular sludge reactors. *Biotechnol Bioeng* **2012**, *109*, (8), 1919-28.
173. Kuba, T.; Wachtmeister, A.; van Loosdrecht, M. C. M.; Heijnen, J. J., Effect of nitrate on phosphorus release in biological phosphorus removal systems. *Wat Sci Tech* **1994**, *30*, (6), 263-269.
174. Smolders, G. J. F.; Meij, J. v. d.; Loosdrecht, M. C. M. v.; Heijnen, J. J., A structured Metabolic Model for Anaerobic and Aerobic Stoichiometry and Kinetics of the Biological Phosphorus Removal Process. *Biotechnol Bioeng* **1995**, *47*, 277-287.
175. Kishida, N.; Kim, J. M.; Kimochi, Y.; Nishimura, O.; Sasaki, H.; Sudo, R., Effect of C/N ratio on nitrous oxide emission from swine wastewater treatment process. *Wat Sci Tech* **2004**, *49*(5-6), 359-371.
176. Camejo, P. Y.; Owen, B. R.; Martirano, J.; Ma, J.; Kapoor, V.; Domingo, J. S.; McMahan, K. D.; Noguera, D. R., *Candidatus Accumulibacter phosphatis* clades enriched under cyclic anaerobic and microaerobic conditions simultaneously use different electron acceptors. *Water Res* **2016**, *102*, (C), 125-137.
177. Wicht, H., A model for predicting nitrous oxide production during denitrification in activated sludge. *Water Sci Tech* **1996**, *34*, (5-6), 99-106.
178. Read-Daily, B. L.; Sabba, F.; Pavissich, J. P.; Nerenberg, R., Kinetics of nitrous oxide (N₂O) formation and reduction by *Paracoccus pantotrophus*. *AMB Express* **2016**, *6*, (1), 85.
179. Zeng, R. J.; Yuan, Z.; Keller, J., Enrichment of denitrifying glycogen-accumulating organisms in anaerobic/anoxic activated sludge system. *Biotechnol Bioeng* **2003**, *81*, (4), 397-404.
180. Ge, S.; Peng, Y.; Wang, S.; Lu, C.; Cao, X.; Zhu, Y., Nitrite accumulation under constant temperature in anoxic denitrification process: The effects of carbon sources and COD/NO₃-N. *Bioresour Technol* **2012**, *114*, 137-43.
181. Bond, P. L.; Hugenholtz, P.; Keller, J.; Blackall, L. L., Bacterial community structures of phosphate-removing and non-phosphate-removing activated sludge from sequencing batch reactors. *Appl Environ Microbiol* **1995**, *61*, (5), 1910-1916.
182. Hesselmann, R. P. X.; Werlen, C.; Hahn, D.; van der Meer, J. R.; Zehnder, A. J. B., Enrichment, phylogenetic analysis and detection of a bacterium that performs enhanced biological phosphate removal in activated sludge. *Syst Appl Microbiol* **1999**, *22*, (3), 454-465.
183. Mao, Y.; Graham, D. W.; Tamaki, H.; Zhang, T., Dominant and novel clades of *Candidatus Accumulibacter phosphatis* in 18 globally distributed full-scale wastewater treatment plants. *Sci Rep* **2015**, 1-10.
184. Zhang, A. N.; Mao, Y.; Zhang, T., Development of quantitative Real-time PCR assays for different clades of "*Candidatus Accumulibacter*". *Sci Rep* **2016**, *6*, 1-7.

185. Kim, J. M.; Lee, H. J.; Lee, D. S.; Jeon, C. O., Characterization of the denitrification-associated phosphorus uptake properties of "*Candidatus Accumulibacter phosphatis*" clades in sludge subjected to enhanced biological phosphorus removal. *Appl Environ Microbiol* **2013**, *79*, (6), 1969-1979.
186. He, S.; Bishop, F. I.; McMahon, K. D., Bacterial community and "*Candidatus Accumulibacter*" population dynamics in laboratory-scale enhanced biological phosphorus removal reactors. *Appl Environ Microbiol* **2010**, *76*, (16), 5479-87.
187. Zhou, Y.; Lim, M.; Harjono, S.; Ng, W. J., Nitrous oxide emission by denitrifying phosphorus removal culture using polyhydroxyalkanoates as carbon source. *J Environ Sci* **2016**, *24*, (9), 1616-1623.
188. Albertsen, M.; Hugenholtz, P.; Skarshewski, A.; Nielsen, K. a. r. L.; Tyson, G. W.; Nielsen, P. H., Genome sequences of rare, uncultured bacteria obtained by differential coverage binning of multiple metagenomes. *Nat Biotechnol* **2013**, *31*, (6), 533-538.
189. Alneberg, J.; Bjarnason, B. S.; de Bruijn, I.; Schirmer, M.; Quick, J.; Ijaz, U. Z.; Lahti, L.; Loman, N. J.; Andersson, A. F.; Quince, C., Binning metagenomic contigs by coverage and composition. *Nat Meth* **2014**, *11*, (11), 1144-1146.
190. Wu, Y.-w.; Tang, Y.-H.; Tringe, S. G.; Simmons, B. A.; Singer, S. W., MaxBin: an automated binning method to recover individual genomes from metagenomes using an expectation-maximization algorithm. *Microbiome* **2014**, 2-26.
191. Kang, D. D.; Froula, J.; Egan, R.; Wang, Z., MetaBAT, an efficient tool for accurately reconstructing single genomes from complex microbial communities. *PeerJ* **2015**, *3*, e1165.
192. Ahn, J. H.; Kim, S.; Park, H.; Rahm, B.; Pagilla, K.; Chandran, K., N₂O Emissions from Activated Sludge Processes, 2008-2009: Results of a National Monitoring Survey in the United States. *Environ Sci Technol* **2010**, *44*, 5405-5411.
193. Agency, U. S. E. P. Summary report: Global anthropogenic non-CO₂ greenhouse gas emissions: 1990-2030.; *Office of Atmospheric Programs*: 2012.
194. Crutzen, P., The Influence of nitrogen oxides on atmospheric ozone content. In *A Pioneer on Atmospheric Chemistry and Climate Change in the Anthropocene*, 2016; Vol. 50.
195. Ravishankara, A. R.; Daniel, J. S.; Portmann, R. W., Nitrous Oxide (N₂O): The Dominant Ozone-Depleting Substance Emitted in the 21st Century. *Science* **2009**, *326*, (5949), 123-125.
196. Beaulieu, J. J.; Tank, J. L.; Hamilton, S. K.; Wollheim, W. M.; Hall, R. O.; Mulholland, P. J.; Peterson, B. J.; Ashkenas, L. R.; Cooper, L. W.; Dahm, C. N.; Dodds, W. K.; Grimm, N. B.; Johnson, S. L.; McDowell, W. H.; Poole, G. C.; Valett, H. M.; Arango, C. P.; Bernot, M. J.; Burgin, A. J.; Crenshaw, C. L.; Helton, A. M.; Johnson, L. T.; O'Brien, J. M.; Potter, J. D.; Sheibley, R. W.; Sobota, D. J.; Thomas, S. M., Nitrous oxide emission from denitrification in stream and river networks. *PNAS* **2011**, *108*, (1), 214-219.
197. Hanke, A.; Berg, J.; Hargesheimer, T.; Tegetmeyer, H. E.; Sharp, C. E.; Strous, M., Selective pressure of temperature on competition and cross-feeding within denitrifying and fermentative microbial communities. *Front Microbiol* **2015**, *6*, 1461.
198. Chen, M.-Y.; Tsay, S.-S.; Chen, K.-Y.; Shi, Y.-C.; Lin, Y.-T.; Lin, G.-H., *Pseudoxanthomonas taiwanensis* sp. nov., a novel thermophilic, N₂O-producing species isolated from hot springs. *Int J Syst Evol Microbiol* **2002**, *52*, (6), 2155-2161.
199. Anantharaman, K.; Brown, C. T.; Hug, L. A.; Sharon, I.; Castelle, C. J.; Probst, A. J.; Thomas, B. C.; Singh, A.; Wilkins, M. J.; Karaoz, U.; Brodie, E. L.; Williams, K. H.; Hubbard,

- S. S.; Banfield, J. F., Thousands of microbial genomes shed light on interconnected biogeochemical processes in an aquifer system. *Nat Commun* **2016**, *7*, 1-11.
200. Zhou, Y.; Pijuan, M.; Zeng, R. J.; Yuan, Z., Free nitrous acid inhibition on nitrous oxide reduction by a denitrifying-enhanced biological phosphorus removal sludge. *Environ Sci Technol* **2008**, *42*, (22), 8260-8265.
201. Lemaire, R.; Meyer, R.; Taske, A.; Crocetti, G. R.; Keller, J.; Yuan, Z., Identifying causes for N₂O accumulation in a lab-scale sequencing batch reactor performing simultaneous nitrification, denitrification and phosphorus removal. *J Biotechnol* **2006**, *122*, (1), 62-72.
202. Andrews, S. FastQC A quality control tool for high throughput sequence data. <http://www.bioinformatics.babraham.ac.uk/projects/fastqc/>
203. Gurevich, A.; Saveliev, V.; Vyahhi, N.; Tesler, G., QUAST: quality assessment tool for genome assemblies. *Bioinformatics* **2013**, *29*, (8), 1072-5.
204. Langmead, B.; Salzberg, S. L., Fast gapped-read alignment with Bowtie 2. *Nat Meth* **2012**, *9*, (4), 357-359.
205. Markowitz, V. M.; Chen, I. M.; Palaniappan, K.; Chu, K.; Szeto, E.; Grechkin, Y.; Ratner, A.; Jacob, B.; Huang, J.; Williams, P.; Huntemann, M.; Anderson, I.; Mavromatis, K.; Ivanova, N. N.; Kyrpides, N. C., IMG: the Integrated Microbial Genomes database and comparative analysis system. *Nucleic Acids Res* **2012**, *40*, (Database issue), D115-22.
206. Parks, D. H.; Imelfort, M.; Skennerton, C. T.; Hugenholtz, P.; Tyson, G. W., CheckM: assessing the quality of microbial genomes recovered from isolates, single cells, and metagenomes. *Genome Res* **2015**, *25*, (7), 1043-1055.
207. Richter, M.; Rosselló-Móra, R.; Oliver Glöckner, F.; Peplies, J., JSpeciesWS: a web server for prokaryotic species circumscription based on pairwise genome comparison. *Bioinformatics* **2016**, *32*, (6), 929-931.
208. Overbeek, R.; Begley, T.; Butler, R. M.; Choudhuri, J. V.; Chuang, H.-Y.; Cohoon, M.; Crécy-Lagard, V. d.; Diza, N.; Disz, T.; Edwards, R.; Fonstein, M.; Frank, E. D.; Gerdes, S.; Glass, E. M.; Goesmann, A.; Hanson, A.; Iwata-Reuyl, D.; Jensen, R.; Jamshidl, N.; Krause, L.; Jubal, M.; Larsen, N.; Linke, B.; McHardy, A. C.; Meyer, F.; Neuweger, H.; Olsen, G.; Olson, R.; Osterman, A.; Portnoy, V.; Pusch, G. D.; Rodionov, D. A.; Ruckert, C.; Stelner, J.; Stevens, R.; Thiele, I.; Vassleva, O.; Ye, Y.; Zagnitko, L.; Vonstein, V., The subsystems approach to genome annotation and its use in the project to annotate 1000 genomes. *Nucleic Acids Res* **2005**, *33*, (17), 5691-5702.
209. Huerta-Cepas, J.; Szklarczyk, D.; Forslund, K.; Cook, H.; Heller, D.; Walter, M. C.; Rattei, T.; Mende, D. R.; Sunagawa, S.; Kuhn, M.; Jensen, L. J.; von Mering, C.; Bork, P., eggNOG 4.5: a hierarchical orthology framework with improved functional annotations for eukaryotic, prokaryotic and viral sequences. *Nucleic Acids Res* **2016**, *44*, (D1), D286-D293.
210. Kanehisa, M.; Goto, S., KEGG: Kyoto Encyclopedia of Genes and Genomes. *Nucleic Acids Res* **2000**, *28*, (1), 27-30.
211. Pearson, W. R.; Lipman, D., J., Improved tools for biological sequence comparison. *PNAS* **1988**, *85*, (8), 2444-2448.
212. Lechner, M.; Findeiß, S.; Steiner, L.; Marz, M.; Stadler, P. F.; Prohaska, S. J., Proteinortho: Detection of (Co-)orthologs in large-scale analysis. *BMC Bioinformatics* **2011**, *12*, (124).

213. Csuros, M., Count: evolutionary analysis of phylogenetic profiles with parsimony and likelihood. *Bioinformatics* **2010**, *26*, (15), 1910-2.
214. Ravenhall, M.; Škunca, N.; Lassalle, F.; Dessimoz, C., Inferring horizontal gene transfer. *PLoS Comput Biol* **2015**, *11*, (5), e1004095.
215. Erik, S. W., Using DECIPHER v2.0 to analyze big biological sequence data in R. *R Journal* **2016**.
216. Buchfink, B.; Xie, C.; Huson, D., H, Fast and sensitive protein alignment using DIAMOND. *Nat Meth* **2015**, *12*, (1), 59-60.
217. Katoh, K.; Standley, D. M., MAFFT multiple sequence alignment software version 7: improvements in performance and usability. *Mol Biol Evol* **2013**, *30*, (4), 772-80.
218. Darling, A. E.; Jospin, G.; Lowe, E.; Matsen, F. A. I. V.; Bik, H. M.; Eisen, J. A., PhyloSift: phylogenetic analysis of genomes and metagenomes. *PeerJ* **2014**, *2*, e243.
219. Yu, K.; Zhang, T., Construction of customized sub-databases from NCBI-nr database for rapid annotation of huge metagenomic datasets using a combined BLAST and MEGAN approach. *PLoS One* **2013**, *8*, (4), e59831.
220. Mao, Y.; Yu, K.; Xia, Y.; Chao, Y.; Zhang, T., Genome reconstruction and gene expression of "*Candidatus Accumulibacter phosphatis*" Clade IB performing biological phosphorus removal. *Environ Sci Technol* **2014**, *48*, (17), 10363-71.
221. Goris, J.; Konstantinidis, K. T.; Klappenbach, J. A.; Coenye, T.; Vandamme, P.; Tiedje, J. M., DNA-DNA hybridization values and their relationship to whole-genome sequence similarities. *The ISME J* **2007**, *57*, (Pt 1), 81-91.
222. Richter, M.; Rosselló-Móra, R., Shifting the genomic gold standard for the prokaryotic species definition. *PNAS* **2009**, *106*, (45), 19126-19131.
223. Heylen, K.; Vanparys, B.; Gevers, D.; Wittebolle, L.; Boon, N.; De Vos, P., Nitric oxide reductase (*norB*) gene sequence analysis reveals discrepancies with nitrite reductase (*nir*) gene phylogeny in cultivated denitrifiers. *Environ Microbiol* **2007**, *9*, (4), 1072-7.
224. Oyserman, B. O.; Noguera, D. R.; del Rio, T. G.; Tringe, S. G.; McMahon, K. D., Metatranscriptomic insights on gene expression and regulatory controls in *Candidatus Accumulibacter phosphatis*. *The ISME J* **2015**, *10*, (4), 810-822.
225. He, S.; McMahon, K. D., '*Candidatus Accumulibacter*' gene expression in response to dynamic EBPR conditions. *The ISME J* **2010**, *5*, (2), 329-340.
226. Mao, Y.; Wang, Z.; Li, L.; Jiang, X.; Zhang, X.; Ren, H.; Zhang, T., Exploring the shift in structure and function of microbial communities performing biological phosphorus removal. *PLoS One* **2016**, *11*, (8), e0161506.
227. Speth, D. R.; In 't Zandt, M. H.; Guerrero-Cruz, S.; Dutilh, B. E.; Jetten, M. S., Genome-based microbial ecology of anammox granules in a full-scale wastewater treatment system. *Nat Commun* **2016**, *7*, 11172.
228. Pfeiffer, T.; Bonhoeffer, S., Evolution of cross-feeding in microbial populations. *Am Nat* **2004**, *163*, (6), 126-135.
229. Hyatt, D.; LoCascio, P. F.; Hauser, L. J.; Uberbacher, E. C., Gene and translation initiation site prediction in metagenomic sequences. *Bioinformatics* **2012**, *28*, (17), 2223-30.
230. Finn, R. D.; Clements, J.; Eddy, S. R., HMMER web server: interactive sequence similarity searching. *Nucleic Acids Res* **2011**, *39*, (Web Server issue), W29-37.

231. Camacho, C.; Coulouris, G.; Avagyan, V.; Ma, N.; Papadopoulos, J.; Bealer, K.; Madden, T. L., BLAST+: architecture and applications. *BMC Bioinformatics* **2009**, *10*, 421.
232. Huson, D. H.; Beier, S.; Flade, I.; Górski, A.; El-Hadidi, M.; Mitra, S.; Ruscheweyh, H.-J.; Tappu, R., MEGAN community edition-interactive exploration and analysis of large-scale microbiome sequencing data. *PLoS Comput Biol* **2016**, *12*, (6), e1004957.
233. Karst, S. M.; Kirkegaard, R. H.; Albertsen, M., mmgenome: a toolbox for reproducible genome extraction from metagenomes. *bioRxiv* **2016**, 059121.
234. Price, M. N.; Dehal, P. S.; Arkin, A. P., FastTree 2 - Approximately Maximum-Likelihood Trees for Large Alignments. *PLoS One* **2010**, *5*, (3).
235. Liu, B.; Yuan, J.; Yiu, S. M.; Li, Z.; Xie, Y.; Chen, Y.; Shi, Y.; Zhang, H.; Li, Y.; Lam, T. W.; Luo, R., COPE: an accurate k-mer-based pair-end reads connection tool to facilitate genome assembly. *Bioinformatics* **2012**, *28*, (22), 2870-4.
236. Zerbino, D. R.; Birney, E., Velvet: algorithms for de novo short read assembly using de Bruijn graphs. *Genome Res* **2008**, *18*, (5), 821-9.
237. Kumar, S.; Stecher, G.; Tamura, K., MEGA7: Molecular Evolutionary Genetics Analysis Version 7.0 for Bigger Datasets. *Mol Biol Evol* **2016**, *33*, (7), 1870-4.
238. Frederick, A. M.; Robin, B. K.; E. Virginia, A., pplacer: linear time maximum-likelihood and Bayesian phylogenetic placement of sequences onto a fixed reference tree. *BMC Bioinformatics* **2010**, *11*, (1), 538.
239. Fish, J. A.; Chai, B.; Wang, Q.; Sun, Y.; Brown, C. T.; Tiedje, J. M.; Cole, J. R., FunGene: the functional gene pipeline and repository. *Front Microbiol* **2013**, *4*, 291.
240. Shi, Y.; Wells, G.; Morgenroth, E., Microbial activity balance in size fractionated suspended growth biomass from full-scale sidestream combined nitrification-anammox reactors. *Bioresour Technol* **2016**, *218*, 38-45.
241. Lettinga, G.; Velsen, A. F. M.; Hobma, S. W.; Zeeuw, S. W.; Klapwijk, A., Use of the upflow sludge blanket (USB) reactor concept for biological wastewater treatment especially for anaerobic treatment. *Biotechnol Bioeng* **1980**, *22*, (4), 699-734.
242. Morgenroth, E.; Sherden, T.; Loosdrecht, M. C. M. v.; Heijnen, J. J.; Wilderer, P. A., Aerobic Granular Sludge in a Sequencing batch reactor. *Water Res* **1997**, *31*, (12), 3191-3194.
243. Beun, J. J.; Hendriks, A.; Loosdrecht, M. C. M. v.; Morgenroth, E.; Wilderer, P. A.; Heijnen, J. J., Aerobic granulation in a sequencing batch reactor. *Water Res* **1999**, *33*, (10), 2283-2290.
244. Mulder, A.; Graaf, A. A. v. d.; Robertson, L. A.; Kuenen, J. G., Anaerobic ammonium oxidation discovered in a denitrifying fluidized bed reactor. *FEMS Microbiol Ecol* **1995**, *16*, (3), 177-183.
245. Strous, M.; Gerven, E. V.; Zheng, P.; Kuenen, J. G.; Jetten, M. S., Ammonium removal from concentrated waste streams with the anaerobic ammonium oxidation (Anammox) process in different reactor configurations. *Water Res* **1997**, *31*, (8), 1955-1962.
246. Adav, S. S.; Lee, D. J., Extraction of extracellular polymeric substances from aerobic granule with compact interior structure. *J Hazard Mater* **2008**, *154*, (1-3), 1120-6.
247. Adav, S. S.; Lee, D. J.; Show, K. Y.; Tay, J. H., Aerobic granular sludge: recent advances. *Biotechnol Adv* **2008**, *26*, (5), 411-23.
248. Cordero, O. X.; Datta, M. S., Microbial interactions and community assembly at microscales. *Curr Opin Microbiol* **2016**, *31*, 227-234.

249. Lee, D. J.; Chen, Y. Y.; Show, K. Y.; Whiteley, C. G.; Tay, J. H., Advances in aerobic granule formation and granule stability in the course of storage and reactor operation. *Biotechnol Adv* **2010**, *28*, (6), 919-34.
250. J.-H, T.; Q.-S, L.; Y, L., The effects of shear force on the formation, structure and metabolism of aerobic granules. *Appl Microbiol Biotechnol* **2001**, *57*, (1-2), 227-233.
251. Adav, S. S.; Lee, D. J.; Lai, J. Y., Aerobic granulation in sequencing batch reactors at different settling times. *Bioresour Technol* **2009**, *100*, (21), 5359-61.
252. Wang, J.; Wang, X.; Zhao, Z.; Li, J., Organics and nitrogen removal and sludge stability in aerobic granular sludge membrane bioreactor. *Appl Microbiol Biotechnol* **2008**, *79*, (4), 679-85.
253. Wang, X.; Zhang, H.; Yang, F.; Wang, Y.; Gao, M., Long-term storage and subsequent reactivation of aerobic granules. *Bioresour Technol* **2008**, *99*, (17), 8304-9.
254. Seviour, T.; Yuan, Z.; van Loosdrecht, M. C.; Lin, Y., Aerobic sludge granulation: a tale of two polysaccharides? *Water Res* **2012**, *46*, (15), 4803-13.
255. Carvalho, G.; Meyer, R. L.; Yuan, Z.; Keller, J., Differential distribution of ammonia- and nitrite-oxidising bacteria in flocs and granules from a nitrifying/denitrifying sequencing batch reactor. *Enzyme Microb Technol* **2006**, *39*, (7), 1392-1398.
256. Innerebner, G.; Insam, H.; Franke-Whittle, I. H.; Wett, B., Identification of anammox bacteria in a full-scale deammonification plant making use of anaerobic ammonia oxidation. *Syst Appl Microbiol* **2007**, *30*, (5), 408-12.
257. Luo, J.; Chen, H.; Han, X.; Sun, Y.; Yuan, Z.; Guo, j., Microbial community structure and biodiversity of size-fractionated granules in a partial nitrification-anammox process. *FEMS Microbiol Ecol* **2017**, *93*, (6), 1-10.
258. Ali, M.; Rathnayake, R.; Zhang, L.; Ishii, S.; Kindaichi, T.; Satoh, H.; Toyoda, S.; Yoshida, N.; Okabe, S., Source identification of nitrous oxide emission pathways from a single-stage nitrification-anammox granular reactor. *Water Res* **2016**, *102*, 147-157.
259. Wang, Y.; Jiang, X.; Wang, H.; Guo, G.; Guo, J.; Qin, J.; Zhou, S., Comparison of performance, microorganism populations, and bio-physiochemical properties of granular and flocculent sludge from denitrifying phosphorus removal reactors. *J Chem Eng* **2015**, *262*, 49-58.
260. Yilmaz, G.; Lemaire, R.; Keller, J.; Yuan, Z., Simultaneous nitrification, denitrification, and phosphorus removal from nutrient-rich industrial wastewater using granular sludge. *Biotechnol Bioeng* **2008**, *100*, (3), 529-41.
261. Vanwonterghem, I.; Jensen, P. D.; Dennis, P. G.; Hugenholtz, P.; Rabaey, K.; Tyson, G. W., Deterministic processes guide long-term synchronised population dynamics in replicate anaerobic digesters. *The ISME J* **2014**, *8*, (10), 2015-2028.
262. DeSantis, T. Z.; Hugenholtz, P.; Larsen, N.; Rojas, M.; Brodie, E. L.; Keller, K.; Huber, T.; Dalevi, D.; Hu, P.; Andersen, G. L., Greengenes, a chimera-checked 16S rRNA gene database and workbench compatible with ARB. *Appl Environ Microbiol* **2006**, *72*, (7), 5069-72.
263. Csárdi, G.; Nepusz, T., The igraph software package for complex network research. *Complex System* **2006**, 1695.
264. Dixon, P., VEGAN, a package of R functions for community ecology. *Journal of Vegetation Science* **2003**, *14*, (6), 927.
265. Stachowicz, J. J., Mutualism, facilitation, and the structure of ecological communities. *BioScience* **2001**, *51*, (3), 235-246.

266. McCann, K. S., The diversity-stability debate. *Nat* **2000**, *405*, 228-233.
267. Faust, K.; Sathirapongsasuti, J. F.; Izard, J.; Segata, N.; Gevers, D.; Raes, J.; Huttenhower, C., Microbial co-occurrence relationships in the human microbiome. *PLoS Comput Biol* **2012**, *8*, (7), e1002606.
268. Braker, G.; Conrad, R., Diversity, structure, and size of N₂O-producing microbial communities in soils-what matters for their functioning? *Adv Appl Microbiol* **2011**, *75*, 33-70.
269. Henry, S.; Bru, D.; Stres, B.; Hallet, S.; Philippot, L., Quantitative detection of the *nosZ* gene, encoding nitrous oxide reductase, and comparison of the abundances of 16S rRNA, *narG*, *nirK*, and *nosZ* genes in soils. *Appl Environ Microbiol* **2006**, *72*, (8), 5181-5189.
270. Griffin, J. S.; Wells, G. F., Regional synchrony in full-scale activated sludge bioreactors due to deterministic microbial community assembly. *The ISME J* **2017**, *11*, (2), 500-511.
271. Burgmann, H.; Jenni, S.; Vazquez, F.; Udert, K. M., Regime shift and microbial dynamics in a sequencing batch reactor for nitrification and anammox treatment of urine. *Appl Environ Microbiol* **2011**, *77*, (17), 5897-907.
272. Bru, D.; Sarr, A.; Philippot, L., Relative abundances of proteobacterial membrane-bound and periplasmic nitrate reductases in selected environments. *Appl Environ Microbiol* **2007**, *73*, (18), 5971-5974.
273. Throback, I. N.; Enwall, K.; Jarvis, A.; Hallin, S., Reassessing PCR primers targeting *nirS*, *nirK* and *nosZ* genes for community surveys of denitrifying bacteria with DGGE. *FEMS Microbiol Ecol* **2004**, *49*, (3), 401-17.
274. Braker, G.; Fesefeldt, A.; Witzel, K.-P., Development of pcr primer systems for amplification of nitrite reductase genes (*nirK* and *nirS*) to detect denitrifying bacteria in environmental samples. *Appl Environ Microbiol* **1998**, *64*, (10), 3769-3775.
275. Santoro, A. E.; Boehm, A. B.; Francis, C. A., Denitrifier community composition along a nitrate and salinity gradient in a coastal aquifer. *Appl Environ Microbiol* **2006**, *72*, (3), 2102-9.
276. Henry, S.; Bru, D.; Stres, B.; Hallet, S.; Philippot, L., Quantitative detection of the *nosZ* gene, encoding nitrous oxide reductase, and comparison of the abundances of 16S rRNA, *narG*, *nirK*, and *nosZ* genes in soils. *Appl Environ Microbiol* **2006**, *72*, (8), 5181-9.
277. Zeng, R. J.; Lemaire, R.; Yuan, Z.; Keller, J., Simultaneous nitrification, denitrification, and phosphorus removal in a lab-scale sequencing batch reactor. *Biotechnol. Bioeng.* **2003**, *84*, (2), 170-178.
278. He, S.; Kunin, V.; Haynes, M.; Martin, H. G.; Ivanova, N.; Rohwer, F.; Hugenholtz, P.; McMahon, K. D., Metatranscriptomic array analysis of 'Candidatus Accumulibacter phosphatis'-enriched enhanced biological phosphorus removal sludge. *Environ Microbiol* **2010**, *12*, (5), 1205-1217.
279. Perez-Garcia, O.; Mankelov, C.; Chandran, K.; Villas-Boas, S. G.; Singhal, N., Modulation of nitrous oxide (N₂O) accumulation by primary metabolites in denitrifying cultures adapting to changes in environmental C and N. *Environ Sci Technol* **2017**, *51*, (23), 13678-13688.
280. Lawson, C. E.; Wu, S.; Bhattacharjee, A. S.; Hamilton, J. J.; McMahon, K. D.; Goel, R.; Noguera, D. R., Metabolic network analysis reveals microbial community interactions in anammox granules. *Nat Commun* **2017**, *8*, 1-12.

281. Caruso, T.; Chan, Y.; Lacap, D. C.; Lau, M. C.; McKay, C. P.; Pointing, S. B., Stochastic and deterministic processes interact in the assembly of desert microbial communities on a global scale. *The ISME J* **2011**, *5*, (9), 1406-13.
282. Vanwonterghem, I.; Jensen, P. D.; Dennis, P. G.; Hugenholtz, P.; Rabaey, K.; Tyson, G. W., Deterministic processes guide long-term synchronised population dynamics in replicate anaerobic digesters. *The ISME J* **2014**, *8*, (10), 2015-28.
283. Leibold, M. A.; McPeck, M. A., Coexistence of the niche and neutral perspectives in community ecology. *Ecology* **2006**, *87*, (6), 1399-1410.
284. Pholchan, M. K.; Baptista Jde, C.; Davenport, R. J.; Sloan, W. T.; Curtis, T. P., Microbial community assembly, theory and rare functions. *Front Microbiol* **2013**, *4*, 68.
285. Zhou, J.; Liu, W.; Deng, Y.; Jiang, Y. H.; Xue, K.; He, Z.; Van Nostrand, J. D.; Wu, L.; Yang, Y.; Wang, A., Stochastic assembly leads to alternative communities with distinct functions in a bioreactor microbial community. *MBio* **2013**, *4*, (2).
286. Lu, H. P.; Yeh, Y. C.; Sastri, A. R.; Shiah, F. K.; Gong, G. C.; Hsieh, C. H., Evaluating community-environment relationships along fine to broad taxonomic resolutions reveals evolutionary forces underlying community assembly. *The ISME J* **2016**, *10*, (12), 2867-2878.
287. Louca, S.; Polz, M. F.; Mazel, F.; Albright, M. B. N.; Huber, J. A.; Connor, M. I. O. x.; Ackermann, M.; Hahn, A. S.; Srivastava, D. S.; Crowe, S. A.; Doebeli, M.; Parfrey, L. W., Function and functional redundancy in microbial systems. *Nat Ecol Evolution* **2018**, 1-8.